Coversheet

Earth ArXiv

MARINE GEOHAZARDS AND GEO-ENGINEERING CONSTRAINTS ON THE GLACIATED EUROPEAN MARGINS

Benjamin Bellwald (corresponding author), NGI, Oslo, Norway, benjamin.bellwald@ngi.no and University of Oslo, Oslo, Norway

Bartosz Kurjanski, University of Aberdeen, Aberdeen, UK, bkurjanski@abdn.ac.uk

Gareth Carter, Arup, Edinburgh, UK, gareth.carter@arup.com

Gareth Wood, bp International, Sunbury on Thames, UK, gareth.wood@bp.com

Leah Arlott, RWE Renewables, Swindon, UK, leah.arlott@rwe.com

Andreia Plaza-Faverola, UiT The Arctic University of Norway, Tromsø, Norway, andreia.a.faverola@uit.no

Heather A. Stewart, Kelpie Geoscience Limited, Edinburgh, UK, hstewart@kelpiegeoscience.com

Berit Oline Hjelstuen, University of Bergen, Bergen, Norway, berit.hjelstuen@uib.no

Helge Løseth, Equinor ASA, Trondheim, Norway, heloe@equinor.com

Katrine Juul Andresen, Aarhus University, Aarhus, Denmark, katrine.andresen@geo.au.dk

Stefan Wenau, ATLAS MARIDAN ApS Germany, Bremen, Germany, stefan.wenau@atlasmaridan.com

Roger Birchall, SSE Renewables, Glasgow, UK, roger.birchall@sse.com

Claire McGhee, AtkinsRéalis, Glasgow, UK, claire.mcghee@atkinsrealis.com

Steven J. Gibbons, NGI, Oslo, Norway, steven.gibbons@ngi.no

Carl B. Harbitz, NGI, Oslo, Norway, carl.bonnevie.harbitz@ngi.no

Brian Carlton, NGI, Oslo, Norway, brian.carlton@ngi.no

Andrew M. W. Newton, Queen's University Belfast, Belfast, UK, a.newton@qub.ac.uk

Mads Huuse, The University of Manchester, Manchester, UK, mads.huuse@manchester.ac.uk

Dieter Issler, NGI, Oslo, Norway, dieter.issler@ngi.no

Finn Løvholt, NGI, Oslo, Norway, finn.lovholt@ngi.no

Carl Fredrik Forsberg, NGI, Oslo, Norway, carl.fredrik.forsberg@ngi.no

Mark Coughlan, University College Dublin, Dublin, Ireland, mark.coughlan@ucd.ie

Simona Caruso, bp International, Aberdeen, UK, simona.caruso@bp.com

Michael Long, University College Dublin, Dublin, Ireland, mike.long@ucd.ie and NGI, Oslo, Norway, michael.long@ngi.no

David Tappin, BGS, Nottingham, UK, drta@bgs.ac.uk

Paul Dimmock, NGI, Perth, Australia, paul.dimmock@ngi.no

Rasmus Tofte Klinkvort, NGI, Oslo, Norway, rasmus.klinkvort@ngi.no

Maarten Vanneste, NGI, Oslo, Norway, maarten.vanneste@ngi.no

This is a non-peer-reviewed preprint submitted to EarthArXiv.

The paper was submitted to Earth-Science Reviews.

MARINE GEOHAZARDS AND GEO-ENGINEERING CONSTRAINTS ON THE GLACIATED EUROPEAN MARGINS

Benjamin Bellwald[1,2], Bartosz Kurjanski[3], Gareth Carter[4,5], Gareth Wood[6], Leah Arlott[7], Andreia Plaza-Faverola[8], Heather A. Stewart[9], Berit Oline Hjelstuen[10], Helge Løseth[11], Katrine Juul Andresen[12], Stefan Wenau[13], Roger Birchall[14], Claire McGhee[15], Steven J. Gibbons[1], Carl B. Harbitz[1], Brian Carlton[1], Andrew M. W. Newton[16], Mads Huuse[17], Dieter Issler[1], Finn Løvholt[1], Carl Fredrik Forsberg[1], Mark Coughlan[18], Simona Carusoack[6], Michael Long[1,18], David Tappin[19], Paul Dimmock[20], Rasmus Tofte Klinkvort[1], Maarten Vanneste[1]

[1]NGI, Sandakerveien 140, Oslo, Norway

[2]University of Oslo, Oslo, Norway

[3]University of Aberdeen, Aberdeen, UK

[4]British Geological Survey, Lyell Centre, Research Avenue South, Edinburgh, UK

[5]Arup, Edinburgh, UK

[6]bp, ICBT, Chertsey Rd, Sunbury-on-Thames, UK

[7]RWE Renewables, Swindon, UK

[8]iC3 – Centre for ice, Cryosphere, Carbon and Climate, Department of Geosciences, UiT the Arctic University of Norway, 9037 Tromsø, Norway

[9]Kelpie Geoscience Limited, Murchison House, 10 Max Born Crescent, Edinburgh, UK

[10]Department of Earh Science, University of Bergen, Bergen, Norway

[11]Equinor ASA, NO-7005 Trondheim, Norway

[12]Department of Geoscience, Aarhus University, Høegh-Guldbergs Gade 2, 8000 Aarhus C, Denmark

[13]ATLAS MARIDAN ApS Germany, Heerenholz 17, Bremen, Germany

[14]SSE Renewables, Glasgow, UK

[15]AtkinsRéalis, Glasgow, UK

[16]Queen's University Belfast, Belfast, UK

[17]University of Manchester, Manchester, UK

[18]University College Dublin, Dublin, Ireland

[19]British Geological Survey, Kingsley Dunham Centre, Keyworth, Nottingham, UK

[20]NGI, Perth, Australia

Abstract

The glaciated European continental margins (spanning 49-82°N and 16°W-36°E) are home to a thriving offshore energy sector and densely inhabited coastal areas. These regions face numerous marine geohazards and geo-engineering challenges due to complex subsurface conditions shaped by large-scale geological and climate processes. The geological complexity of this area is among the highest globally, featuring dynamic processes such as distinct ice-sheet oscillations and sea-level changes, which have led to rapidly evolving paleo-geographic and depositional environments. Consequently, the soil conditions are highly variable and heterogeneous, both vertically and laterally, requiring meticulous evaluation for engineering projects, such as offshore wind developments.

This study reviews the marine geohazards and geo-engineering constraints along the glaciated European margins, with a particular focus on the Quaternary period, during which the most significant environmental changes occurred. We examine the implications of shallow subsurface deposits and fluids on engineering foundations and hazards for offshore activities, including offshore wind energy, carbon storage, hydrocarbon exploration, marine infrastructure, and marine ecosystems. Additionally, we assess the risks of tsunamis and earthquakes related to the Quaternary evolution of the Northern European margin. This array of hazards presents substantial risks and challenges to both coastal communities and offshore industries.

Keywords: *Geohazards; Geo-engineering; Quaternary geology; Data integration; Glacial and marine sediments; Shallow gas; Gas hydrates; Fluid flow; Strength variability; Boulder; Gravel; Weathered bedrock; Peat; Glaciotectonic deformation; Glacigenic landforms; Ocean currents; Slope instabilities; Glacio-isostatic adjustment; Seismicity; Tsunami*

1. Introduction

The Quaternary is the current and most recent period of Earth's geological history, spanning from 2.58 million years ago to the present day (Walker and Geissman, 2022). It is divided into two epochs: the Pleistocene (2.58 million to 11.7 thousand years ago) and the Holocene (11.7 thousand years ago to present; Walker and Geissman, 2022). The Pleistocene is characterized by repeated cycles of glaciation, with ice sheets periodically advancing and retreating across much of North America, Europe, and Asia, leaving a distinct imprint on the geomorphology, lithology, and stress history in the sedimentary sequences (Svendsen et al., 2004; Batchelor et al., 2019; Newton et al., 2024a).

The Quaternary deposits along the glaciated European margins and the crustal response related to the spatio-temporal loading and unloading of these deposits by large-scale Pleistocene ice sheets have resulted in a variety of marine geohazards and geo-engineering constraints (Eyles, 2013). Broadly speaking, geohazards have the potential to cause damage to health, environment, marine developments, offshore infrastructure, and/or loss of life both in coastal communities and on offshore assets. Geo-engineering constraints can have wide-ranging negative impacts on the development of offshore projects, ranging from increased costs and timelines to making a project uneconomical or technically infeasible (Bienen et al., 2015; Watts et al., 2021).

There are multiple definitions and interpretations of what constitutes a marine geohazard, especially in the context of geo-engineering and geo-risk management activities (Table 1.1; e.g., Vanneste et al., 2014; Giles, 2020a; IAEG, 2022; OSIG, 2022; Dimmock et al., 2023). In marine geoscience, a geohazard is often regarded as an event that can occur naturally or can be triggered anthropogenically (induced geohazard), with consequences for coastal communities. On the other hand, for offshore industries, a marine geohazard includes any unforeseen natural geological conditions that have any adverse effects on human life, operations (project timeline, budget, and safety), infrastructure, or environment (ISO 19901-10; SUT, 2022). The definition formulated by Vanneste et al. (2014) states that a marine geohazard is "a geological condition which represents – or has the potential to develop further into – a situation leading to damage or uncontrolled risk". The definition of hazard (and geohazard in this instance) can also be adapted from the occupational health and safety (OHS) approach. For example, according to Standards Australia/Standards New Zealand a (geo)hazard is “a source or a situation with a potential for harm in terms of human injury or ill-health, damage to property, damage to the environment, or a combination of these” (Standards Australia, 2001). Another approach uses the idea of energy release to define (geo)hazards. In this context, (geo)hazards are ‘sources of potentially damaging energy which either exist naturally or as a result of humankind’s modification of the naturally occurring world ... where damage (injury) is the result of an incident energy whose intensity at the point of contact with the recipient exceeds the damage threshold of the recipient (Viner, 1991)’.

Dimmock et al. (2023) separates geohazards from geo-engineering constraints: Geohazards are defined as dynamic geo-events/processes that are a risk to the development and are addressed by project management frameworks whereas geo-engineering constraints are defined as existing, static ground features that pose an engineering challenge to the development and that are addressed by routine geo-engineering solutions.

Table 1.1. Selected definitions of geohazards.

Organization	Geohazard Definition
British Geological Survey	Geohazards, such as volcanoes, earthquakes and landslides, are the natural geological processes that present a direct risk to people or an indirect risk by impacting development.
Dimmock et al. (2023)	It is proposed to restrict the term 'geohazard' to dynamic processes that impact the development. Another term 'geo-engineering constraint' is proposed to cover pre-existing features, static in nature, that require engineering consideration.
European Marine Board	A geohazard (or geological hazard) is a geological condition which represents - or has the potential to develop into - a situation leading to damage or uncontrolled risk.
Giles (2020a)	A geological hazard (geohazard) is the consequence of an adverse combination of geological processes and ground conditions, sometimes precipitated by anthropogenic activity. The term implies that the event is unexpected and likely to cause significant loss or harm.
International Association for Engineering Geology and the Environment (2022)	Geological and geomorphological processes or phenomena that can adversely impact a project.
International Ocean Discovery Program	Natural geological processes and phenomena, such as earthquakes, tsunamis, landslides, and volcanic eruptions, that pose significant risks to human life, infrastructure, and the environment.
ISO 19901-10	A geological condition that has the potential to have adverse effects on persons, operations, infrastructure, or the environment.
National Oceanography Centre (Southampton)	Marine Geohazards are a range of underwater phenomena all of which can either directly or indirectly represent a threat to humans and the environment. These include underwater landslides, volcanic eruptions, turbidity currents and tsunamis.
Natural Resources Canada	Marine geohazards are geological conditions at the sea floor or within sub-bottom sediments that, if unrecognized, could result in dangerous or catastrophic events with attendant risks to life and/or infrastructure. Examples of such hazards include earthquakes and submarine landslides that can trigger tsunamis, iceberg scouring of the seabed, and gas migration or build-up that can lead to locally overpressurized sediments and potential terrain instability and/or blowouts.
Offshore Site Investigation and Geotechnics (2022)	A geological state, feature, or process that presents a risk to humans, property, or the environment.
United States Geological Survey	Marine geohazards, or 'dangers in the deep' include earthquakes, volcanic eruptions, submarine landslides, and tsunamis, as well as dissociation of gas hydrates—which can cause seafloor collapse—and oil spills or toxic seeps that affect deep sea life or change the physical characteristics of ocean environments.
Vanneste et al. (2014)	Geohazards are defined as a geological condition which represents – or has the potential to develop further into – a situation leading to damage or uncontrolled risk.
Viner (1991)	Geohazards are sources of potentially damaging energy which either exist naturally or as a result of humankind's modification of the naturally occurring world ... where damage (injury) is the result of an incident energy whose intensity at the point of contact with the recipient exceeds the damage threshold of the recipient

Risk is defined as the combination of likelihood (or frequency of occurrence) and the severity of consequence of a process or constraint (i.e., hazard) impacting infrastructure and development. The consequences of geohazards can be divided into the ones i) affecting life, health, and environment, ii) causing material losses, and iii) disturbing global economy. For offshore industries and coastal communities, the marine geohazard identification is the first step of risk assessment.

Induced (or operational) geohazards are manifested on a small, subregional to borehole scale. Often associated with drilling and emplacement of subsea infrastructure on the seafloor, they are the main focus of scientific drilling, energy-industry drilling, and offshore development activities (Shipp, 2017). Prominent induced offshore geohazards along the glaciated European margins cover blowouts, loss of well control, and loss of well stability. One of the best documented, and most tragic, induced geohazards in our study area is the shallow gas blow-out at the West Vanguard platform on the mid-Norwegian margin (Table 1.2; Figures 1.1c and 1.2). Although shallow gas is recognised as a potential geohazard, and pre-drilling site surveys are mandatory, accidents can still occur such as the UK22/4b platform blowout in 1990 (Table 1.2; Figure 1.1d).

Naturally occurring geohazards, often manifested on a larger regional scale, are historically more frequently threatening larger areas than induced ones and preferentially affecting coastal communities. A good example is the wave run-up and inundation associated with a rock-avalanche-triggered tsunami, such as the Tafjord event in 1934 (Table 1.2; Figure 1.1a). The tsunami related to the Storegga landslide around 8100 years ago might have impacted settlements located on the formerly terrestrially exposed Doggerland (Hill et al., 2014) and classical coastlines (Walker et al., 2020). Several tsunamis also occurred in lakes located on the glaciated European margins (e.g., Loen rock avalanche and tsunami in 1905 and 1936 with 61 and 74 fatalities; Grimstad and Nesdal, 1990; Waldmann et al., 2021), but these events are not part of this paper. Slope instabilities along the coastlines, and in fjord systems, often result in road closures (Figure 1.1b; NVE 2021; Lacasse et al., 2022), or, in worst case, in injury or loss of life.

Table 1.2. Selected offshore accidents and natural disasters on the glaciated European margins related to geohazards and engineering challenges since 1900 AD. Listed are only published and known events in the marine realm, and thus the table is under-representative for the incidents that occurred along the margin.

Event	Area	Consequences	Cause	Reference
Tafjord tsunami, 1934	Western Norwegian fjord	40 fatalities	Tsunami triggered by rock avalanche	Harbitz et al., 1993; Braathen et al. 2004
West Vanguard, 1985	Mid-Norwegian margin	1 fatality	Shallow gas blow-out	Vinnem and Røed, 2020
High Seas Driller platform UK22/4b-4, 1990	North Sea	0 fatalities	Shallow gas blow-out	Leifer and Judd, 2015
Horns Rev III OWF, Wind Turbine Foundation, 2019	North Sea	0 fatalities	Liquefaction, likely due to jack-up operations and low strength subsurface	Vattenfall, 2019
Kråkneset quick clay landslide, Alta, 2020	Northern Norway	0 fatalities; road closed	Low initial slope stability and placement of fill, eventually triggered by unfavourable ground water pressure from snow melt	NVE, 2021; Lacasse et al., 2022



Figure 1.1. Historic accidents along the glaciated European margins. **a)** Tafjord rock avalanche and tsunami in 1934. Photo by Alfred Skar, Arbeiderbevegelsens arkiv og bibliotek. **b)** Quick clay landslide at Kråkneset in Alta in 2020. Photo by Anders Bjordal/NVE. **c)** Shallow gas blowout at West Vanguard platform in 1985. Photo by Øyvind Hagen/Equinor. **d)** MODU High Seas Driller – UK22-4b-4 Blowout – North Sea. Photo from https://the-norwegian.com/north-sea-blowouts-and-fires-1964-2020/.

Glaciated margins are burdened with a complex set of geological conditions linked to of ice-sheet dynamic and resulting in a spatially and temporally heterogeneous glacial and interglacial sedimentary package further affected by sea-level oscillations, and glacio-isostatic rebound. These complex Quaternary conditions are encountered in the shallow subsurface directly at and under the seabed in a zone critical for engineering where all offshore infrastructure (e.g. offshore windfarms, pipelines, cables and O&G platforms) has been placed since the mid-20th century (Figures 1.2, 1.3, and 2.1). A variety of industries (offshore wind, carbon capture and storage, oil and gas, shipping traffic, fishing activities; Figure 1.4) compete for acreage within these areas (e.g., de Jonge-Anderson and Underhill, 2022; Paolo et al., 2024), which are also unique habitats for a variety of birds, fish and for marine mammals (e.g., Virtanen et al., 2022; Danish Maritime Authority, 2023). The challenge for decision makers and authorities is to manage the multiple conflicts of interests and seek synergies and opportunities between the various industries, public safety, and the natural environment (Virtanen et al., 2022).

The aim of this paper is to review and systematise marine geohazards and geo-engineering constraints present on the formerly glaciated European margins. The study area includes the Barents Sea, the mid-Norwegian margin, the North Sea, the areas West of Shetland and the Outer Hebrides, the Baltic Sea including the Gulf of Bothnia, the Irish Sea, the Celtic Sea, and the Rockall Trough (Figure 2.1). We also discuss the impact of ice sheet loading on the regional tectonic stress history, and the effect it exerted on the mechanical properties of sediments and rocks. We summarize lithologies and landforms of the study area, as these give valuable insights into the extent and progressive decay of ice sheets, the existing fluid flow, and structural properties of the subsurface. Finally, we describe in depth geo-engineering constrains and geohazards specific to the study area and glacial and post glacial processes. We also discuss the implications of each hazard and constrain for offshore engineering undertakings.

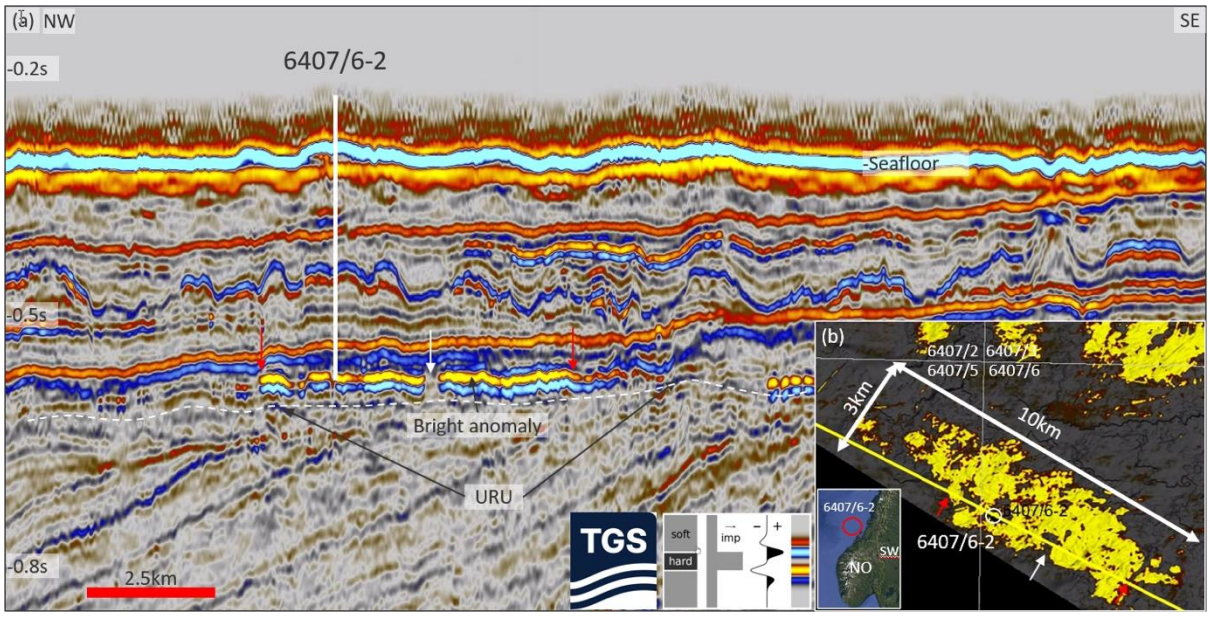


Figure 1.2. Location of the West Vanguard gas blow-out in well 6407/6-2 on Haltenbanken, mid-Norwegian shelf. **a)** Seismic profile across the West Vanguard gas field. The position of the well 6407/6-2 is shown on a new seismic section (inline 24016 of the 3D: PGS 18M01). A bright anomaly is present immediately above the Upper Regional Unconformity (URU). **b)** Extent of the minimum amplitude anomaly extracted from the 3D seismic data (shown in yellow), covering an area of approximately 19 km^2 (3 km x 10 km). This bright low impedance anomaly is interpreted as a gas charged sand. The red and white arrows show the same position on seismic profile and map view. Data courtesy of TGS.

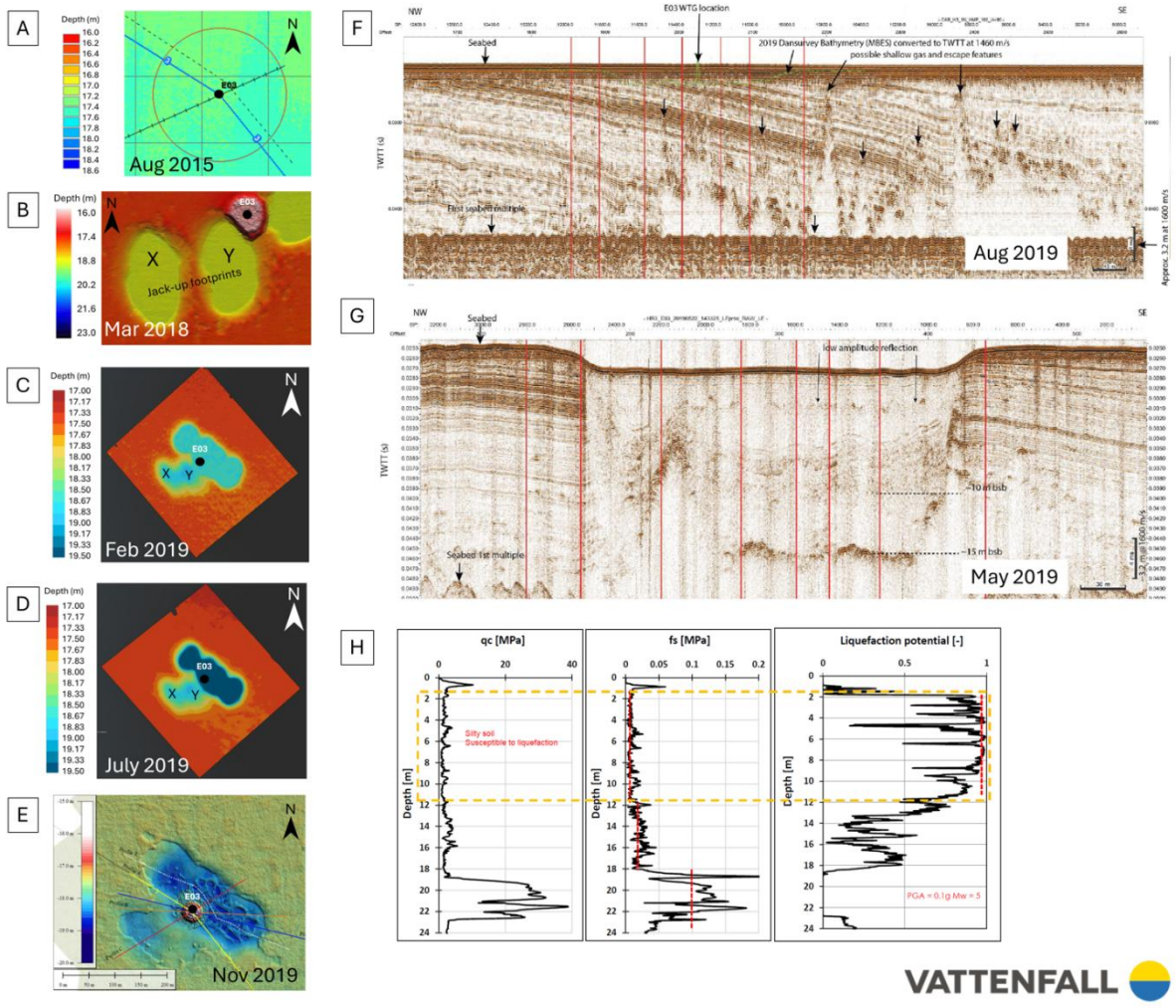


Figure 1.3. Time series illustrations of multibeam echosounder data (MBES) (**a-e**), sub-bottom profiles (**f-g**) and CPT (**h**) before and after the liquefaction event at the E03 wind turbine foundation site in the Horns Rev III offshore wind farm, Danish North Sea. The site comprised a thick post-glacial silt unit with low strength and high liquefaction potential (**h**). The causes for the liquefaction remain uncertain but likely relate to multiple jack-up operations at the site, that involved jetting and soil displacement. Further triggers may relate to repeated storm events during spring 2019 and shallow gas in the silt (Vattenfall, 2019). **a)** MBES data from August 2015 prior to installation of scour protection. **b)** MBES data from March 2018 showing deep (1.4 m) jack-up footprints (X and Y) and damage to scour

protection. **c)** MBES data from February 2019 showing enlarged depressions around the E03 site. **d)** MBES data from July 2019 showing deepened depressions around the E03 site. Seabed lowering was reported to an approximate rate of 0.2-0.5 cm/day (~6-15 cm/month). **e)** MBES data from November 2019 after remediation (initiated in August 2019) and reconstruction of scour protection. **f)** Sub-bottom profile from August 2015 across the E03 site showing a flat seafloor, gently dipping reflections within the post-glacial silt layer and shallow gas 3-9 m below the seabed. **g)** Sub-bottom profile from May 2019 across the E03 site showing the ca. 2.5 m deep seafloor depression and the altered acoustic signal within the post-glacial silt unit down to a level of ca. 15 m below the seabed. **h)** D-CPT at site E03 from 2015, showing a high calculated liquefaction potential within the uppermost ~11 m of the post-glacial silt unit. Data and figures provided by Vattenfall (Vattenfall, 2019).

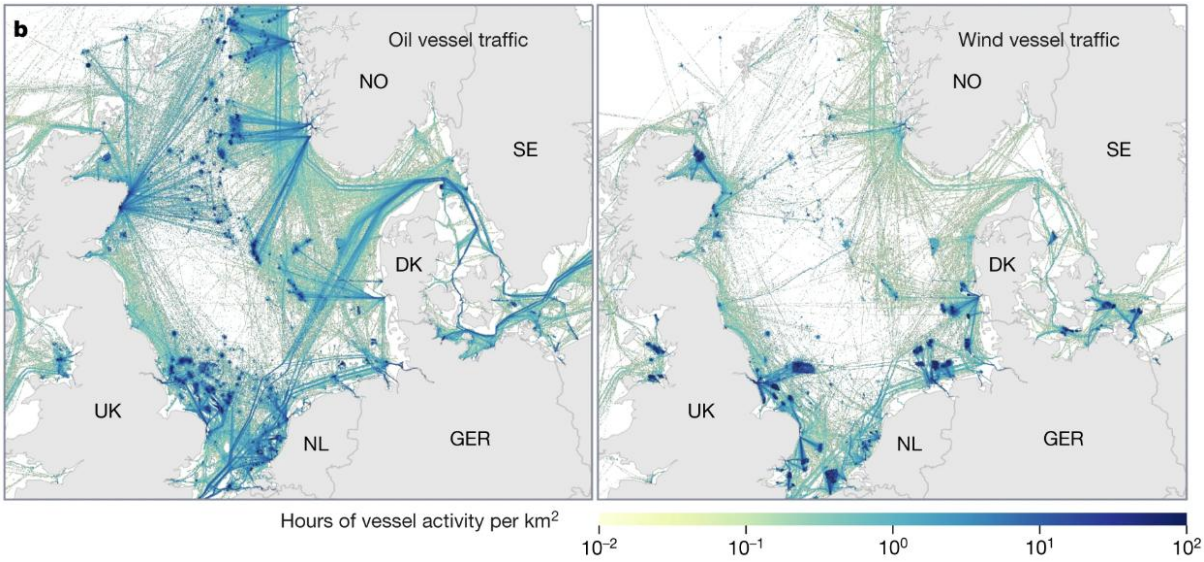


Figure 1.4. Examples of competing interests in the North Sea. Global Fishing Watch uses AI and satellite imagery to map vessel traffic and offshore infrastructure to provide an unprecedented view of previously unmapped industrial use of the ocean, as seen here in the North Sea). Figure from Paolo et al. (2024).

2. Regional setting, glacial history, and paleogeography

The intensification of the global glacial-interglacial cycle at the onset of the Quaternary (~2.58 Ma) was a critical tipping-point in Earth's recent climate history (e.g., Raymo et al., 2006; Westerhold et al., 2020). The increased severity of cold intervals at the Plio-Pleistocene boundary triggered the development of large-scale continental ice sheets in the Northern Hemisphere (Sejrup et al., 2005; Batchelor et al., 2019). The European continental margins throughout the Pleistocene have experienced multiple episodes of glaciation as and when the Eurasian Ice Sheets (EIS) advanced and covered vast areas of land and seabed (Lee et al., 2012). These episodes of glaciations are separated by interglacial periods during which the ice sheet is melted completely or significantly reduced in size. As a result, the European offshore basins and continental margins preserve the most comprehensive sedimentary record

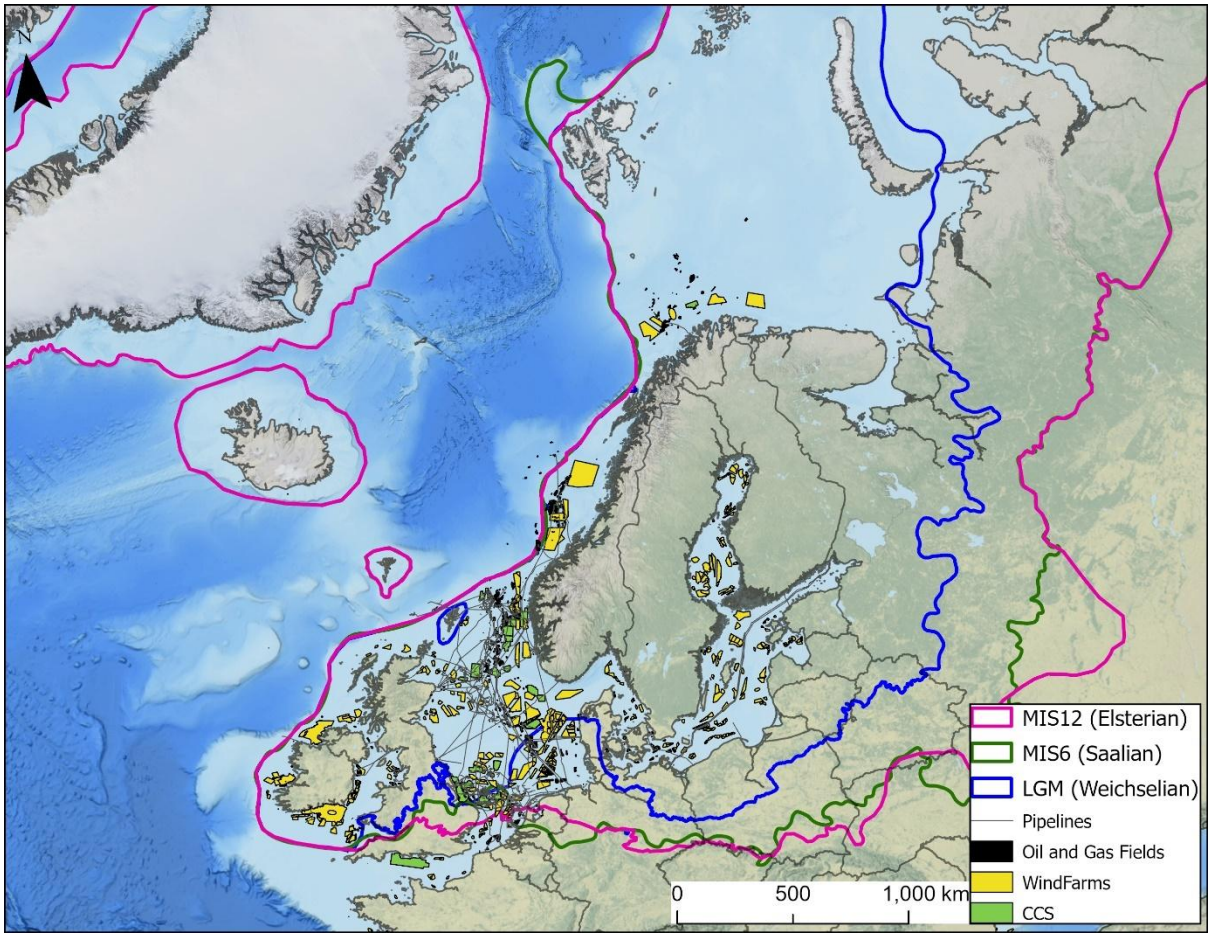
of the EIS and interglacial conditions, including the large river systems supplying sediments to those basins (e.g., Svendsen et al., 2004; Sejrup et al., 2005; Lee et al., 2012; Hughes et al., 2016; Batchelor et al., 2019). The EIS itself can be separated into the Kara-Svalbard–Barents Sea Ice Sheet (SBIS), the Fennoscandian Ice Sheet (FIS), and the British–Irish Ice Sheet (BIIS; Figure 2.1) which nucleated and evolved separately for large parts of their existence but also coalesced on multiple occasions forming a continuous ice mass covering a large part of the continent and adjacent continental seas, but also extended periodically all the way to the continental shelf break. These EIS ice domes were drained by many, fast flowing ice streams which were time transgressive, and their flow was re-organized in response to changes in ice sheet geometry.

The Quaternary glaciations strengthened further during the Mid-Pleistocene Transition (MPT ~1.3-0.7 Ma), with three major glaciations (Elsterian/Anglian, Saalian/Wolstonian, and Weichselian/Devensian) recognised since 500 ka. These glaciations often left distinctive unconformities in the sedimentary package, such as the Upper Regional Unconformity in the Barents Sea (Bellwald et al., 2019c). The traditional view, whereby the Early Pleistocene is characterized by minor ice coverage with regional shelf-edge glaciations, and the Middle- and Late Pleistocene glaciations were more extensive and reached the shelf-edge, is being challenged by new landform and sedimentary records providing evidence of widespread glaciations during the Early Pleistocene although there remain many questions regarding Pleistocene glaciation both in Europe and globally (e.g., Rea et al. 2018; Newton et al., 2024a; Ottesen et al., 2024; Lien et al., 2022; Bellwald et al., 2024a, vs. Sejrup et al., 2005; Nygård et al., 2005; Knies et al., 2009). Nevertheless, during the Pleistocene, glacial processes redistributed large volumes of sediments from the hinterland across the continental shelves and onto the slopes, forming prograding sequences and large trough mouth fans or filling offshore basins (Vorren and Laberg, 1997; Lamb et al., 2017; Rea et al., 2018; Gales et al., 2019; Hjelstuen et al., 2021).

This complex mosaic of glacial and interglacial sediments recording multiple episodes of deposition, incision, reworking and erosion is now occupied by numerous industries with competing interests and is posed to play a key role in the process of energy transition. (Figure 1.4). The offshore areas, in particular the shallower waters of the shelves with an active hydrocarbon exploration, have been the focus of a large coverage of geophysical, geological, and geotechnical datasets. Industrial activity in the harsher and more remote environments of the Arctic Barents Sea has so far been far lower than in the North Sea.

There is ongoing work to better understand and corelate the onshore and offshore stratigraphical schemes across the wider formerly glaciated European margins and link them to the deep-ocean oxygen isotope record. However, correlation remains difficult and is largely inferred in areas where the units lack good chronostratigraphic control (Newton et al. 2024b). Some direct links can be made in well-dated sections of the offshore stratigraphy (e.g., Rea et al., 2018). Existing regional seismostratigraphic

frameworks (e.g., Faleide et al., 1996; Kuhlman and Wong, 2008; Rise et al., 2010; Stoker et al., 2011; Rydningen et al., 2016; Ottesen et al. 2018; Løseth et al., 2022; Newton et al., 2024a) are presented here to illustrate the Quaternary evolution of the glaciated European margins and are valuable for an early assessment of the expected ground conditions but should be carefully evaluated against site-specific datasets. Figure 2.1 illustrates the study area of this review and denotes specific regions that are described in greater detail in terms of their Quaternary evolution and resulting region-specific ground conditions.



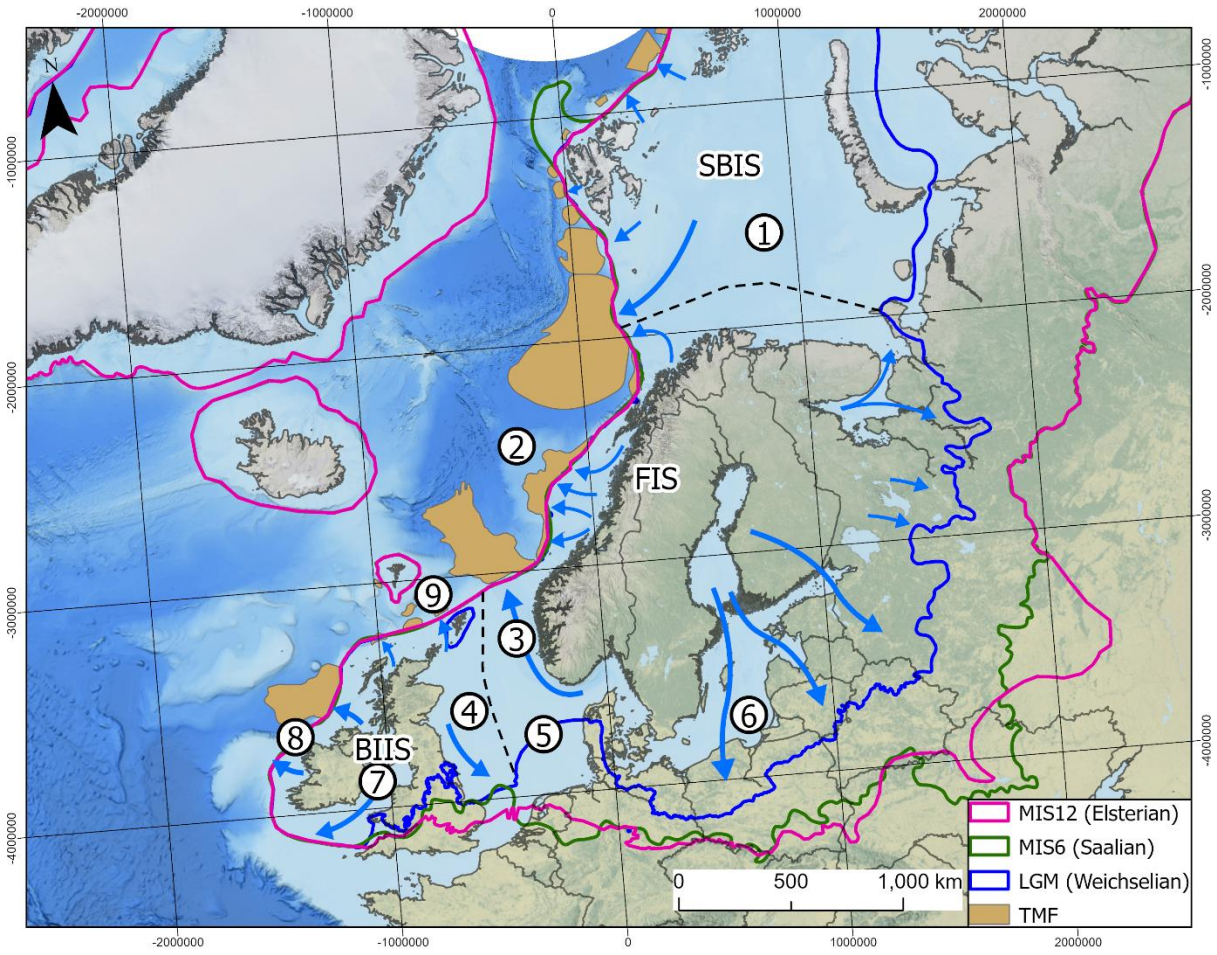


Figure 2.1. The glaciated European margins. **a)** Offshore energy activities ongoing in the region. Shown are blocks for offshore wind and CCS, Oil and Gas discoveries, and pipelines. Ice-sheet extents from Batchelor et al. (2019). **b)** Study area showing the Weichselian, Saalian, and Elsterian ice sheet extents (after Batchelor et al., 2019), major drainage routes of the Eurasian Ice Sheet complex (as for Last Glacial Maximum), trough mouth fans (both after Patton et al., 2017; and references therein), and ice divides (Hughes et al., 2016). Numbers indicated different regions of the glaciated European margin: 1: Barents Sea, 2: Mid-Norway, 3: Northern North Sea, 4: Central North Sea, 5: Southern North Sea, 6: Baltic Sea and Gulf of Bothnia, 7: Irish Sea and Celtic Sea, 8: Outer Hebrides and Rockall, 9: West of Shetland. BIIS: British–Irish Ice Sheet, FIS: Fennoscandian Ice Sheet; SBSIS: Svalbard–Barents Sea Ice Sheet (also named Kara–Barents Sea–Svalbard Ice Sheet).

2.1 Quaternary evolution

2.1.1 Barents Sea

The Barents Sea (Figure 2.1) is a shallow epicontinental sea with an average water depth of 230 m and a maximum water depth of 500 m, and it is one of the widest continental shelves on Earth. In the Pliocene to Early Pleistocene, the Barents Sea was an exposed land area (Dimakis et al., 1998; Butt et al., 2000). The area experienced erosion depths that varied regionally from 10 to >1000 m, caused by repeated glaciations throughout the Pleistocene (Fjeldskaar and Amantov, 2018, Faleide et al., 1996).

297 Field data constrained ice-sheet models suggesting that sub-glacial erosion can account for up to ca.
298 200 m of bedrock excavation, accumulated through the last glacial cycle (for the last ca. 100 kyr; Patton
299 et al., 2022). These erosive episodes resulted in a glacial unconformity (Upper Regional Unconformity),
300 that divides Quaternary sediments (mainly subglacial till) from the underlying pre-Quaternary
301 sedimentary bedrock. Deep troughs such as Bjørnøyrenna formed during ice-streaming phases, and
302 some of the Earth's largest trough mouth fans are depocenters of these processes (Figure 2.1; e.g., the
303 Bear Island Fan and Storfjorden Fan). The glacial processes shifted the shelf topography from a
304 terrestrial platform to the present shelf geometry (Løseth, 2023). The Quaternary sediments are 0 to 70
305 m in thickness on the shelf but can reach thicknesses of up to 4 kilometres on the slopes (Figure 2.2;
306 see also Figure 6.4; Faleide et al., 1996; Hjelstuen and Sejrup, 2021; Alexandropoulou et al., 2021;
307 Lasabuda et al., 2023; Bellwald et al., 2024a). The Quaternary stratigraphy around the modern shelf
308 break is dominated by turbidites, slide debrites, and subglacial till, and the Bjørnøya Contourite Drift
309 at the base (Figure 2.2; Rydningen et al., 2020).

310 During the Last Glacial Maximum, the SBSIS extended all the way to the continental shelf break in the
311 north and west and was coalescent with the FIS in the south (Svendsen et al., 2004; Hughes et al., 2016).
312 The Quaternary deposits of the shelf are mainly of Late Weichselian age (Mangerud et al., 1998; Laberg
313 et al., 2010). The thick sequences on the slopes, in contrast, record the Quaternary processes since the
314 onset of the Pleistocene (Figure 2.2; Vorren et al., 1998; Laberg et al., 2010; 2012; Alexandropoulou et
315 al., 2021; Bellwald et al., 2024a). The last major deglaciation started at c. 18–16.9 ka (ka: thousands of
316 years before present) in the SW Barents Sea (Rüther et al., 2011), with the SBIS and FIS separating by
317 c. 16 ka (Sejrup et al., 2022). A complex assemblage of glaciogenic landforms and sediments is
318 preserved at the seabed, including multiple paleo-ice stream troughs, ice-marginal ridges, grounding
319 zone wedges, meltwater channels, and iceberg ploughmarks (e.g., Winsborrow et al., 2010; Newton and
320 Huuse, 2017). Less than 2 m of Holocene sediments cover most of the Barents Sea, covering some of
321 the glacial landforms (Elverhøi and Solheim, 1983).

322 The modelled glacio-isostatic response is around 800 m for the last one million years but varies strongly
323 across the Barents Sea (Fjeldskaar and Amantov, 2018). The glacial history of the Barents Sea combined
324 with complex tectonics (i.e., marked by cycles of isostatic rebound and subsidence, erosion and
325 sedimentation, fault reactivation, and fracturing) has contributed to a highly dynamic fluid flow regime
326 (Kishankov et al., 2022). Vast hydrocarbon prone basins have been contributing fluids to the shallow
327 subsurface, sustaining widespread gas accumulations, seafloor seepage, and gas hydrate formation. The
328 gas hydrate stability zone (GHSZ) thickness across the Barents Sea can be up to ~400 m in troughs and
329 basins, while at shallow water depths (200–300 m) the upper tens of meters of the sedimentary column
330 are prone to complete gas hydrate dissociation in response to bottom water temperature variations
331 (Vadakkepuliyambatta et al., 2017). On the uppermost continental slopes, thick contourite drifts host
332 widespread gas hydrates and associated free gas accumulations within the uppermost 200 m bsf (e.g.,

Hustoft et al., 2009). Salt tectonics and volcanic sill intrusions also had impact on fluids and gas hydrate dynamics and Quaternary deformation in the western Barents Sea region (e.g., Chand et al., 2008; see also Figures 5.32 and 5.38). Overpressure-prone contourites and beds underlying glacigenic debris flows are often associated with slope failure and mass transport events along the continental slopes of the Barents Sea and the west Svalbard margins (e.g., Bellwald and Planke, 2019).

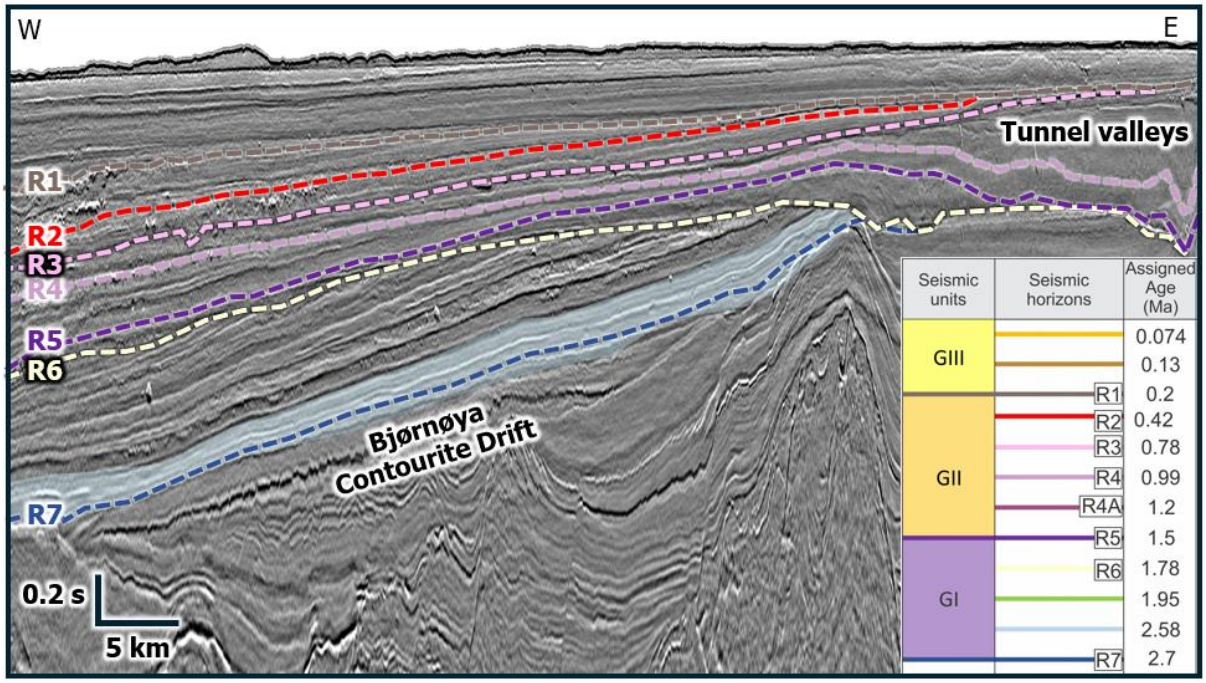


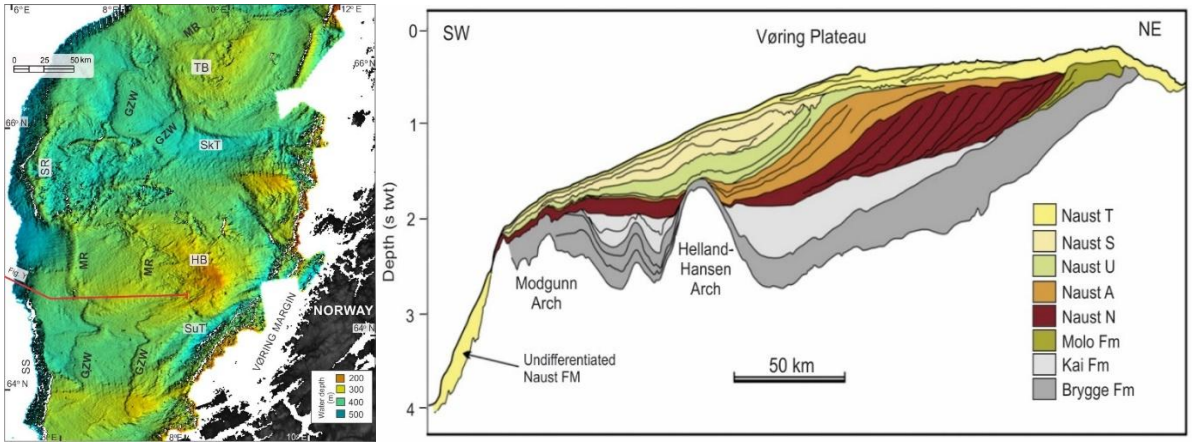
Figure 2.2. Seismic stratigraphy of the SW Barents Sea margin. Chronostratigraphy from Alexandropoulou et al. (2021), and seismic profile modified after Bellwald et al. (2024a). Data courtesy of TGS.

2.1.2 Mid-Norway

The Mid-Norwegian margin (Figures 2.1 and 2.3) comprises three segments; the Møre, Vøring, and Lofoten-Vesterålen. The Møre margin is characterized by a narrow continental shelf, reaching approximately 40 km wide, and where the seabed of the upper continental slope is imprinted by the 8200 ka BP Storegga Slide (e.g., Haflidason et al., 2005). A broad continental shelf region, where the present shelf edge is located about 200 km west of the Norwegian coast, characterizes the Vøring margin (Figure 2.3). The seabed in this region is dominated by prominent cross-shelf troughs, such as the Trænadjupet, Sklinnadjupet, and Suladjupet, that reach water depths of approximately 400 m, and shallow banks, such as the Haltenbanken and Trænabanken, characterized by water depths of around 200 m (Ottesen et al., 2005; Rise et al., 2005). The Lofoten-Vesterålen margin segment consists of an outer narrow part, the Lofoten and Vesterålen basements highs and the inner Vestfjorden and Andfjorden sedimentary basins. The continental slope is intersected by several canyons (Figure 2.4; Rise et al., 2013).

Most of the Vestfjorden, Lofoten, and Vesterålen area (Figure 2.4) was a land area at the initiation of the Pleistocene ice-age as recorded by the immediate pre–Quaternary Molo Formation interpreted as a coastal shelf delta located west of Røst (Henriksen and Weimar 1996; Eidvin et al., 2007; Løseth et al. 2017; Løseth 2021; 2023). Southward and northward-flowing ice streams in the Vestfjorden and Andfjorden, respectively, eroded deep into the sediment succession and fed the prograding shelf in Mid Norway and Troms regions (Figure 2.4) (Ottesen et al., 2005; Laberg et al., 2009). Westward-bound ice flows from the Lofoten and Vesterålen basement highs reached the shelf edge where the associated sediments mostly continued down the fifteen submarine canyons incised along the steeply dipping (5–8°) continental slope, without building out a shelf edge (Figure 2.4; Rise et al., 2013). A mostly thin layer of sediments from the last glaciation covers the URU, including thick recessional moraines in Vestfjorden (Ottesen et al., 2005; Laberg et al., 2009). The strandflat in Lofoten and Vesterålen is limited to the subcropping basement areas, is submerged in the south and, rises northwards to be subaerially exposed. (Løseth, 2023).

The present-day configuration of the Mid-Norwegian margin is intrinsically linked to the Quaternary development of the region, when this margin was repetitively influenced by ice sheets that advanced to the shelf edge (e.g., Sejrup et al., 2005; Montelli et al., 2017), causing huge quantities of sediments to be transported to the continental shelves and slopes (e.g., Hjelstuen and Sejrup, 2021). During this period, the prominent Naust Formation developed as a prograding wedge, up to 1200 m thick (Figure 2.3; Ottesen et al., 2009, Dowdeswell et al., 2010, Chand et al., 2011). The seabed of the Mid-Norwegian continental shelf is dominated by a wide range of glacial landforms, including terminal moraines and grounding zone wedges (e.g., Bachelor et al., 2023; Ottesen et al., 2022; Nygård et al., 2004; Rydningen et al., 2015; Sejrup et al., 2022; Figure 2.3). The Mid-Norwegian margin was affected by several sub-marine slide events during the Quaternary period (e.g., Solheim et al., 2005a) and sediment remobilization related to ooze diapirism and overpressure release (e.g., Hjelstuen et al., 1997; Riis et al., 2005; Bellwald et al., 2024b). Along the entire Mid-Norwegian margin, contourite deposits are commonly identified (e.g., Laberg et al., 2016; Bellwald et al., 2022a), and such layers may represent "weak layers" in the sediment stratigraphy that can behave similar to gas hydrates identified on the southern Vøring Margin (Bűnz and Mienert, 2004), representing a pre-conditioning factor of sub-marine slides. Polygonal faults, frequently observed in pre-Quaternary sediments, penetrate locally into the Quaternary sediment package and have been suggested to be important fluid flow pathways with regards to pore-pressure build-up in the region (Solheim et al., 2005b) and so could also create favourable pre-conditions of submarine landslides. Soft bright anomalies, interpreted as shallow gas, are frequently observed in the Quaternary Naust Formation sediments (Figure 1.2).



388

389 **Figure 2.3.** Bathymetry and subsurface of the Vøring margin. **a)** Seabed imagery of the Vøring margin
390 continental shelf, characterised by up to 400 m deep cross shelf troughs and shallow banks at a water
391 depth of around 200 m. Terminal moraines (MR) and grounding zone wedges (GZW) are frequently
392 identified. SkT: Sklinnadjupet Trough, SuT: Suladjupet Trough, TB: Træna Bank, HB: Halten Bank,
393 SR: Skjold Ridge, SS: Storegga Slide. Figure modified from Nygård et al. (2004) and Hjelstuen and
394 Sejrup (2023). **b)** Interpreted 2D multichannel seismic profile from the southern Vøring margin,
395 showing the characteristics of the Quaternary prograding wedge, the Naust Formation, in this region.
396 Figure modified from Rise et al. (2010).

397

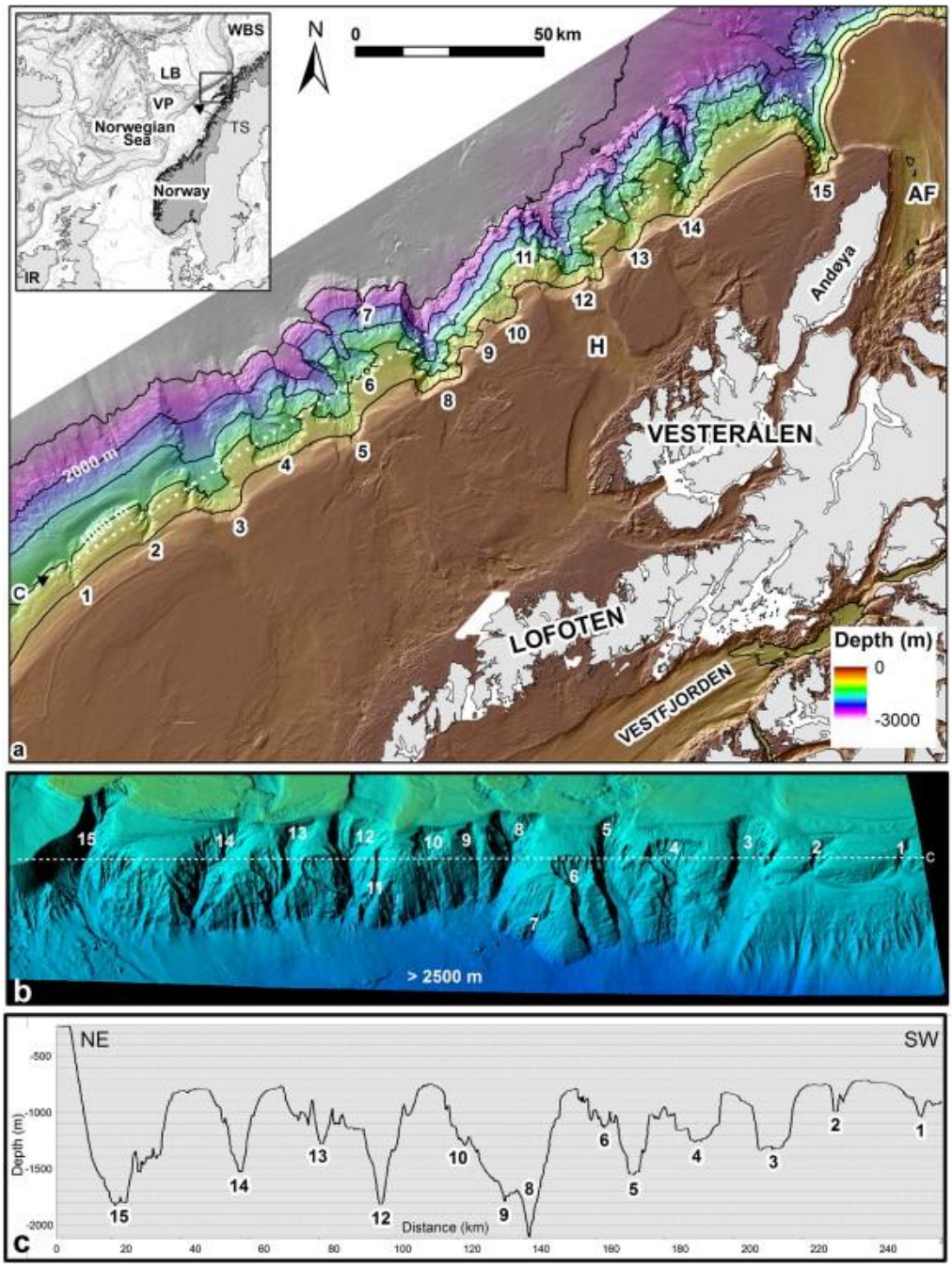
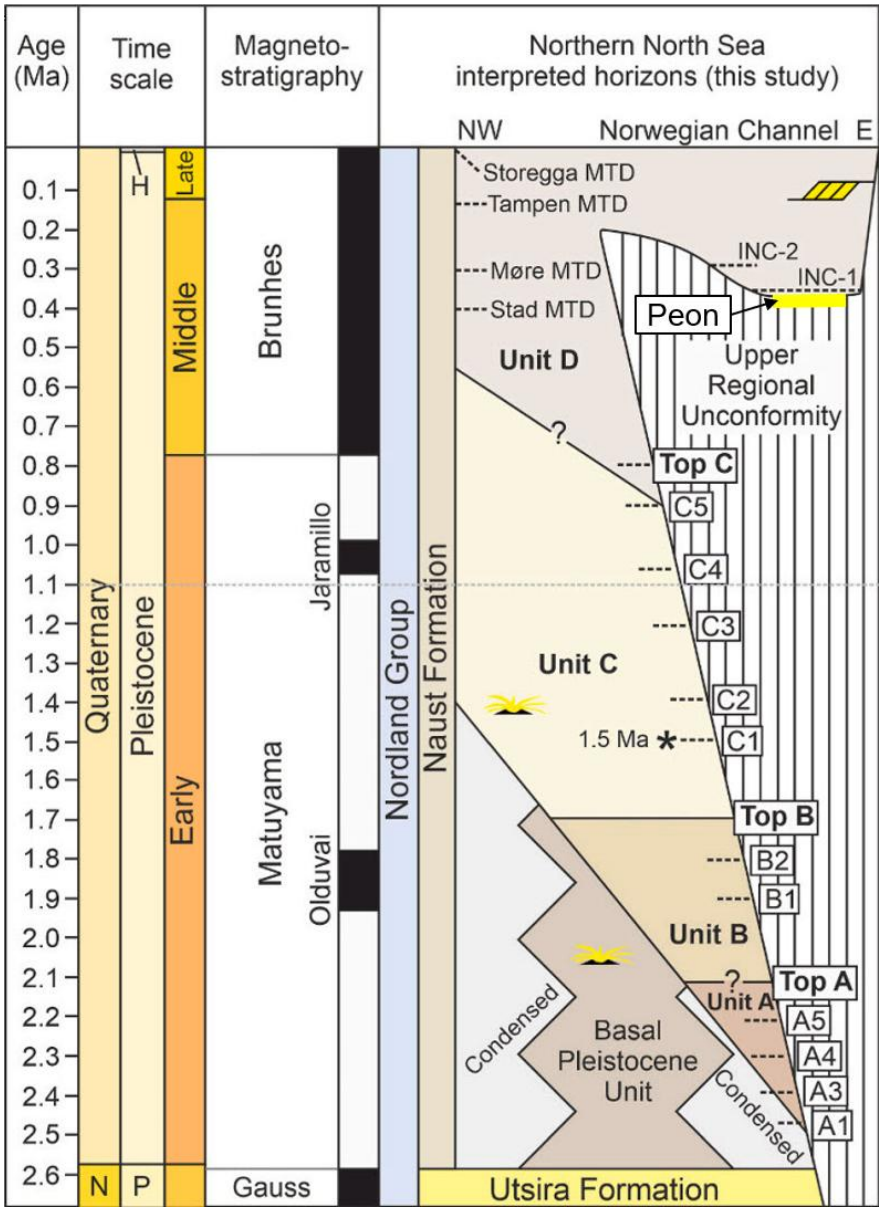


Figure 2.4. Canyons along the Lofoten-Vesterålen margin (from Rise et al., 2013). **a)** High-resolution bathymetric relief image of the Lofoten-Vesterålen margin. AF: Andfjorden; H: Hola cross-shelf trough; VP: Vøring Plateau; LB: Lofoten Basin; IR: Ireland; WBS: Western Barents Sea; TS: Headwall of Trænadjupet Slide. **b)** 3D view of canyons incised into the continental slope seen from the northwest. Canyons defined by Rise's criteria are annotated with numbers. Bleiksdjupet northwest of Andøya is canyon 15. **c)** Vertical profile along the slope. See a and b for location.

2.1.3 Northern North Sea

The Northern North Sea, from 60°N to 62°N, comprises of the western shallow sea area (<200 m deep) and the deep NNW-SSE striking Norwegian Channel with water depths up to 400 m. Regional 3D

broadband seismic data covering the entire northern North Sea reveal a detailed Pleistocene geological history (Figure 2.5). It is suggested that the inception of the Pleistocene ice age came with locally sourced ice entering the North Sea from the former Sognefjord valley, Western Norway (Løseth et al. 2020). Glacial shelf deposits built out on top of the Utsira East Formation in the N-S-elongated deep marine North Sea Basin (Ottesen et al. 2018). The westward prograding shelf grew wider and their buried shelf surfaces show evidence of glaciogenic debris flows (Løseth et al. 2020). At the same time, an early Quaternary fluvial delta built out eastwards from the East Shetland Platform and the associated deep marine deposits interfingered with the westward prograding glacial debris flows from Norway (Løseth et al., 2022). At around 1.5 Ma, the deep marine strait filled up and the glacial shelves continued to build NW-ward and SW-ward until the entire deep marine North Sea Basin was filled up northward to 62°N at around 1.0 Ma (Ottesen et al. 2018; Løseth et al 2022). The infill of the deep basin encouraged the initiation of the northward flowing Norwegian Channel Ice Stream which delivered glacial sediments to the North Sea TMF (King et al., 1996, Nygård et al. 2005; Løseth et al 2022). The ice flow in the Norwegian Channel eroded locally more than 500 m of sediments and the angular Upper Regional Unconformity (URU) was formed (Sejrup et al. 1995; Ottesen et al., 2018; Baig et al. 2019; Løseth et al., 2022). The delivery of large volumes of sediment in the North Sea TMF led to permanent isostatic subsidence and tilting of the northern North Sea. This gave accommodation room for sediments to deposit within the Norwegian Channel (Løseth et al. 2022). Strata above the URU have been tied from the Norwegian Channel to the North Sea TMF (Løseth et al. 2022) and suggest that subglacial fluvial sands, basal tills and marine clays were deposited within the Norwegian Channel during the last 0.35 Ma (Løseth et al. 2022), which is converse to previous studies (e.g., Sejrup et al., 1995). Some of these sands, like the Peon glaciofluvial outwash fan (Ottesen et al., 2012; Mikalsen, 2015; Bellwald et al., 2022b), were later charged with gas (Figure 2.6).



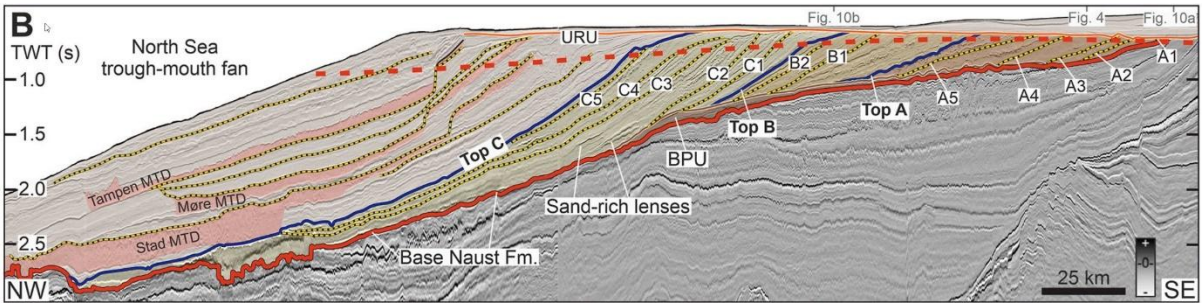
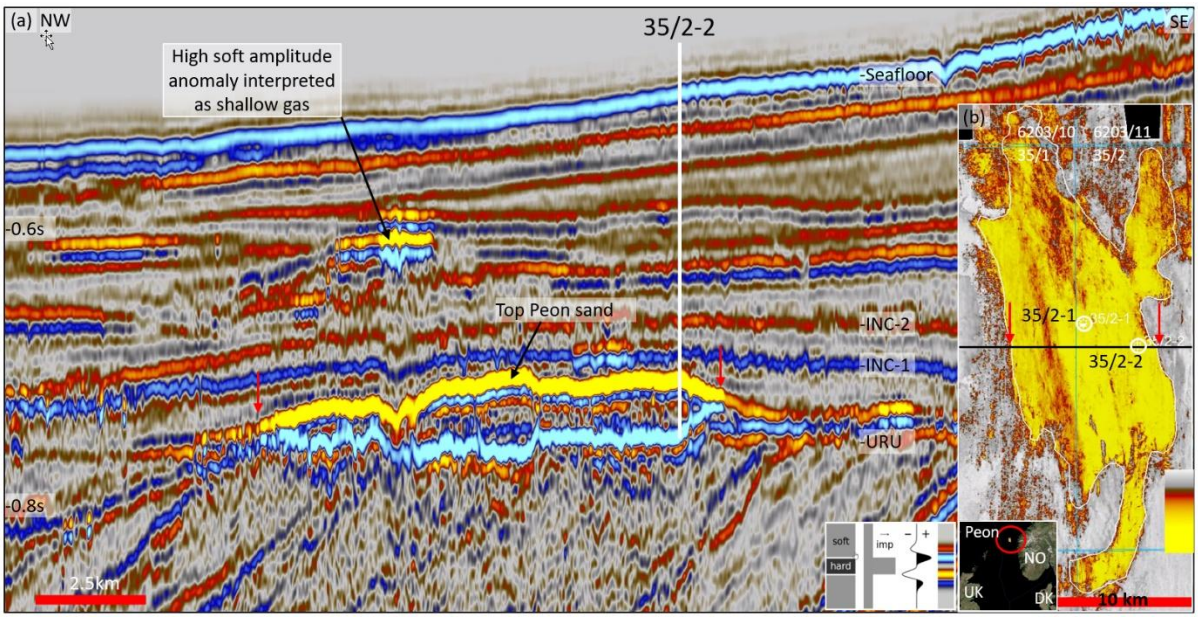


Figure 2.5. a) Stratigraphy of the Quaternary Naust Formation in the Northern North Sea from Løseth et al. (2022). The Upper Regional Unconformity was formed by fast ice sheet erosion that formed the Norwegian Channel from 0.8-0.35 Ma. **b)** A seismic section showing the Quaternary Naust Formation units in the Northern North Sea (Løseth et al. 2022).



437

438 **Figure 2.6.** Peon shallow gas discovery. Well 35/2-1 proved gas in the Quaternary Peon sand, located
439 above the Upper Regional Unconformity (URU). **a)** Seismic section (inline 34410 of the CGG2018 3D)
440 showing the gas filled sand as a high-amplitude, soft bright amplitude. **b)** Extent of the minimum
441 amplitude anomaly at the top sand reflection extracted from 3D seismic data. The sand is covered by a
442 till layer and a marine clay, which tops are termed Intra Norwegian Channel-1 (INC-1) (0.35 Ma) and
443 Intra Norwegian Channel-2 (INC-2) (0.3Ma), respectively (Løseth et al. 2022). Red arrows show the
444 extent of the gas anomaly on seismic and amplitude map. Data owner: Viridien.

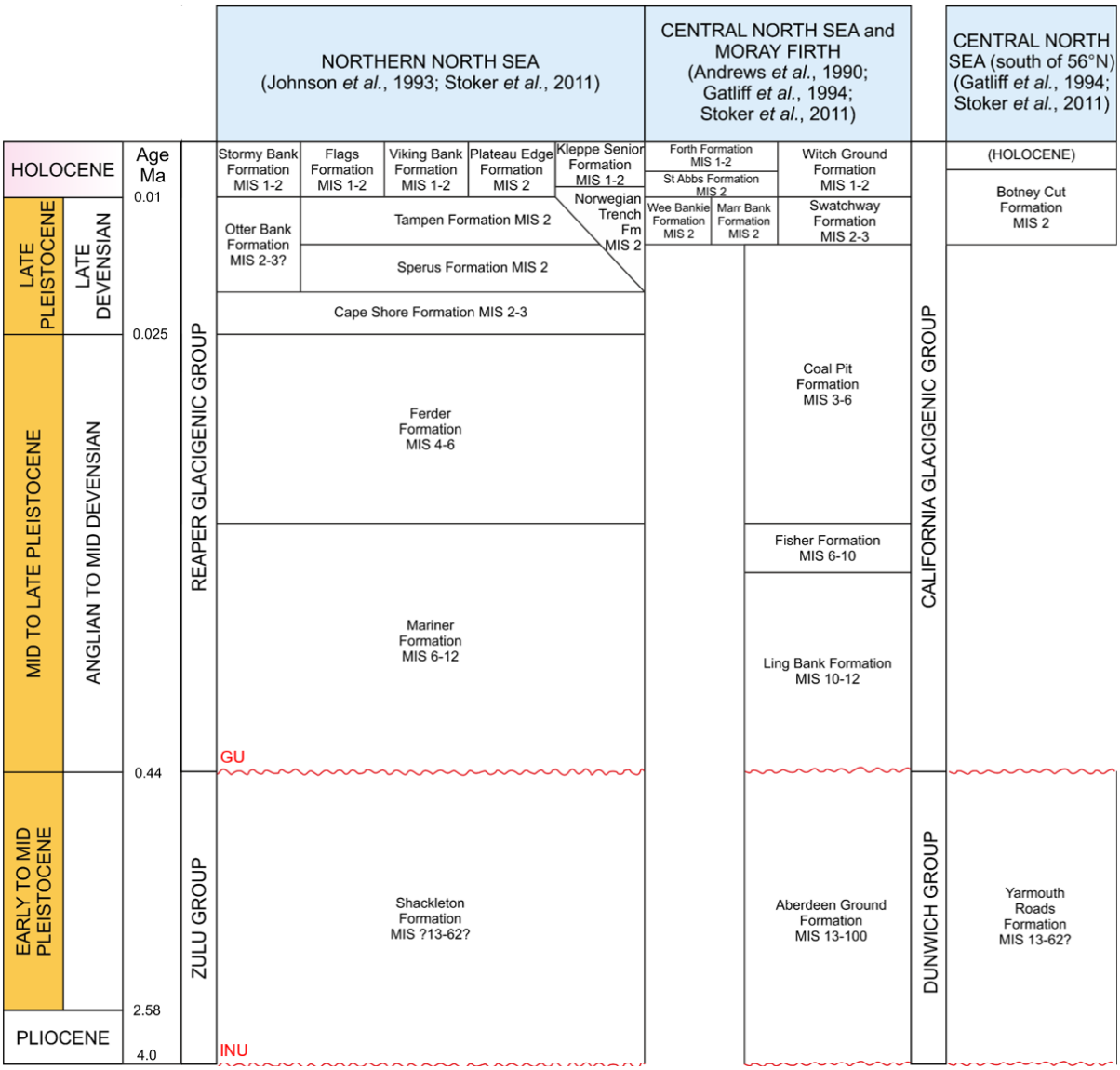


Figure 2.7. Summary of the Quaternary stratigraphy in the Northern and Central North Sea. Note that recent studies in the region using 3D seismic datasets (e.g. Ottesen et al., 2018; Løseth et al., 2022) utilise an alternative regional stratigraphy (Figure 2.5a), correlated by Newton et al. (2024a). GU = Glacial Unconformity, INU = Intra-Neogene Unconformity.

2.1.4 Central North Sea

Since Neogene times, up to 2 km of sediment accumulated in the Central Graben, of which up to ~1.2 km is of Quaternary age in the central and southern North Sea (see also Figure 6.4; Ottesen et al. 2014; Lamb et al. 2018; Newton et al., 2024a; Figure 2.7). Basin-scale 3D-seismic data show that at ~2.6 Ma the North Sea formed an elongate depression with a narrow marine connection to the north (Lamb et al. 2018). North-westward progradation of shelf deltaic systems in the southern North Sea and glaciogenic-linked progradation in the central/northern North Sea gradually infilled the Early Pleistocene basin with sediments from glacial erosion and deposition sourced from both the FIS and the BIIS, and the Baltic and Rhine-Meuse river systems (Lamb et al. 2017, 2018; Ottesen et al. 2018; Newton et al. 2024a).

Plio-Pleistocene intensification of Northern Hemisphere glaciation strengthened further during the MPT and is captured within the North Sea Basin (Newton et al. 2024a). While direct glacial evidence is scarce (e.g., Graham et al. 2011), 3D-seismic data reveal extensive Early Pleistocene glacial landforms on clinoforms (e.g., Knutz 2010; Arfai et al. 2018; Rea et al. 2018; Newton et al. 2024a). In the North Sea Basin scant direct evidence of Early Pleistocene glaciations are found in glacigenic sediments recovered from below the Bruhnes–Matuyama palaeomagnetic reversal (~780 ka BP): within borehole 81/27 (Stoker et al. 1983); a buried sub-glacial till within borehole 81/26 (Sejrup et al. 1987; Ekman and Scourse 1993; Sejrup et al. 2000); and a glacial diamicton from commercial well 22/07a-5 and 22/07a-6Z (Rea et al. 2018; Rose et al. 2018). Early studies suggested the subglacial Fedje Till sampled within the Norwegian Channel was deposited ~1.1 Ma based on micropaleontology, Sr-isotopes, paleomagnetism and amino acid geochronology (Sejrup et al. 1995; 2000). However, Løseth et al. (2022) present evidence using 3D seismic data to suggest that the Norwegian Channel Ice Stream initiated ~0.8 Ma and that sediments preserved at the base of the Norwegian Channel, such as the Fedje Till, were instead deposited much later, about to or prior to 0.35 Ma. 3D seismic datasets have revealed the presence of iceberg ploughmarks and mega-scale glacial lineations imaged on Early Pleistocene clinoform horizons (Kuhlmann et al. 2006; Buckley 2017; Dowdeswell and Ottesen 2013; Rea et al. 2018). From ~2.53 Ma (MIS 100), Rea et al. (2018) provide the first evidence of large icebergs within the central and northern North Sea sourced from non-confluent FIS and BIIS ice sheets to the east and west. These icebergs were likely locally sourced as palaeo-bathymetric evidence reveals the presence of a bathymetric sill north of 60° N preventing entry of icebergs from the northeast Atlantic Ocean (Lamb et al., 2017; Rea et al., 2018). These studies suggest extensive glaciation within the North Sea ~1.4 Myr earlier than previously accepted (Sejrup et al., 1995, 2000; Rea et al., 2018) although the FIS and BIIS only coalesced in the centre of the North Sea from ~1.87 Ma, as indicated by ice flow landforms (Rea et al. 2018). Furthermore, Rea et al. (2018) postulate that both the FIS and BIIS ice sheets were significantly more extensive during the early Quaternary than previously thought (Dowdeswell and Ottesen 2013; Ottesen et al. 2014), which is a matter of controversy at present due to ambiguity in landform interpretation (Batchelor et al. 2021). A more detailed discussion on the inconsistency in ice sheet reconstructions is presented in Newton et al. (2024a) and Ottesen et al. (2024).

Recent studies, imaging tunnel valleys in 3D seismic data (e.g. Ottesen et al., 2018, 2020; Kirkham et al., 2024), show unequivocal evidence of grounded ice-sheet glaciations prior to the LGM as tunnel valleys are considered to form subglacially. By separating the extensive networks of cross-cutting tunnel valleys into generations, these studies suggest that there have been seven (or more) extensive glaciations prior to MIS 2 (e.g. Stewart and Lonergan, 2011; Ottesen et al., 2020), indicating repeated advance and growth of Pleistocene ice sheets in northwest Europe since the Bruhnes–Matuyama reversal (Figure 2.8).

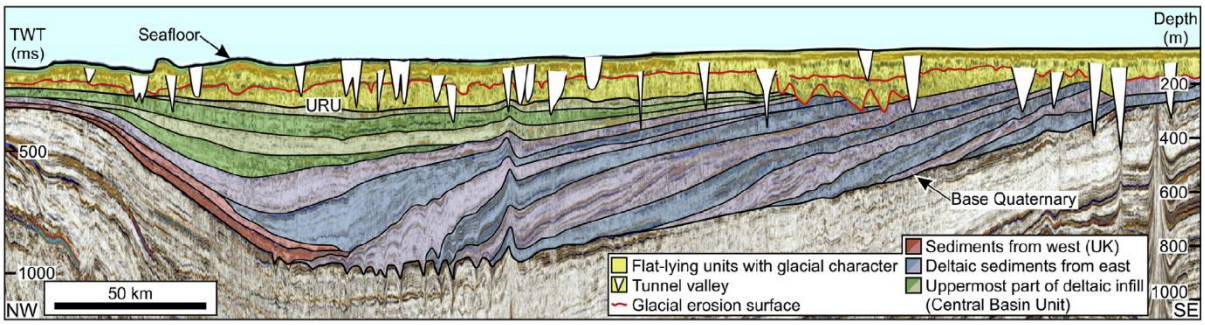


Figure 2.8. Regional 2D seismic line across the North Sea Basin (NW-SE) showing the distribution of tunnel valleys within the Quaternary stratigraphy, provided by TGS. Figure from Ottesen et al. (2020). URU: Upper Regional Unconformity. A velocity of 1800 m/s is used for depth conversion. See Figure 2.10 for location.

Numerous studies have presented and reviewed the evidence for ice-sheet glaciation of the North Sea Basin during the Late Pleistocene with good evidence for at least two phases of extensive ice-sheet development in the Early Weichselian (MIS 4; ~50–60 ka) and Late Weichselian (MIS 3/2) (e.g. Gatliff et al., 1994; Graham et al., 2011). High-resolution seismo-acoustic profiles, bathymetric elevation models and shallow marine cores have contributed to a relatively good understanding of the last glacial phase (MIS 2). During this time the BIIS expanded into the central and northern North Sea, extending to, or close to, the continental shelf edge from the Norwegian Channel to the NW of Ireland (e.g. Bradwell et al., 2008; Graham et al., 2009; Sejrup et al., 2016; Clark et al., 2017; Bradwell et al., 2019a; Roberts et al., 2019; Stewart et al., 2021, 2023; Evans et al., 2021). The last ice sheet reached its maximum extent ~30–24 ka, during or slightly after global Last Glacial Maximum (LGM; ~22–27 ka BP). Within the North Sea Basin the FIS and BIIS ice sheets coalesced on multiple occasions (Stoker and Bent, 1985; Cameron et al., 1987; Gatliff et al., 1994; Sejrup et al., 2000; Graham et al. 2011; Stoker et al., 2011; Sejrup et al., 2016; Newton et al., 2024a), with a number of scenarios presented for maximum extent of the LGM.

Much of the present-day topography of the seabed is directly related to the last glacial cycle (~32–11.5 thousand years ago), which had a pronounced impact on the morphology and composition of the modern seabed. Mega-scale geomorphological features such as grounding zone wedges, channels, moraines, drumlins and deeply incised tunnel valleys formed beneath an ice sheet (e.g. the Devil's Hole Deeps) (e.g. Bradwell et al. 2008; Clark et al. 2017; Stewart et al. 2021). In addition, previous glaciations within the Mid- and Early- Pleistocene may have influenced the materials underlying these Late Pleistocene deposits. These varying conditions will have had significant implications on the deposition, glaciotectonic disturbance (e.g., Figure 2.9), diagenesis and erosion of the soils together with the erosion, weathering and load history of the rocks. Meltwater channels, some with associated eskers, are also present oriented roughly coast parallel extending from Arbroath in the south to Peterhead in the north incised into the Marr Bank and Aberdeen Bank, again related to melting of the retreating ice sheet

(Golledge and Stoker, 2006). Detailed seabed mapping of these glacial landforms has permitted reconstruction of the pattern of deglaciation following the LGM, at a time of rapidly rising sea levels (e.g. Bradwell et al., 2008; Dove et al., 2017; Clark et al., 2017; Stewart et al., 2021; Figure 2.10). Geomorphological evidence strongly suggests a dynamic switch in glacial styles, from terrestrial to strongly marine-influenced, ice-sheet retreat, resulting in rapid ice-mass losses at key time intervals (Bradwell et al. 2008, 2019a, 2019b; Clark et al. 2012; Sejrup et al. 2016; Evans et al. 2021).

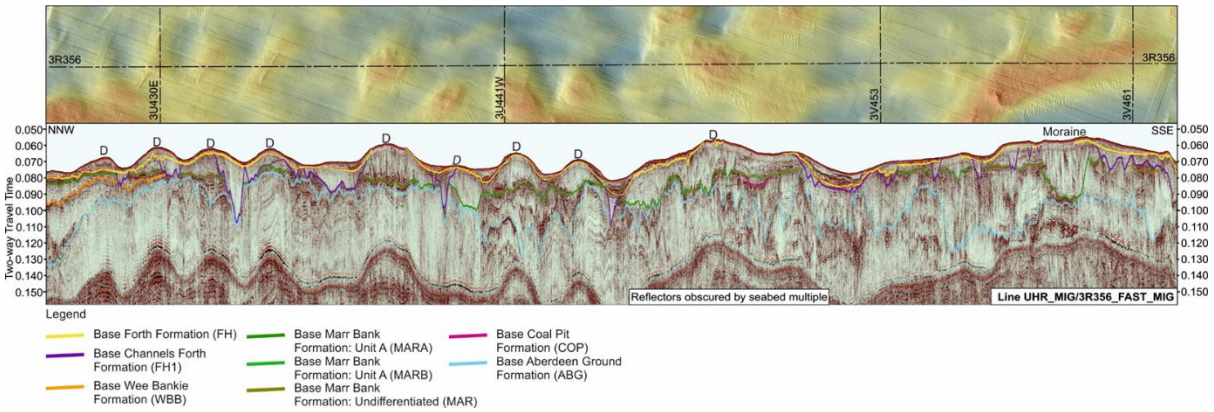


Figure 2.9. Glaciotectonism observed coincident with smaller topographic features identified as drumlins and areas of ribbed moraine (also known as hummocky terrain) offshore eastern Scotland, central North Sea. The top panel displays corresponding Marine and Coastguard Agency multibeam bathymetry data gridded at 8 m resolution. Abbreviations: D = drumlin; *D* = buried drumlin. Data courtesy of SSE Renewables.

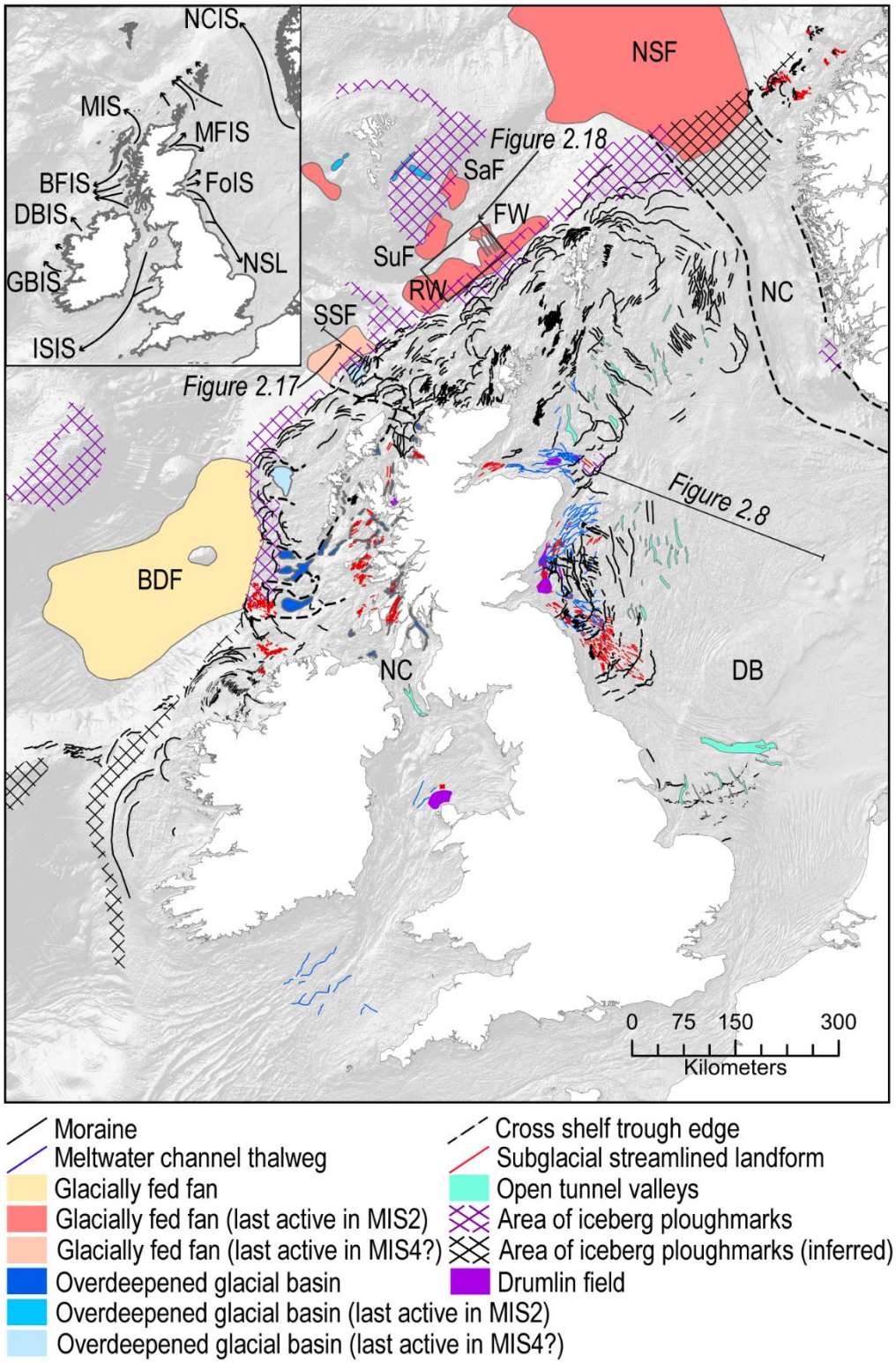


Figure 2.10. Selected large-scale glacial landforms including tunnel valleys and subglacial streamlined landforms, ice-marginal landforms represented by large moraines, glacimarine landforms such as trough-mouth fans and iceberg ploughmarks (adapted from Clark et al. (2017) and Stewart et al. (2021)). BDF = Barra–Donegal Fan, DB = Dogger Bank, FW = Foula Wedge, NC = North Channel, NSF = North Sea Fan, RW = Rona Wedge, SaF = Sandoy Fan, SSF = Sula Sgeir Fan, SuF = Suduroy Fan.

Inset map depicts generalised direction of offshore palaeo-ice streams. BFIS = Barra Fan Ice Stream (also known as the Malin Sea Ice Stream and includes the unlabelled North Channel Ice Stream), DBIS = Donegal Bay Ice Stream, FoIS = Forth Ice Stream (including the unlabelled Strathmore Ice Stream), GBIS = Galway Bay Ice Stream, ISIS = Irish Sea Ice Stream, MFIS = Moray Firth Ice Stream, MIS = Minch Ice Stream, NCIS = Norwegian Channel Ice Stream, NSL = North Sea Lobe (including the unlabelled Tweed, Tyne Gap and Eden-Stainmore ice streams). Note that areas devoid of mapped landforms are commonly areas of poor seafloor data rather than indicative of an absence of landform assemblage. Regional Bathymetry from GEBCO Compilation Group (2024).

2.1.5 Southern North Sea

The Southern North Sea, defined in the context of this paper as the Danish, German, Dutch, Belgian and British North Sea sectors south of Dogger Bank (Figure 2.1), comprises a wide (up to 300 km) shallow water continental shelf. Water depths are generally less than 70 m except for the Norwegian Channel where depths increase to over 600 m. During the Cenozoic, the epicontinental North Sea Basin experienced very little subsidence, due to thermal relaxation from Jurassic rifting, however, significant water depths within the basin enabled deposition of thick siliciclastic deltaic successions sourced mainly from the Fennoscandian shield and the northwestern European continent (Huuse et al., 2001; Overeem et al., 2001; Schiøler et al., 2007; Rasmussen et al., in press). As for the central and northern North Sea, the southern North Sea was significantly influenced by the Pleistocene glaciations. While the Elsterian and Saalian ice sheets advanced across the full area, the southern extent of the ice during the LGM (MIS2) was close to the present day bathymetric high Dogger Bank (Figure 2.1; e.g. Hughes et al., 2016). Evidence for potential earlier glaciations of the region is scarce making it extremely difficult to reconstruct pre-mid Pleistocene ice sheet extents (Lee et al., 2012).

The Quaternary sedimentary record in the southern North Sea mainly comprises coarse-grained glacial deposits including sand and gravels from the Elsterian and Saalian glaciations, while the Weichselian deposits are dominated by sandy outwash (glacio-fluvial) deposits (Rijsdik et al., 2005; Coughlan et al., 2018).

The pre-Elsterian Quaternary record is less well defined but also contains mainly sands originating from Neogene delta topsets in the southeastern parts of the North Sea (Overeem et al., 2001; Thöle et al., 2014) presumably reworked during early Quaternary sea-level cycles and compacted by subsequent glacial loading (Coughlan et al., 2018, Fleischer et al., 2023). Neogene delta deposits below the Quaternary strata are present westwards into the Dutch sector (Benvenuti et al., 2012; Moreau and Huuse, 2014) while further westwards, older bedrock are encountered, e.g. Upper Cretaceous Chalk (Mellett et al., 2019). The record furthermore holds local deposits of finer grained interglacial sediments from the Holsteinian and Eemian interglacials, as well as highly heterogenic successions within buried tunnel valley system (e.g., Hepp et al., 2012; Coughlan et al., 2018; Eaton et al., 2020; Fleischer et al.,

2023; Figure 2.9). The Late Weichselian (late glacial) and early Holocene record is particularly well preserved within younger buried valley systems, where there is often a continuous record from fluvial and estuarine to shallow and open marine conditions (Andresen et al., 2022; Prins and Andresen 2019, Özmaral et al., 2022; Hepp et al., 2019), reflecting the late Pleistocene to early Holocene flooding of the southern North Sea region. Peat and fine-grained siliciclastic are typically found within or in the proximity of such valleys, whereas the marine Holocene sedimentation has resulted in deposition of a fine-grained sand cover that is present in various thicknesses over most of the southern North Sea. These marine Holocene sand deposits show various degrees of mobility depending on the present-day oceanographic setting. The bottom current systems and tidal regimes in the southern North Sea were generally established after the opening of the English Channel (ca. 9 ka) and the submergence of Dogger Bank (ca. 7 ka) (Sturt et al., 2013). Ice marginal processes from all three glaciations are clearly evidenced by occurrence of tunnel valley systems, glacio-tectonic complexes and the extensive glacial outwash deposits (Andersen et al., 2004; Pedersen and Boldreel, 2016; Bendixen et al., 2017; Winsemann et al., 2019; Mellett et al., 2019; Cartelle et al., 2021; Andersen, 2004; Figures 2.8 and 2.11). Several authors have furthermore suggested the occurrence of a large proglacial lake south of the Dogger Bank (Hjelstuen et al., 2018; Andresen et al., 2022), in part spatially coinciding with the Elbe Paleo Valley (Özmaral et al., 2022).

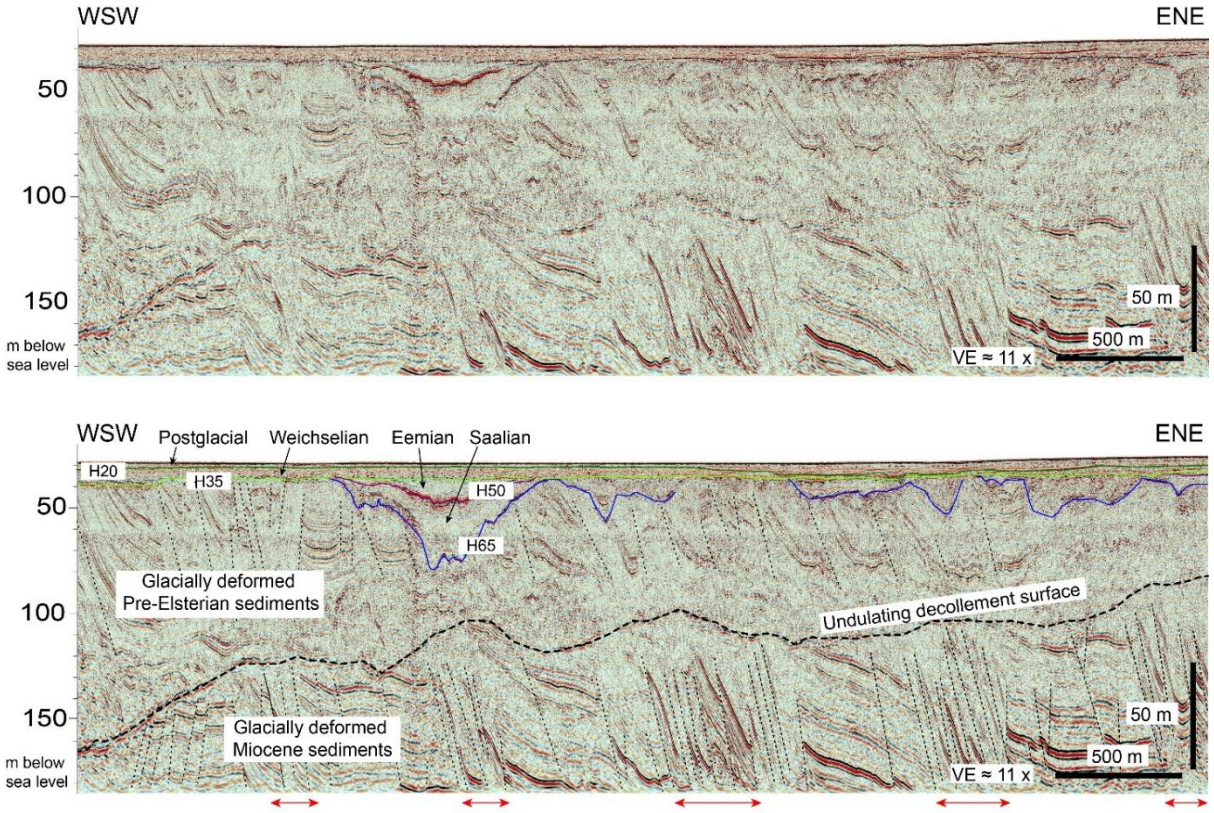


Figure 2.11. Uninterpreted (top) and interpreted (base) 2D UHRS sparker profile from the North Sea 1 offshore wind farm area in the Danish North Sea. The profile shows two sets of glaciotectonic thrust structures (black dashed lines) separated by an undulating decollement surface. Red arrows in the base

indicate areas with intense deformation in the lower thrust set. The upper deformed succession is incised by Saalian valleys. Shown mapped surfaces are based on interpretations from Fugro (2024): H20 – base Unit 20 (postglacial fresh water and marine sediments), H35 – base Unit 35 (Weichselian glacial meltwater deposits), H50 – base Unit 50 (Eemian interglacial marine sediments), H65 – base Unit 65 (Saalian glacial deposits), H70 – base Unit 70 (Elsterian glacial deposits).

2.1.6 Baltic Sea

The Baltic Sea (Figure 2.1) is a shallow intracontinental sea extending between Scandinavia and Finland in the North and Central and Eastern Europe to the South (Figure 2.12; Jakobsson et al., 2019; Rosentau et al., 2017) with a very limited connection to the global ocean via the Danish straights and the North Sea. The pre-Quaternary basement of the basin consists of crystalline and metamorphic bedrock of the Baltic Shield in the north, which is often exposed at the seafloor and along the coast. Sedimentary rocks of Palaeozoic and Mesozoic ages are subcropping further south or fill basins in the Gulf of Bothnia. Towards the central and southern basin, the basement consists of various sedimentary rocks of Palaeozoic and Mesozoic origin, including Cretaceous and Danian chalk, and even poorly consolidated Paleogene/Neogene sediments underneath Quaternary deposits (Uścinowicz, 2014; Rosentau et al., 2017).

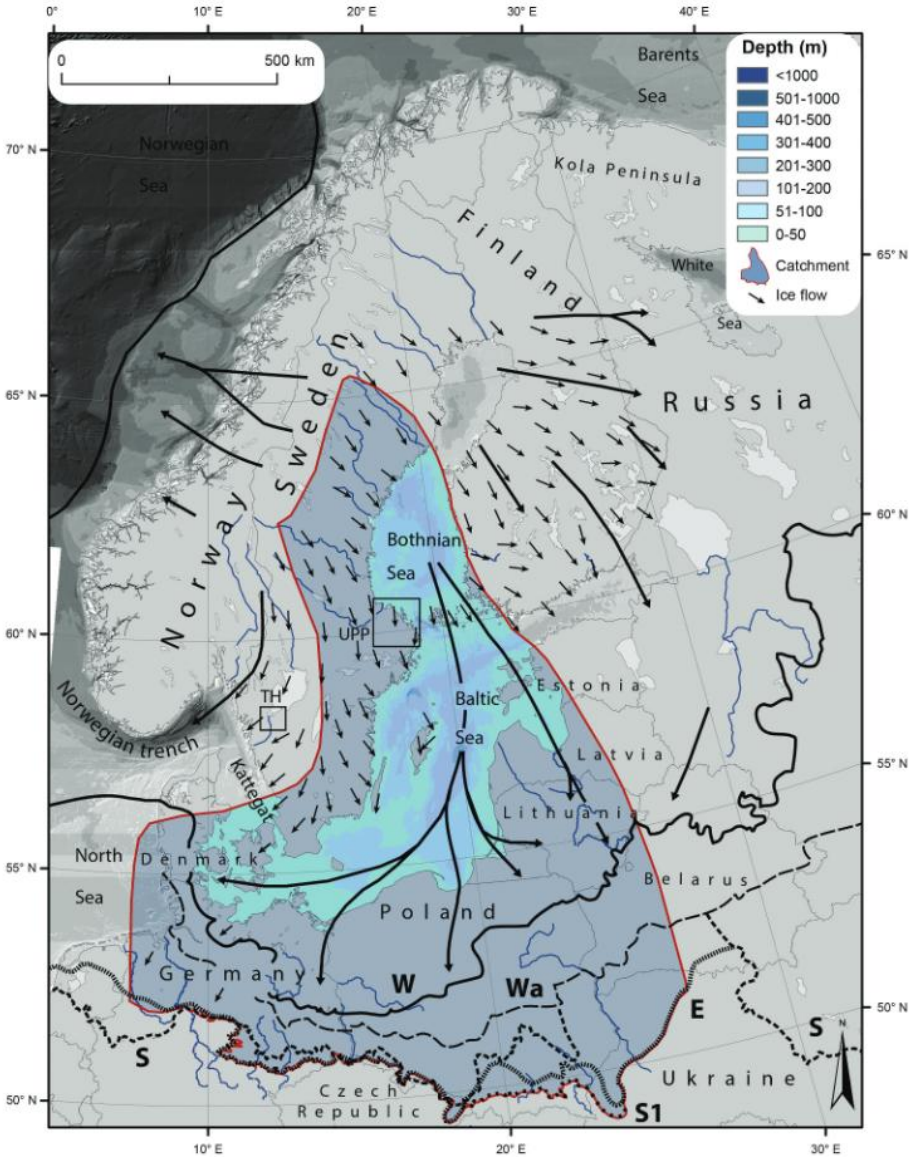


Figure 2.12. Bathymetry of the Baltic Sea basin with Pleistocene ice limits and flow lines. W Late Weichselian. Wa Warte. S1 Sanian 1, E Elsterian. S Saalian. Image from Hall and van Boeckel (2020).

In the Quaternary, the Baltic Sea area underwent multiple, repeated glaciations (Figure 2.12) and deglaciations that resulted in extensive erosion of pre-existing sediments and bedrock, leading to the formation of the basin (Overeem et al., 2001; Tuuling and Flodén, 2016; Hall and van Boeckel, 2020).The Quaternary geologic record comprises Pleistocene glaciogenic and Holocene terrestrial, lacustrine and marine sediments, often distributed irregularly depending on erosion of bedrock and ice sheet dynamics (Obst et al., 2017; Hall and van Boeckel, 2020). Subglacial tunnel valleys (Figure 2.13) are present in many parts of the basin but do not reach the depths known from the neighbouring North Sea basin (Flóden et al., 1997).

The Baltic Sea basin was fully covered by the FIS for the last time during the LGM between 23 and 19 cal kyr BP (Figure 2.12) followed by ice retreat from 17-16 cal kyr BP onwards (Hughes et al., 2016).

The retreat was punctuated by ice margin stabilisations and/or re-advances. Pro-glacial and glaciomarine deposits that formed during this halting ice retreat can be observed in bathymetric data throughout the basin (Jakobsson et al., 2019, Tylmann and Uścinowicz, 2022; Greenwood et al., 2017; 2024). Ice contact glaciofluvial deposit (ice contact fans and deltas) as well as recessional moraines were formed at the margin of the retreating ice sheet and in front of it. Glaciotectonic deformations (faulting and folding) are widespread in the southern Baltic. As a consequence, in the southern and central Baltic, pre-Quaternary strata are blanketed with variable thicknesses of glaciogenic sediments including tills deposited sub- and proglacially as well ice marginal and proglacial glaciofluvial deposits (Obst et al., 2017). Glacial landforms and glacially sculpted bedrock surfaces become more prominent in the north towards the coast of Sweden and Finland as well as into the Gulf of Bothnia. Subsequent flooding of the basin initially formed isolated proglacial lakes and kettle holes formed in front of the retreating ice margin around 15.5 cal kyr BP in the southern Baltic. Ice margin retreat in the northern part, i.e. the Gulf of Bothnia, continued until significantly later and this part of the basin only became ice free between 10-12 cal kyr BP. The freshwater Baltic Ice Lake (BIL) formed during the ice retreat and covered large parts of the formerly glaciated landscape, itself isolated from the global ocean. The lake drained during the Younger Dryas when two major BIL drainage events occurred though a topographic low near Mount Billingen around 11.7 cal kyr BP with subsequent drainage events inferred through Fehmarn Belt and Mecklenburgh Bight as the ice sheet margin was positioned across southern Sweden and Finland, leading to ~25 m water level fall in a very short time. The geometry of the basin combined with ice margin position during its retreat, global sea level fluctuations and glacial isostatic adjustment of the region resulted in periodical isolation of the Baltic basin (Baltic Ice-Lake and Ancylus Lake stages) and drainage and connection to the global oceans (Yoldia Sea, Mastogloia Sea and Littorina/ Postlittorina Sea stages) (Uścinowicz, 2006; Andrén et al. 2011). During the Late Pleistocene and Holocene, the postglacial fine grained organic-rich lacustrine and marine deposits can be found mainly in deeper or isolated parts of the basin whereas shallower parts are often dominated by sandy and gravelly deposits due to waves and currents reworking the glacial substrate. Boulders, as well as shallow gas pockets, organic rich soils and laterally heterogeneous glaciogenic sediments and glacial and mobile bedforms are common across the basin.

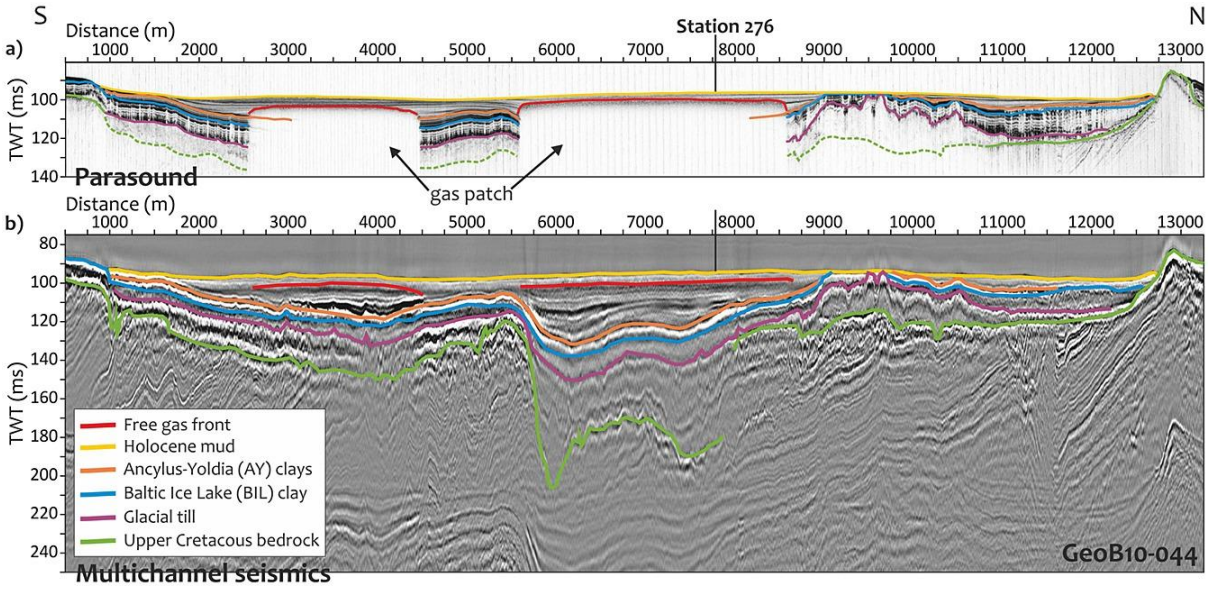


Figure 2.13. Interpreted sub-bottom profiler data (**a**) and seismic (**b**) profile in the Bornholm Basin showing typical basin filling geology. Above a Mesozoic basement lie glaciogenic till deposits followed by the typical late- and post-glacial sequence of limnic and marine sediments. Modern Holocene mud shows high organic content and shallow biogenic gas formation in the basins. Image from Tóth et al. (2014a).

2.1.7 Irish Sea and Celtic Sea

While the exact number of glacial periods to have directly influenced the Irish and Celtic Sea basins remains poorly constrained, it is generally accepted that the Elsterian, Saalian, and Weichselian ice sheets (the three most recent and largest glaciations in the Mid to Late Quaternary) were responsible for depositing the sedimentary packages that form the present-day Quaternary framework across this region (Figure 2.1; Jackson et al., 1995; Mellett et al., 2015). Naturally, there is a preservation bias as the BIIS of Weichselian age is likely to have reworked a significant portion of Elsterian and Saalian deposits and, as such, the majority of the Quaternary sequence across this region is associated with the Weichselian glaciation (Mellett et al., 2015).

Fed by ice domes over Ireland, Scotland, the Lake District and Wales, fast moving ice started to develop sometime after 36 ka (Roberts et al., 2007), with Chiverrell et al. (2021) finding that ice build-up and expansion took place substantially between 30 ka through to ~26 ka. This area (i.e., Irish Sea sector) of the BIIS was unique in that it represented a bifurcating system with two distinct outlets; the Irish Sea Glacier (ISG), a non-streaming terrestrial terminus that extended over present-day Cheshire–Shropshire lowlands and into the English Midlands, and the Irish Sea Ice Stream (ISIS), a marine-terminating ice stream comprising fast flowing, generally grounded, ice which expanding south through the Irish Sea Basin and out across the Celtic Sea (Scourse et al., 2021). Ice sheet reconstruction work by Scourse et al. (2021) and Clark et al. (2022) showed that the maximum extent of the ISIS reached the shelf break

679 of the Celtic Margin, completely covering the Irish and Celtic Sea region, by around 26-25.5 ka (Praeg
680 et al. 2015; Scourse et al. 2019; Smedley et al., 2017). Across the Irish Sea and Celtic Sea sector, this
681 period of advance of the ISIS is recorded by the deposition of subglacial till, till deformation and
682 subglacial erosive features. In the north and central Irish Sea, tunnel valleys are understood to have been
683 initiated during this phase, with existing features often down-cut into bedrock (Whittington, 1977;
684 Jackson et al., 1995; Callaway et al., 2011; Coughlan et al., 2020a). Mega-scale glacial lineations
685 (MSGL) initiated during this phase with examples noted in the north Irish Sea (Michel et al., 2023) and
686 offshore Anglesey (Van Landegehm and Chiverrell, 2020). Deposition of sub-glacial till and the
687 deformation and erosion of pre-Weichselian deposits are recorded off the southeast Irish coast (Tóth et
688 al., 2020), as well as southwest of Ireland (Giglio et al., 2022). Giglio et al. (2022) identified a drumlin
689 field more than 25 km offshore southwest Ireland signifying grounded ice in this area during the initial
690 ISIS advance. The legacy of this advance phase was to have a significant control over the deposition of
691 units and formation of other geomorphological features subsequently.

692 Scourse et al. (2021) conclude that this expansion of the ISIS would have been a relatively short-lived
693 but rapid event, resulting in thin ice forming a marine calving margin at the shelf break. Having reached
694 its maximum extent, rapid deglaciation followed as the ice margin collapsed and retreated 400 km
695 northwards across the Celtic Sea, where it stabilised in the region of St. George's Channel around 24.2
696 ka (Small et al., 2018). This period of retreat is recorded by a grounding zone wedge and recessional
697 moraines southwest of Ireland (Giglio et al., 2022), as well as the formation of an extensive subglacial
698 drainage system represented by tunnel valleys implying significant amounts of erosive meltwater
699 discharge (Giglio et al., 2021). Further evidence for subglacial drainage is recorded in the north Celtic
700 Sea through esker formation (Tóth et al., 2020). In this area, Tóth et al. (2020) infer the deposition of
701 ice-marginal, glacial outwash deposits, possibly in an ice-dammed lake that formed during the retreat
702 of the ISIS. The retreat of the ISIS margin in this nearshore area also un-impinged terrestrial ice,
703 allowing it to advance from inland centres reaching more than 15 km beyond the present coastline,
704 tectonising ISIS-related deposits (Tóth et al., 2020).

705 The subsequent ISIS withdrawal from the Irish Sea Basin was not a simple, continuous process.
706 Between St George's Channel (ca. 24 ka) and a line from Llŷn Peninsula – Wicklow approximately (ca.
707 21 ka), ISIS retreat slowed down with a series of stillstands, and oscillations recorded along the
708 coastlines of Ireland and Wales (Chiverrell et al., 2013, 2018; Smedley et al., 2017; Small et al., 2018).
709 This appears to be largely controlled by topographic pinning points and constrictions of the ice stream
710 (Scourse et al., 2021). This phase allowed for the further development of sub-glacial drainage in the
711 form of channel systems and tunnel valleys (Coughlan et al., 2020a; Michel et al, 2023) as well as mega-
712 scale glacial lineations (Van Landeghem and Chiverrell, 2020).

713

The ISIS reached the north Irish Sea Basin by approximately 21.9 ka where, according to Scourse et al. (2021), it began to retreat rapidly again, primarily due to increased retreat space afforded by trough geometry, and deeper waters. Pronounced ice margins are recorded across the northern Isle of Man dated at 19.1 ka (Scourse et al., 2021; Clark et al., 2022). In the eastern Irish Sea, offshore Anglesey, evidence for this deglaciation of the Irish Sea Basin is well captured by seafloor and sub-seabed geomorphological assemblages, including substantial drumlin fields, ribbed and De Geer moraines, eskers, iceberg scour marks and flutes (Figure 2.15), and emphasising the continued oscillation of the ISIS margin during retreat, as well as the transition from old- to warm-based ice (Van Landeghem et al., 2009a; Van Landeghem and Chiverrell, 2020). To the north and northwest of the Irish Sea Basin, this glacial landscape has largely been buried by post glacial sedimentation, in particular by thick accumulations of marine sediment during the Holocene (Belderson, 1964, Pantin, 1978; Coughlan et al., 2019; Chiverrell et al., 2018).

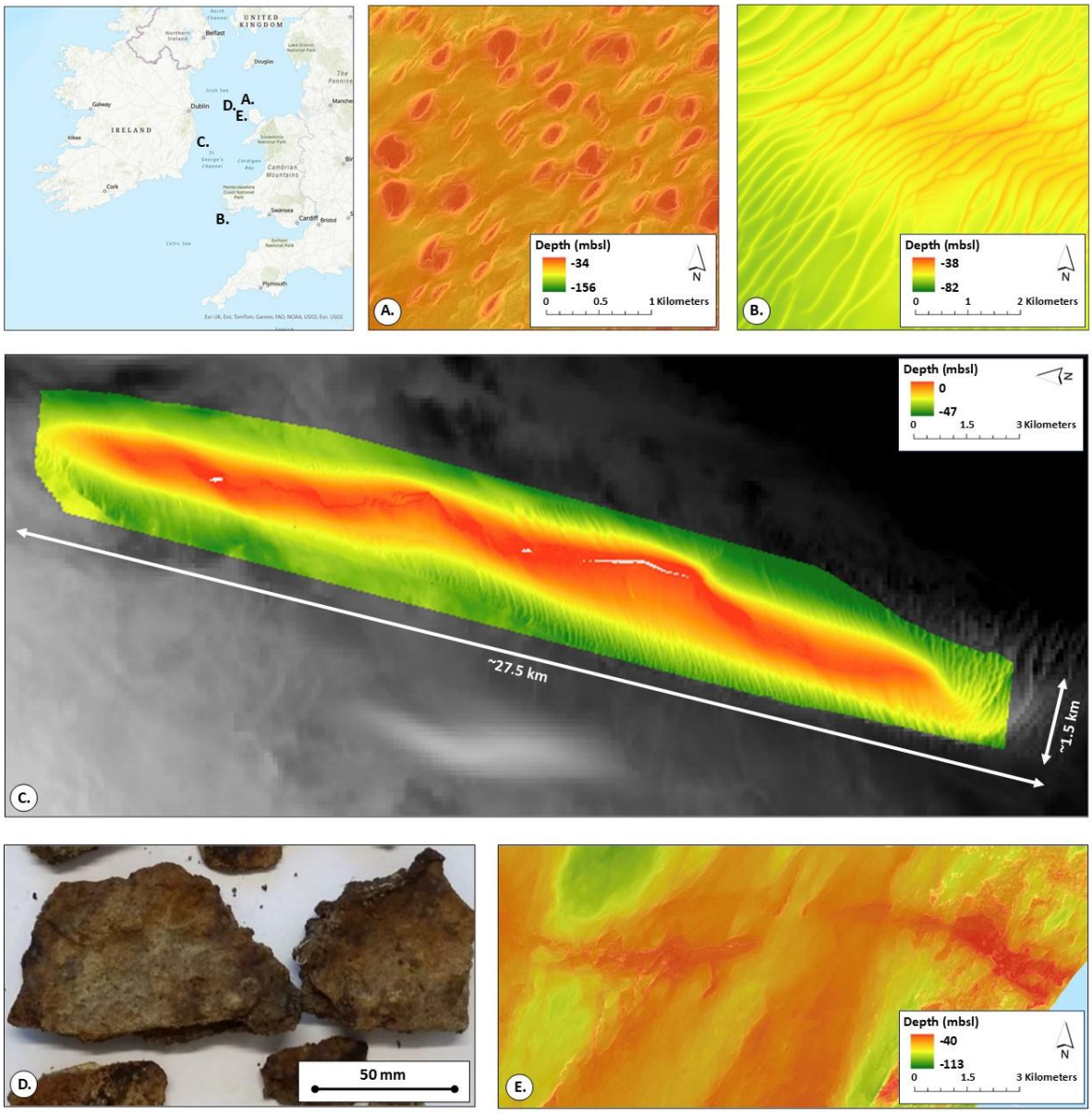


Figure 2.15. Examples of present-day seabed geomorphology across the Irish and Celtic Sea area. **a)** An extensive drumlin field offshore of Anglesey, with varying morphologies suggesting periods of both ice-streaming and slower-moving/static ice flow behaviour. **b)** A significant sand-wave field located on the margins of the Outer Bristol Channel. **c)** The Arklow Bank, a major N-S orientated linear, elongated sand bank, is located off the south-east coast of Ireland and measures approximately 27.5 km in length and 1-2 km in width (Creane et al., 2023a). **d)** The Croker Carbonate Slabs are methane derived authigenic carbonates deposited on the seabed through fluid escape. **e)** The remnants of a roughly E-W orientated moraine, located west of the island of Anglesey. Multibeam bathymetry sourced from the UK Hydrographic Office (UKHO) and Maritime & Coastguard Agency (MCA), EMODnet Bathymetry, and INFOMAR. MDAC photo is courtesy of The British Geological Survey (c) UKRI 2025.

739 The ice margin eventually pulled back onto the terrestrial highs across the north of Ireland and SW
740 Scotland at approximately 17 ka, which represented the final phase of retreat with complete deglaciation
741 of the Irish Sea Basin being achieved in a fully marine setting (Scourse et al., 2021; Clark et al., 2022).
742 This final deglaciation was punctuated by minor, local ice readvances during the Clogherhead Stadial
743 (~18.4 ka BP) and Killard Point Stadial (~17.3 to 16.6 ka BP) which are well constrained onshore
744 (McCabe et al., 2005, 2007; Chiverrell et al., 2018). Offshore, some evidence is found in the form of
745 moraine development, for example in Dundalk Bay (Michel et al., 2023). Evidence of an unstable,
746 calving ice front is also seen though the presence of buried iceberg scours (Michel et al., 2023).

747 The lithostratigraphical framework for Quaternary deposits in the Irish Sea and Celtic Sea sector is
748 summarised in Table 2.1, according to Stoker et al. (2011), and Figure 2.16 shows a seismic section
749 through the Quaternary sequence in the eastern Irish Sea.

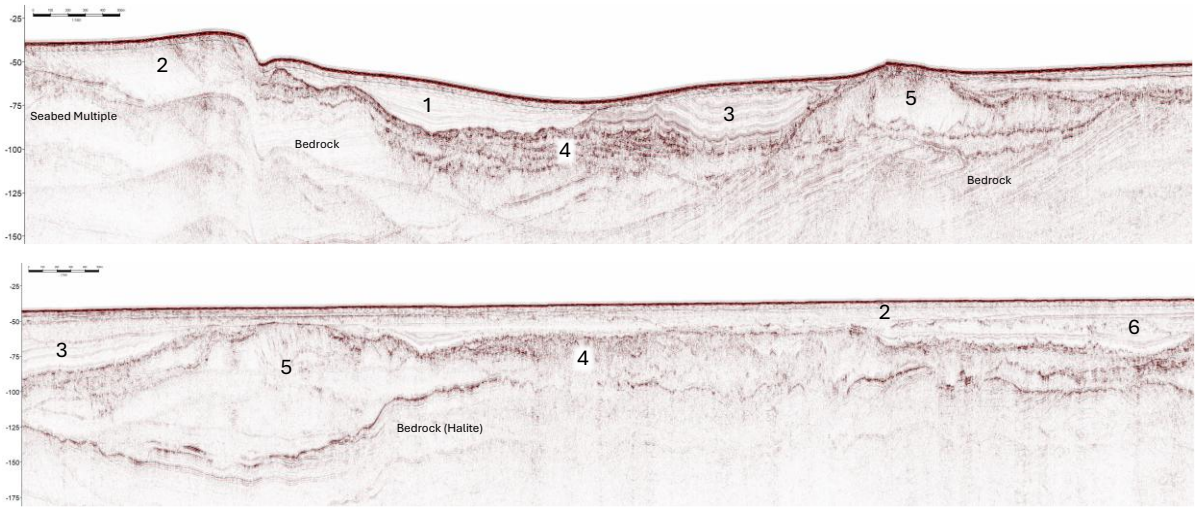
750

751 **Table 2.1.** Detailed formations of the Demetae Group and Brython Glacigenic Group as per Stoker et
752 al. (2011).

Group	Formation	Member	Description
Brython Glacigenic Group	Surface Sands	Seabed Depression	
		Surface Layer 1	
		Surface Layer 2	
	Western Irish Sea	Codling Bank Facies (offshore Wicklow only)	A very clast-rich (cobble-boulder size) deposit possibly laid down as a diamicton through subaqueous ice-rafting and sediment gravity flows, or sandur deposits.
		Mud facies	Black to greenish grey, shelly silts, representing ice-distal glaciomarine deposits that pass upwards into fully marine deposits.
		Prograded facies	fine- to medium-grained sand representing prodeltaic and glaciomarine deposits
		Chaotic facies*	tabular-stratified deposits, likely to have been laid down under glaciolacustrine or glaciomarine ice-proximal settings.
	Cardigan Bay	Upper Till (late Weichselian)	Stiff or very stiff diamicton of clay containing clasts up to boulder size (>1 m diameter).
		Bedded and Infill member (late Saalian to early Weichselian	Sands with subordinate clay beds passing upward into fine-grained silty sands and sandy clays
		Lower Till member (Saalian)	Very stiff clay with abundant cobbles to a shelly sand with lithic gravels and occasional cobbles
	St George's Channel		Shelly glaciomarine muds
	Caernarfon Bay	Upper Unstratified member (early Saalian)	Till or sandy to muddy diamicton with drops stones (probably an ice-sheet-proximal, glaciomarine deposit).
		Incision Infill member (late Elsterian to Holsteinian)	diamictons of stiff clay with lithic clasts, muds with clasts up to boulder size, sands, muds and clays
		Bedded member (Elsterian)	depositional environment unknown but consists of shelly sand with occasional clay beds and scattered cobbles.
		Lower Unstratified member (Elsterian)	Probable subglacial to proglacial olive-grey till

Demetae Group	Bardsley Loom		heterogeneous mix of clay, sand, gravel and peat layers
Notes: * Geoscience data acquired for Offshore Wind Developments has allowed for a greater understanding of the depositional and glacial setting, but at the time of writing was yet to be publicised			

753



754

755

756 **Figure 2.16.** Seismic section (west to east) through the Eastern Irish Sea Quaternary Sequence. 1. Mud
757 Facies [Glaciomarine], 2. Prograded Facies [Glaciomarine], 3. Chaotic Facies [Glaciolacustrine with
758 crevasse squeeze ridges], 4. Chaotic Facies [Pro-glacial outwash and lakes], 5. Upper Till [Glacio-
759 tectonised Moraine], 6. Chaotic Facies [Sandur Plain and Glaciofluvial]. Walney Wind Farm, publicly
760 available data.

761 Post-glacially, the Irish Sea and Celtic Sea seafloor has been heavily influenced by marine transgression
762 and contemporary hydrodynamics. As a result of glaciation, the seafloor sediment of this area largely
763 comprises reworked glacial or post-glacial material forming a mosaic of sediment types, that are often
764 reworked into bedforms. Linear sediment mega-ridges in the Celtic Sea have been interpreted as tidal
765 features, with a subglacial basement control, that formed under stronger current conditions in the past
766 (Lockhart et al., 2018; Praeg et al., 2015). In the Irish Sea, a series of linear, north-south trending
767 sandbanks are found close inshore and parallel to the Wexford, Wicklow and South Dublin coast. These
768 features form bathymetric highs relative to the surrounding seabed and are understood to formed under
769 more energetic tidal regimes in the geological past (Uehara et al., 2006; Wheeler et al., 2001) or with a
770 partly glacial origin (Whittington, 1977). They are currently considered quasi-stable and in equilibrium
771 with present hydrographic conditions, with some minor morphological changes (Creane et al., 2023a;
772 2023b). These banks form sites for planned offshore wind development. In general, the Irish Sea
773 seafloor is dynamic with high levels of sediment erosion, transport and deposition due to the energetic
774 tidal regime (Coughlan et al., 2021a; Ward et al., 2015). These conditions help maintain and drive
775 bedform development and migration, including extensive sediment wave fields (Creane et al., 2022;
776 Van Landeghem et al., 2009b). This dynamic seafloor also creates engineering issues such as scour,
777 which has impacted on offshore wind turbine stability previously (Whitehouse et al., 2011). The

present-day seafloor in the Irish Sea also shows evidence of fluid escape. Pockmarks and sub-surface gas accumulations in the Quaternary sequence has been documented in the north Irish Sea (Coughlan et al., 2021b; Yuan et al., 1992) with methane derived authigenic carbonates (MDAC) and mounds found in sandier deposits further south (Croker et al., 2005; O'Reilly et al., 2014; Van Landeghem et al., 2015).

Despite the substantial sediment reworking and seafloor modification by post-glacial processes, the present-day seabed captures this diverse and complex Quaternary history across this region. The growth in national seabed mapping programmes, such as INFOMAR, has provided key large-scale datasets that have allowed for the regional classification of glacial features (e.g. Arosio et al., 2023), and to identify key geological constraints to the development of offshore infrastructure related to Quaternary processes and deposits (Coughlan et al., 2020b; Guinan et al., 2020).

2.1.8 Outer Hebrides and Rockall

From Early Pliocene times onshore uplift of the northwest European Atlantic margin (west of Shetland, Outer Hebrides, Rockall and west of Ireland) was accompanied with accelerated offshore subsidence, coupled with seaward tilting of the continental margin that resulted in basinal progradation of the northwest Atlantic Margin (Stoker and Varming, 2011; Stoker 2013). Progradation and development of the Atlantic margin, of up to 50 km in the Hebridean region (Stoker 2013), was further enhanced by multiple Late Pliocene to Pleistocene glaciations (Stoker and Varming, 2011; Stoker 2013) with much of the sediment forming these wedges younger than around 2.5 Ma (Stoker, 2002; Stoker et al., 2005).

Across the Atlantic margin, regional mapping has shown that the Quaternary succession can be divided into two separated by a widespread Mid-Pleistocene glacial erosion surface correlated with the Anglian glacial stage (the Glacial Unconformity on Figure 2.17) dated to about 0.44 Ma on the continental margin (Stoker et al., 2005). The glacial unconformity separates sediments of the Hebrides Margin Group (below) from the Eilean Siar Glacigenic Group. Unlike the North Sea Basin, multiple glaciations during the Mid and Late Pleistocene have removed much of the Early Pleistocene/Pre-Elsterian deposits from the outer continental shelf (Stoker et al., 1993). Across the continental shelf the Quaternary succession is comparatively thin, only attaining a thickness of up to around 200 m (Figure 6.4). At their maximum extent, the BIIS delivered sediments directly to the continental slope generating large glacigenic depocentres such as the Foula and Rona wedges in the Faroe Shetland Channel, and the Sula Sgeir (Figure 2.18) and Barra–Donegal glacigenic fans in the Rockall Trough (Figure 2.10), accumulating sequences up to around 800 m thick (Figure 6.4). The margin of the southern Rockall–Porcupine area was largely sediment starved during Quaternary times (Stoker et al., 2005).

The Sula Sgeir and Barra–Donegal glacigenic fans are composed predominantly of stacked accumulations of debris-flow diamictons interbedded with hemipelagic and contouritic marine/glacimarine muds and thin-bedded turbidites (Stoker et al., 2005; Stoker, 2013). British

Geological Survey boreholes and a limited number of commercial wells located on the Hebridean margin suggest that the regional Glacial Unconformity separates underlying sand-dominated strata of the Hebrides Margin Group from overlying mud-dominated sediments of the Eilean Siar Glacigenic Group (Stoker, 2013; Figure 2.17). Borehole 88/07,7A located on the Hebrides Slope proved ice-rafted debris in the form of scattered dropstones at 86.0 m, more or less coincident with the Gauss–Matuyama polarity transition (2.48 Ma) measured at 85.8 m (Stoker et al., 2005). This contrasts with palaeontological evidence of warmer environmental conditions during deposition of the underlying Pliocene section suggesting deterioration of climatic conditions from latest Pliocene to earliest Pleistocene times (Stoker, 2013).

The planar to irregular, regional Glacial Unconformity typically truncates older Plio-Pleistocene prograding strata, and is overlain by a flatter lying sequences that displays an aggrading geometry, preserves glacial moraines on the continental shelf, and gives way to glacial-fed trough-mouth fans on the slope (Figure 2.18; Stoker et al., 2005). This early Mid-Pleistocene stratigraphic expression marks the switch from restricted (down to coastline) to expansive (shelf-wide) glaciations (Stoker, 2013).

Regional-scale geomorphology along the mid and outer shelves is dominated by a series of arcuate and sometimes overlapping ice-marginal moraines (Figure 2.10). These ubiquitous bedforms relate to the extent and retreat of grounded ice on the shelf. Large moraines show a clear geographic association to glacially eroded troughs, and the depositional trough-mouth fans on the continental slope (Figure 2.10; e.g. Sula Sgeir and Barra–Donegal fans), revealing the terminal positions of a number of palaeo-ice streams extending out across the continental shelf to the shelf break. The excavated troughs and depositional trough-mouth fans have been formed over successive glacial stages, while the moraines are more likely associated with the most recent glaciation to impact the seabed as ice sheets tend to remove surficial evidence from previous events. Some of the transverse ridges on the mid-shelf have been interpreted as grounding-zone wedges (marking position between grounded ice and floating ice shelf) rather than moraines, depending on the relative sea level at the time. These are particularly well developed for the Minch Ice Stream (Bradwell et al., 2021), Barra–Donegal Ice Stream (Arosio et al., 2018; Callard et al., 2018), Donegal Bay Ice Stream (Benetti et al., 2021), and Galway Bay Ice Stream (Peters et al., 2015; Callard et al., 2020), suggesting punctuated or episodic retreat of the grounding line from their maximum LGM extent.

As ice sheets retreat from the mid and outer shelf, proximal glacimarine sedimentation proceeded, and these deposits still mantle the seabed in several places (e.g. near and beyond shelf break, North Lewis and North Minch Basins). Acoustic gas-blanking is commonly reported within the sediments of the Jura Formation, likely to be the result of very high rates of deposition and associated rapid burial of organic matter (Fyfe et al., 1993). Where sheltered, low-energy coastal and estuarine conditions dominate, accumulations of fine-grained sands and muds exhibit small areas of pockmarks on the seabed surface (Audsley et al., 2021). Extensive basement platforms occur on the inner continental shelf in the vicinity

of the Outer Hebrides and Sea of the Hebrides. West of the Outer Hebrides these basement rocks comprise scoured Lewisian strata (>2500 million years old) cropping out at seabed across a large region, extending at least 150 km from north to south. Bedrock landforms produced by glacial erosion (e.g. bedrock crag-and-tails and streamlined rock drumlins), provide evidence of intense subglacial erosion by powerful fast-flowing ice, and key information regarding former ice-flow dynamics. Bedrock highs within the Minch and Sea of Hebrides, represent a marked increase in bed strength and a topographic pinning point that may provide vital stability of the marine-terminating margin during overall ice-stream retreat (Bradwell et al., 2019b, 2021; Stewart et al., 2022). Predisposed in places by the underlying structural geology, glacial troughs, up to ~100 m deeper than the surrounding seabed, are present in the North Channel and Inner Hebrides (Figure 2.10).

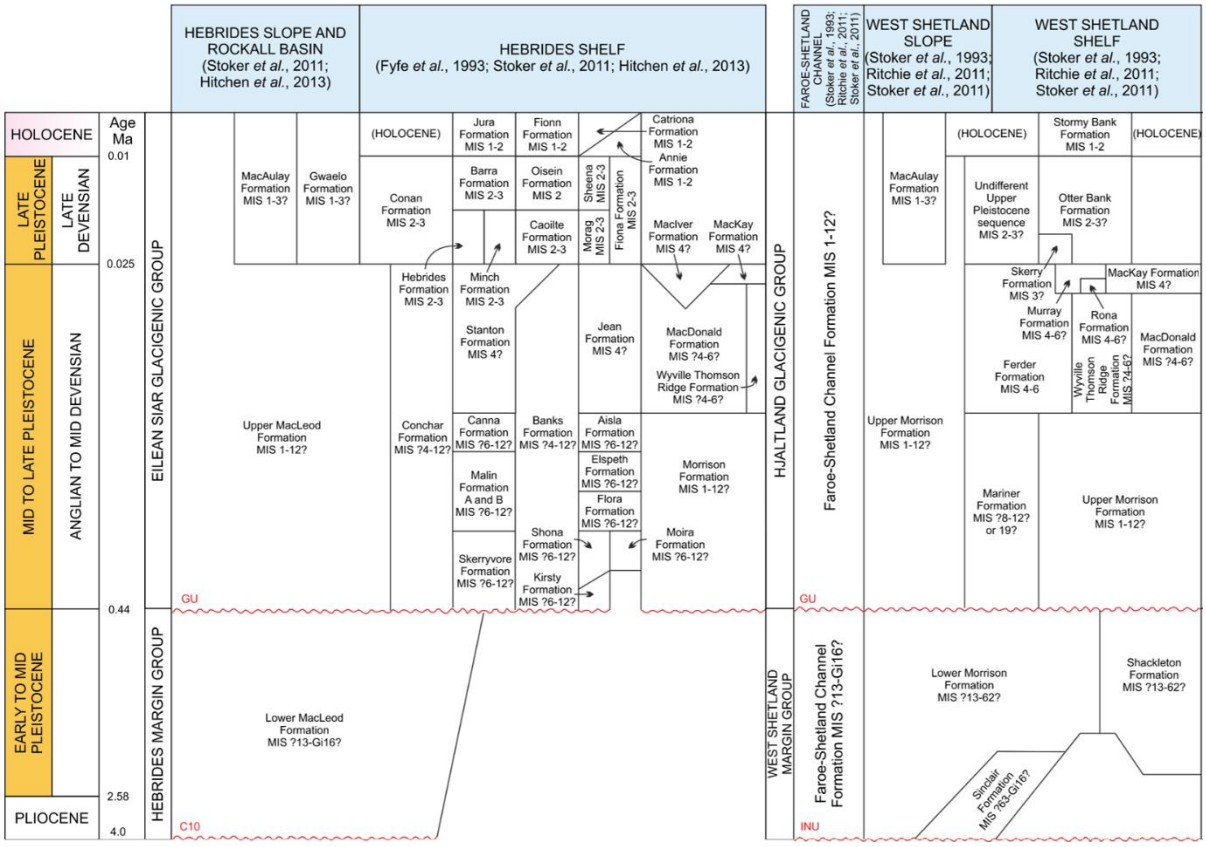


Figure 2.17. Summary of the Quaternary stratigraphy in the Hebridean, Rockall and West of Shetland regions. GU = Glacial Unconformity, INU = Intra-Neogene Unconformity, C10 = Early Pliocene unconformity.

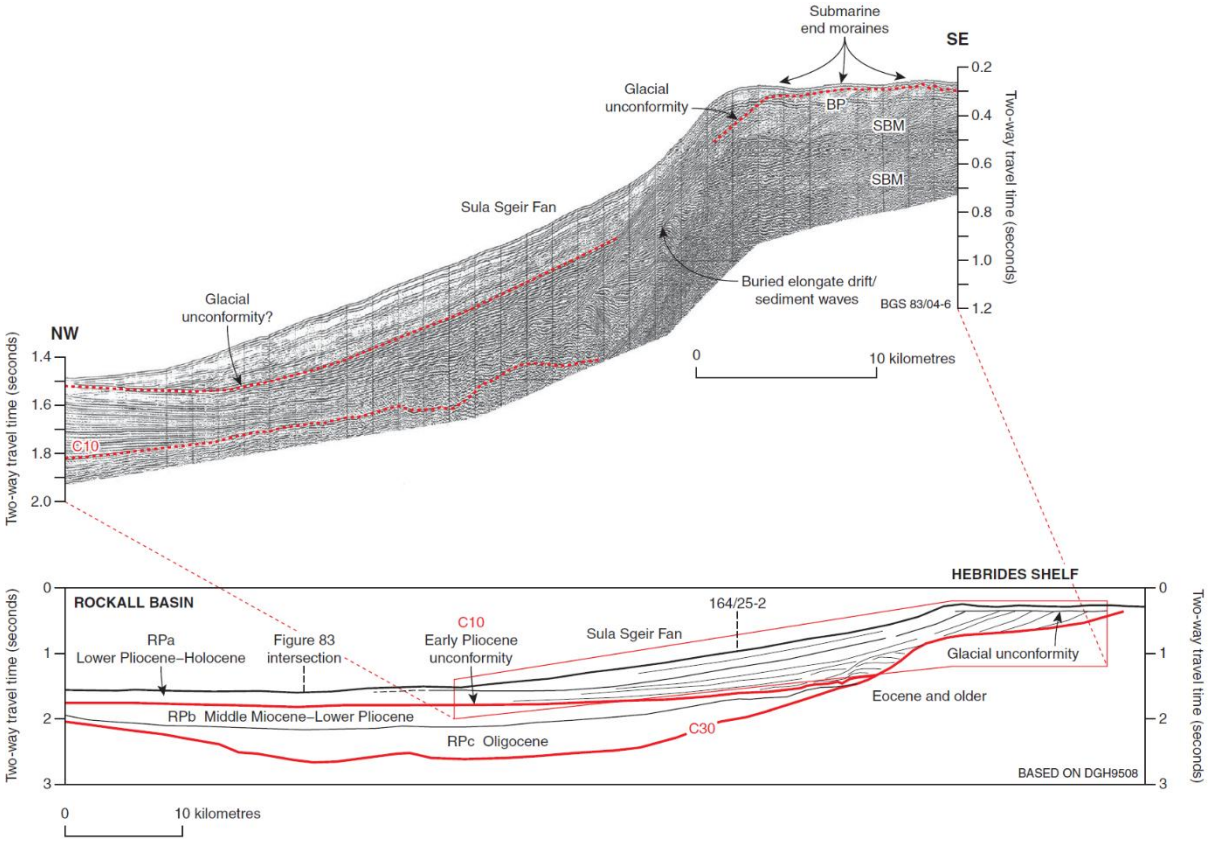


Figure 2.18. British Geological Survey airgun profile 83/04-6 across the Hebridean margin showing the Lower Pliocene–Holocene slope apron of the prograding Sula Sgeir Fan overlying and partly interbedded with onlapping and upslope migrating contourite drift and sediment waves, which both comprise the RPa megasequence (sediments of both the Hebrides Margin and Eilean Siar Glacigenic groups). Submarine end moraines are preserved above the Mid Pleistocene glacial unconformity on the Outer Hebrides shelf. Modified after Stoker et al. (2005). For location see Figure 2.10. Image British Geological Survey © UKRI 2025.

2.1.9 West of Shetland

The Late Pliocene to Pleistocene history of the West of Shetland (WoS) margin, like the Outer Hebrides and Rockall margin, is also characterized by a dynamic interplay between glacial advances and retreats, fluctuating sea levels, and bottom current activity. This period witnessed significant progradation, with the margin extending seaward by up to 50 km since the early Pliocene (Stoker and Varming, 2011). The progradation can be broadly categorized into two distinct phases: a first phase as part of the Faroe Shetland Neogene 1 (FSN-1) mega-sequence followed by a second phase of the formation of the Glacial Unconformity, marking the onset of extensive shelf glaciation around 0.44 million years ago (Ma) (Stoker, 1995; Stoker and Varming, 2011; Clark et al., 2018).

Prior to the Mid Pleistocene glaciation, progradation was initially restricted to the outer shelf, gradually extending into deeper water over time (Stoker and Varming, 2011). Borehole data reveal a sand-dominated sequence underlying the Glacial Unconformity, attributed to the Sinclair and Morrison (unit

1) formations (Figure 2.17), which together comprise the older portion of the Rona and Foula wedges (Stoker and Varming, 2011; Figure 2.10). These formations exceed 100 meters in thickness, with the older Sinclair sequence occupying the innermost portion. Biostratigraphic dating suggests a Pliocene to Early Pleistocene age for the Sinclair sequence.

The Glacial Unconformity separates the underlying sand-rich strata (Morrison 1 Sequence) from the overlying mud-dominated sediments (Morrison 2 Sequence; Stoker and Varming, 2011; Figure 2.17). Mid-Pleistocene orbital shifts (100 ka cycles) drove extensive glaciation across the British continental shelf, impacting sedimentation and margin development (Rea et al., 2018). Resulting glacial cycles led to unconformities and prograding glacial wedge deposits on the shelf/slope. Since the Mid Pleistocene, progradation has extended from the shelf to the Faroe-Shetland Basin (FSB) (Stoker and Varming, 2011). The uppermost sediments form, between 59.5ºN and 61ºN latitude, large, wedge-shaped deposits (prograding wedges) and apron-like layers (slope aprons) as part of Trough Mouth Fan systems (Figures 2.10 and 2.19).

British Geological Survey borehole data indicate that many post-Glacial Unconformity units on the outer shelf, such as, Foula and Rona sequences, are dominated by diamicton (glacigenic debris flow), sand, and gravel (Stoker and Varming, 2011; Figure 2.17). These debris flow deposits are alternated to contouritic clays and sands, alongside glacimarine clays and sands deposited by ice-rafted debris and meltwater plumes (Davison, 2004; Knutz and Cartwright, 2003) with finer glaciomarine and contouritic sediments. Further north, between 61ºN and 62ºN, these deposits transition into elongated, mounded features, associated to bottom currents flowing along the continental slope. The latter represent the West of Shetland Drifts (WSD) and are mirrored by sheeted contourite drifts across the Faroe-Shetland Channel basin. These deposits are attributed to ice-marginal processes associated with the growth and retreat of the BIIS (Stoker and Holmes, 1991) and successively by the combined BIIS and the FIS at, or near, the WoS shelf break between 26-25 k yr BP (Stoker and Varming, 2011; Clark et al., 2018; Hall et al., 2019; Ballantyne and Small, 2019; Bradwell et al., 2019). Notably, the Otter Bank sequence displays mounded accumulations forming prominent seabed ridges (Stoker and Varming, 2011).

During glacial maxima, large ice sheets deposited thick sediment wedges (hundreds of meters) on the continental slope. On the WoS slope, the prograding succession is primarily assigned to the Morrison 2 sequence, with a late to postglacial MacAulay sequence occupying the uppermost portion. Further downslope from the Foula Wedge, the characteristic gully and basin floor fan systems imprinted in the present-day seafloor suggests the lower slope experienced minimal sediment deposition, with most material bypassing this area and accumulating across the basin area to form the triangular-shaped complex glacigenic basin floor fan deposits, part of the distal Foula Wedge (Stewart and Long, 2012; 2016; Caruso et al., 2022).

Since the last glaciation and throughout the Holocene, the region has seen minimal terrestrial sediment input. Seafloor sediments are linked to postglacial vertical rainout from meltwater plumes, including ice-rafted debris and reworked Pleistocene sediments. Postglacial sedimentation is thought to be largely controlled by ocean currents, with fully marine interglacial circulation established around 9,500 years ago (Masson et al., 2004). Current sedimentation rates are typically less than 1 centimetre per thousand years (Masson, 2001).

Notably, the southern WoS margin lacks significant head scarps or classic marine slides on the seafloor. The large slides observed to the north and northeast of the Faroe Shetland basin are located within the WSD slope body, with the Afen slide being a particularly well-studied example. Recent research suggests that in low-angle, layered contourite drifts, specific sediment boundaries are more important factors for slope failure than the overall slope geometry. The location of the Afen slide, free from glaciogenic debris flows, suggests less influence from glacial activity on downslope sedimentation in this region compared to the northern and southern ends of the FSC (Davison, 2004). This highlights the contrasting depositional environments along the continental slope, resulting in distinct compositions of the shallow sediments. In the Afen slide area the shallow sediments are dominated by bottom current-related deposits which are considered a major preconditioning factor in past slope failures within the region (Stoker and Varming, 2011; Gatter et al., 2020), similar to what has been observed on the Norwegian margin (e.g., Storegga Slide; Bryn et al., 2005b;).

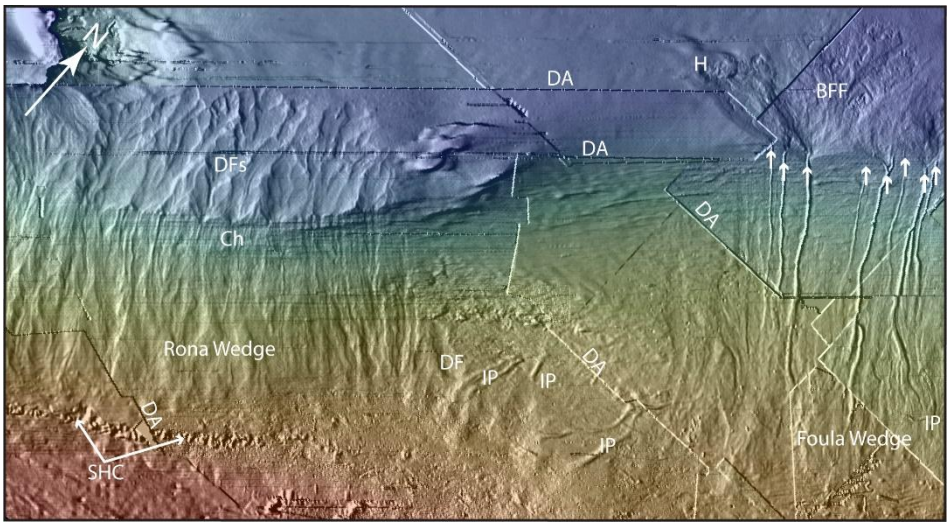


Figure 2.19. Seafloor image showing the glacigenic debris flows the of Rona and Foula wedges adapted from Stewart and Long (2016). Image derived from first returns from commercial 3D seismic surveys (methodology in Bulat and Long 2001). Arrows indicate downslope slope gullies. BFF = Basin floor fan, Ch = Channelised features, DA = Data artefact, DF = Debris fans, H = Hollow, IP = Iceberg ploughmarks, SHC = Scour-hole complex. For location see Figure 2.10. Image British Geological Survey © UKRI 2025.

3. Deglaciated continental margins: Processes

The glacial source-to-sink systems along the glaciated European margins are different compared to other sedimentary source-to-sink systems that do not account for glacial and ice-sheet processes as direct components of the system (Figure 3.1; Castelltort and Van Den Driessche, 2003; Vimpere et al., 2023). Sinks of the glacial source-to-sink system are diverse and time transgressive and include lakes, fjords, shelves, trough mouth fans, and ultimately the deep sea depending on the ice sheet or glacier catchment area and the concomitant ice margin position. (Figure 3.1). These sinks act as valuable archives for a variety of deposits during different parts of the glacial cycle (Figure 3.2; Sejrup et al., 1996). While lake and fjord basins record marine and glacio-marine sedimentation following ice retreat (Bellwald et al., 2016), they rarely preserve glacial tills recording subglacial conditions under the ice sheet. In contrast, ice-stream troughs on continental shelves, such as the Norwegian Channel in the North Sea or the Bear Island Trough in the Barents Sea comprise >70% glacial till, and are thus better archives for this type of glacial sediments (Figure 3.2; Sejrup et al., 1996).

A wide variety of processes shaped the glaciated European margins, and in the following chapter, we discuss these processes throughout a glacial cycle, separated into glacial (incl. periglacial), deglacial, and interglacial time periods (Figure 3.3). Ice-sheet dynamics and hydrological evolution are crucial to define the interaction and (dis)connectivity of different systems. The ice-margin position of glaciers at a given time is an important location for the sedimentary activity as it can be used as an approximate location of a depocenter or a sink at a given time and which marks a boundary between lithological different sediments and landforms developed under and in front of the ice margin (Boulton, 1986, Kurjanski et. 2020). For marine-terminating ice sheets, the location of the grounding line, defined as the transition from grounded into floating ice, is a key parameter for the study of processes and deposits. In glacial source-to-sink systems, significant changes in grain-size distribution, clast morphology, and mineral properties can occur on short lateral scales (<250 m; Kjær, 1999). The source-to-sink systems can further be modified during the engineering phase.

Bathymetric and side-scan sonar data allow for detailed reconstruction of processes shaping the seafloor, whereas conventional 2D/3D seismic, (ultra-)high-resolution 2D/3D seismic, and sub-bottom profiler data are commonly used to characterize landform assemblages buried by several meters of sediments (e.g., Dowdeswell et al., 2016; Hill et al., 2024).

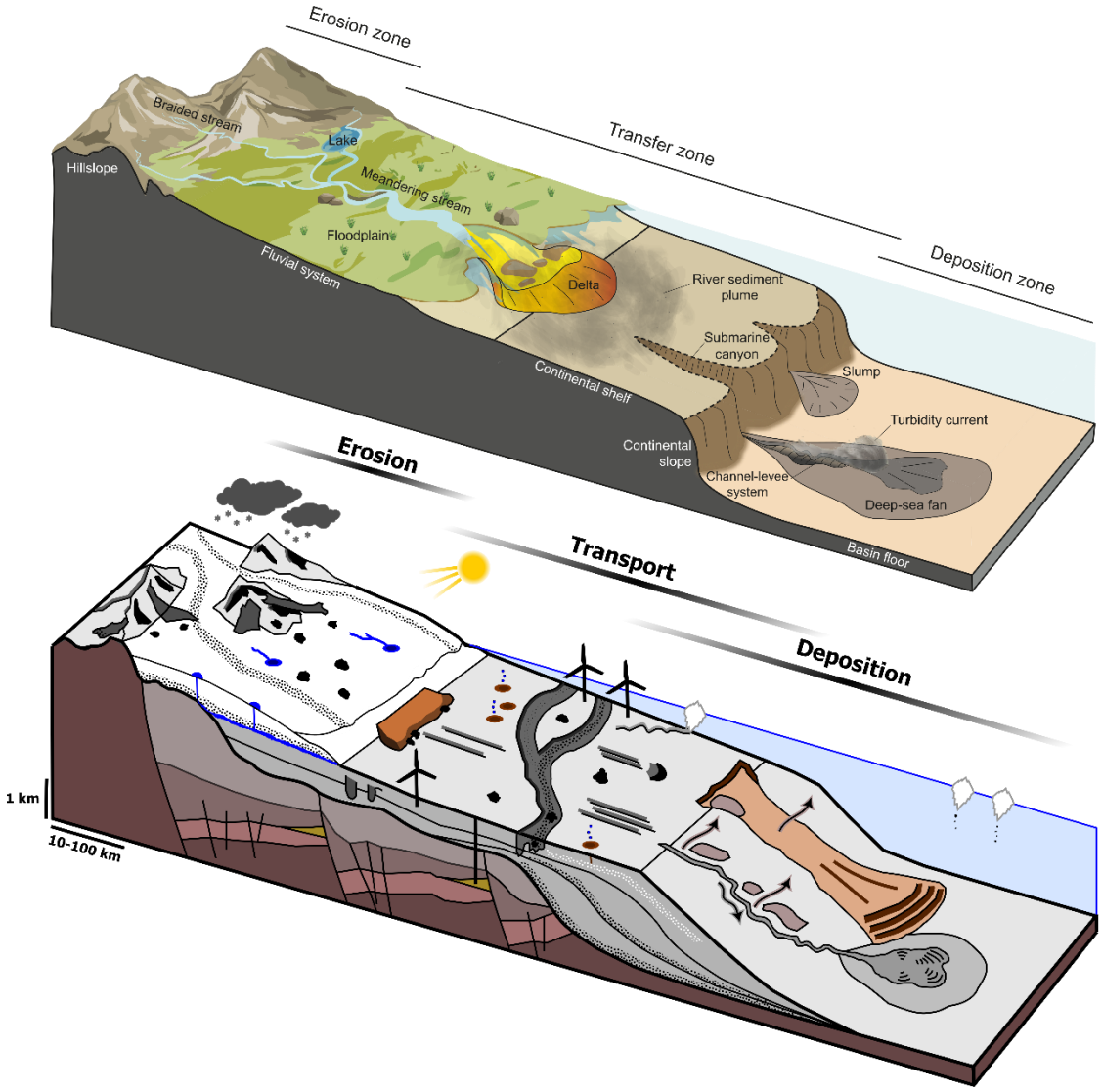
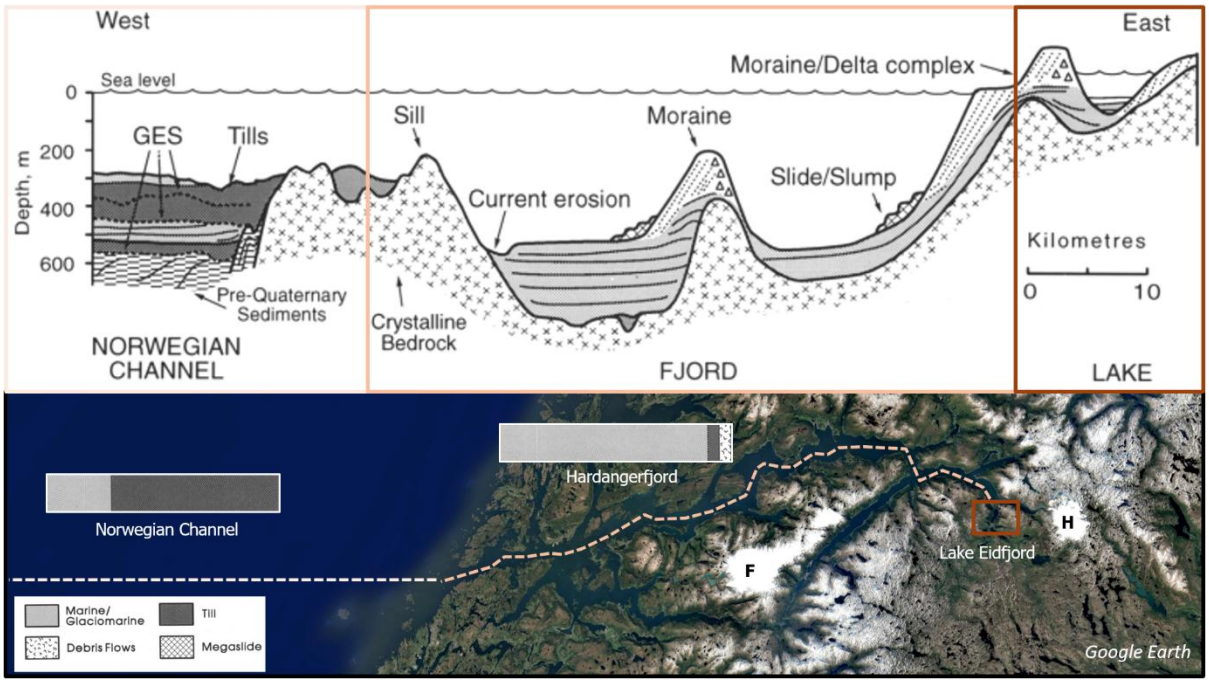


Figure 3.1. The concept of source-to-sink systems. Comparison of **a)** classical source-to-sink systems (from Vimpere et al., 2023) with **b)** glacial source-to-sink systems dominated by marine-terminating ice sheets (water depths >120 m).



976

977 **Figure 3.2.** The Hardanger fjord system in Western Norway and neighbouring Northern North Sea as
978 a modern glacial source-to sink-system. Bars show the relative quantity of sediment types in different
979 archives (after Sejrup et al., 1996). H: Hardanger Glacier, F: Folgefonna Glacier. Satellite image from
980 GoogleEarth.

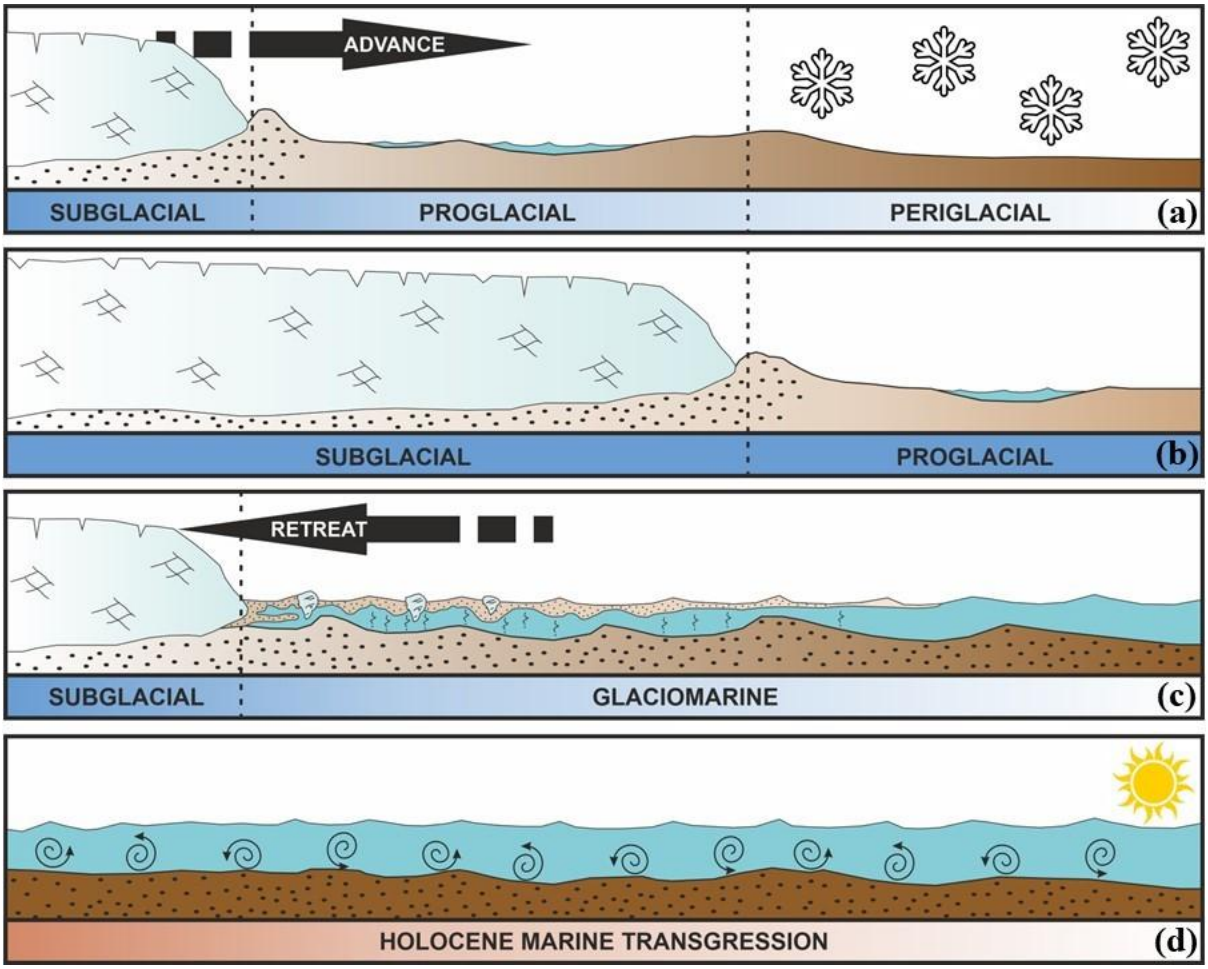


Figure 3.3. Processes and deposits during a glacial cycle. **a)** Periglacial. **b)** Glacial. **c)** Deglacial. **d)** Interglacial.

3.1 Glacial

At the onset of the cold climate, the ice sheets start to build-up and advance, and the sea-level drops, resulting in emerged platforms with occasional rivers forming proglacial fluvial channels (Prins and Andresen, 2019; Andresen et al., 2022). Large parts of presently submerged continental shelves of the study area were terrestrially exposed during the Pleistocene glaciations (Dimakis et al., 1998; Butt et al., 2002, Patton et al. 2017, Clark et al. 2022). During ice-sheet build-up, these platforms formed a periglacial environment dominated by the development of permafrost in the upper rock and soil units (Figure 3.3a). Climate was sufficiently cold to allow for freezing temperatures to propagate below the ground surface. Freeze-and-thaw processes often weakened the bedrock exposed to the atmosphere, and contribute to a bedrock weathering that commonly reaches depths of 5-10 m. However, in extreme cases where perennial freezing (scales of two yrs to hundreds of thousands of years or more) occurs, permafrost can propagate to subsurface depths of 1,500 m in temperatures of 0°C to ca. -24°C (Murton and Ballantyne, 2017).

Erosion, transport and deposition of pre-existing sediments and bedrock occurred simultaneously during the build-up of these ice sheets (Figure 3.3b). The main subglacial processes are the accumulation of subglacial till and boulders as ice sheet grew and advanced as well as, glaciotectonic deformation at ice sheet margins, and reworking at the base of the ice streams. The interplay between subglacial erosion and deposition results in large vertical and lateral variability of soil properties through the glacial time period.

During shelf-edge glaciations, ice streams rapidly deposited huge sediment quantities to the slopes (Hjelstuen and Sejrup, 2021). Sediment deposition on the slopes was dominated by submarine mass movements, such as glacigenic debris flows downslope and contour currents alongslope (Nygård et al., 2005; Newton and Huuse, 2017). Contour currents are documented to be weakened during the glacial time period (Batchelor et al., 2021; Bellwald et al., 2024a). The tectonic stress field during glaciations was a different one compared to the modern stress field, with kilometers of ice covering the shelves (ice loading), and erosion and deposition resulting in a new sediment balance.

Gas hydrates formed to subsurface depths of up to 200 m in regions with active hydrocarbon systems, such as the North Sea and the Barents Sea (Vadakkepuliyambatta et al., 2017). Ice streams were locally frozen to the subsurface, and gas hydrates potentially acting as sticky spots (Winsborrow et al., 2016; Bellwald et al., 2023a).

3.2 Deglacial

Deglaciation is dominated by ice mass loss, either through iceberg calving (marine ice sheet margins) or ablation (marine and terrestrial ice sheets) (Figure 3.3c). Icebergs released from marine terminating ice sheets were often dragging their keels along the seabed forming a complex network of furrows known as iceberg ploughmarks. Subglacial meltwater discharge was enhanced during deglaciation and often resulted in erosion of tunnel valleys and meltwater channels subglacially on the continental shelves, as well as deposition meltwater turbidites on the continental slopes (Ó'Cofaigh et al., 2018, Bellwald et al., 2020; Garcia et al., 2024). The contour currents were still weakened during the deglacial time periods (Batchelor et al., 2021). As the ice margin stepped back from, the shelf edge during deglaciation the sediment sinks shifted from TMFs towards continental shelves, ice marginal and proglacial lakes, ponds, and kettle holes. Sediment distribution and sink areas were often constrained by previous glaciogenic landforms and pre-existing topography forming a series of backstepping mini basins constrained between the contemporaneous ice margin and former ice-marginal moraine. In some cases, catastrophic drainage of ice-dammed lakes formed outburst floods (Gupta et al., 2007; Høgaas and Longva, 2016). These outburst floods could transport boulders with diameters of up to 2 m and often produced erosive boundaries in the stratigraphic record. Otherwise in terrestrial setting, proglacial rivers acted as sediment conduits on these, then emergent, shelves (Bellwald et al., 2021). On the flat shelves, water was often not forced into one river channel, but formed braided river systems known also

as sandar, which may have changed in time due to erosion of the riverbanks and variations in the amount of water.

Glacio-isostatic rebound (see Section 6.4), and related seismic activity, started to increase, and likely reached its peak during deglaciation. In fjord systems, both terrestrial and marine slope instability was enhanced during at that time as the ice and permafrost support was removed. (Bøe et al., 2004; Böhme et al., 2015; Hermanns et al., 2017; Bellwald et al., 2019a). Warmer waters resulted in the disintegration of gas hydrates, often documented by pockmarks and blow-out craters formed on deglacial surfaces (Forsberg et al., 2007; Andreassen et al., 2017; Tasianas et al., 2018).

3.3 Interglacial

During interglacials, the sea-level generally continued to rise, resulting in a marine transgression and full marine inundation of previously glaciated landscape but the sea relative sea level change was spatially variable as some areas experienced more isostatic rebound (cf. Section 6.4) (Figure 3.3d; Clark et al., 2022). Postglacial channels are often found to be incised in regions with active discharge and shallow waters, resulting in an increase of terrestrial soil material especially during the interglacial transitions. As the Sea level was rising hydrodynamic forces acted on the unconsolidated, often terrestrially deposited, glacial substrate, remobilising and reworking the sediments in shallow marine environments. Sand banks, sand waves, and megaripples are common interglacial landforms on the shelf (Bellec et al., 2019; see Section 6.1). The interglacial sedimentation of the slope is dominated by contourites, which are more active during interglacial time periods compared to their glacial counterparts (Batchelor et al., 2021). Several megaslides removed sediments from the upper slope into the deeper basins (Solheim et al., 2005a; Hjelstuen et al., 2007). Tsunami deposits are reported for some of these megaslides (Bondevik et al., 2005a; 2005b). Most of the glacio-isostatic rebound and subsidence is completed in interglacial periods. However, rebound- related earthquakes are still reported as a potential trigger mechanism for submarine slides in interglacial times (Bellwald et al., 2019a) and slope instabilities in fjord systems (Sørensen et al., 2023).

3.4 Land-sea correlations and modern analogues

The shelves within the study area have water depths of up to 400 meters. During the Pleistocene glaciations, most of these shelves represented a different sedimentary environment, with ice directly delivered into proglacial terrestrial and glaciomarine settings (e.g., Walker et al., 2024). A sketch summarizing glacial environments and sedimentary environments is shown in Figure 3.4.

The Barents Sea, with water depths of 200-400 m, was in the Early Pleistocene a subaerial platform (Dimakis et al., 1998; Butt et al., 2002), most likely having similar sedimentary environments as the North Sea in the Late Pleistocene (Bellwald et al., 2024a). Environments similar to these paleo-shelves occur today in SE Iceland, Svalbard, Alaska, Greenland, Patagonia, and Antarctica (Figure 3.5). It is beneficial to use outcrops of such settings as modern analogues, and terrestrial outcrops allow

correlations with less accessible submarine (and potentially buried) landscapes (Figure 3.6). Sediments recovered from present-day submarine environments are valuable archives for the Quaternary evolution of the area (Figures 3.6 and 3.7).

Landforms, sediments and associated structures, as well as fossils are all proxies that allow conclusions on time periods during which long-term observations are lacking. For instance, the well-preserved ice-marginal geomorphology is beneficial in order to localize the development site in relation to the palaeo-ice margin and predict possible depositional domains based on the understanding of processes unique to areas under the ice, at the margin, and in front of it. Diatoms and mollusc can be used to provide chronological correlation and ultimately help to define the paleogeographic environment and site stratigraphy. Recovered sediments and glacial erratics originating from different provenances allows the separation of river/ice-sheet systems and definitions of catchment areas.

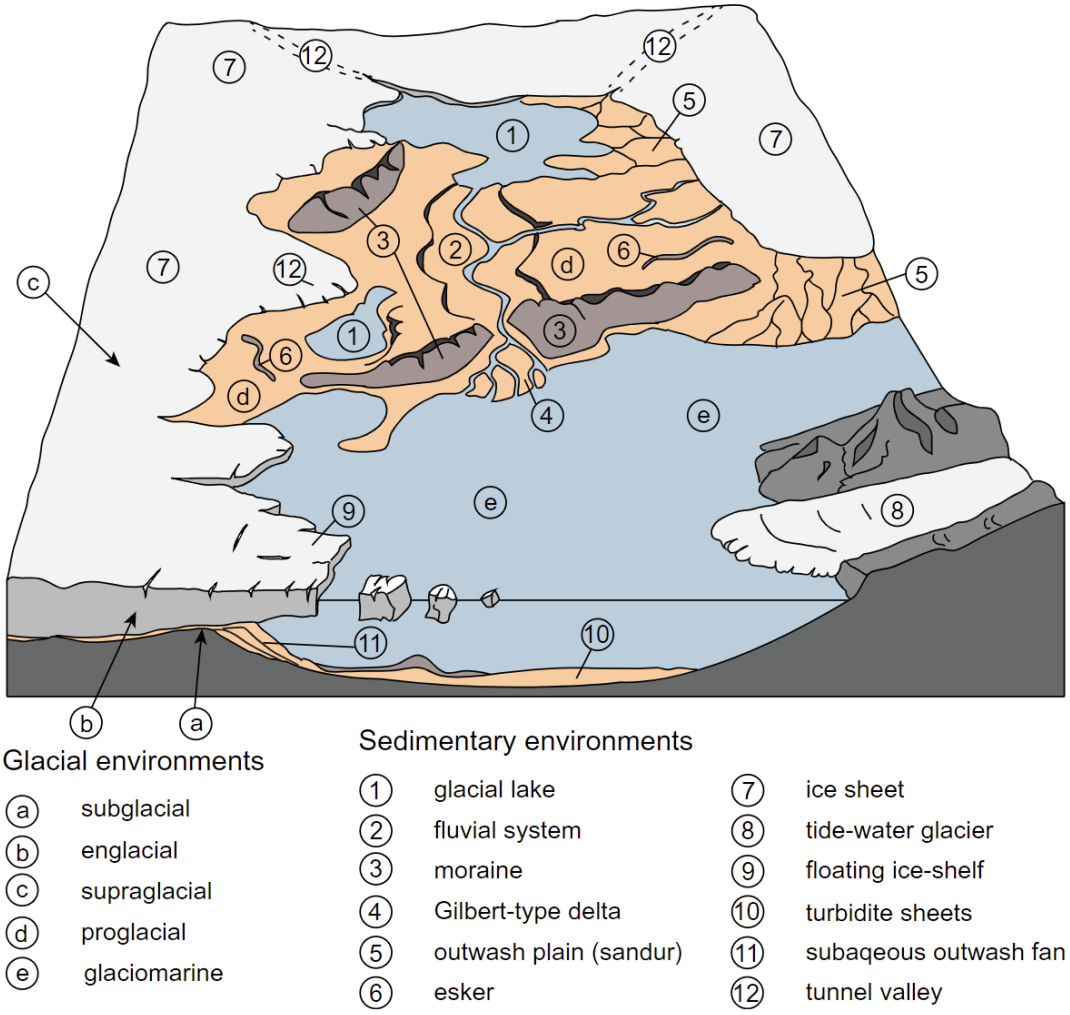


Figure 3.4. Glacial environments (from Huuse et al., 2012).

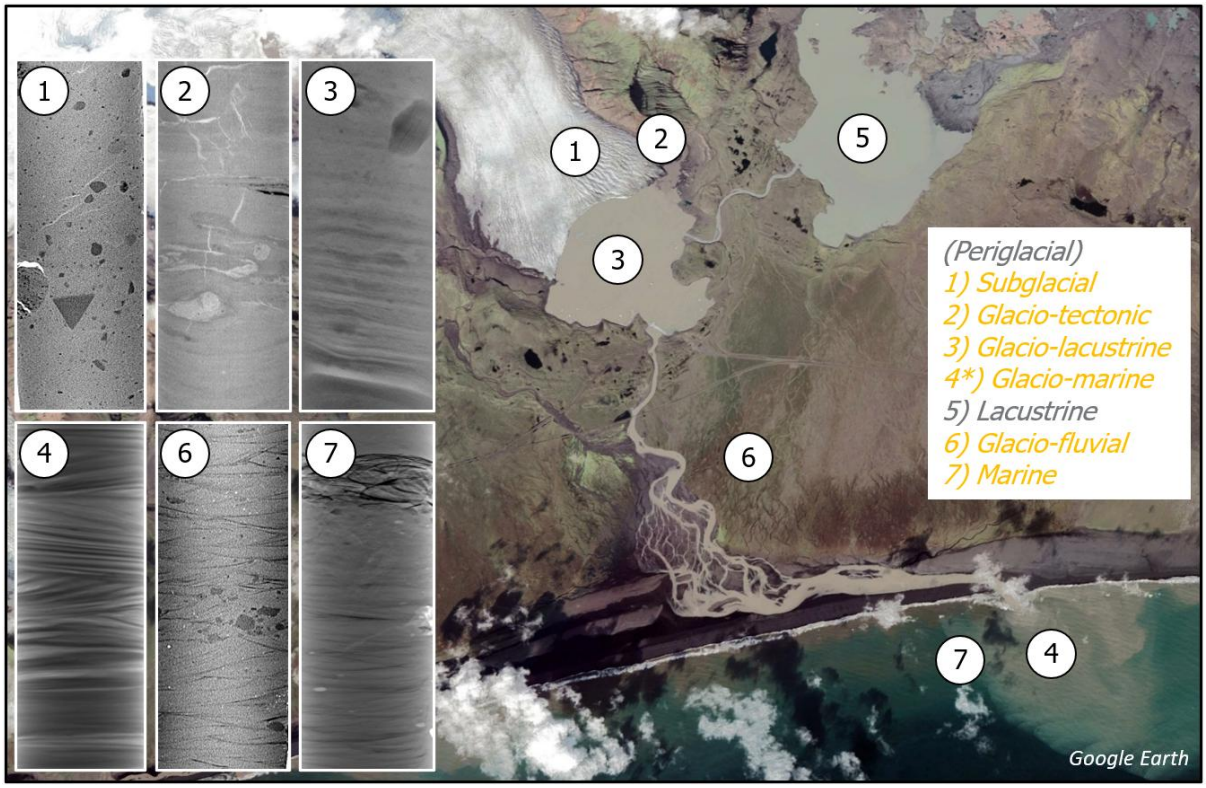


Figure 3.5. Modern terrestrial environments as analogues for sedimentary units identified in subsurface data from the marine domain of the glaciated European margins. Satellite image shows Fjallsárlón, SE Iceland. Computer tomography imagery from different Offshore windfarm projects of the glaciated European margins.

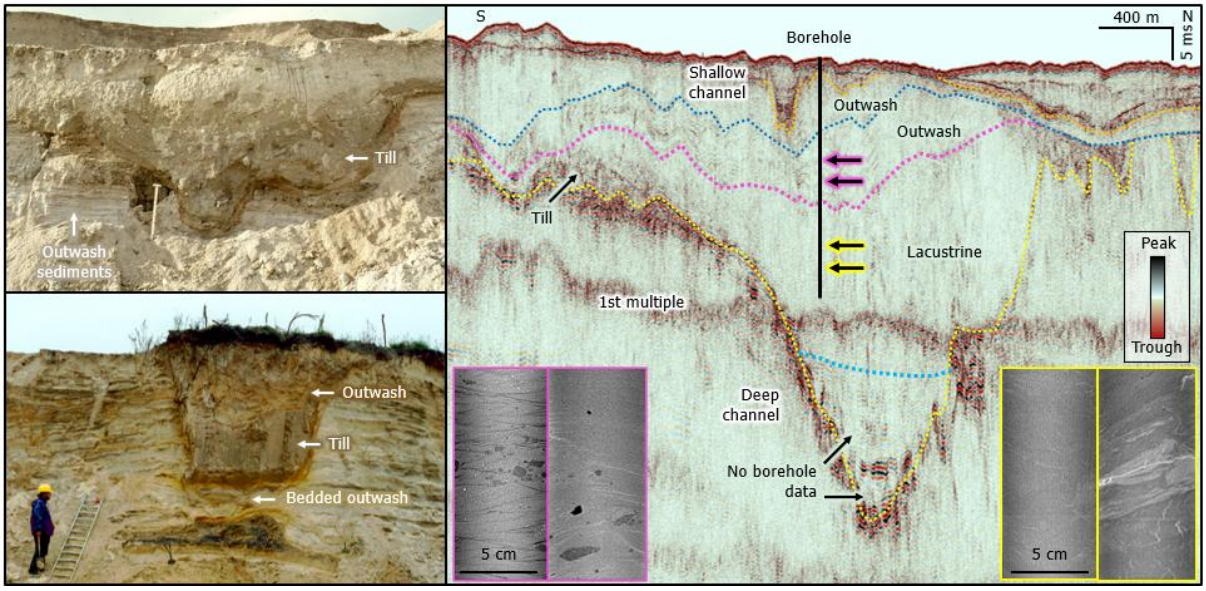


Figure 3.6. Integration with outcrops to further advance the geological understanding of offshore windfarm sites (from Bellwald et al., 2023b). **a)** Infilled subglacial channel at Brügge (N Germany). **b)** Infilled subglacial channel at Welzow South (E Germany). Both photos by Jan Piotrowski. **c)** Expression of an infilled subglacial channel on UUHR seismic profile of the Southern Baltic Sea.

Computer tomograph images show sedimentary structures of different glacial sequences (pink: outwash, yellow: lacustrine).

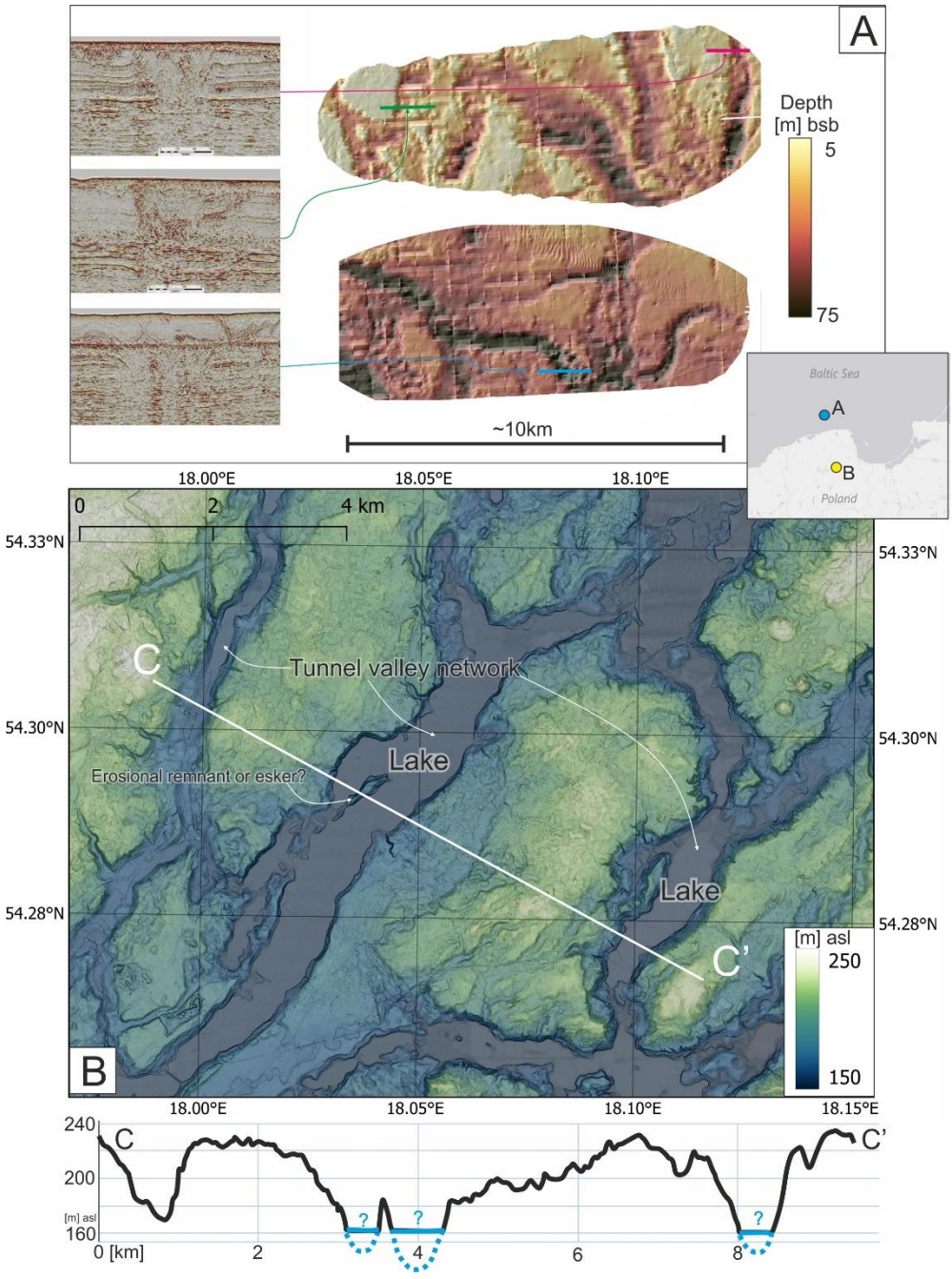


Figure 3.7. a) Tunnel valleys mapped within the subsurface across an OWF site in the Southern Baltic in the Slupsk Bank area. All valleys are fully filled with sediment leaving no expression at the seabed. **b)** Underfilled tunnel valleys on land in Northern Poland shown in 1 m resolution lidar dataset. Lakes are currently filling the overdeepened valleys. Both images are comparable in scale. Note the similarities in dimensions and morphologies between tunnel valleys in both locations.

4. Deglaciated continental margins: Deposits

Processes described in Section 3 produced a diverse, and laterally and vertically heterogeneous, complex depositional record on formerly glaciated European continental margins as well as a rich variety of geomorphic features at the seabed and within the subsurface (e.g., Newton et al., 2024a, Kurjanski et al. 2020). Typical sedimentological and geotechnical characteristics of the different glacial and interglacial facies observed along the glaciated European margins, and their potential engineering implications are presented in Table 4.1. Note that that the description of 'typical' deposits for a given area or environment is a generalisation aiming to characterise most of the sedimentary package. Small-scale or local variations of grainsize, lithology or geometries within depositional environments are normal and should be expected.

4.1 Deposits of the shelves

The deposits of the shelves can range significantly in thickness (Fjeldskaar and Amantov, 2018; Hjelstuen and Sejrup, 2021; Newton et al., 2024). They can be absent or very thin when bedrock is close to the seabed but also can form basin fill often >100s of meters thick if accommodation is available. In such cases, for example in the North Sea, Quaternary sequences can be traced and correlated regionally for long distances (Figure 4.1). The deposits affected by ice loading and bulldozing can be overconsolidated and glacio-tectonically deformed, having high strengths. The sediments of the shelf are in general more coarse-grained, and boulders and gravel beds can frequently occur when compared to deposit accumulated along the slopes and within trough mouth fans. Although the glacial sediments of the shelf tend to be less sorted than deposits compared to sediments from other environments (e.g. shallow marine, fluvial, etc), in certain glacial environments, the sorting can be good: For example, the clean sands of an outwash fan deposited by the Norwegian Channel Ice Stream form the Peon discovery, one of the largest gas discoveries of the North Sea (Bellwald et al., 2022b; Figure 2.6). The organic content is enhanced in shelf deposits compared to the deeper waters of the slopes, and decomposition of this material can often result in shallow, biogenic gas generation and accumulations frequently observed as acoustic blanking in shallow subsurface seismic data (Arosio et al., 2018).

Lacustrine deposits form in closed basins isolated from the global ocean and saltwater input or within localised depressions within formerly terrestrially exposed shelves. These lacustrine deposits mainly consist of clays with dropstones delivered by icebergs, have a low to medium shear strength, and can be laminated or varved as a result of seasonal changes in sedimentation rates and energy within the environment. Glacio-fluvial channels frequently observed to be cut into the subsurface neighboring the lake environments. The channels cut by glacially-fed rivers are hotspots of complex infill, with multiple cut-and-fill sequences commonly preserved filling the incision. The channel infill can have all types of seismic facies, and shear strengths vary from low to very high.

On formerly terrestrially exposed glaciated shelf's, large meltwater outflows with suspended sediment load and bedload of proglacial streams and rivers typically resulted in the deposition of extensive, gently sloping outwash plains known by the Icelandic term sandar (singular sandur). The deposits regionally are characterized by a general fining grainsize trend in a downstream direction which may not be evident locally as erosional nature of periodical/ seasonal high flows could result on removal of finer fractions and transport of coarser material further downflow. Fluvial deposits are often marked as a regional planar unconformity, with a prograding geometry and dipping reflections in all directions.

4.2 Deposits of the slopes

The deposits of the continental slopes are dominated by down-slope processes (turbidites, debris flows, landslides, and along-slope processes (contourites) that often are trackable for several 10s of kilometers (e.g., Rydningen et al., 2020). These deposits often form several kilometers-thick sequences (Figure 4.2; Hjelstuen and Sejrup, 2021) sediments better sorted and more fine-grained compared to the deposits of the shelf.

Turbidites can bypass parts of the slope or deposit sediments, and form normally graded sediment sequences (vs. inverse grading of contourites). The turbidites consist of muddy sand (Bellwald et al., 2024a) up to sandy mud. Glacigenic debris flows have often a lens-shaped, homogenous facies in cross sections and lobate shapes in planar view (Laberg and Vorren, 2000; Nygård et al., 2005; Løseth et al., 2020). These debris flows are mud-dominated (Baeten et al., 2014; Bellwald et al., 2024a). Landslides mainly consist of removed material of previously deposited debris flows and turbidites (Barrett et al., 2021). Contourites are enriched in mud, and have occasional sands (Baeten et al., 2014; Batchelor et al., 2021; Bellwald et al., 2022b; 2024a). Turbidites and debris flows are sudden and quick processes, remobilizing sediment downslope including sharp erosive contacts. Contourites are rather inversely-graded, compared to the normally graded turbidites. Contourites can have classical mounded geometry (Rydningen et al., 2020), but can also be more sheeted (e.g., sand sheets in Bear Island Fan) and filling megaslide escarpments (e.g., North Sea Fan; Garcia et al., 2024). Contourites are formed by continuous and slow processes (compared to turbidites and debris flows) and accumulate as sediment mounds or drifts along-slope in a rather continuous trend with gradational internal grainsize changes (Rydningen et al., 2020; Batchelor et al., 2021; Bellwald et al., 2024a).

Boulders, cobbles and gravels dropped by meltout from icebergs (often referred to as ice rafted debris; IRD) are more commonly identified on the paleo-shelves but can also be deposited along the slopes of the NE Atlantic Ocean. Boulders are very few to absent on the slopes.

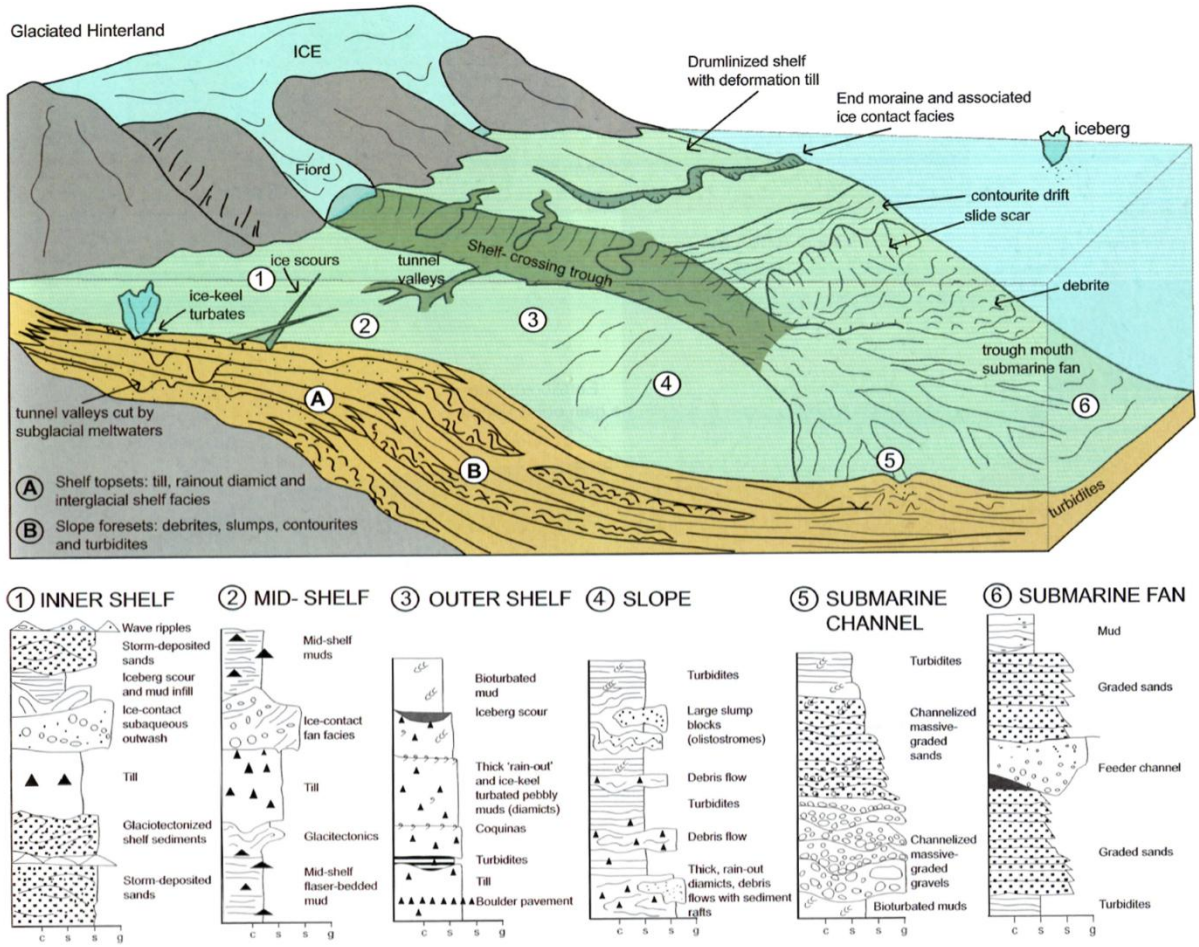


Figure 4.1. Cartoon showing the typical sedimentological characteristics associated with different proximities and relationships with the retreating ice sheet margin. Figure modified from Eyles and Eyles (2010).

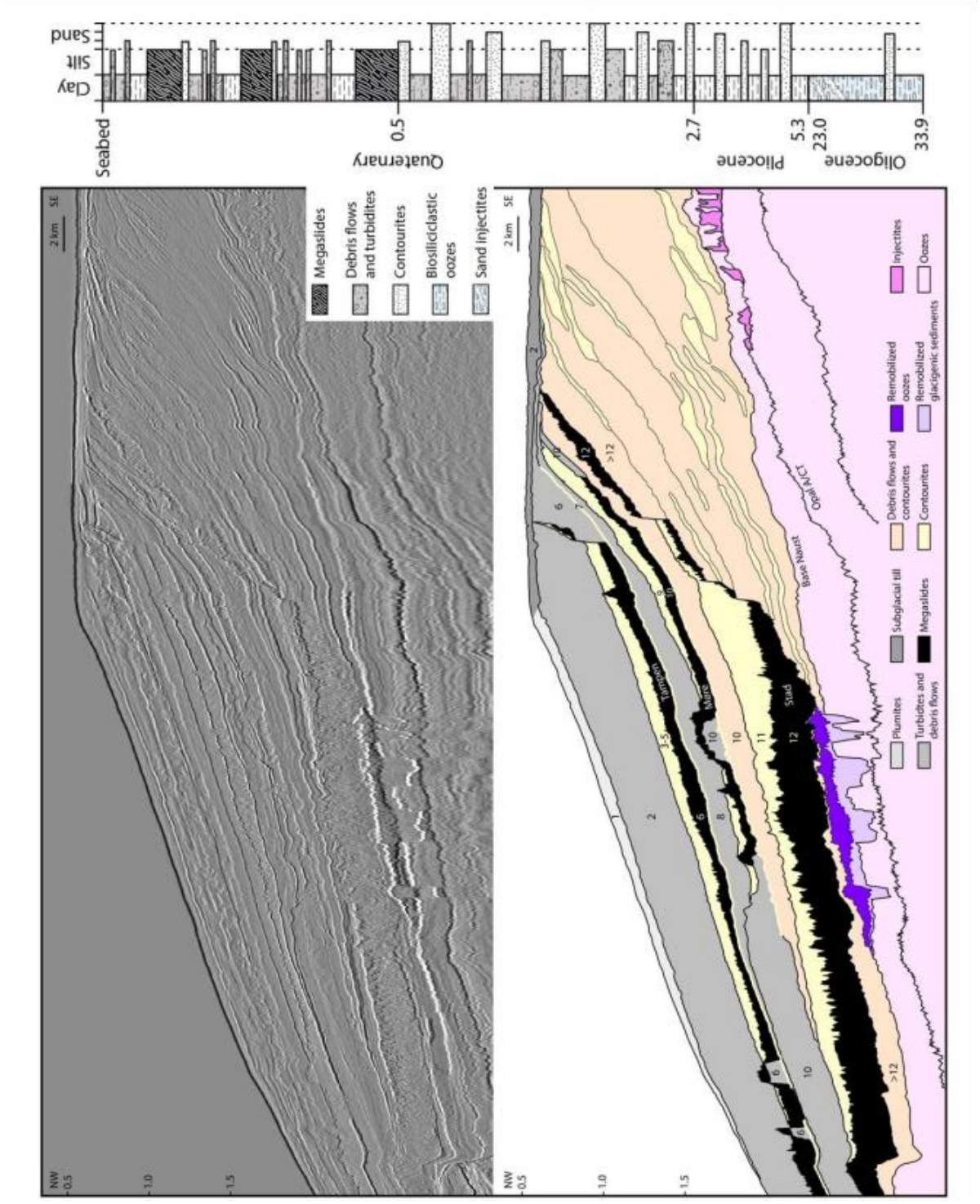


Figure 4.2. Stratigraphy and lithology of the North Sea Fan. Seismic profile across the fan with representative well log. Numbers indicate marine isotope stages (MIS) for different sedimentary units (updated from Nygård et al., 2005). Data courtesy of TGS.

Table 4.1. Typical sedimentological and geotechnical characteristics of the different glacial, deglacial, and interglacial facies observed along the glaciated European margins, and their potential engineering implications. Stage *indication based on likelihood of formation during an ice advance (Glacial), retreat (Deglacial) or Interglacial conditions. Facies description ordered based on their prevailing stage of formation (from glacial to interglacial). Wording in bold indicates main stage of formation, whereas wording in parentheses as potential stage when such facies can be formed but are less prevalent. *Oversteepening, sediment delivery, and location within source-to-sink system are key.*

Facies Type	Stage	Sedimentology and Structure	Geotechnical Characteristics	Engineering Implications
Till (e.g., traction, lodgement, and deformation)	**Glacial** (Deglacial)	• Contains a wide range of particle sizes, including clay, silt, sand, gravel, and boulders (often gravelly, matrix-supported clay). • Often unstratified and unsorted to poorly sorted. • Can show large variations over short distances. • May contain large boulders (erratics) and incorporated rafts of pre-existing sediments or bedrock • New and overridden sediments may contain faults and folds from cm- to km-scale.	• Generally, very low permeability, high density, variable strength (often very high to extremely high shear strengths). • Variable compressibility but often highly overconsolidated. • Can be highly heterogenous. • Traction till can be much softer compared to lodgement till. • Deformed tills have heterogenous properties.	• Challenging for construction due to potential inconsistency due to variable composition. • Difficult to excavate. • Requires thorough site investigation and may require ground improvement techniques. • Often challenging to map transition from till into weathered or competent bedrock. • Potential for boulders. • Lithology within tills can vary significantly.
Ice-contact (e.g., against ice margins)	**Glacial Deglacial**	• Range from till (e.g., potentially boulder-rich) to sorted sands, gravels, cobbles and even boulder beds/units. • Heterogeneous due to direct ice contact. • Show often evidence of deformation and compaction due to ice push. • Dimensions: Typically, more continuous parallel to the palaeo-ice margin and forming sets of distinctive discrete sediment belts or ridges. From 1m in height and width (for example small push moraines) up to 100s-1000m wide and 10s m high complex ice marginal systems deposited when ice oscillated/stagnated in one location for a longer time.	• Variable permeability. • Compressibility and strength dependent upon level of overconsolidation.	• Can provide excellent foundations, but variable strength requires thorough site investigation and potential ground improvement. • Challenging due to variable material properties and potential for encountering deformed layers.
Glacioaeolian	**Glacial** (Deglacial)	• Well sorted fine sands and silts, which can be homogeneous in extensive deposits. • Can show regular stratification and layering. • Shows often extensive sorting and rounding. • Loess covers: Mixed quarts and feldspar silt grade deposits	• Variable permeability. • Variable compressibility. • Strength can vary significantly.	• Poor foundation material due to potential for erosion, low strength and high compressibility. • Requires additional considerations for techniques and monitoring during construction.
Supraglacial	**Deglacial** (Glacial)	• Primarily coarse debris composed of a mix of poorly sorted particle sizes from clay to boulders. • Poorly stratified, chaotic; may have melt features.	• Low to moderate permeability. • Variable compressibility. • Variable strength due to heterogeneity.	• Often unstable, difficult to excavate and may require further considerations during site development.

		• Shows often evidence of debris flows.		• Requires extensive site investigation due to heterogeneity and potential instability.
Glaciofluvial	**Deglacial** (Glacial)	• Composed primarily of sands and gravels with minor silts and clays. • Stratified, cross-bedding, ripples and foresets. • Can show evidence of high-energy water flow. • Multiple, clear erosive surfaces. • Esker: Subglacial/englacial channel fill consisting of (sometimes sheeted) gravel, cobble and boulder-sized sediments and sands	• High permeability, good bearing capacity. • Low compressibility, high (low to very high) shear strength. • Has typically good drainage properties. • Eskers: Presence of boulders.	• Generally good foundation material due to good bearing capacity. • Requires assessment of stratification and compaction / degree of consolidation. • Stacked sequences of cut-and-fill is a challenge for ground models. • Eskers: Steep slopes, discrete, lateral variability, curvilinear and irregular zones of coarse sediment in ridges with steep slopes; cable trenching and pile driving may be difficult.
Glaciomarine	**Deglacial** (Glacial)	• Often composed of silts and clays with interbedded sands and gravels. • Can be laminated and may contain dropstones and ice-rafted debris. • May show evidence of tidal influences. • Can contain marine fossils and organic material.	• Variable permeability. • High compressibility and shear strength. • May have elevated pore water pressures. • Potential for gas hydrate presence.	• Variable properties requiring site investigation. • Potential instability from dropstones or gas hydrates. • Intercalation with impermeable layers can weaken shear strength if overpressured.
Glaciolacustrine and lacustrine	**Deglacial** (Glacial) (Interglacial)	• Sands, silts and clays, may contain dropstones. • Laminations or varves create regular stratification. • Organically enriched sediments and peats are likely to be associated with glaciolacustrine deposits	• Low permeability, low to medium strength if fresh, high or very high strength when dried out or overconsolidated. • High compressibility due to clay content. • Low shear strength and low densities. • Very high compressibility of organic rich sediments and peats when present within the sequence.	• Poor foundation material due to high compressibility and low shear strength. • Requires significant ground improvement. • Requires careful drilling and monitoring. • Variable strengths: From very soft/weak (soil-profile inversion in geotechnical terms) in their primary form to extremely hard and over-consolidated after being subject to subaerial exposure and drying or subsequent loading depending on site evaluation. • Possible issues with slope instability or unstable trench sides • Thermal properties of clays and organic rich strata may negatively impact installation process and power cable heat dissipation (high thermal resistivity) .
Turbidites	**Deglacial** (Glacial) (Interglacial)	• Well sorted, normal grading; consist of sand, silt, and mainly clay. • May have sharp basal contacts, rip-up clasts, and flame structures.	• High to moderate permeability. • Shear strength and compressibility varies depending upon the dominant grain size.	• Grading can impact load-bearing properties of the sediments. • Potential for reactivation of turbidity currents and further erosion and/or deposition.

Debris flows and slides	**Deglacial*** (Glacial*) (Interglacial*)	• Poorly sorted, deformed, and consist of sand, silt, and mainly clay, with occasional boulders. • Slide deposits often consist of reworked debris flows, including glaciogenic debris flows. • Can occur at a wide range of scales, including megaslides (e.g., Storegga).	• Low to very low permeability. • Chaotic structure, with random clast orientations leads to highly heterogenous properties. • May contain variable levels of pore water content. • Low shear strengths and high compressibility.	• High water content may promote further mobility and flow behaviour of deposited sediments. • Potential for further debris flows or slides in the source area need to be considered. • Deposited materials may prevent fluid migration and elevate subsurface pore water pressure.
Fluvial and deltaic	**Deglacial** **Interglacial**	• Well-sorted sands and gravels with interbedded silts and clays. • Structures may include cross-bedding, channel fills, and point bars.	• Permeability and compressibility depend on dominant grain size and sorting. • Moderate to high shear strength in coarser deposits.	• Generally good foundation material but surveying is required to map heterogeneity of deposits. • Potential for subsidence of finer grained overbanks.
Contourite	**Interglacial** (Deglacial)	• Typically consist of well-sorted clays, silts and fine sands. • Commonly exhibit lamination and bioturbation. • May show features such as graded or inversely graded bedding, indicative of fluctuating current velocities.	• Moderate permeability due to the well-sorted nature of the sediments. • Shear strength can vary depending on sediment composition and degree of consolidation.	• Structures built in areas with active contour currents need to account for erosion and sediment reworking. • Fine-grained layers within contourites can pose issues for slope stability and consolidation (forming weak layers).
Marine	**Interglacial**	• Typically consists of well-sorted fine-grained materials, dependent on distance from the coast. • Often display laminated bedding. • May contain bioturbation.	• Compressibility and permeability are grain size dependent. • Often show low degree of overconsolidation • Typically, homogenous clay/silt but may grade to sands closer to the coast. • High pore water content. • Low density	• Can have well known geotechnical properties that lowers site investigation requirements, but still requires study. • Structures may need to consider potential winnowing/erosion of marine sediments. • Can be issues with slope instability / unstable trench sides
Organic-rich sediments /Peat	**Interglacial**	• Decomposed plant material and organic matter. • Often displays a fibrous structure with visible plant remains, arranged in layers. • May contain inorganic/lithic materials.	• Generally, very low shear strength due to high levels of organic content. • Geotechnical properties vary depending on the magnitude of peat decomposition and compression.	• Potential for stored gases. • Possible settlement over time and unsuitable for heavy structures without ground improvement. • Low thermal conductivity (overheating of cables). • Low load bearing capacity (implications for cable trenching and installation process)
Periglacial	**Interglacial**	• Primary sediments altered by freeze-thaw cycles and permafrost processes. • Ice wedge casts filled downwards with sediments from overlying strata forming thermal contraction polygons	• Laterally heterogeneous sediment properties • Weakened primary rock/ sediment strength due to frost weathering • Overconsolidation due to drying of sediments in cold conditions	• Poorly predictable sediment properties and load bearing capacity. • Discrete zones of different engineering sediment properties within ice-wedge casts. • Base of frost-weathered zone may be difficult to identify from boreholes and geophysical data

1178

5. Geo-engineering constraints

A geo-engineering constraint is here defined as an existing, statistic ground feature that poses an engineering challenge and that is addressed by routine geo-engineering solutions (see also ISO 19901-10). Geo-engineering constraints are dominated by static features, landforms, and deposits, whereas geohazards are more dynamic processes that can affect these static features (Figure 5.1). Glacial deposits are thus geo-engineering constraints, but can develop into a geohazard when triggered and affected. However, if these constraints are identified, mitigation is in general feasible. For instance, shallow gas is a geo-engineering constraint as it is static.

This chapter reviews geo-engineering constraints characteristic for deglaciated continental margins. It is separated into sections related to fluids in the subsurface (Sections 5.1-5.3), effects of changes in grainsize distribution and lithology (Sections 5.4-5.7), the effect of weathering and presence of bedrock (Section 5.8), the presence of organic materials and peat (Section 5.9), subsurface features formed by tectonic processes (Sections 5.10-5.12), and glacigenic landforms (Section 5.13).

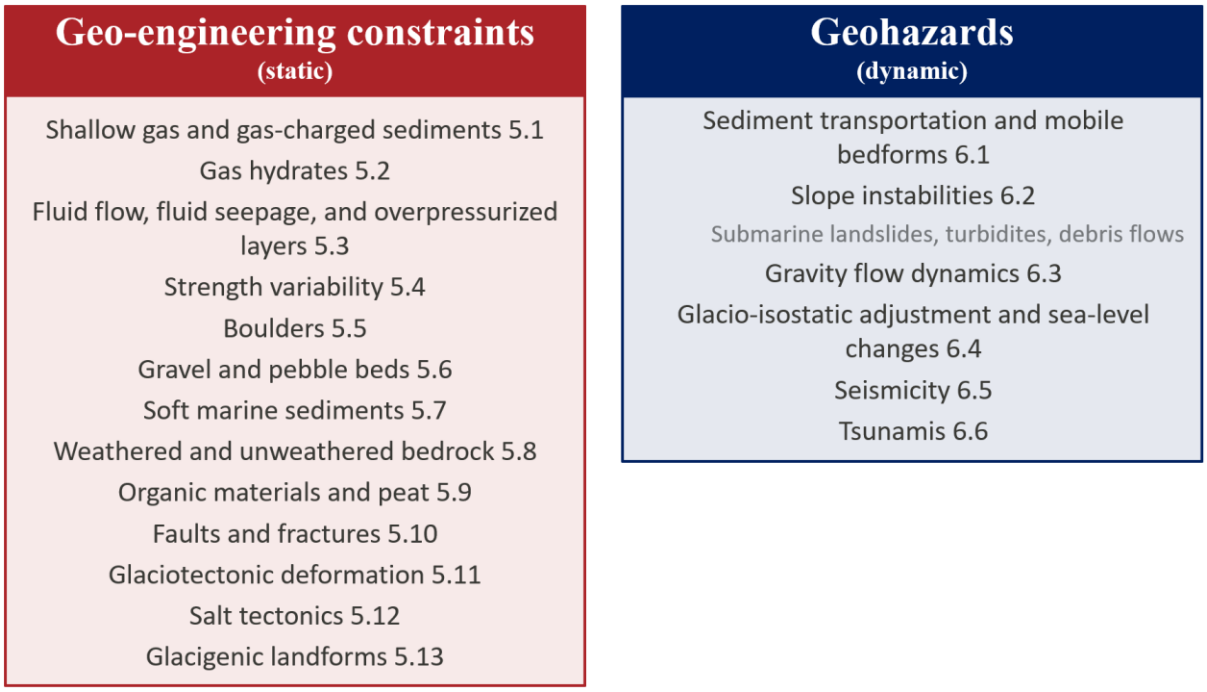


Figure 5.1. Geo-engineering constraints and geohazards along the glaciated European margins included in this review.

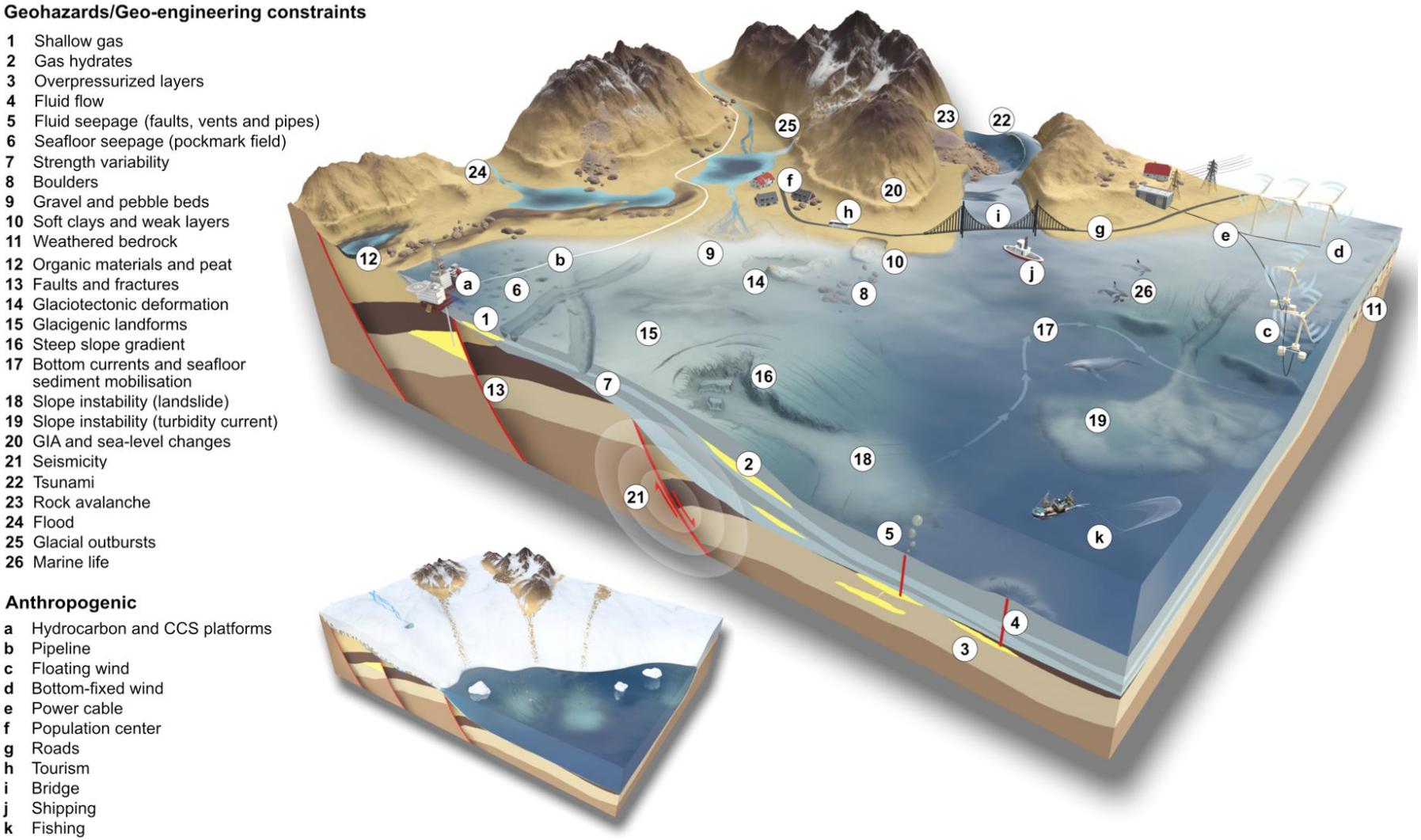


Figure 5.2. Conceptual sketch of geohazards and geo-engineering constraints along the glaciated European margins. Shown are the deglaciated margin (modern setting) in large, and the ice-covered margin during glacial maxima in small. CCS: Carbon Capture and Storage, GIA: Glacio-isostatic adjustment.

5.1 Shallow gas and gas-charged sediments

The presence of gas in the subsurface can have major implications for engineering behaviour of sediments and is considered a major constraint and, when triggered, hazard to offshore engineering projects, particularly in drilling operations (Davis, 1992, and papers therein). The term "Shallow Gas" is loosely defined as 'gas pockets or entrapped gas below impermeable layers at shallow depth' by the Norm ISO 19905-1:202, and is alternatively defined as 'gas-charged sediment occurring within the upper 1000 m of the seafloor' (Judd and Hovland, 2009). Gas observed on seismic data is frequently used to define various forms of gas presence. Notably, even low concentrations ranging from 0.5% to 2 % can result in significant seismic responses, such as acoustic blanking and turbidity (e.g., Schroot and Schüttenhelm 2003 and references therein; Morgan et al., 2012). However, in terms of risk to an offshore installation, not all gas poses the same level of threat. Therefore, to differentiate between gas that poses the largest threat in terms of safety, from other forms of gas presence, the following definitions are suggested in Table 5.1.

Table 5.1. Proposed definitions of shallow gas.

Low permeability gas	Defined as gas in low porosity and permeability sediments/ rock that does not have sufficient concentration to cause an amplitude response on seismic data but may appear as areas of acoustic blanking (turbidity) on sub-bottom profiler data (frequency of c. 3000 Hz and above).
Solution gas	Solution gas (sometimes referred to a "fizz gas") is defined as gas dissolved in water and hence not in the free gas phase and therefore undetectable on seismic data.
Shallow gas	Over-pressured free gas within a trap (structural or stratigraphic), which results in a significant increase in amplitude on seismic data. This type of gas is a serious threat to drilling operations if encountered when the well is in underbalance conditions.

Engineering Considerations

The primary risk, in terms of offshore drilling, is posed by significant accumulations of free gas that are over-pressured, but of insufficient pressure to fracture the overburden (shallow gas - Table 5.1). Hence, once drilled into, the overpressure causes a rapid influx of gas into the wellbore if the retaining pressure inside the wellbore is not maintained in equilibrium, or slightly overbalanced. This is generally not an issue when drilling at depth (beyond surface casing depth), as pressure within the well is maintained by drilling mud and secondly, mechanical methods for controlling pressure within the well can be employed if a sudden increase in pressure were to occur, e.g. the blowout preventor, which "shuts the well in".

However, in the shallow overburden (Top-hole), where Quaternary soils are encountered (e.g., Figure 5.3), the soils are too weak for the well to be "shut in" as the pressure within the wellbore would fracture the surrounding formation, and any chance of controlling the flow would be lost. Therefore, the internal

wellbore pressure must be controlled using drilling fluid to maintain pressure equilibrium. This can be achieved with sea water if subsurface pressures permit, but often drilling muds of higher specific gravity are required, which increase the cost of a drilling operation. The SINTEF Offshore Blowout Database (2011) provides a full history on Industry events from the 1950's through to the present day, many of which incurred tragic loss of life (e.g., West Vanguard platform blowout in 1985, Figures 1.1c and 1.2)

The use of high-resolution (HR) seismic data to identify shallow gas has been the Industry Standard since the early 1980's. Shallow gas is readily identifiable on seismic data as an anomalously high-amplitude, phase-reverse reflection (bright spot in clastic soils, see Figure 5.3). Other seismic indicators of the presence of shallow gas include velocity pull-down, polarity reversal, high-frequency attenuation, amplitude blanking (Figure 5.4) and a Class 3 AVO (amplitude-versus-offset) response. HR and EHR seismic provides the industry with a tool with which to evaluate risk and avoid or mitigate gas presence through well design and procedure, whereby 3D seismic gives better results for shallow-gas identification compared with 2D seismic (Figure 5.5). Shallow gas is still generally best avoided wherever possible.

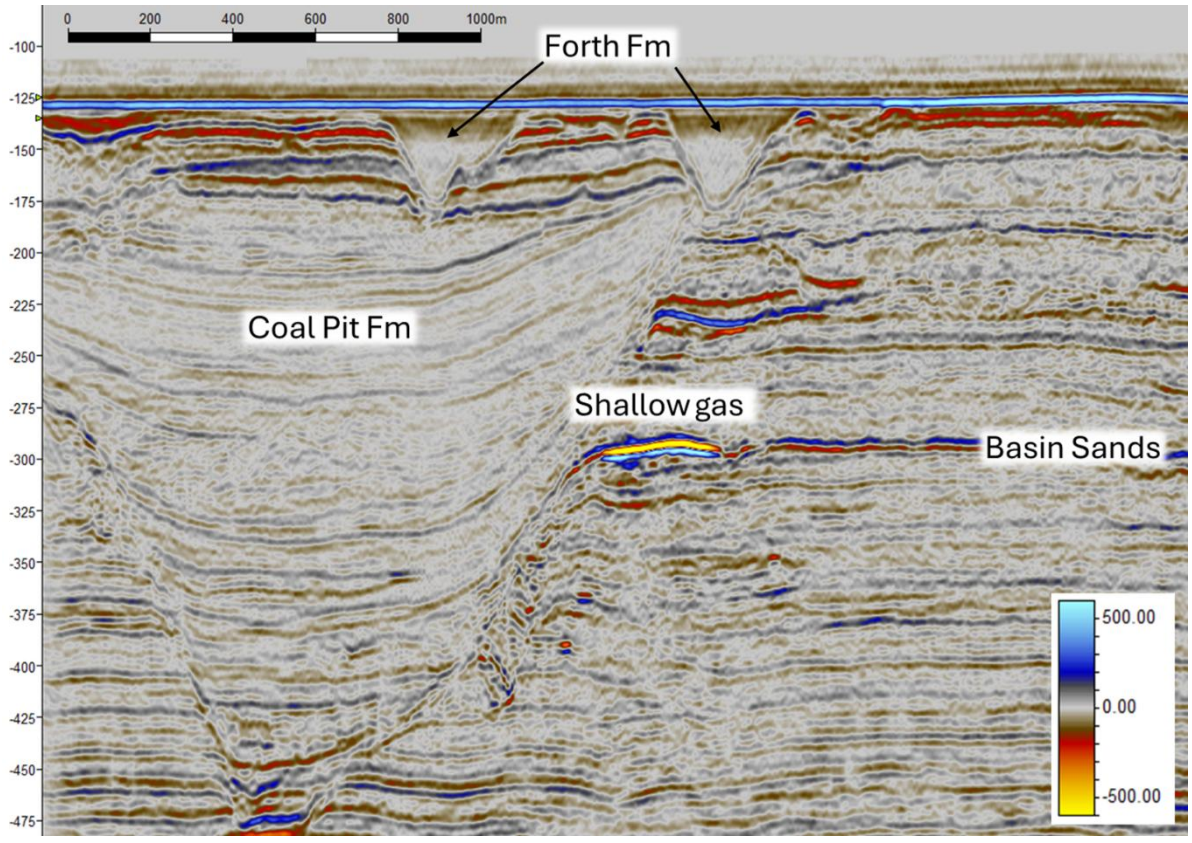


Figure 5.3. Example of a shallow gas accumulation trapped against a tunnel valley infilled by the Coal Pit Formation, Central North Sea. Courtesy of bp Plc. Shallow gas is here indicated as an anomalously high-amplitude, phase-reverse reflection. Scale indicates the strength (amplitude) of the reflection.

However, gas can exist in other states within the soil (see Table 5.1), and while not an immediate threat to a facility or its personnel, can influence long term integrity of structures.

Depending on the configuration of seismic data acquisition, low permeability gas may cause zones of acoustic blanking on sub-bottom profiler data (Figure 5.4) and while not a significant threat to Oil and Gas well drilling, can be an issue for geotechnical borehole drilling. There have been recorded incidents where gas has been brought to the drill floor through swabbing caused by temporary and local reductions in the borehole fluid and a disruption of the in-situ gas-fluid-soil equilibrium (Kortekaas et al, 2008). This can be challenging to mitigate for, especially in large offshore wind park projects, as this occurrence of gas can be widespread and unavoidable (e.g., in the Baltic Sea).

Not only is low permeability gas an issue for geotechnical drilling, but also for detailed mapping of the subsurface, and identification of other hazards, as the acoustic scattering and attenuation create areas of blanking, below which, all acoustic energy is lost, and no reflections are recorded (Figure 5.4).

Long-term exposure to low permeability gas, and gas in solution may be the cause of low state bubbling observed around Oil and Gas wells through channelling around the cemented casings and conductors. In extreme cases, this could lead to cratering around the conductor, loss of bearing capacity and well integrity. The same threat is posed to long term foundations such as deep piled structures, monopiles, and suction caissons/buckets.

So far, this section has dealt with the presence of biogenic methane gas. However, hydrogen sulphide (H_2S) is also a significant threat in certain environments and indications of H_2S have been noted in offshore wind sites around monopile foundations (Soraghan, 2016; Blumenberg et al., 2022). H_2S is colourless gas with the characteristic smell of rotten eggs in small concentration and becomes odourless in concentrations increase above 100 ppm. The gas is poisonous, corrosive, flammable and explosive in certain concentrations, and represents a significant risk to personnel, and long-term integrity of steel structures.

In the southern North Sea, soils with high-organic content typically led to increased sulphate reduction rates and higher concentrations of sulphide (e.g., Blumenberg et al., 2022). Under anaerobic conditions, such as in submerged peat (see Section 5.9), sulphate reduction produces hydrogen sulphide (H_2S), contributing to the anaerobic decomposition of organic matter. If there is evidence of H_2S and a concern of risk, H_2S concentrations in shallow marine sediments should be understood. As samples for H_2S concentration are not easy to obtain, a better understanding can be achieved by analysing sediment and pore-water chemistry. Such analysis helps assess anoxic conditions and the sediment's scrubbing potential. Generally, the presence of minerals like pyrite in sediments indicates H_2S generation and reaction with iron, while abundant iron-oxide-bearing minerals suggest low H_2S levels.

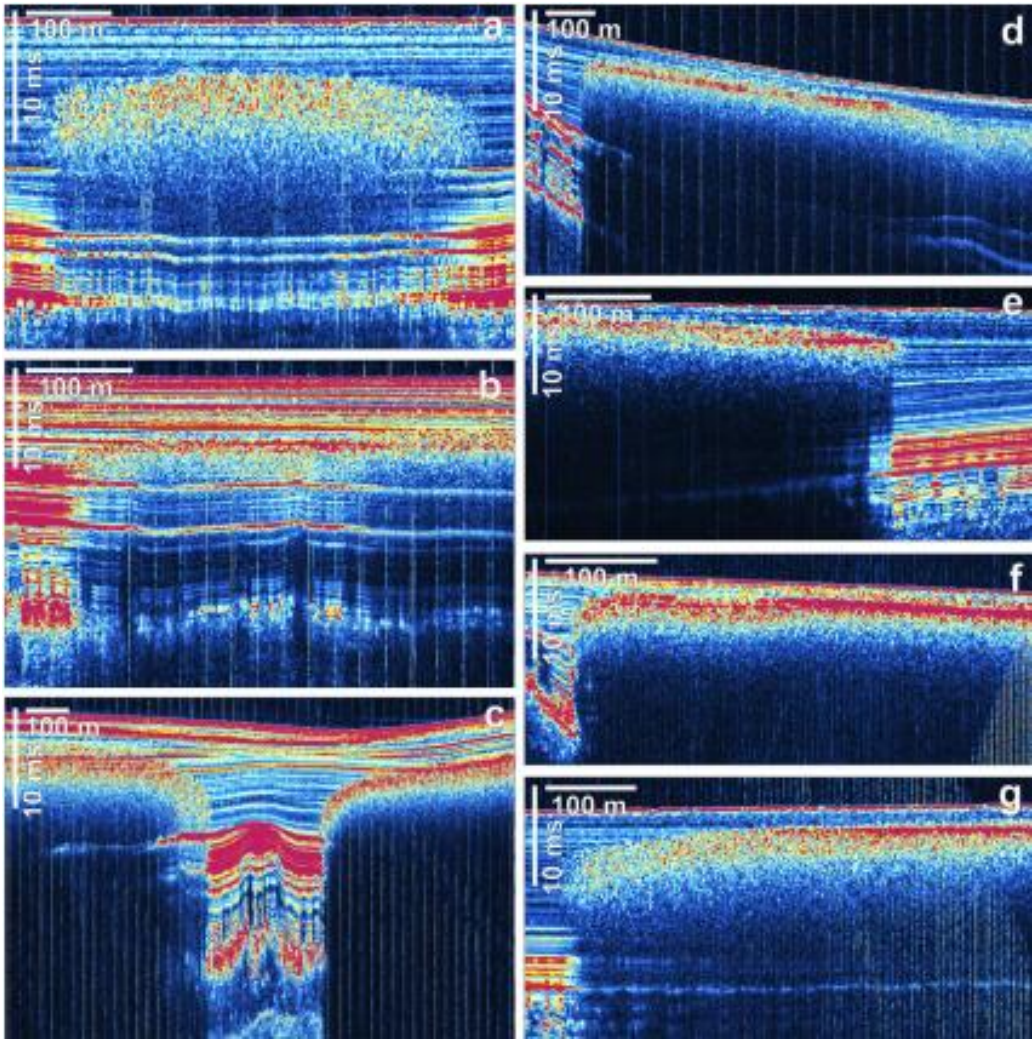


Figure 5.4. Shallow gas imaged with the Parasound sediment echosounder (SLF 4.3 kHz, envelope display). Gas bubbles in the Holocene mud appear as a patch or layer of point scatterers with highly variable amplitudes, and they cause acoustic blanking as the scattering in the gassy layer disrupts the sediment layering. From Tóth et al., 2014a.

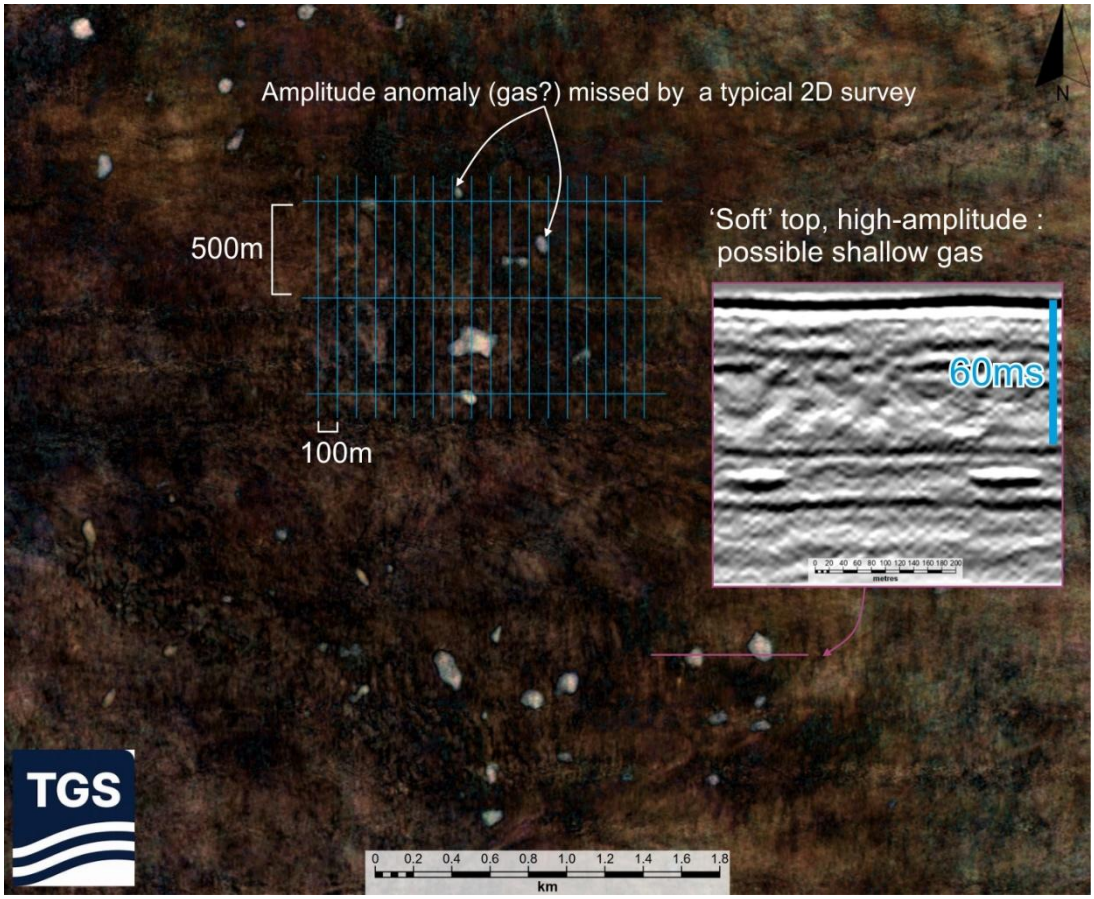


Figure 5.5. 3D high spectral decomposition time slice showing small high-amplitude, soft-topped seismic anomalies interpreted as shallow gas accumulations. Note small size of gas 'speckles' making them challenging to image by conventional 2D UHRS/ EHRS survey. Data courtesy of TGS

5.2 Gas hydrates

Gas hydrates are solid compounds of water molecules encaging molecules of natural gas (example in Figure 5.6). Although methane hydrates are the most widespread type of hydrate in continental margins, any gas derived from chemical and biochemical processes within the sedimentary column (i.e., hydrocarbons and non-hydrocarbons, organic and inorganic) can form hydrates. Depending on the size of the molecular cages and their crystalline structure, natural gas hydrates have been classified into: type I, can trap methane, ethane and molecules with comparable diameter such as CO_2 and hydrogen sulphide; type II, in addition to methane and ethane can trap larger-order hydrocarbons, e.g., propane; and type H, the least commonly observed in nature (and perhaps the least understood) can have cages even larger than type II (Sloan, 1998a; 1998b). Natural gas hydrates are found in continental margin settings at combined low temperatures and high-pressure conditions, with factors such as salinity and gas saturation and composition also controlling their stability (Kvenvolden, 2000).

The theoretical stability of gas hydrates can be estimated using relationships between geothermal gradient, bottom water temperatures and pore pressures at specific depths for given salinities and gas compositions (e.g., Sloan and Koh, 2007). In nature the presence of hydrates can be confirmed by sampling in sedimentary cores (Figure 5.6b) but also based on various geophysical and geochemical observations (e.g., Minshull et al., 2020):

1) One of the most straightforward indications of gas hydrate in the sediment is the presence of bottom simulating reflections (BSR) in seismic data at the approximate depth of the theoretical base of the gas hydrate stability zone (e.g., Hyndman and Spence, 1992; Figures 5.7a and 5.7b). Provided suitable seismic resolutions and survey orientations, a BSR is typically a high-amplitude reflection, characterized by a reverse polarity, with respect to the seafloor reflection, and in dipping layer settings it appears as a cross-cutting reflection (Figures 5.7a and 5.7b). Gas hydrate may be present even if a BSR is not observed in seismic data (i.e., the strength of the BSR reflection is mainly controlled by the accumulation of small amounts of free gas under lower permeability gas-hydrate bearing layers; Figure 5.7a). However, the presence of a BSR implies that hydrates are present and acting as a seal for upward migrating fluids. A free gas zone (often reaching tens of meters) develops under the BSR in settings with substantial gas generation or migration (e.g., Hornbach et al., 2004; Figure 5.7c);
2) Observation of vertical fluid migration pathways and associated seafloor pockmarks and authigenic carbonate mounds, can often indicate gas hydrate related past methane seepage events (Figure 5.7a; see also Figure 5.11 in following section). When the gas hydrate stability zone is known, high interval P- and S-wave velocities (measured from multi-channel seismic data and/or ocean bottom seismometer experiments) and high resistivities (measured using controlled source electromagnetic methods), can be used as indicators of gas hydrates and methane-derived authigenic carbonate accumulations within vertical fluid pathways and sub-seabed faults and fractures (e.g., Goswami et al., 2015; Singhroha et al., 2020);
3) Cone penetration tests (CPTU) integrated with seismic velocity analyses allow identifying gas hydrate bearing layers (i.e., often characterized by low density and high excess pore pressures upon penetration). The presence of authigenic carbonates commonly associated with focused fluid flow, seepage and gas hydrate dynamics may be also identified as anomalously low pore pressures, (i.e., in cases where fluids dissipate easier through higher permeability areas in the sediment surrounding the carbonates (e.g., Sultan et al., 2007).
4) Often, the presence of a clear methane-sulphate transition zone (MSTZ), indicates how much methane reaches the seafloor. A several meters deep MSTZ indicates that low amounts of methane reach the seafloor and therefore limited gas hydrate accumulations can form. Similarly, high salinity inhibits gas hydrate formation and anomalously low salinities in the pore water may indicate gas hydrate dissociation (e.g., Paull et al., 2005).

In glaciated continental margins, the stability of gas hydrates has been significantly affected by both temperature and pressure relevant processes associated with ice-sheet dynamics (e.g., the advance and retreat of large ice-masses, significant erosion of pre-glacial strata, increased sedimentation rates in catchment zones, crustal uplift and subsidence, fracturing, fault reactivation, among others). For example, large craters (< 1 km wide) in the Bjørnøyrenna trough in the Barents Sea (Figure 5.6b), have been suggested to be an expression of massive blow outs triggered by abrupt pressure changes following ice-sheet retreat after the LGM (Andreassen et al., 2017). Both microbial and thermogenic gas tend to migrate to the shallow subsurface and accumulate beneath gas-hydrate bearing sediments over millions of years, forming what is known as the free gas zone (e.g., Plaza-Faverola et al., 2012). Ice sheets keep the stability of these systems. However, upon ice-sheet retreat, gas hydrate may dissociate and the interactions with the associated free gas may lead to sediment deformation, fracturing, vertical fluid migration and seafloor expulsion (e.g., Forsberg et al., 2007). In addition, intervals of increased sedimentation along the continental slopes (e.g., glacigenic debris flows along the mid-Norwegian margin) can lead to basal gas hydrate dissociation events via a relative shift of gas hydrate bearing strata out of the base of the GHSZ that sustain fast vertical fluid migration (i.e., leading to pipe formation and seafloor pockmarks (Karstens et al., 2018; Plaza-Faverola et al., 2012). Post-glacial subsidence and uplift is another mechanism that leads to sub-seabed deformation and destabilization of gas hydrates and associated free-gas accumulations (e.g., Wallmann et al., 2018).

On the upper continental slopes, the GHSZ pinches out at the seafloor (landwards) and forms the feather edge. The spatial location of this zone varies but it lays at water depths usually around the shelf break. The extent of the GHSZ is particularly sensitive to ocean warming, both locally and regionally, and at various scales (i.e., seasonal and diurnal as well as long term changes). Whilst relative sea-level changes typical of glacial-interglacial transitions has a more regional impact on gas hydrate stability. Multiphase fluid flow models from the west-Svalbard margin show that present day gas seepage at the feather edge can be sustained by temperature-controlled gas-hydrate dissociation in the recent past (Trivedi et al., 2023). These episodes of recent gas hydrate dissociation have an impact on the pore water salinity and likely on the sediment hydromechanical properties.

The Norwegian Channel running from Skagerrak along the Norwegian coastline into the North Atlantic Ocean contains numerous pockmark fields (e.g., Troll field; see Chapter 5.3). Investigations of the pockmarks around the Troll hydrocarbon field have not revealed presently active pockmarks. However, these pockmarks have formation ages corresponding to the climatic amelioration at the end of the last ice age and are believed to have formed by gas from decomposing gas hydrates (Mazzini et al., 2017; Mazzini et al., 2016; Forsberg et al., 2007).

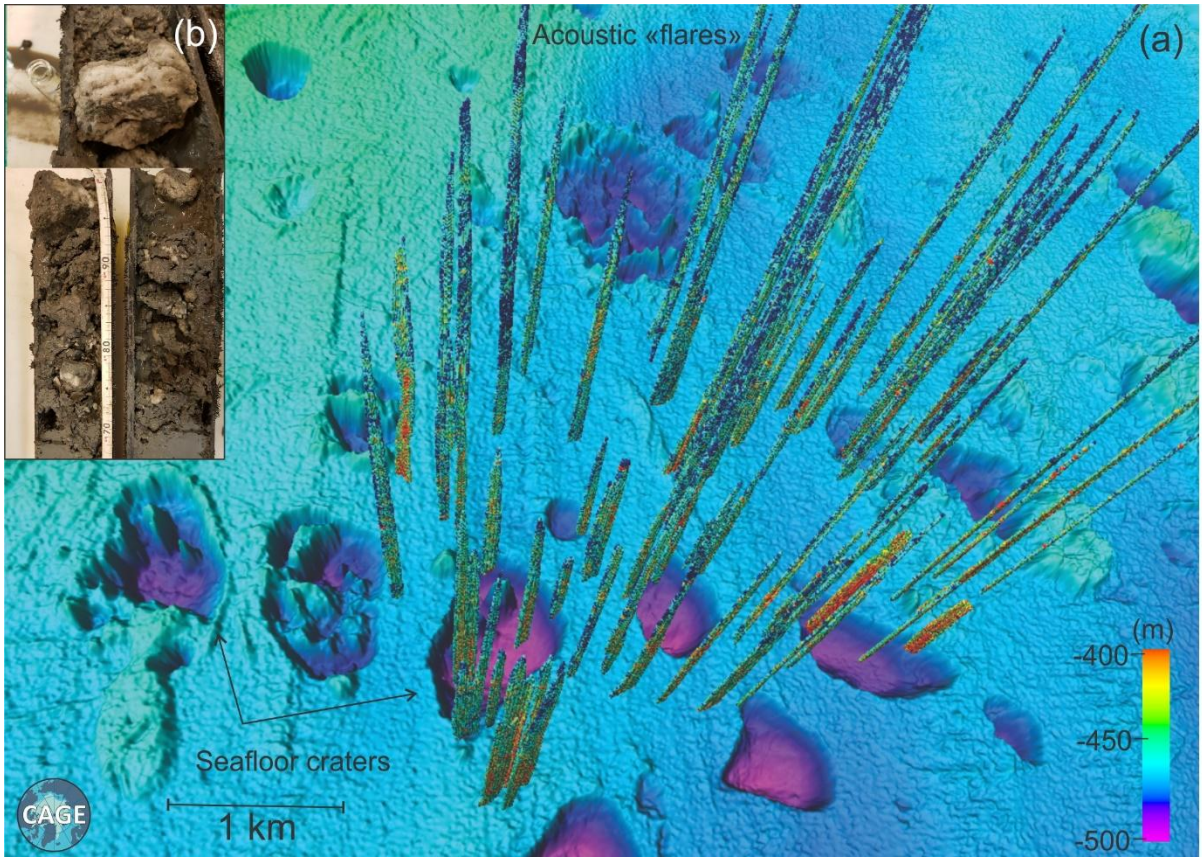


Figure 5.6. Gas hydrates related fluid dynamics on the shelves of the Arctic. **a)** Bathymetry data from Bjørnøyrenna/Barents Sea collected with ship mounted multibeam on board R/V Helmer Hanssen. The data show kilometer scale seafloor craters suggested to be caused by abrupt collapse of gas hydrate charged sediment upon ice-sheet retreat during the Last Glacial Maximum (Andreassen et al., 2017). Gas bubbles in the water column are indicated as vertical anomalies in hydroacoustic data and referred to as acoustic "flares" in the literature; **b)** Inset showing an example of gas hydrate accumulations retrieved within the upper 2 meters of sediment in a sediment core collected off the west-Svalbard coast. The presence of sub-seabed gas hydrates and methane accumulations in fine-grained sediment have been documented as direct sampling and as pressure and temperature pulses in piezometer data (Sultan et al., 2020).

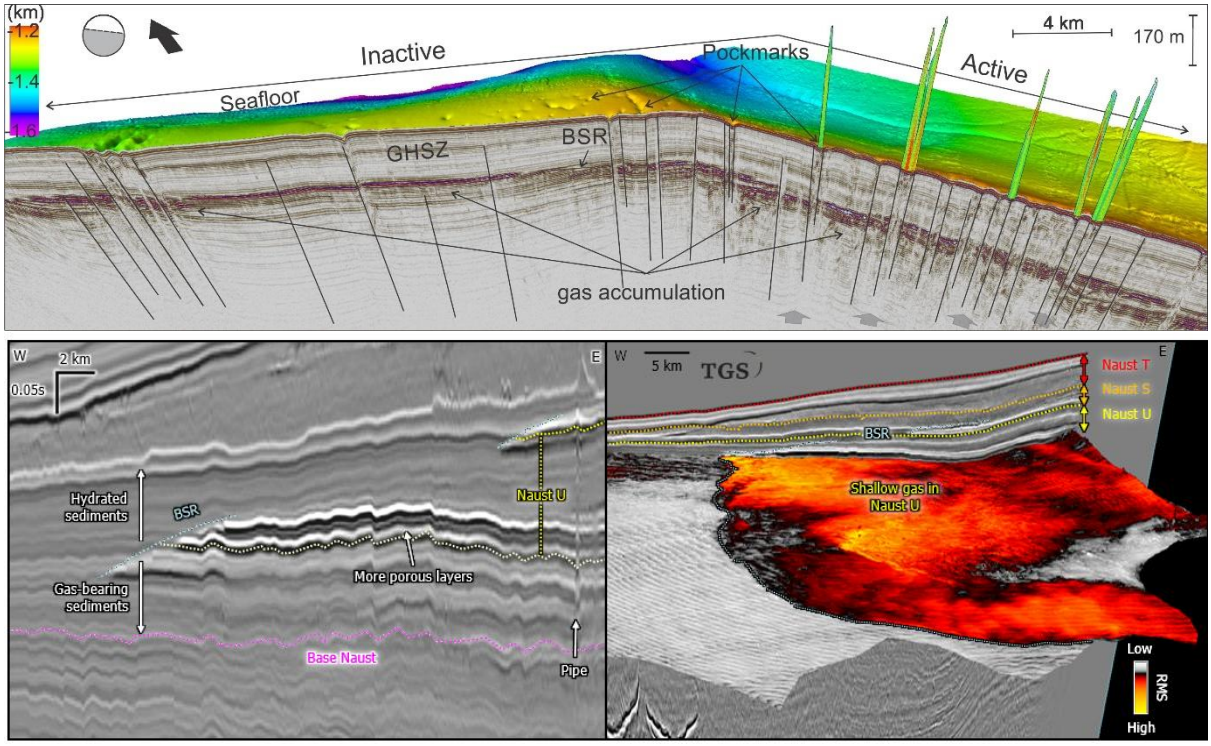


Figure 5.7. Gas hydrates, shallow gas, and fluid flow as expressed in seismic data. **a)** Composite 3D image of a deep marine gas hydrate system offshore west-Svalbard, the Vestnesa Ridge (from Plaza-Faverola et al., 2017). The gas hydrate stability zone (GHSZ) in this area is 160-200 m thick and its base is characterized by a well-defined bottom simulating reflection (BSR) in seismic data. A free gas zone (tens of meters thick) has developed over geological time through accumulation of upward migrating thermogenic gas as well as in-situ generated microbial gas. Widespread seafloor pockmarks and associated authigenic carbonate indicate gas release over geological time scales. Today only a few pockmarks are still releasing gas via advection through open cracks possibly regulated by changes in the glacial stress regime (e.g., Vachon et al., 2022). **b)** Example of a typical BSR cross-cutting the stratigraphic layers (here contourites within Naust Unit U), and associated free gas accumulation from conventional 3D seismic data from the mid-Norwegian margin, north of the Storegga Slide (modified from Bellwald et al., 2022b). Strong seismic amplitudes represent stratigraphically-bound, gas-charged layers. **c)** The Naust Formation and its units are characterized by glacimarine sediments. The surface shows the RMS amplitude within the Naust U sub-unit. The BSR limits the western extent of the gas-charged layers (modified from Bellwald et al., 2022b).

5.3 Fluid flow, fluid seepage, and overpressurized layers

Overpressure in sedimentary basins is caused by disequilibrium between compaction and sedimentation. In different settings, overpressure can be attributed to sedimentation outpacing the ability of low-permeability strata to evacuate physical and chemical compaction-derived fluids, and/or from hydrocarbon generation or rapid tectonic or glacial loading and unloading (Figure 5.8).

Overpressure can thus happen at numerous time- and spatial scales, from bed-scale to the scale of multi-km of overburden deposited over tens of millions of years.

In the context of the glaciated European margins and the North Sea Basin, all of these factors are significant and sediment wedge deposition during the Quaternary (e.g., Lamb et al., 2018) is particularly important in providing a permanent load, tilting of the basins by very localised and (geologically-speaking) very quick sedimentation (>1km accumulated at >1mm/yr), on top of sequences characterised by much slower sedimentation (<0.1mm/yr; e.g., Bellwald et al., 2024b). The presence of petroleum systems, reservoirs and effective seals has resulted in a prominent pressure cell in the central North Sea and locally along the Norwegian margin (e.g. Evans et al. 2003; Morency et al. 2007; Vejbæk 2008; Lamb et al. 2018; Løseth et al. 2022).

The presence of pressure disequilibrium leads to flow in cases where the system is open and may lead to catastrophic seal-breach where a system is effectively closed, and the fracture gradient is exceeded (Figures 5.8 and 5.9). Seal-breach may manifest itself as seepage or catastrophic depending on the depth of the pressure compartment and the rheologies involved in the sealing and the pressurised layers (Figure 5.10). Some of the most spectacular geology in the world results from catastrophic seal breach, including mud volcanoes, sandstone intrusions, blow-out pipes and pockmarks, which can range from metric to kilometric scales (Figures 5.8, 5.9, 5.10, and 5.11; Van Rensbergen et al., 2003; Judd and Hovland, 2007; Huuse et al., 2010). Smaller-scale pockmarks are often widespread and seen in abundance in fine grained units, suggesting they may be related to de-watering and/or very shallow de-gassing triggered by sea-level changes whilst larger pockmarks may represent cross stratal fluid conduits, evacuating fluids, often gas, from deeper levels (Judd and Hovland (eds) 2007; Böttner et al. 2019; Figures 5.10 and 5.11).

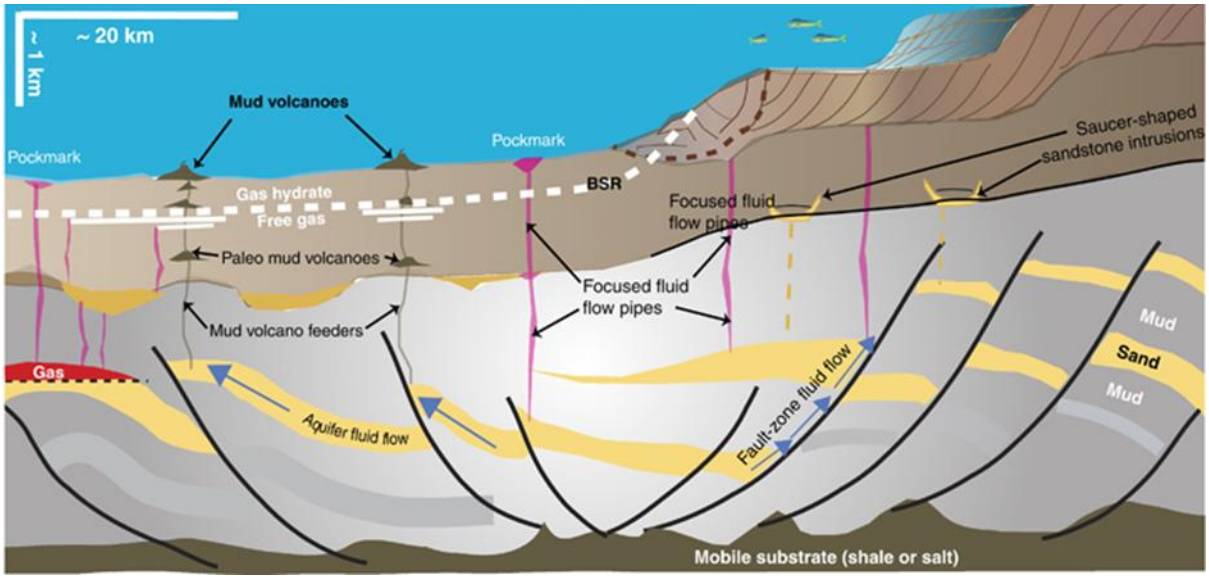


Figure 5.8. Fluid flow in basins can take many forms and are a function of tectono-stratigraphy, rates of subsidence, nature of sedimentation, sediment porosity and permeability through time and modified

during burial, diagenetic processes and triggered by external factors such as glacial loading and unloading, earthquakes, tilting, and human interventions such as drilling (Huuse et al. 2010).

Processes involved in fluid flow and blowouts can be subdivided into primers and triggers, many of which can happen on different magnitudes and time scales and thus can sometimes be considered both primer and trigger. Primers include deposition, erosion, compaction whereas triggers may include tectonics, diagenesis including oil and gas generation, silica diagenesis at shallow burial and smectite-illite transformation and quartz cementation at few km burial. These processes release significant volumes of water from the sedimentary column and are thus implicated in overpressure generation at depth whenever the fluids encounter barriers to fluid flow.

In the Quaternary stratigraphy of the European margin, the most common features related to fluid flow, fluid seepage, and overpressurized layers are: i) gas flares in the water column (Plaza-Faverola et al., 2017; Serov et al., 2023; Figures 5.6 and 5.7), ii) pockmarks at the seafloor and within the buried stratigraphy (e.g., Judd and Hovland, 2007; Böttner et al. 2019; Tasianas et al., 2018; Figures 5.10 and 5.11), iii) chimneys vertically crossing to modern and paleo-seafloors (e.g., Hustoft et al., 2009; Figure 5.10); and iv) remobilized ooze mounds at multiple Quaternary stratigraphic levels with associated evacuation craters at the Base Quaternary (e.g., Riis et al., 2005; Bellwald et al., 2024b). A summary of fluid-flow phenomena is shown in Figure 5.9 (Andresen, 2012). The identification of fluid-flow related landforms increases the understanding of shallow fluid migration paths and mechanisms, which ultimately contributes to reduce risks associated to blowouts and changes in soil strength (Prins et al., 2025).

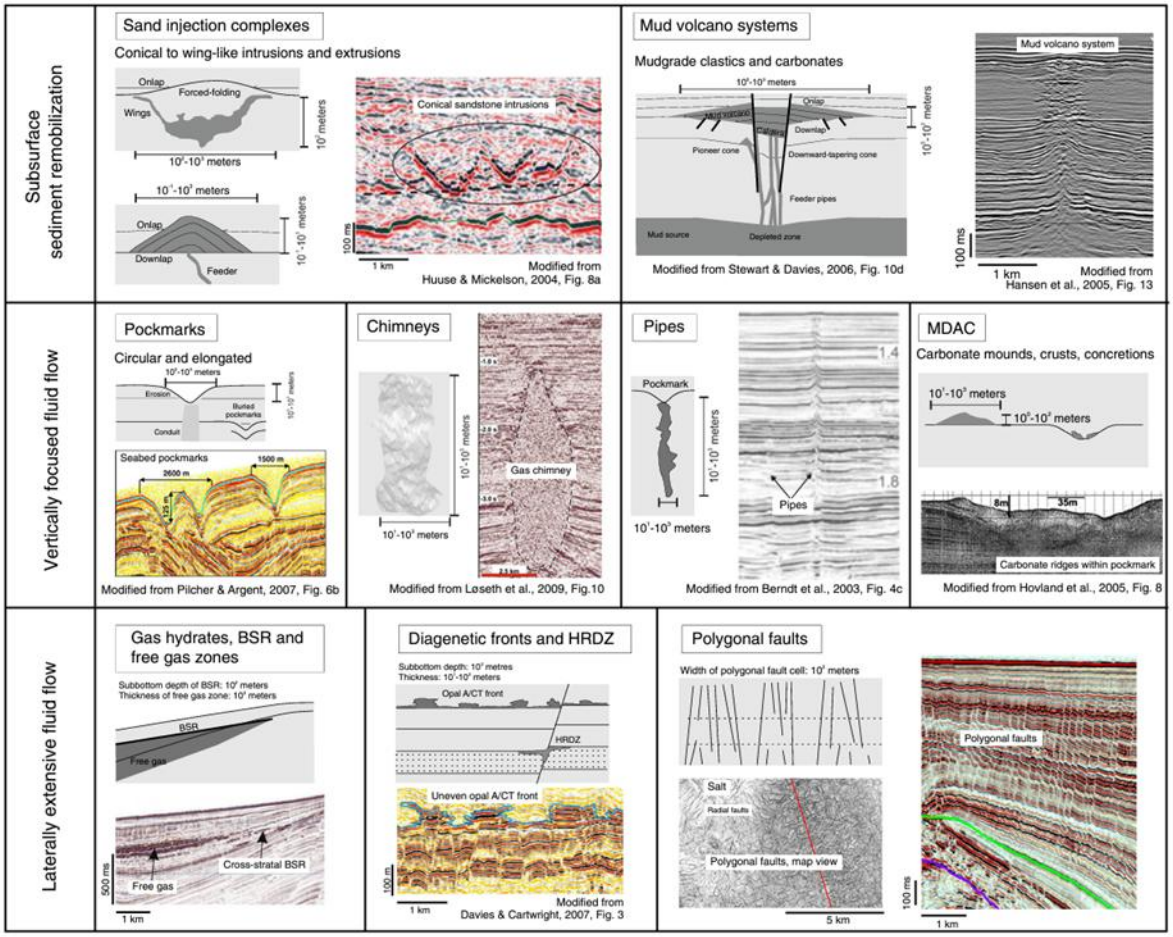


Figure 5.9. Fluid flow phenomena in seismic data (Andresen, 2012).

Fluid flow and human activity

The drilling of a borehole for geotechnical testing, insertion of monopiles for wind turbines or wells exploring explore for petroleum, geothermal or storage space would be considered a triggering process due to their highly invasive nature, perforating sealing units and connecting reservoirs/aquifers at different levels and to the surface. This connection between reservoirs at various stages of overpressure and with different degrees of lateral transfer of pressure due to reservoir dip and any ongoing diagenetic processes can cause internal and external blowout and fluidisation of unconsolidated aquifers, potentially leading to the eruption of sediments (e.g. Davies et al. 2007). Evacuation of excess fluids can lead to rapid compaction and seafloor subsidence (as seen on top of some producing North Sea fields) whilst evacuation of sediments can lead to subsurface cavity formation and collapse as seen around active mud volcanoes (Stewart and Davies 2006) and in association with deep-seated submarine landslides (Bull et al. 2009).

Pressure connections notwithstanding drilling can also cause release of non-aqueous fluids, dissociation of gas hydrates, and drilling associated events can lead to knock-on effects including landslides and blowouts.

The hazards associated with fluid flow and triggering by human intervention are undergoing a significant change from petroleum fluid extraction and produced water injection towards widespread installation of wind turbines, affecting the top 100-200 m of the seabed and large-scale injection of CO_2 which in some cases will cause pressure waves in aquifers and in the case of depleted fields, may cause whole-scale uplift of the overburden. The latter effects may open new connections and could also destabilise legacy boreholes and cause cross-stratal fluid flow in ways not experienced previously. There is a strong need for monitoring to detect and action any evidence for such fluid flow and much of the associated equipment will be deployed in near-surface environments. Any interventions would need to be quick and effective and could lead to unexpected fluid flow phenomena (see also Figure 1.3).

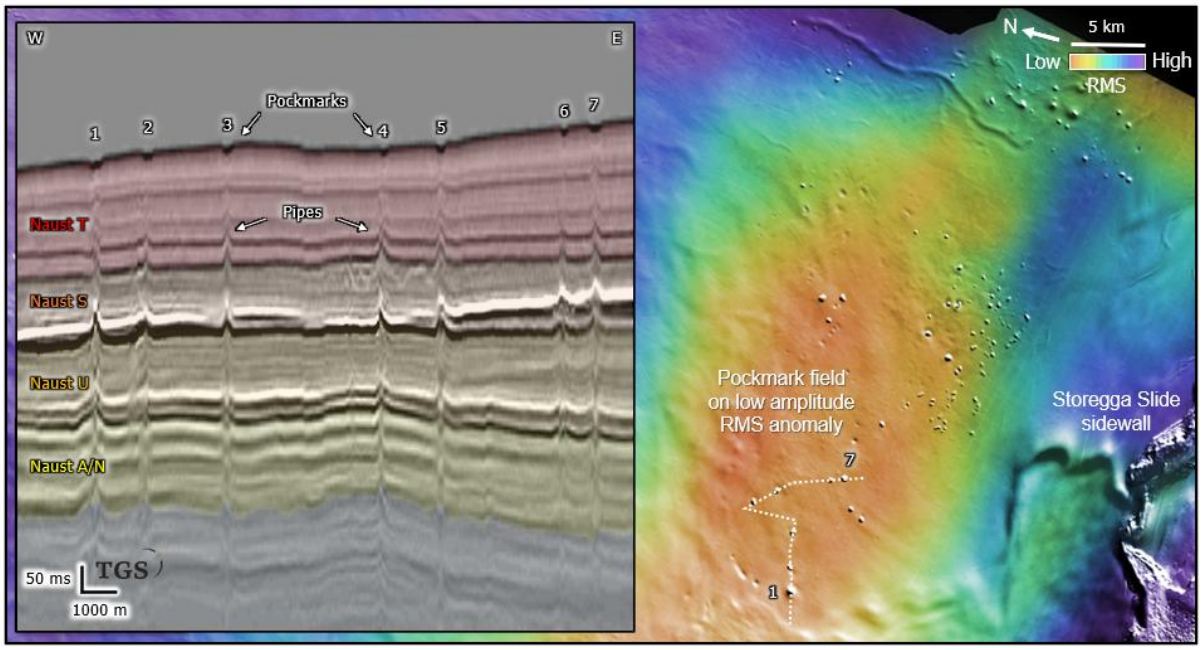


Figure 5.10. Fluid flow along the mid-Norwegian margin. **a)** Association between indications of fluid escape features in the Quaternary and the seabed, and gas hydrates in the subsurface. Seismic profile showing the subunits of the Quaternary Naust Formation and pipe structures crossing a BSR (black arrow). **b)** Structure map of the seabed blended with RMS amplitude of the Naust S subunit. Pockmarks at the seabed correlate with low RMS amplitudes of Naust S sub-unit and pipes in the subsurface data. Data courtesy of TGS.

The formation of pockmarks is often concluded to be triggered by fluid release, i.e. gas hydrate dissociation (Hovland et al., 2002; Forsberg et al., 2007; Mazzini et al., 2017; Tasianas et al., 2018). High-resolution bathymetric examples from the Troll field in the Northern North Sea (Mazzini et al., 2017; Figure 5.11) and high-resolution 3D seismic interpretation of the seafloor of the Snøhvit field in the Southwestern Barents Sea (Tasianas et al., 2018) show different types of pockmarks: i) Larger, but fewer "normal pockmarks" c. 100 m wide and c. 10 m deep (e.g., Septagram on Figure 5.11), and ii) smaller, but more numerous "unit pockmarks" (Hovland et al., 2002) some 10s of meter wide and c. 1 m deep (e.g., numerous points on Figure 5.11). Pockmark fields as locations of focused fluid seepage

are often associated to habitats formed by chemosynthetic organisms using methane and precipitating authigenic carbonate, and may thus present issues due to marine habitat protection (e.g., Noble-James et al., 2020; Prins et al., 2025). ROV footage shows that pockmarks are refuges for marine benthic biodiversity (Figure 5.11c; d; Webb et al., 2009). Although mentioned as the most common trigger mechanism for pockmark formation, processes causing these depressions may not always relate to fluid release (Krämer et al., 2017), and remain unclear in some cases (Böttner et al., 2024).

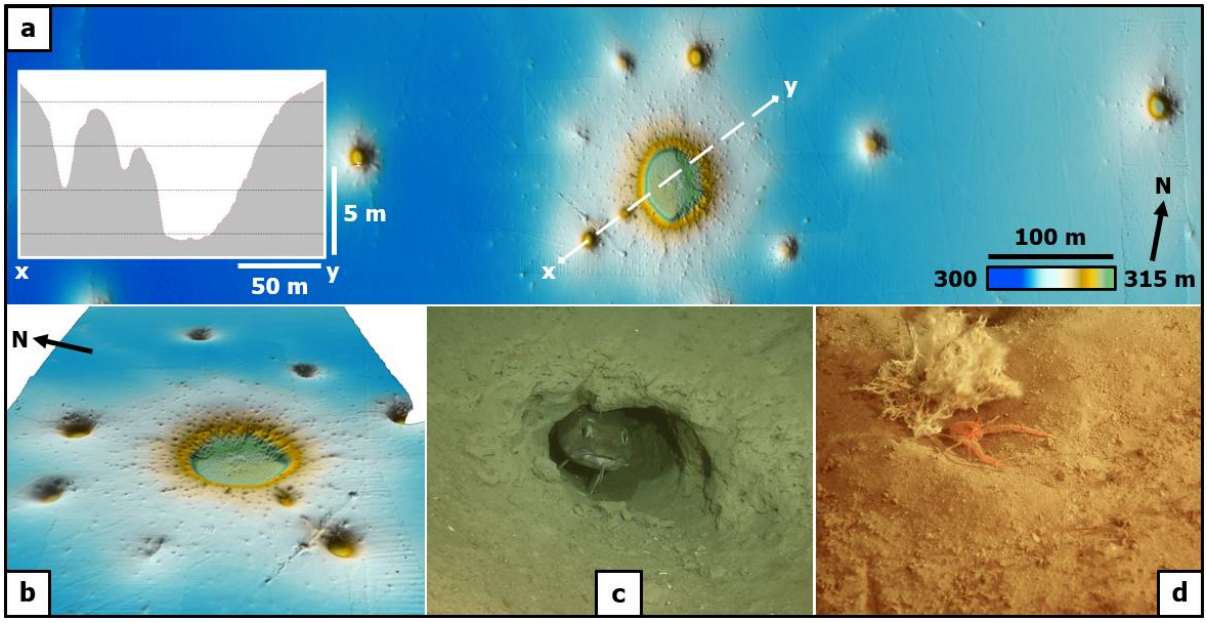


Figure 5.11. Pockmarks on the seafloor of the Troll hydrocarbon field. **a)** Example of high-resolution bathymetry (0.2 m resolution) of the Septagram pockmarks with profile across different types of pockmarks. **b)** 3D view into the Septagram pockmarks. Note the numerous smaller dots referred to as unit pockmarks. **c+d)** Marine life identified in the Troll pockmark field. Data courtesy: Equinor.

5.4 Strength variability

Soil strength can be defined as how much shear stress a soil can withstand without deformation or failure. In the simplest description, low strength soils are easily deformable, whereas high strength soils are more resistant to deformation. Strength variability is a product of multiple factors; the physical makeup of soil particles (in terms of grain size, grain shape, and proportions of different grain sizes, and type of grains), and the stress history of the soil (what the soil has gone through, since it was deposited). Soils in glaciated environments can have a very complex stress history, and as such can be extremely laterally and vertically variable (see Chapter 5.13).

Consolidation specifically refers to the volume of water and physical particles within a soil and how these change over time. Soils that are experiencing the same loads in the past as they are currently experiencing, for example, recently deposited soils, are normally consolidated. Soils which have previously experienced loading which has subsequently been removed are over-consolidated (e.g.,

subglacial traction tills). Under-consolidated soils can be described as soils which have had a load applied, but there has yet been insufficient time for pore water pressures to equilibrate. Depending on the type of soil, consolidation can take a very long time, sometimes hundreds of years to fully equilibrate, assuming no other changes to the load applied on the soil.

The three main stages of consolidation are: immediate settlement, where a soil fills a space without any change to the volume of water; primary consolidation where water in voids and pore spaces is expelled; and secondary consolidation where the physical grains undergo deformation. Whether or not a soil will behave in a plastic or brittle manner lies beyond the scope of this paper.

Soils deposited or modified in glacial or periglacial environments have both a complex depositional setting, sometimes over very short time periods, with variations in grain size, type and water content, and complex post-depositional stress history. Much of north-west Europe has experienced repeated glacial and interglacial cycling and therefore over short lateral and vertical distances, soils can have very different geotechnical properties (Figures 5.12 and 5.13). These soils are often over-consolidated but under-consolidated soils also exist.

Over-consolidated soils can occur in formerly glacially effected environments in three key settings: i) Soils that have been loaded directly by ice cover from above, such as subglacial tills; ii) soils that have been loaded regionally by nearby ice (indirect ice contact), such as on the margins of ice sheets or glaciers but not directly covered, as is exhibited in late-glacial glaciolacustrine sediments on the Dogger Bank, or soils which are immediately adjacent glacial systems, for example push moraines; and iii) permafrost environments where the expansion and freezing water can cause over-consolidation on the soil fabric scale.

Due to the variability in stress history that can occur even to the same depositional unit over short distances, it can be difficult to predict how soils will behave under new loading for example the installation of offshore infrastructure (Figure 5.13).

Measuring soil variability

Measuring the shear strength of soils in such a variable stratigraphic setting can be challenging. The correct tooling for geotechnical sampling and testing should be considered based on the expected ground conditions that includes the number of locations, location selection, sampling and testing methodology, and appropriate twinning of locations. Some units will have a high proportion of granular material and care should be taken not to wash these out during borehole drilling. Similarly, very high strength, overconsolidated units or very dense sands can cause early refusal in Cone Penetration Tests (CPTs). As many of these soils are boulder-prone, early refusals can be a concern unless they are well tied into the geophysics and geological model.

Subsequent parameter derivation of these soils can also be difficult. The lateral and vertical variability will often result in wide-ranging lower-bound and higher-bound estimates, which can lead to conservatism in any design for offshore infrastructure.

Seismic characteristics

Geophysics works best when the subsurface comprises layers with increasing strength with depth; usually, erosive surfaces result in an impedance contrast between the eroded surface, which is often over-consolidated, and the overlying units. However, in regions that have undergone multiple phases of glacial advance and retreat, lower strength or less consolidated layers can occur beneath higher strength/more consolidated layers. This leads to a difficulty interpreting boundaries for the top of the underlying units, and subsequently challenges mapping separate seismostratigraphic units across sites; particularly where different parts of a single seismostratigraphic unit may have undergone different levels of consolidation under subtly different circumstances, i.e., tills deposited as moraine at the front of a glacier versus the same till unit, which might have no obvious lateral boundary, but deposited directly beneath the glacier (for lateral variability in the same packages, see Figure 5.13).

High levels of vertical and lateral variability also make velocity modelling across these regions challenging, resulting in inaccurate depth conversion and difficulty tying in geotechnical data correctly. It is important to integrate available geophysical, geotechnical and geological data to understand likely depositional environments to have the best chance of maximising the use of all datasets in these areas of high variability (Figure 5.13).

Engineering implications and considerations

High levels of lateral and vertical soil variability often result in a need for more detailed site investigations to reduce uncertainties in design parameters. Wide scatter in results will lead to larger uncertainties in design profiles and un-optimised design, and increased difficulties predicting how soil bodies will behave under new loads.

For piles, incorrect assessment of required foundation weights and lengths lead to different scenarios, and can result in both over- and under-conservatism in design: i) Where soils are lower strength than characterised and designed for, the installation method may not be appropriate and over-heavy piles can experience excessive or rapid pile run beyond the expected settlement; ii) Where soils are higher strength than anticipated, this can result in excessive installation times when driving or pile refusal.

During installation, issues may arise across the footprint of the foundation if soil strength variability is high. In some regions with high levels of glaciotectonism, such variability may be within the metre scale, and geotechnical response can be significantly different only few meters apart (e.g., at bump-over locations can be significantly different). To mitigate this, some larger structures may benefit from

multiple CPT locations or extremely high-resolution 3D seismic data if lateral variability is expected to be high (Hill et al., 2024).

For cables and pipelines, geospatial variability in soil conditions requires careful consideration of tool selection to prevent issues with achieving the desired depth of burial in over-consolidated soils, but also the risk of equipment loss in unexpectedly low-strength soils.

The presence of strength variations within the very shallow foundation depths can pose a significant threat to mobile bottom-founded rigs and barges. Temporary works including jacking-up next to a jacket structure or installing a wind turbine may experience rapid leg penetration, or punch-through if there are stronger layers located over lower strength materials. This is especially important in glacifluvial or glaciolacustrine sedimentary environments processes. Figure 5.12 shows a CPT profile depicting 3 m of dense sand over approximately 3 m of low strength clay in relatively shallow water. This profile represents a high chance of a punch-through incident occurring if not carefully assessed and managed. Procedures such as pre-loading and spud can foot design can help mitigate the risk.

In order to mitigate the risks associated with soil strength variability, any project should make effective use of ground modelling to understand the soil depositional and post-depositional stress history (Figure 5.13). Such an approach requires full and proper integration of geophysical, geotechnical and geological data; if one of these data sets has not been fully considered, knowledge gaps can provide results which may be open to misinterpretation. Therefore, a careful planning of all geophysical and geotechnical site investigations is required to ensure good coverage of expected soil units and seismostratigraphic units present across the site.

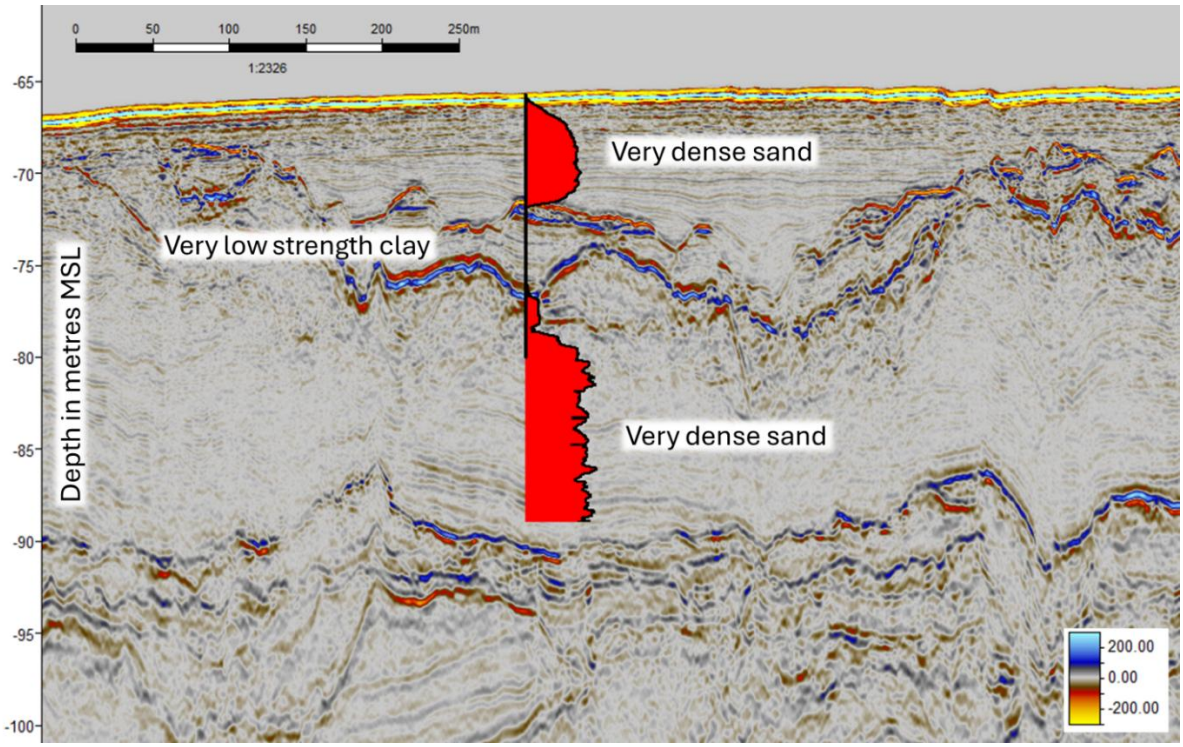


Figure 5.12. CPT profile showing near surface strength inversion from dense sand over low strength clay. UK Central North Sea. Source: Anonymous.

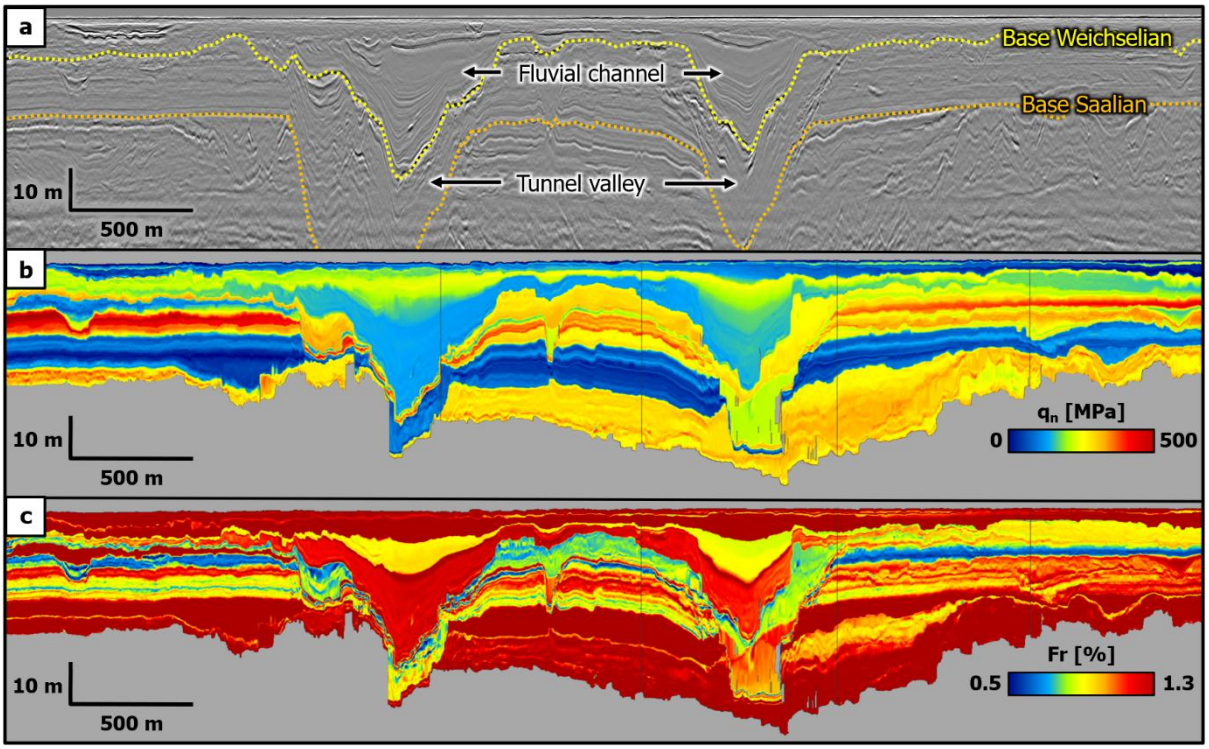


Figure 5.13. CPT-response models of the shallow subsurface offshore the Netherlands highlighting distinct variations, both horizontally and vertically. **a)** Seismic profile showing the base of the last two glaciations. The area has only been covered by the ice of the FIS during the Saalian glaciation. **b)** Normalised cone resistance. Blue values indicate soft sediments, red values are hard sediments. **c)** Normalized friction ratio. Blue indicates sandy sediments or desiccated clays. Red indicates clayey sediments. CPT-response models generated by Eliis. Data courtesy of RVO.

5.5 Boulders

Boulders can be defined as "A smooth rounded mass or rock … that has been shaped by erosion and transported by ice or water from its original position" (collinsdictionary.com), although a boulder may also be moved from its original position by human action or under the effect of gravity. There are several definitions of the size of boulders, but most standards indicate a boulder is a rock that will not pass through a 0.3 m square opening (Table 5.2). This implies that there is often some overlap in the size spectrum between cobbles and boulders.

Table 5.2. Different definitions of boulders according to object size.

Reference	Boulder Size
EN ISO 14689:2017	>0.2 m
BS 5930:2015	>0.2 m
Wentworth	>0.25 m

ASTM	>0.3 m

Boulders represent the largest grain sizes that are deposited in glacial environments, being transported on (supraglacial), within (englacial), and under (subglacial) the ice, bulldozed in front of it, and transported by high-energy meltwater flows. Due to the range of depositional mechanisms associated with glacial processes, single, as well as concentrations of boulders (boulder fields), may occur anywhere within glacial deposits, and especially glacial tills. Boulders are ubiquitous along the coastlines of previously glaciated margins, documenting their abundance within glacial deposits (Figure 5.14). Concentrations of boulders, known as boulder lag or palimpsest lag, may be expected at the base of till deposits due to the very high level of energy involved with the deposition (e.g. Obst et al., 2017), in positions of subsequent winnowing of finer material (e.g. channel bases, or the top of glacial deposits effected by subsequent erosion) or within outwash plain deposits (Griffiths and Martin, 2017) (Figure 5.14)

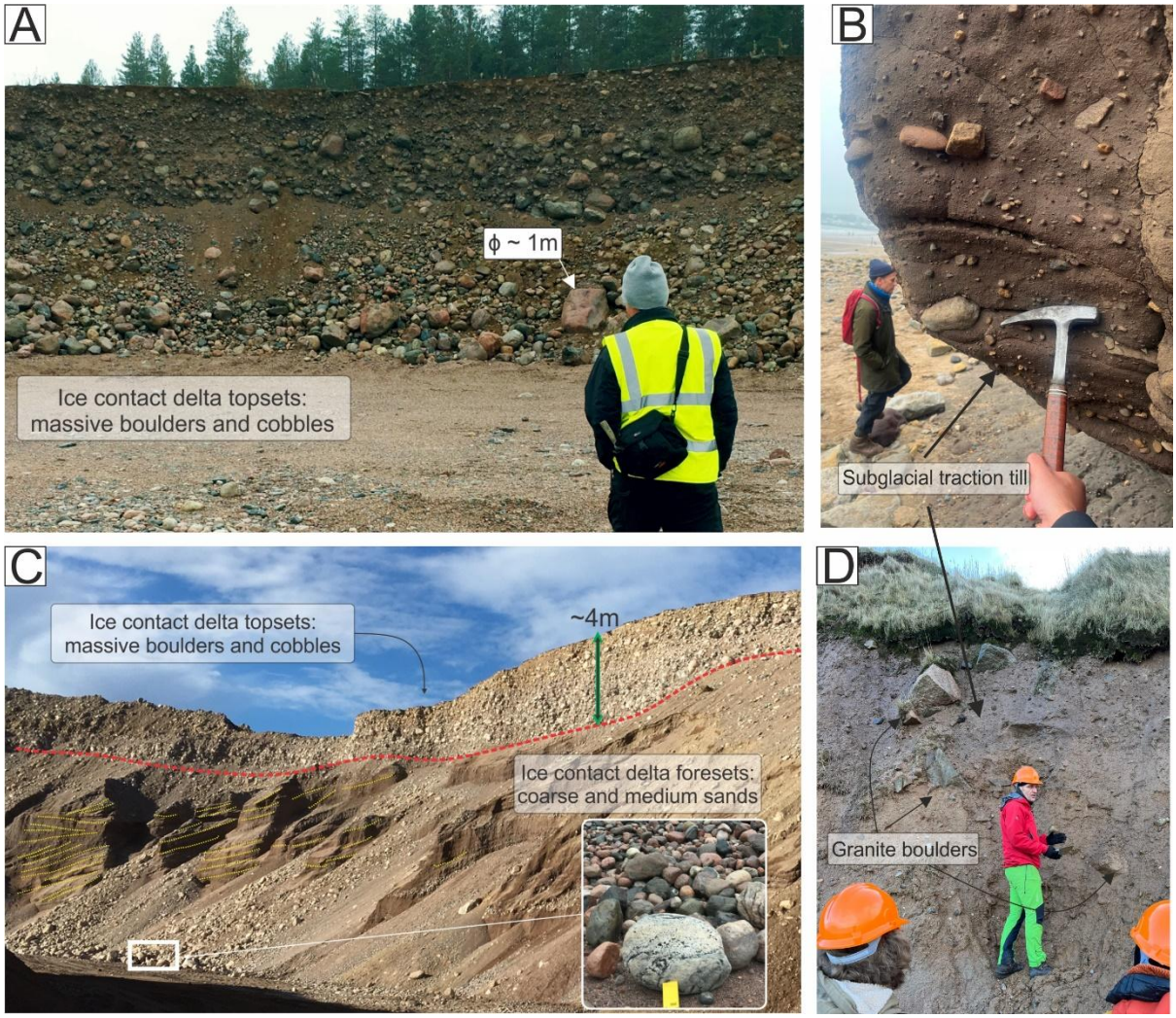


Figure 5.14. a) Massive boulder and cobble deposit forming the proximal part of an ice contact-delta within Salpausselka moraine near Lahti, Finland. **b)** Cobble and gravel clast-rich till from Filey Bay, Yorkshire, UK. **c)** last supported boulders and cobble-rich conglomerates forming topsets and sandy, steeply dipping forests of an ice contact delta near Lahti, Finland. The delta formed when the FIS margin was grounded in the Palaeo Baltic Ice Lake ~11.5 ka. Similar, but older, deposits can be expected from Slupsk Bank, Southern Middle Bank, and Northern Middle Bank offshore in the Baltic Sea. **d)** Boulder-rich sandy till from Sandford Bay near Peterhead, Scotland. Pictures: Bartosz Kurjanski

Other sources of boulders that occasionally need to be considered include ice rafted boulders, commonly called "drop stones" (Griffiths and Martin, 2017; Donovan and Pickerill, 1997). These are often present in glaciomarine or glaciolacustrine deposits and can occur anywhere in the sequence of generally much finer-grained materials. However, it is important to note that ice rafted material can potentially be transported for a considerable distance from the glacial source.

Boulders affected by glacial processes are representative of the rocks present in the path of glacial movement (provenance area), for example ice streams originating in Scandinavia will transport rocks from the crystalline and metamorphic basement; glacial deposits in the North Sea can contain rocks from the UK and/or Scandinavia. By assessing the lithology of these glacial erratics, it is possible to relatively reconstruct glaciations and ice flow pathways within specific ice-related deposits (e.g., Obst et al., 2017). Depending on the rock catchment of an ice sheet, boulders might be preserved to a lesser degree during the transport and erosion processes; igneous rocks might have a higher preservation potential than sedimentary rocks.

Geotechnical relevance

Boulders can be detrimental to several stages in offshore project development, depending on their size and distribution at and below seafloor within the area of interest. The prediction of boulder occurrence in previously glaciated margins is difficult and a holistic site appraisal is needed to understand its geologic development and to utilize available and suitable geophysical and geotechnical data. By understanding potential depositional environments, potentially boulder prone geological units such as glacial tills, channels, fans, or glaciomarine deposits can be investigated appropriately.

During site investigation, boulders can cause early refusal during cone penetration testing (CPT), and numerous boulders can cause acoustic scattering during geophysical surveys. It is therefore important to consider how best to investigate areas known or expected to be boulder prone; even early site investigation "failures", such as refusals and acoustic scattering, is information that can help inform future site investigation in these areas.

Subsurface boulders may hinder the installation of piled foundations or damage piles during installation (Holeyman et al., 2015). Near-surface or surface boulders may damage jackup spud cans during

installation or maintenance as well as hinder cable installation and burial. Engineering mitigation for the presence of boulders may include a review of the location of cable routes or pile installations to avoid local boulder presence (Figure 5.15). This may include the avoidance of areas of high boulder-probability (e.g. bases of tunnel valleys) or limited micro-siting to avoid identified individual objects. At the seafloor, boulders that are small enough to be lifted and still pose a risk may be removed to clear installation corridors, but larger boulders or those identified sub-seafloor need to be avoided or the installations hardened against them (e.g. pile tip reinforcements). For subsurface boulders, the strength of the surrounding matrix should be considered against the size of object considered a risk, as large infrastructure may effectively push objects aside in softer material. A 1 m boulder at depth in a low-strength clay will likely be pushed aside during monopile installation and not present an installation problem.

Boulder mapping and risk assessment

Boulders on the seafloor can generally be mapped out reliably using standard seismo-acoustic methods such as multibeam echosounders and side-scan sonars (SUT OSIG, 2022; IHO, 2020; Figure 5.15) and recent advances in technology mean other techniques, such as synthetic aperture sonar, can also be used, as they usually provide cm-scale horizontal resolution. Therefore, it is important to specify the minimum size of object that will pose an obstruction to engineering activities. Mapping all boulders on a site may be neither necessary nor cost-efficient and the focus should be on boulders of a critical size that is considered a risk (e.g. >0.5 m). Advances in automated data interpretation aid in dealing with large data volumes and target counts, however, these still require significant effort for quality control. It should be noted that seafloor imaging may only detect the surface expressions of buried boulders and further inspection, e.g. using remotely operated vehicles, may be needed to investigate complex areas (Figure 5.15).

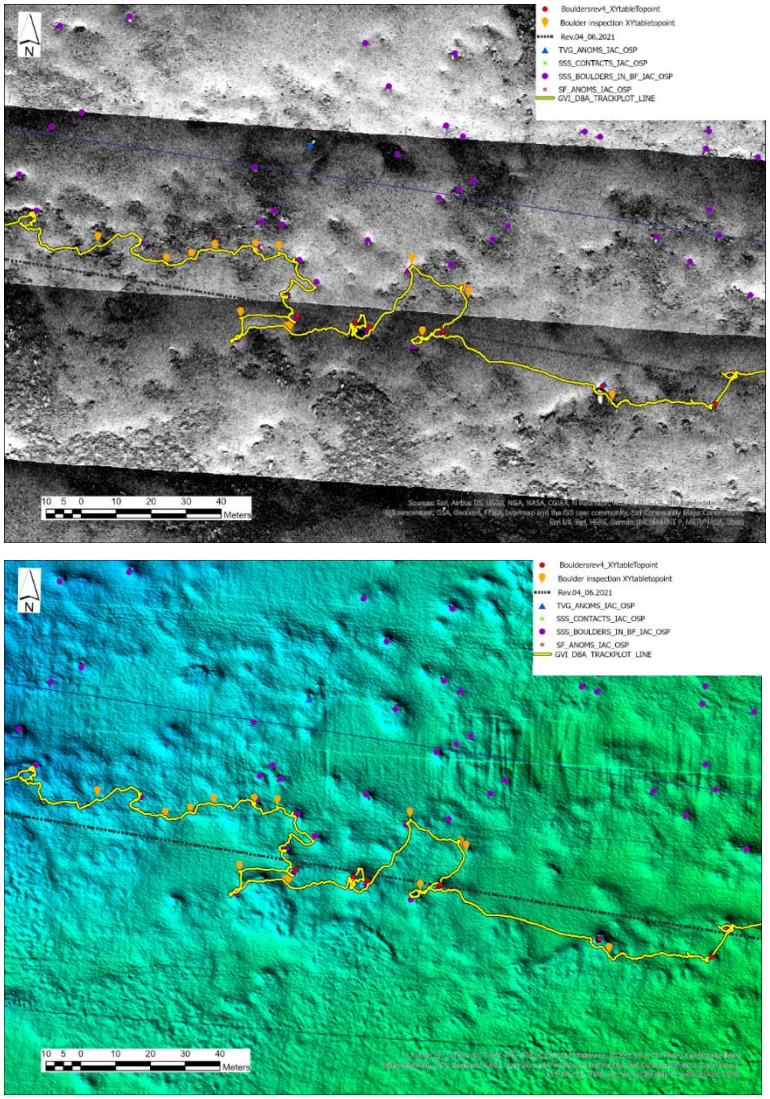


Figure 5.15. Boulders identified in different datasets. ROV track (yellow) and additional boulders identified in ROV data (orange tags) compared to the side-scan-sonar targets (top) and multi-beam echo sounder targets (bottom). Data courtesy of SSE Renewables.

Depending on the site geology, the subsurface may also contain significant boulder content that is not as easily mapped. Boulders pose a significant challenge for geophysical methods due to their small size and their characteristic as acoustic scatterers (Figures 5.16 and 5.17). Seismic methods are the predominant means of subsurface boulder mapping, relying on the identification of diffraction energy to pinpoint boulders. Due to the point-nature of the objects, such measurements need to be carried out in 3D for accurate mapping (Figure 5.17), thus require a high effort in data acquisition, processing and interpretation. The object size requires an extremely high resolution (EHR) seismic setup (see ISO 19901-10; Hill et al., 2024) to image objects in the relevant size range (e.g., Monrigal et al., 2017). It is important to note that even for advanced 3D EHRS setups, the mapping of boulders within complex glacial geology with a background of high impedance contrasts and spatially heterogenous unit distribution is a challenging task. It is also important to consider that many EHRS setups will also be

capable of detecting much smaller objects (<20 cm diameter), especially close to the seafloor, which might in reality be below the size threshold considered a risk for engineering. This could lead to alarming numbers of subsurface contacts and the potential for unnecessary engineering mitigations. However, determining exact object sizes at depth from seismic diffraction signals remains difficult and often leads to ambiguity during interpretation (e.g. Römer-Stange et al., 2022). The use of 3D EHRS techniques to map subsurface targets should therefore be proportionally balanced with the potential risk to projects, taking into consideration the limitations of the seismic equipment and the determined risk to engineering works.

Boulders (or discontinuities) may also stand out on 2D UHRS (Figure 5.16), however, due to the localization ambiguity for out-of-plane events, 3D EHRS is required for detailed subsurface contact mapping (Figure 5.17). 2D UHRS from site characterization surveys should be used for initial risk assessment and a precursor to dedicated boulder mapping activities where needed.

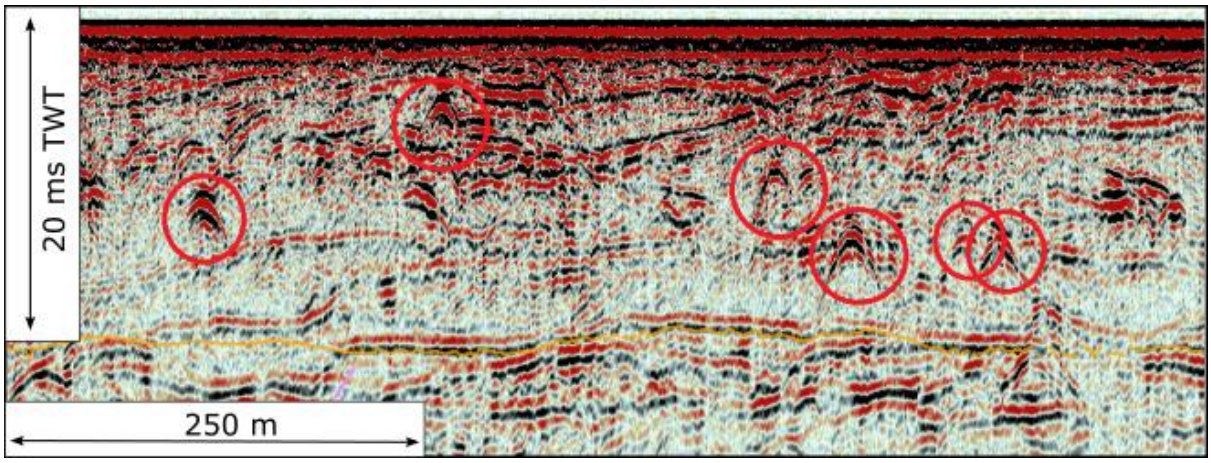


Figure 5.16. Multichannel UHRS line in the southern North Sea showing diffractions visible in unmigrated data within the upper ~30 ms TWT. These diffractions in 2D UHRS data are interpreted as potential boulders and used as a risk indication for the area. Source: BSH, 2023.

At different phases of a development, the risk posed by the presence of boulders should be revisited and survey equipment choice should be optimized to achieve the desired level of accuracy and detection, both for surface and sub-surface boulder presence. A phased approach may include (OWA, 2020):

- Detection phase: Boulder-prone areas are identified and, at best, avoided during development
- Zonal phase: If an area cannot be avoided, a perimeter with a defined boulder density classification is established
- Locate and Measure phase: A targeted survey aims at determining the size and position of boulders in a defined area that require consideration and intervention
- Mitigation phase: Micro-siting of cable, installation footprint, or foundation to avoid boulders

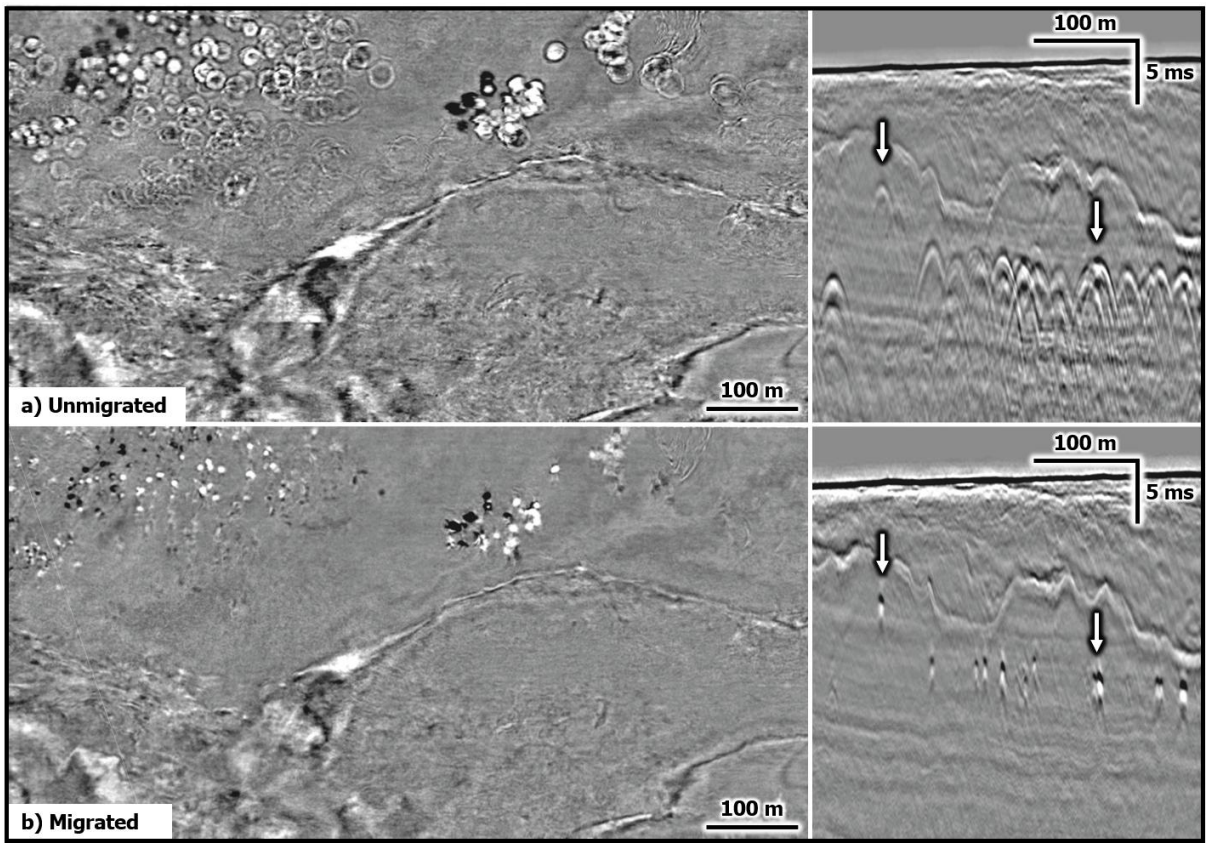


Figure 5.17. Boulder identification using diffractions in ultra-high-resolution 3D seismic data of the Southern North Sea. **a)** Unmigrated data showing clear hyperboles. **b)** Migrated data showing point anomalies. Hard kicks in black. Data courtesy of Vattenfall.

5.6 Gravel and cobble beds

Gravel lag deposits have been reported at various locations across the North Sea and North-East Atlantic Margin in variable water depths (e.g., Carr, 1999; Howe et al., 2001; Diesing et al., 2009). Lag deposits are often formed when bottom currents achieve adequate velocities to enable the winnowing of finer particles (e.g., clay and silt) from the seabed soil unit, leaving behind a blanket of coarser materials. Alternatively, high-energy depositional environments can also lead to the accumulation of thick gravel and cobble deposits.

The Dogger Bank and Bolders Bank Formations comprise soils deposited under glacial conditions, often being lain down under and immediately in front of ice sheets that extended across the North Sea during the Last Glacial Maximum (LGM). They occur extensively across the Central and Southern North Sea and are often found within the uppermost 50 m of stratigraphy, occasionally outcropping at seabed. Diesing et al. (2009) noted gravel lag deposits within bathymetric lows across the Dogger Bank area, and attributed these soil units to the reworking of underlying glacial deposits. Clasts contained within the Dogger Bank and Bolders Bank Formations comprise a wide variety of lithologies, however clasts derived from weaker bedrock units (e.g., chalk, sandstone and mudstone) can become

disaggregated through erosion which typically results in a gravel lag dominated by stronger lithologies (e.g., igneous and metamorphic origins, and flint clasts from chalk units), which reflects the relative high strength of these clasts within a high-energy setting. Studies of these gravel clasts have shown that they originate from bedrock sources typically in Scotland and Northern England (Carr, 1999; Diesing et al., 2009). In addition to the lithic fragments, biogenic gravels comprising shell debris and tests were noted to have accumulated at various locations across the Dogger Bank site; these deposits are Holocene in age and have built up over the past 7.5 ka following the complete inundation of Dogger Bank during the Holocene marine transgression (Diesing et al., 2009).

Gravel lag deposits have previously been identified in boreholes, cores, seabed samples and shallow geophysics from across the wider Central and Southern North Sea, typically overlying glacial deposits and blanketed by Holocene sands. Figure 5.18 illustrates examples of such surface and near-surface gravel lag deposits from the Dogger Bank area, including a section of core comprising 45 cm of dark greyish brown sand (Holocene sands) overlying 17 cm of gravel and cobbles, which in turn is underlain by dark greyish brown slightly sandy clay containing chalk clasts (glacial diamicton; Figure 5.18c).

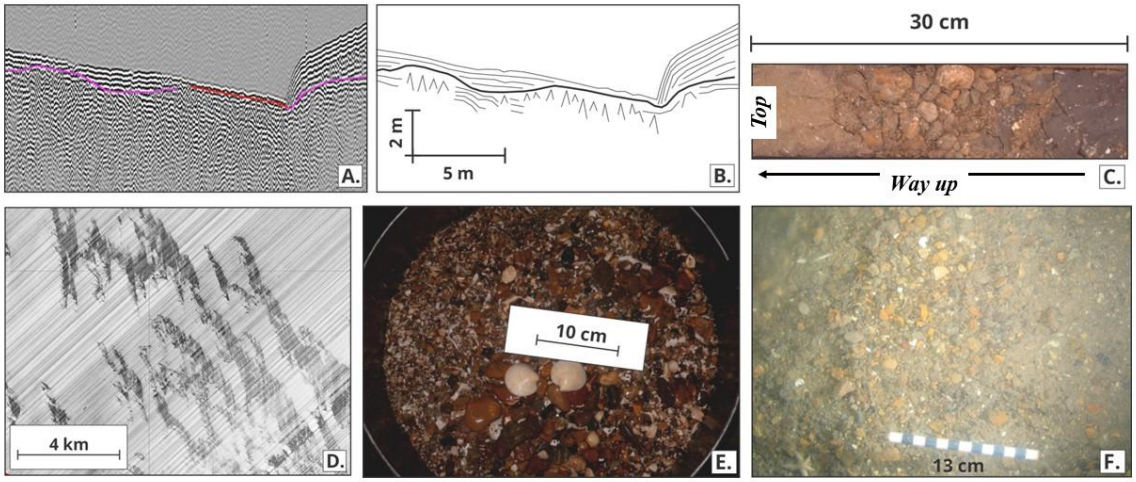


Figure 5.18. Examples of seabed and shallow subsurface gravel lag deposits from the Dogger Bank area of the North Sea. **a+b)** Multiple hyperbolae along a discrete horizon of high-resolution shallow geophysics (pinger data), corresponding with surface and near-surface gravels. **c)** Sediment core illustrating a gravel lag preserved between an underlying glacial diamicton and overlying Holocene sand deposits. **d)** Sidescan Sonar (SSS) with darker grey representing surface gravels and cobbles in NNW-SSE orientated troughs. **e)** Surface gravels recovered in grab samples. **f)** Evidence of gravel beds preserved on the seafloor in sledge camera footage. Data examples courtesy of the British Geological Survey and Dogger Bank Offshore Wind Farm (SSE and Equinor), modified from Carter et al. (2025).

Engineering considerations

In all stages of site and route selection, the presence of gravel beds can cause issues. Gravel beds on the seafloor are generally detected by the use of high-frequency side-scan sonar and multi-beam echo sounder (often using a by-product that measures the intensity of the reflection termed backscatter, to classify the seafloor composition). Gravel beds are used by several important commercial and protected fish species as spawning and nursery grounds (Ellis et al., 2012; Stewart et al., 2022) and as such can be a protected habitat that needs to, at least, be considered as part of any consenting requirements for a project and may be critical in cable routing, foundation location selection and installation planning (Figure 5.19).

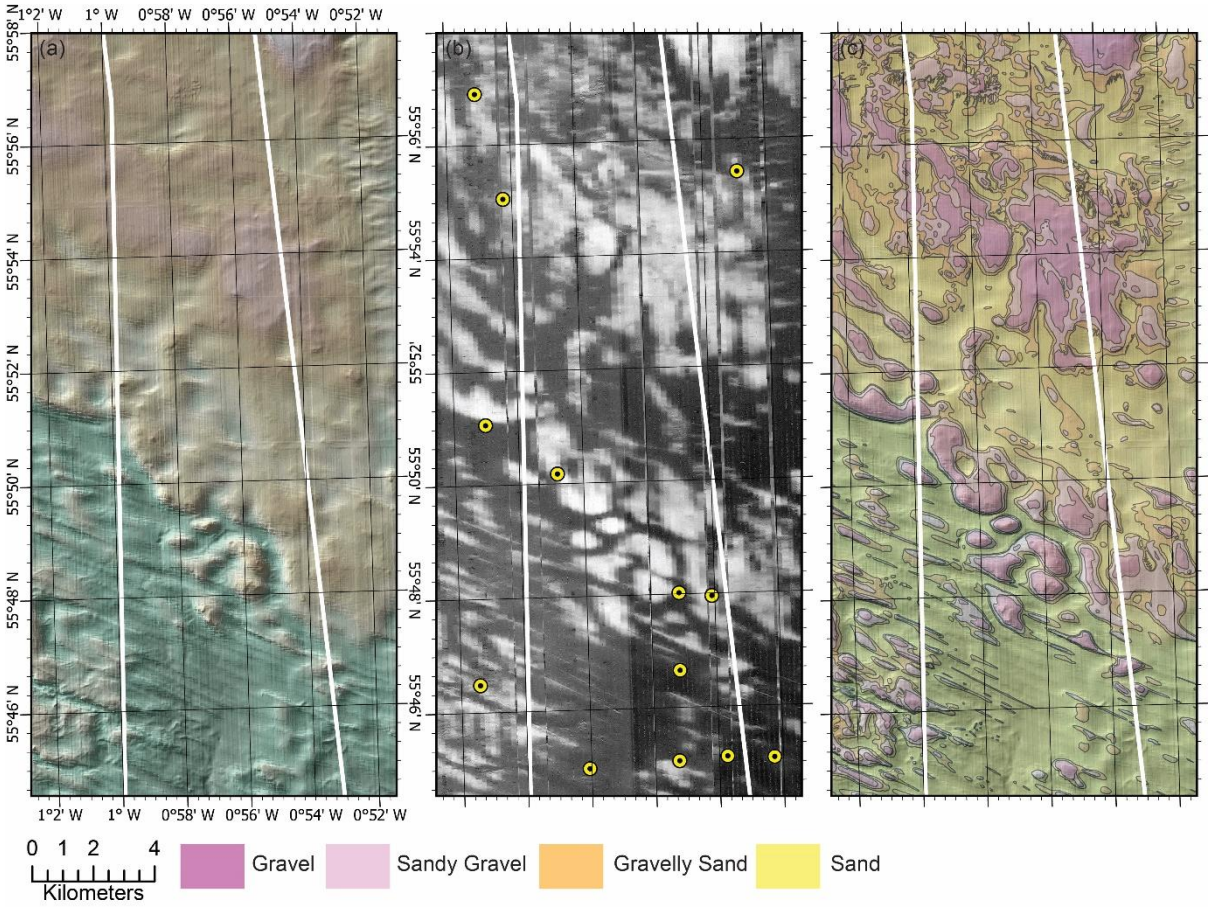


Figure 5.19. Example of Benthic Habitat mapping related to gravel distribution along a proposed cable route (white outline) as part of the consent requirements for route selection. Example from the offshore expression of the North Sea Lobe palaeo-ice stream, an area of glacial ice streaming and deposition of moraines and grounding zone wedges. Multibeam bathymetry **(a)** and backscatter intensity **(b)** data acquired as part of the Civil Hydrography Programme (CHP) on behalf of the Maritime and Coastguard Agency (MCA) from survey HI1083. Ground-truthing data (yellow dots (b)) and seafloor substrate interpretation **(c)** by H.A. Stewart available online via the British Geological Survey Offshore GeoIndex (www.bgs.ac.uk/map-viewers/geoindex-offshore/ British Geological Survey © UKRI 2025).

At the site investigation stage, gravel beds can cause early refusal during cone penetration (CPT), vibrocore, or borehole testing, by acting as a physical barrier to effective penetration of the tool. However, if well sorted and more fine-grained, CPTs might get pushed through these beds. Gravel beds, either on the seabed or subsurface can also cause acoustic scattering during geophysical surveys and therefore mask underlying structure, this property though, is also important in being able to detect the depth and areal extent of buried gravel beds so they can be avoided or planned for. Figures highlight that understanding the paleo-geographic environment (see Section 3.4), and the establishment of solid ground models, are crucial for the planning and success of geotechnical site investigations: The gravels and cobbles deposited in subglacial environments are a larger engineering constraint compared to the gravels deposited on an outwash fan.

Gravel lag deposits can also be of interest to site developers as they have the potential to influence cable trenching activities and parameters; certain trenching methods may have more difficulty with excavating dense gravels when compared with finer-grained, looser sands and silts, resulting in trench instability, high tow forces and/or planned Depth of Lowering (DoL) not being achieved in a single vessel pass. Whilst not only being unsuitable for jetting methods of trench excavation, gravel lags may also result in greater resistance and potential deviation of seabed ploughs leading to unexpected poor performance (Dyer, 2011). This may result in the need to use larger and more costly devices. In addition to impeding cable burial operations, gravel-rich soils can also prove problematic for certain foundation types such as suction caisson, especially when interbedded with other soil units of different grain size, providing a high degree of soil heterogeneity within the foundation zone of interest.

5.7 Soft marine sediments

Across the glaciated European margin, normally consolidated or (sometimes) underconsolidated (i.e. incomplete consolidation) soft to very soft marine sediments, typically muds (clays and silts), occur at or near the seafloor. The definition of "soft" refers to the relationship of undrained shear strengths, with ISO standards designating Extremely low (< 10 kPa), Very low (10 to 20 kPa) and Low (20 to 40 kPa) categories (ISO 14688-2). Common values of between 5 and 20 kPa have been reported for such units in the Irish Sea for example (Coughlan et al., 2023; Mellet et al., 2015). The British Standards also describe a set of standardised field tests for soil strength, which can be used to identify "soft" material (Table 5.3).

Table 5.3. Standardised field tests for soil strength to describe soft sediments.

BS 5930:2015	
Very Soft	Finger easily pushed in up to 25 mm. Exudes between fingers
Soft	Finger pushed in up to 10 mm. Moulded by light finger pressure
BS 5930:1999	
Very Soft	Finger easily pushed in up to 25 mm. Exudes between fingers

Soft	Finger pushed in up to 10 mm; moulded by light finger pressure
BS 5930:1981	
Very Soft	Exudes between fingers when ssqueezed in hand
Soft	Moulded by light finger pressure

During the Quaternary, the oscillation between glacial and interglacial periods has created a number of low-energy environments across the glaciated European margin, allowing for the deposition of these sediments, including glaciomarine to marine, glaciolacustrine and estuarine settings. Presently, accumulations of these sediments on the continental shelf generally form under low bed-stress, or depositional, conditions and are usually late-glacial to Holocene in age (e.g. Ward et al., 2015; Coughlan et al., 2021a). They can form thick deposits in depocenters in a variety of settings under differing environmental conditions and processes (Hanebuth et al., 2015; Porz et al., 2021). Well studied examples of these deposits include the Witch Ground Formation in the North Sea (Paul and Jobson, 1991), the Mud Facies of the Western Irish Sea Formation (Coughlan et al., 2023), and the contouritic infill in the northern Storegga escarpment (Bryn et al., 2005a). In the north Irish Sea, up to 40 m of soft marine sediments were recorded in the British Geological Survey borehole 89/15 forming a valuable palaeoenvironmental archive (Woods et al., 2019). A thick succession of weakly consolidated glaciomarine clays have been identified in a recent desktop study in the Danish North Sea (Jensen and Benniken, 2022). Extensive areas of surface soft marine sediments typically exhibit an overall flat seabed, and these areas are typically targeted by bottom trawling activity as they form habitats for many burrowing invertebrates (Eigaard et al., 2017) in addition to forming reservoirs of organic carbon (Diesing et al., 2017). Deposits of silty to clay sediments can be found having been deposited under conditions associated with palaeo-proglacial lakes (Andresen et al., 2022; Hjelstuen et al., 2018). Depending on the subsequent geological history of the area they were formed in, they can be soft. Their extent in terms of vertical thickness and lateral continuity can be difficult to constrain.

Identification Criteria

At the site investigation stage soft marine sediments can be identified by multibeam echosounder backscatter data at the surface. Where thick deposits occur, these deposits typically exhibit a laminated or transparent character in reflection seismic profiles. Efforts have been made to characterise soft marine sediments using shear wave velocity (V_s) values with promising results (e.g. Coughlan et al., 2023; Trafford et al., 2022; Figure 5.22d), however this is not carried out normally as part of the site investigation process.

Retrieving good quality borehole and core samples of these deposits can be difficult. Box corers can provide relatively intact and good quality samples but typically have shallow penetration and recovery depths of 20–60 cm below the seafloor. Vibrocores and gravity corers can recover deeper cores, reaching up to 15 m below the seafloor, although sediment disturbance and profile shortening can be

significant issues (e.g. Dück et al., 2019). Piston corers provide higher sample quality, and to greater depths, but are expensive and more difficult to operate (Lunne and Long, 2006; Tommasi et al., 2019).

As a result, in-situ testing using cone penetration testing (CPT) with selected boreholes with piston sampling remains the tool of choice when characterising these sediments as it can deliver reliable, high-resolution, geotechnical profiling to depths of up to 50 m to International Standards Organisation (ISO) standards (ISO 22476-1:2022; Andersen et al., 2008; Lunne et al., 2011; Figure 5.22a-c). The accuracy and applicability of CPTs in soft marine sediments can be improved through the use of "add on" devices such as the T-bar, ball, and plate penetrometers (Qiao et al., 2023). Data acquired through CPTs can be used to estimate sediments based on their soil behaviour type (SBT) according to certain parameter ranges, including normalized cone resistance (Q_t) and the pore pressure parameter B_q or normalized friction ratio (F_r) (Robertson et al., 1986). It has been reported that the use of the sleeve friction (f_s) data acquired by CPTs in soft marine sediments in some cases are unreliable (Lunne et al., 2018). Similarly, Robertson (1990) demonstrated that for soft soils normalised SBT charts are not overly sensitive to variations in f_s. Furthermore, these charts rely on the corrected cone resistance (q_t), requiring accurate pore pressure measurements to make the correction. In soft fine-grained sediments, the difference between uncorrected (q_c) and corrected cone resistance (q_t) can be significant where q_c is less than 1 MPa. The application of a soil behaviour type index (I_c) to the Robertson (1990) Q_t - F_r showed a simplification in characterisation (Robertson, 2016). However, the applicability of these charts depends on the accurate measurement of parameters, and obtaining reliable in-situ pore water pressure measurements in soft sediments remains a challenge and the similarity to the soils the diagrams were calibrated to (Peuchan and Terwindt, 2014). Data acquired through CPTs can be used to estimate other soil properties, such as undrained shear strength (s_u), stiffness, unit weight and pre-consolidation stress (Lunne et al., 1997).

Aside from CPT data, V_s values can be used to estimate undrained shear strength (L'Heureux and Long, 2017; Oh et al., 2017), although such approaches heavily depend on locally derived correlations with good quality samples. Therefore, despite the applicability of CPT approaches to characterising soft marine sediments for engineering design, these data are often used in tandem with an extensive programme of laboratory-based testing (e.g. Andersen et al., 2023).

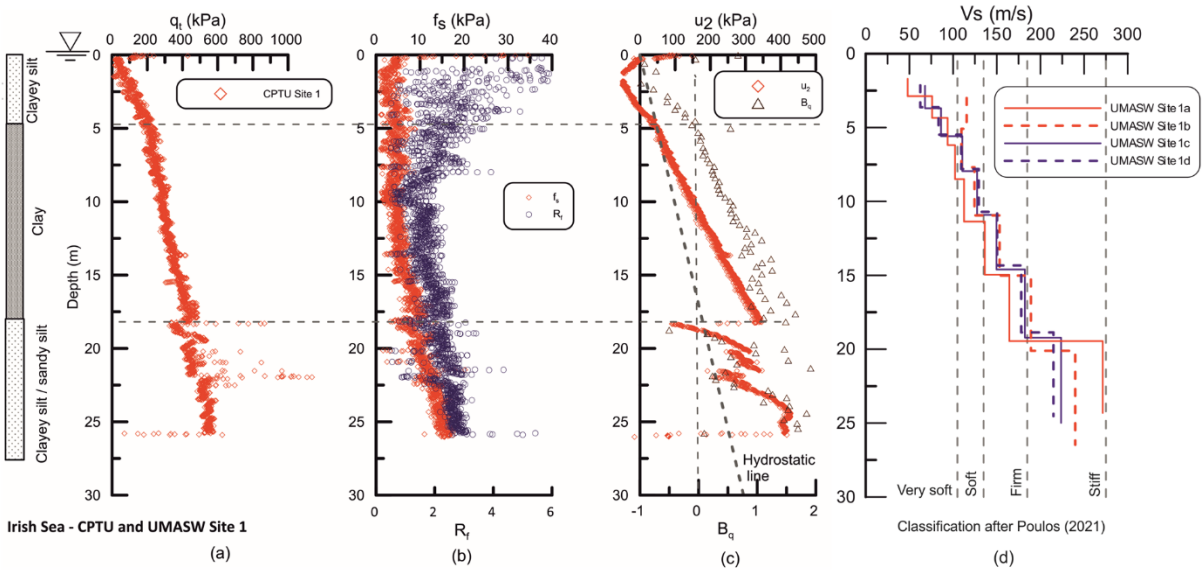


Figure 5.22. Typical CPTU and UMASW profile form the north Irish Sea consisting of soft marine clays from 0 - ~17.5 mbsf, overlying coarser glacial outwash sediments. CPTU data versus depth for Site 1. **a)** CPTU q_t. **b)** CPTU f_s and R_f. **c)** CPTU u_2, u_0 and B_q. **d)** V_s derived from UMASW at the same site superimposed limits for material classification from Poulos (2022). CPTU: In-situ cone penetration testing with pore pressure measurement. UMASW: Underwater multichannel analysis of surface waves.

Engineering Considerations

Soft marine surficial sediments of typically <2 m thickness may pose problems for shallow foundations as for example GBS or suction caissons but do not pose an issue for piled foundations. However, these soft sediments have the potential to allow for much deeper anchor penetrations than expected, which has implications for floating wind anchor systems (Petrie et al., 2022). With regard to cables, the low bearing capacity of soft marine sediments poses a potential geo-constrain in terms of sinking as well as trenching of the cable (DNV, 2014). When these deposits occur in thick packages, foundation sizes increase significantly. Aside from low shear strength, other geotechnical characteristics associated with soft marine sediments are high water content, high compressibility and low permeability. As a result, these sediments can be challenging for foundations due their low bearing capacity, excessive settlement and susceptibility to stiffness degradation. The presence of more resistant, stiffer underlying units (e.g. glacial till) creates a strong mechanical contrast of sub-surface geological, increasing vertical heterogeneity, and offering complex ground conditions. Furthermore, where significant accumulations of soft marine sediments occur, they have been reported as being gas-bearing, as documented in the Irish Sea (Coughlan et al., 2021b; Yuan et al., 1992), North Sea (Böttner et al., 2019) and the Baltic Sea (Tóth et al., 2014b), which forms another constraint (see Section 5.1).

Soft marine sediments are also prone to scouring. Whilst typically occurring in accretionary settings where they form a flat, featureless seabed topography, the introduction of obstacles can induce vortex

shedding and enhanced current flow causing erosion and transport of sediment from around the base of the structure (e.g. Callaway et al., 2009). The extent of this phenomena in muds (i.e. silts and clay) depends on the degree of compaction (Whitehouse et al., 2011), whilst they are also prone to liquefaction (Sumer and Kirca, 2022). Dewatering in soft marine clays has also been reported in the Horns Rev III windfarm site (Vattenfall, 2019; Figure 1.3).Scour is both an issue for foundation stability, as well as free-spanning in cables.

The presence of soft sediment layers at depth below the seafloor are also known to play a significant role in controlling submarine landslide formation (Gatter et al., 2021). On the slopes offshore Norway, the glide planes and infill of mega-slide escarpments is often correlated to soft, contouritic clays (Haflidason et al., 2003; Bellwald et al., 2022a), which show strain-softening behaviour which is very different from the glacial clays (e.g., Bryn et al., 2005a; 2005b; Kvalstad et al., 2005b). In near-shore environments, quick clays pose a significant threat as well for engineering (L'Heureux et al., 2018). Quick clays are sensitive marine clays with unique behaviour when disturbed (e.g., vibrations, changes in stress state), rapidly losing their strength and becoming fluid. They form from normal clays deposited in marine environments, which become uplifted in response to glacio-isostatic rebound, and over time, the salt in the pore water is leached by freshwater leading to a change in the clay's structure and properties (Thakur et al., 2017). Quick clay failures are some of the most devastating hazards in formerly glaciated margins (e.g., Finneidfjord, Rissa, Kråknes, and Gjerdrum landslides in Norway; e.g., L'Heureux et al., 2013b; Giles, 2022b).

5.8 Weathered and unweathered bedrock

If bedrock is within the depth of interest for the installation of foundations, pipelines, or cables, understanding its character, depth and distribution is critical to avoiding damage to the assets and costly delays to projects due to unforeseen ground conditions. Within the glaciated European margins, generally the likelihood of encountering bedrock within the depth of interest can be established early on in a project during the initial desk-top study phase by conducting a review of the various Nation States published geological information such as the British Geological Survey in the UK (e.g. the British Geological Survey). It is important to anticipate the presence and the type of bedrock as early in site development as possible, as the weathering profiles of rocks can vary significantly, which in turn can impact upon individual wind turbine generator (WTG) foundation selection right from the Front-End Engineering Design (FEED) phase of a project. Early work should also include careful consideration of relative sea level curves and wider geo-evolutionary history, to understand the likelihood of sites being subaerially exposed or affected by other processes such as periglacial frost shattering or desiccation.

If the presence of bedrock at the depth of interest at a site or along a cable or pipeline route is shown to be a potential issue for foundation selection, cable installation and design, then it becomes a primary objective of the geophysical survey and subsequent geotechnical survey to investigate the nature of that

bedrock. The primary concern is the potential for encountering unexpectedly strong to extremely strong rockhead within the depth of interest resulting in early pile refusal or cable burial not achieving the required depth. Conversely, the situation can be further complicated when the interface between Quaternary sediments and the underlying bedrock is not clearly defined due to subglacial and periglacial processes having acted upon the bedrock, creating a weathering zone (e.g., Dudgeon Offshore Wind Farm, Mellett et al., 2020). This can result in the overlying Quaternary deposits having higher densities (granular sediments) or shear strengths (cohesive sediments) than the underlying bedrock unit(s), especially where the Quaternary sedimentary sequence has been overconsolidated through ice loading (e.g., subglacial lodgement tills). In many cases, this can lead to the weathered 'bedrock' zone acting more like an unlithified sedimentary deposit (e.g., a firm to stiff clay consistency) in terms of its associated geotechnical properties and geomechanical behaviour.

An example of this scenario of inverse geotechnical properties at the sediment-rock interface can be seen in the Irish Sea, between the mainland UK and Ireland, where the overlying tills and glacifluvial deposits associated with the Cardigan Bay Formation are often observed to have much higher cone resistance (q_c) values from Cone Penetration Tests (CPTs) than the underlying Triassic rocks of the Mercia Mudstone Group (Figure 5.24). Similar inverse profiles have been observed at many locations where rockhead is within foundation depths across the NW European Margin (e.g., the Chalk Group and Smith Bank Formation of the Central-Southern North Sea), with weathering being particularly amplified when the underlying bedrock is composed of fine-grained sedimentary strata (e.g., mudstones and various carbonates; Figure 5.24).

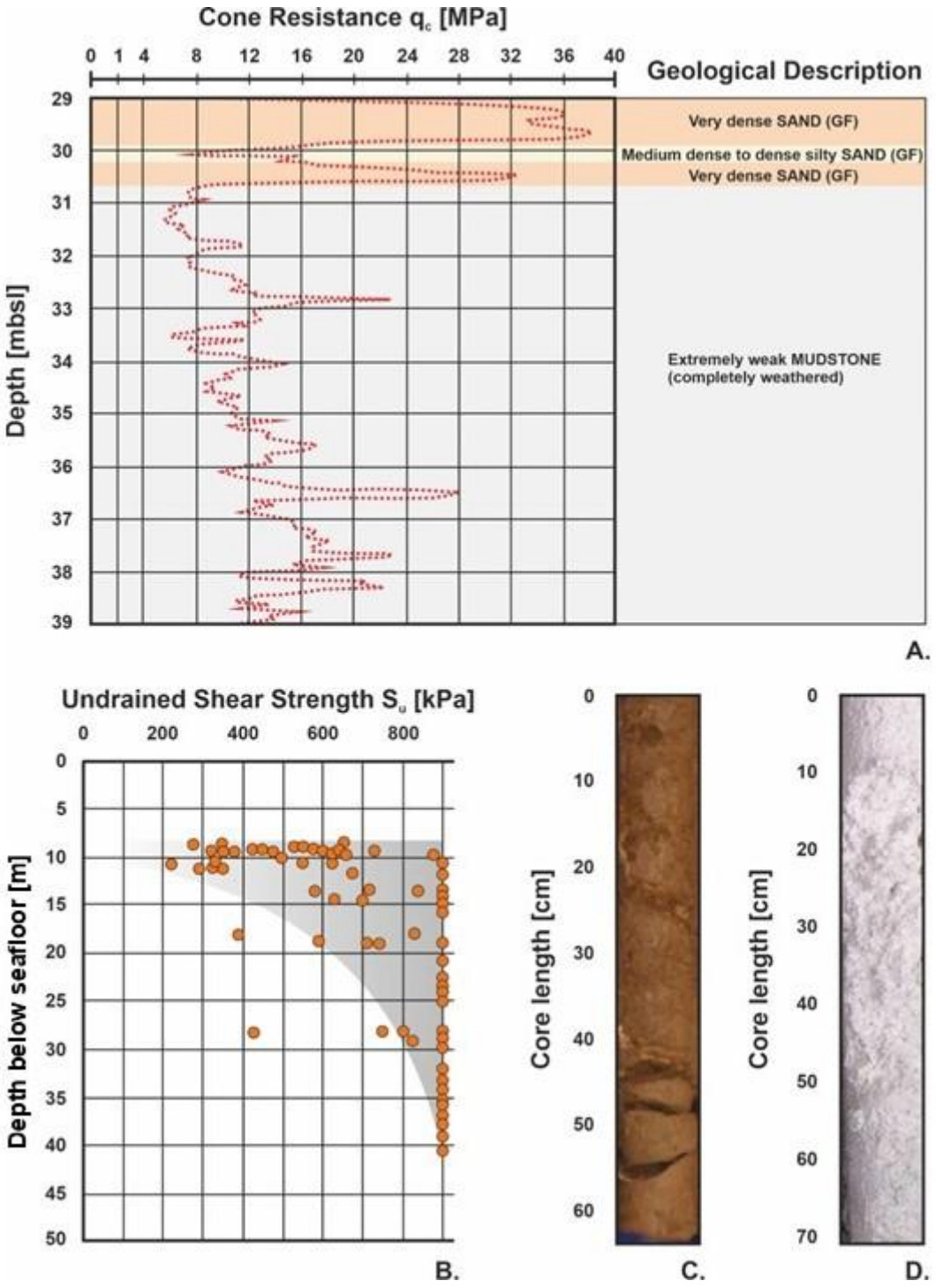


Figure 5.24. Examples of engineering properties and core images from weathered bedrock units. **a)** Example CPT plot demonstrating reduction in cone resistance (q_c) when penetrating down through dense to very dense glacifluvial (GF) sands and into less resistant completely weathered Mercia Mudstone. Plot adapted from southern Irish Sea location (Fugro, 2013). **b)** Shear Strength (S_u) plot demonstrating a weathered surface in Mercia Mudstone, Irish Sea, with low (200-300 kPa) strength properties, increasing in strength with depth (grey shading to demonstrate increase curve). Plot adapted from Mellett et al. (2015). **c)** Core image showing completely weathered Mercia Mudstone Group from

the southern Irish Sea (Fugro, 2013). **d)** Core image showing completely weathered Chalk Group with 'putty' consistency from the southern North Sea (Johnson et al., 2023).

A further challenge lies in the structural framework of the bedrock unit(s) underlying the Quaternary sediments, whereby the orientation of individual subunits/beds within the overall bedrock formation can be steeply dipping with differing weathering profiles. An example of this would be the Chalk Group of the southern North Sea, where moderately to steeply dipping strata have given rise to differential weathering profiles on a metre-scale between beds of completely to moderately weathered chalk and more weathering-resistant flint bands. This Quaternary/bedrock interface will typically vary greatly, in terms of physical properties, over very short distances which can be in the order of <10 m and well within the average radius of modern pile foundation design; the problem is exacerbated when considering potential for difference across jacketed foundations or mooring/anchor solutions for floating offshore structures, which can have a much wider footprint.

While all bedrock types will have unique challenges regarding weathering profiles, particular attention must be paid in areas that have been subaerially exposed (or affected by subglacial water) and may also contain dissolution features, such as voids, infilled pipes, and sinkholes. All of these in turn present their own specific engineering considerations. These are commonly associated with calcium carbonate rocks, such as chalk or limestone, but can also occur in areas with other water-soluble minerals such as halite or gypsum. Considering this further, there are many sub-units of these rocks which will have individual weathering profiles, and it is important to appraise which specific units are present on site, for example as outlined in Mortimore (2014).

When seen in geological profile, within the footprint of a typical monopile, the potential for a pile to encounter an irregular surface of varying localized properties within a short distance is high, as illustrated in Figure 5.25.

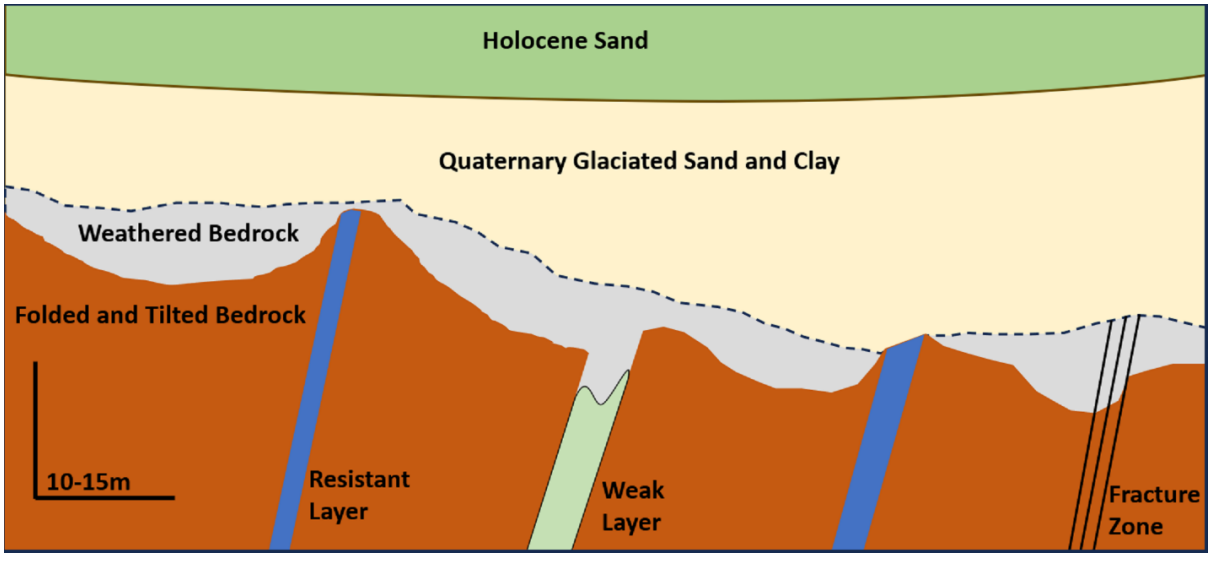


Figure 5.25. Variation in rock properties occurring over very short distances. This variation is further

complicated by the presence of a weathered layer above that can affect the clear understanding of where the interface occurs between Quaternary sediments and the underlying bedrock.

This presents a problem in dealing with the types of open-ended piles typically favoured for WTG foundations. The likelihood of encountering bedrock uniformly over the full cross-section of the pile is low (Pile Buck, 2022) within an area of high variability in the local depth of the (weathered) rockhead. This can generate significant risks to safe pile driving operations, when the forces required to drive the pile are distributed unevenly across its base, creating the potential for pile buckling and penetration failure to occur (Figure 5.26).

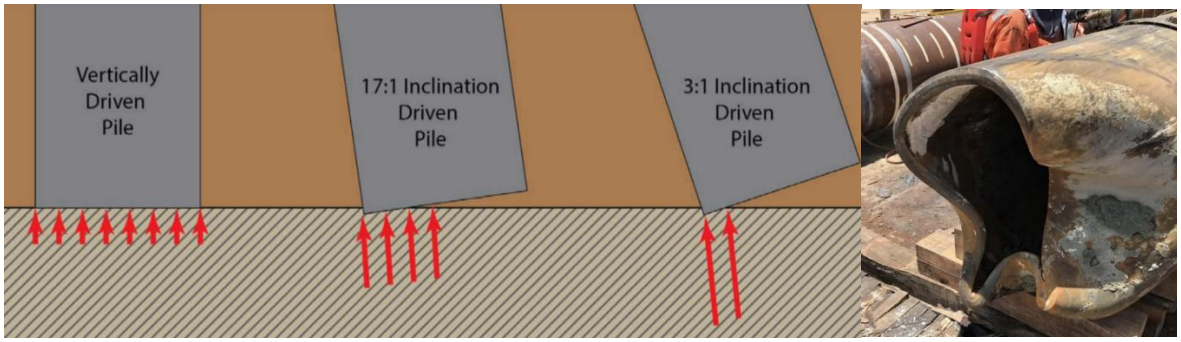


Figure 5.26. Engineering implications of resistant layers. **a)** Illustrates how a change in the orientation of the resistant layer can lead to buckling of a pile (Pile Buck, 2022). **b)** Illustrates the results of a 1070 mm (OD) pile that has been extracted having encountered a calcarenite (hard) layer within a weaker limestone unit on one side of the pile (Pile Buck, 2022).

The aforementioned issues can be exacerbated when there is not a clear understanding of the local variation that may be encountered due to the nature of the datasets that are typically gathered for offshore renewable projects. Well-developed ground models can anticipate the likelihood of specific bedrock units and in some cases, when geophysical and geotechnical data are properly integrated with geological understanding, the likely behaviour of those rocks can be anticipated. For example, properly integrating all available geotechnical data can in some cases help determine the weathered layer from the non-weathered surface, indicated by subtle changes in P-S wave velocities and other records such as Natural Gamma and even calliper logs. However, the combination of using CPT and/or borehole information alongside 2D ultra-high-resolution seismic data can only hint at local variability. A CPT or borehole will be <120 mm in diameter and is probably not located directly on a corresponding seismic line, even an offset of 10 m can make all the difference (see also Chapter 7.2.1). Any mismatch between geotechnical and geophysical data can result in additional conservatism in design, and may not sufficiently de-risk sites from installation-related issues. The pile itself is sometimes sited off traditional 2D-sesimic lines, and a great deal of uncertainty exists as to the actual depth to (weathered) rockhead in the immediate vicinity of the pile footing.

A solution to this problem can be the use of advanced techniques using 3D ultra-high-resolution or 3D extremely high-resolution seismic data (Hill et al., 2024) and processing techniques such as inversion and studies of basic geotechnical properties such as porosity (Vardy et al, 2017). These should be used in areas where the depth to the (weathered) rockhead is anticipated within the depth of interest and is capable of giving a much more accurate and informed picture of the distribution and character of the (weathered) rockhead (Sauvin et al, 2019).

5.9 Organic materials and peat

The organic matter in soils originates from living plants, animals and organisms, forming biogenic matter in contrast to mineral matter. Organic soils are formed by the decomposition of the organic substances, a process which takes place mainly by bacterial activity, but which is intensified by a warm climate, humidity, and access to oxygen (Larsson, 1990). However, too much oxygen in the environment will result in complete organic matter decomposition therefore no organic rich soil or peat will be preserved. Generally speaking, peat is an organic soil with a very high organic content, whereas "organic soils" contain some fine-grained material of non-organic, mineral origin.

Different countries have used various organic content thresholds which allow a soil to be termed a "peat" from an engineering point of view. For example, in the US an organic content limit of 75% is used to permit soil to be classified as "peat" (ASTM, 2010). In contrast, the Dutch National Annex to Eurocode 7 suggests that a soil can be classified as "peat" if the organic content exceeds 30% (ASTM, 2010; Lengkeek and Brinkgreve, 2022). Peat is generally associated with high latitudes, and most existing peatlands globally were formed since the end of the last glacial period (Minasny et al., 2019).

Across Europe, fluctuations of Quaternary sea level due to growing and shrinking ice sheets, combined with the effect of glacial isostatic adjustment and other complex factors resulted in periodic emergence and subsequent submergence of vast land areas that, at present, are inundated and form part of the European continental shelves.

Relatively cold and wet climate following deglaciation combined with low-laying ground and undulating topography close to the water table formed favourable conditions for the formation of organic rich soils and peat (Figure 5.27 and 5.28). Conditions were favourable for early colonizing plants and the colder climate conditions hindered decomposition of organic matter and allowed for accumulation of organic-rich sediments (soils) and peats. The subsequent inundation of those areas as the sea level rose resulted in the burial and preservation of such sediments under shallow marine strata. Quaternary peats and organic-rich soils are typically associated with interglacial and post-glacial conditions and, if encountered at or under the seabed, are an important consideration for offshore engineering projects due to their varied physical properties, particularly their property as a thermal insulator. Well known examples of submerged organic rich sediments and peat were described from the southern North Sea and dated to 9.5-9 ka BP when large areas of present day-seabed were emergent

(Brown et al., 2018; Hazell, 2008; Tappin et al., 2011; Hepp et al., 2019; Waller and Kirby, 2021; Özmaral et al., 2022; Eaton et al., 2024).

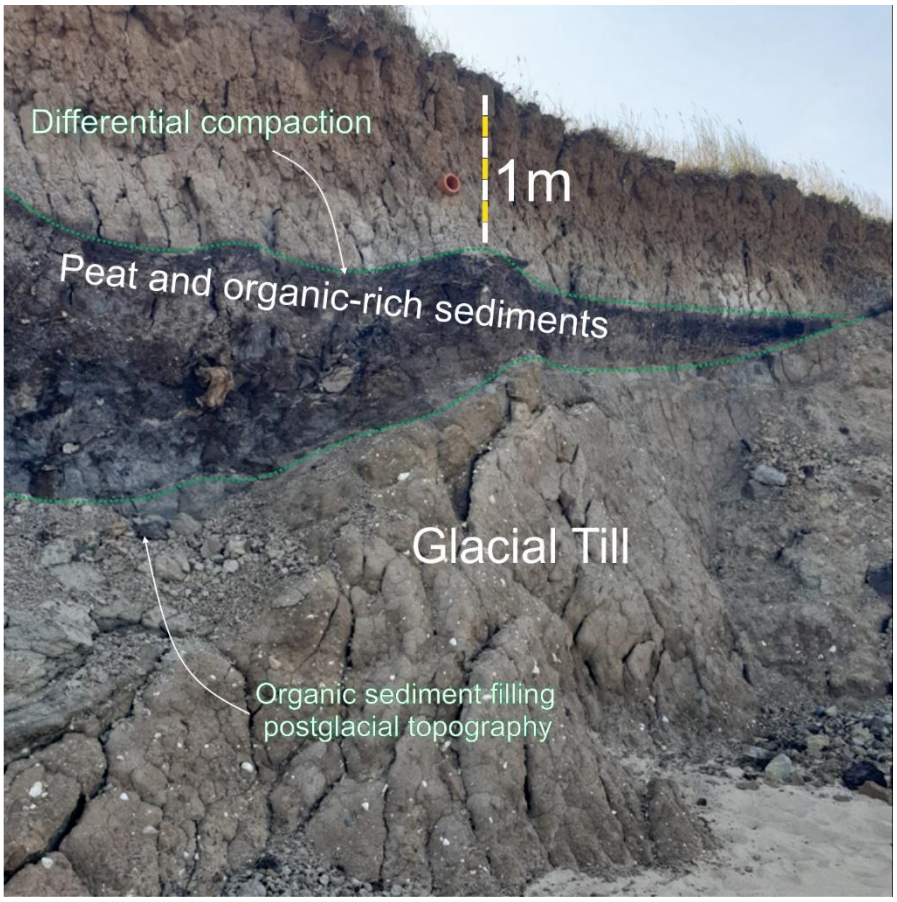


Figure 5.27. Coastal outcrop from Holderness coast near Skipsea, UK, showing peat and organic-rich sediments filling undulating topography of the top of glacial till. Peat accumulated in water-logged low ground areas following the ice retreat from the region. Note wood fragments within the peat. Unique finding of Beaver hair, suggesting a possible beaver dam and lodge, allowed to date the top of nearby peat succession at Withow Mere to ~4ka (http://www.hullgeolsoc.co.uk/beaver.htm). Photograph source: Leah Arlott.

Types of organic sediments and their depositional environments

Soils are generally considered to be slightly organic, or low content when the organic matter content in the sediment is greater than 2%, organic or medium content when above 6% and very organic or high content when above 20% (ISO 14688-1, 2017; ISO 14688-2, 2017). There are several subdivisions of organic soil types, including but not limited to peat, gyttja, dy, and sapropels, all varying in chemistry, source material and typical environment and conditions in which they form. Such deposits are referred to here as organic rich sediments as their detailed description and differentiation is beyond the scope of this paper.

Definitions of peats vary between regions and standards but in general they are characterised as poorly consolidated sediments with organic matter content greater than 30-75% (ASTM, 2010; Huat et al., 2014; ISO 14688-1, 2017; ISO 14688-2, 2017; Larsson, 1990; Lengkeek and Brinkgreve, 2022). They are formed from partially decomposed plant matter deposited in waterlogged hypoxic or anoxic conditions, which allows for accumulation and preservation of organic material. Present day peats and peatlands can be found in most climates but are most prevalent in wetter and colder settings, particularly in high latitudes, where decomposition of organic matter is slower (Huat et al., 2014; Stolt and Lindbo, 2010).

In coastal settings, peats and organic-rich deposits can typically be associated with estuaries, or lagoonal environments behind which salt marshes or fringe peat deposits form. Peats and organic rich sediments can also be found in lacustrine, and fluvial settings where organic-rich deposits firstly accumulate in lakes, ponds and overgrown river channels (e.g. oxbow lake or abandoned channels after avulsions) or in vegetated deltaic and floodplain settings where gradual rise of water table due to transgression allows for preservation of organic detritus and eventual flooding of terrestrial vegetation (Waller and Kirby, 2021).

Physical Properties of Peat and Organic Sediments

The texture of organic soils can vary significantly, depending on both the environment of deposition and the level of decomposition. The type and quantity of organic material can vary substantially ranging from barely discernible organic matter to large fibrous clasts, such as tree roots or other pieces of wood of substantial size.

Offshore, due to the fibrous and/or unconsolidated nature of some peat and organic-rich sediments, these samples may be difficult to collect in vibrocore samples, push tubes or rotary cored samples, particularly if they are only partly decomposed peats with large woody pieces.

Peat and organic-rich soils can be difficult to identify from cone penetration tests (CPTs), as they can sometimes be associated with an increase in tip resistance, or a drop in resistance in other cases. Research has shown that organic rich soils are often associated with high CPTU friction ratio values (f_s/q_t), e.g. in excess of 6% (Long et al., 2024). Organic-rich soils also show much lower shear wave velocity that purely mineral soils and this factor could also be potentially used to help in their characterisation (Trafford and Long, 2020).

In settings where the presence of peat or organic-rich sediments is probable offshore, the use of thermal conductivity cones is essential to be able to aid determination of peat and should be employed as standard on any cable projects in areas where peat may be present.

When logging cores, organic soils often have a distinctive odour due to their anaerobic decomposition; this can be “eggy” or sulphurous. They are also often dark in colour; black, dark brown, and dark

greenish shades are most common, but they may be yellow or grey in some circumstances. The ISO 14688-1 standards offer a specific guidance on sediment/soil colour to aid organic content identification within samples and cores.

Geotechnically, peats and organic soils are generally characterised by low bulk density and high water content between particle density (PD) can range between 1.3 g/cm^3 to 1.6 g/cm^3 (average: ~1.4 g/cm^3) depending on the level of decomposition (typical mineral soil PD 2.4-2.7g/cm^3). The bulk density of peats and organic-rich soils depends on the level of compaction, water content and porosity which can reach up to 96% and typically ranges between 20 and 70%. This implies that peat in the subsurface can be characterised by bulk densities between 1.0 and 1.4 g/cm^3 (typically around 1.05 g/cm^3; M. Long - pers. comm.) depending on the level of compaction, decomposition, mineral content and pore water volume. (Huat et al., 2014). Physical properties of peats and their geotechnical parameters also differ between regions (e.g., Carsten, 2020; Den Haan and Kruse, 2007; Landva, 2006; Mesri and Ajlouni, 2007).

Peats and organic-rich soils are prone to shrinkage and cracking if exposed to atmospheric conditions. Cracks start to develop when moisture content is reduced by 50% and are prominently visible when moisture reaches 30%

Geophysical/Seismic characteristics

Because of the varying nature of the physical properties of organic-rich soils and the range of depositional environments in which they occur, geophysical signatures of peat or other organic material can vary significantly. Peats and organic-rich soils can be complex to characterise using geophysical data and care must be taken to ensure a suitable geotechnical campaign to confirm the type of soil identified.

Peats and terrestrial organic-rich soils were confirmed by boreholes from present-day offshore settings extensively across northwest Europe, particularly in the central and southern North Sea and shallow settings within the Irish Sea (Figures 5.28 and 5.29). Where identified in seismic data, peats and organic-rich sediments are sometimes characterised by high-amplitude, negative-polarity reflections (Figure 5.28). The amplitude of these reflectors can vary significantly and in some cases be indiscernible from reflections representing different geological boundaries, which makes the lateral distribution of peat in some locations difficult to quantify (e.g. Plets et al. 2007).

Terrestrial peats can form continuous or semi-continuous reflectors on top of other tabular units or may be confined to a specific bed or layer within a filled channel or depression (Figure 5.28). They may be preserved as a land surface below modern bedforms such as sandbanks, which is common off the Norfolk coast beneath the Norfolk Banks.

Presence of biogenic gas associated with decomposition of organic matter often is shown as dim-out or acoustic blanking directly at or beneath suspected peat or organic-rich horizons but may also form a dissociated front in areas where organic-rich materials, such as those formed in eutrophic lake environments, fill deep incisions. These soils may also have low strength values (see Chapter 5.7 on low-strength clays.)

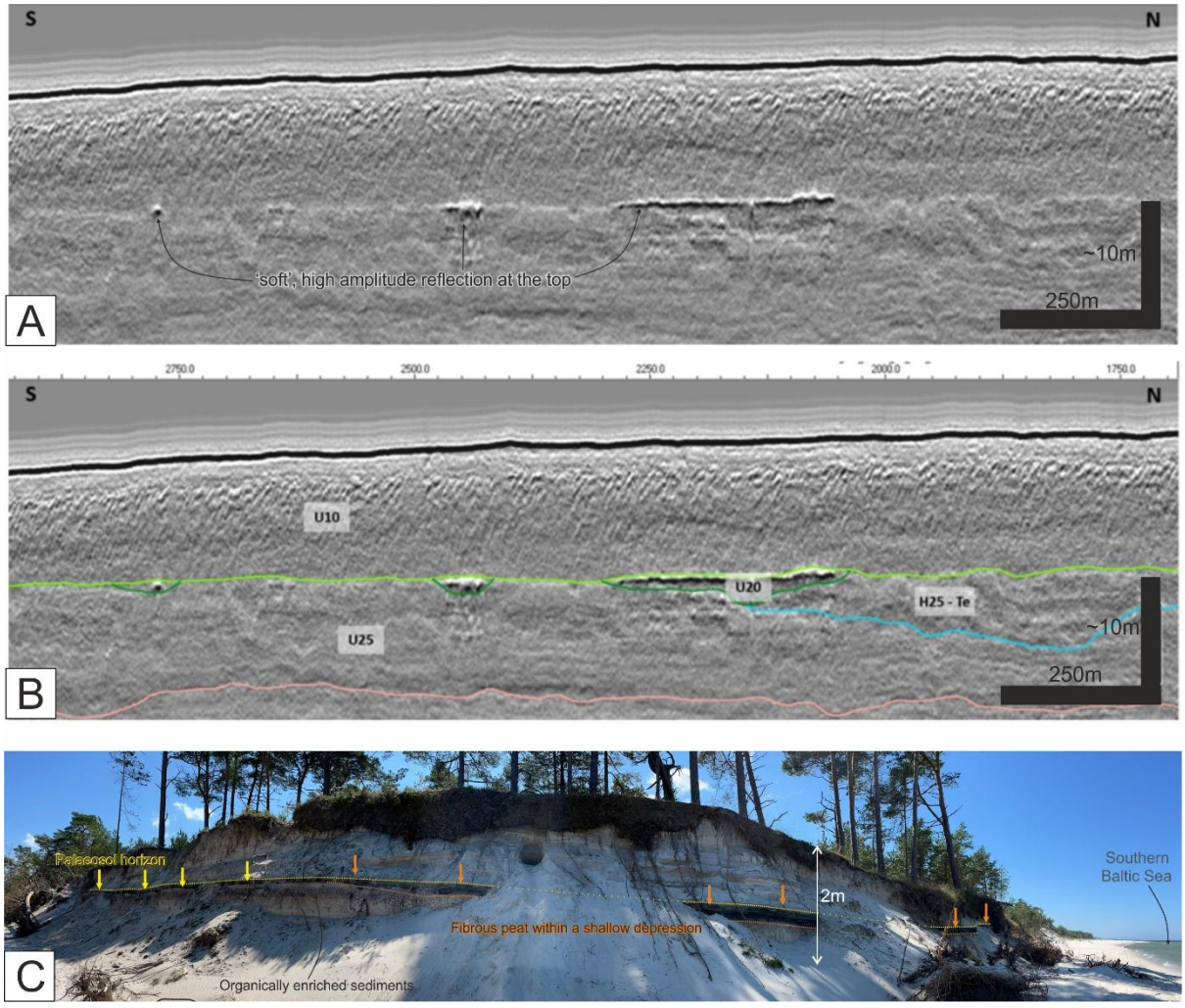


Figure 5.28. Peat beds in seismic profiles and outcrop. **a)** Uninterpreted and **b)** interpreted UHR seismic profile showing high-amplitude 'soft' topped reflection linked to the presence of organic-rich sediments along a palaeosol (green horizon) and confined to local depressions and channels. U10: Marine Holocene sand deposits. U20: Infills of small basins and channels, likely in a restricted marine-tidal setting, partially associated to a subaerial fluvial system. U25: Fine sediments: fine sands-silts (?) deposited in a relatively low-energetic setting, possibly a glacial lake or a transgressive estuary. Subdivided into subunits U25-Te and U25. Danish Energy Agency (2023). **c)** Example of laterally continuous palaeosol horizon buried by coastal dunes on the coast of Southern Baltic Sea in Poland. Note that ~30 cm beds of fibrous peat are only locally present along the surface and confined to a

shallow depression. The bed in the picture extends for ~300 m. Laminae and beds of organic rich sands are present below the paleosol horizon. Photo: B. Kurjanski – private archive.

Important contributions to the topic have been made for the Elbe Paleovalley (Hepp et al., 2019; Özmaral et al., 2022) and for a windfarm site 50 km offshore of East Anglia (Figure 5.29; Eaton et al., 2024). The origin of the organic rich deposits in both areas are described in detail. The Elbe Paleovalley deposits are aged as being deposited between 8250 and 9900 years before present (Özmaral et al., 2022). This study was also able to outline some details on the early stages of the Paleovalley formation. Cuts were infilled with estuarine muds, peat and silty clay in freshwater marshes or in brackish/lagoonal environment. The peat is described as "very dark brown", but no index testing results are given to help assess whether the material is truly peat or an organic-rich soil.

The East Anglia work (Eaton et al., 2024) is of particular value as it also includes the results of some in situ CPTU tests (Figure 5.29). A seismic anomaly unit (SAU) was identified and found to comprise peat, organic-rich sands and silts and clays. The peat is described as a "dark brown, humified and amorphous with wood fragments" but again no engineering index parameters are given. The peat was formed between approximately 13,900 and 9,500 years before present in both laterally extensive sheets, which are now discontinuous, and along the margins of channels. Occasionally peat clasts were found in the overlying sandy soils providing evidence of erosion of the upper organic rich layer. It was found that a high friction ratio (Rf > 5%) and a low cone resistance (qc < 1MPa) corresponded well with the SAU (Figure 5.29).

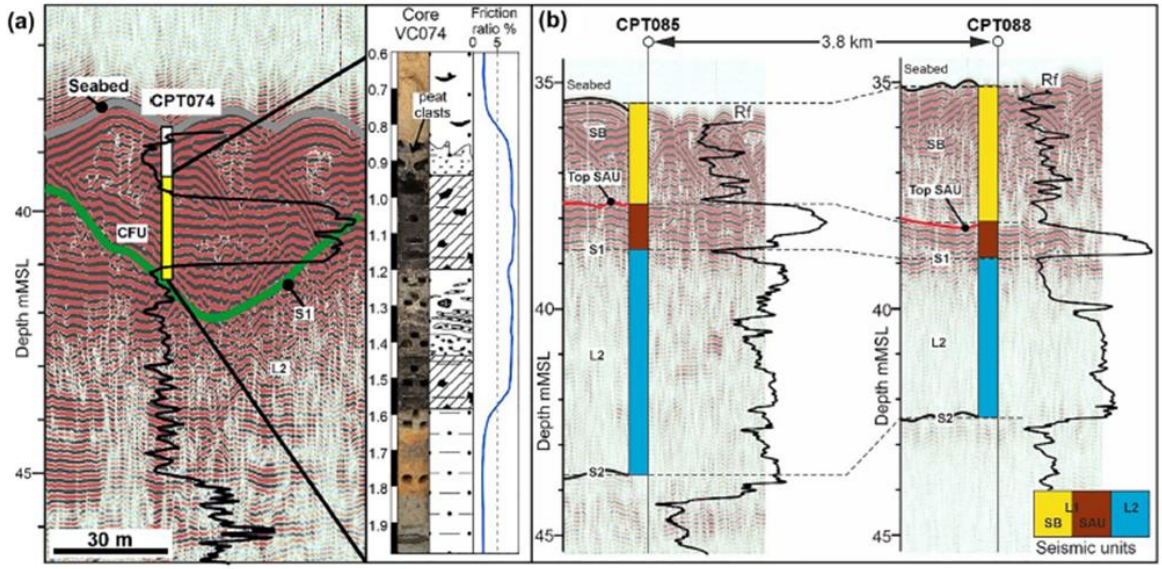


Figure 5.29. Peat identified in seismic, core, and CPT data in a windfarm project offshore East Anglia. CPT parameter (Rf: friction ratio) overlain in black. **a)** VC/CPT 074, with vibrocore path overlain on the seismic data. Yellow indicated the cored unit with the organic-rich interval, including peat within the channel-fill unit (CFU). Note the peat clasts in the overlying sand. **b)** CPT 085 and 088 to show the

clear response in Rf of the seismic amplitude unit (SAU). SB: Seabed bedforms unit, S1: Surface 1, L1: Seismic unit 1, L2: Seismic unit 2. From Eaton et al. (2024).

Some CPTU and MSCL data for a site in the Central North Sea are shown on Figure 5.30 (Smith et al., 2024). The lower density and higher porosity of the organic-rich sediments, as cleary deliniated by the MSCL measurements, are consistent with the high Rf values from the CPTU. The organic rich and low organic content material have similar cone resistance (qc) values thus confirming the usefulness of the Rf data.

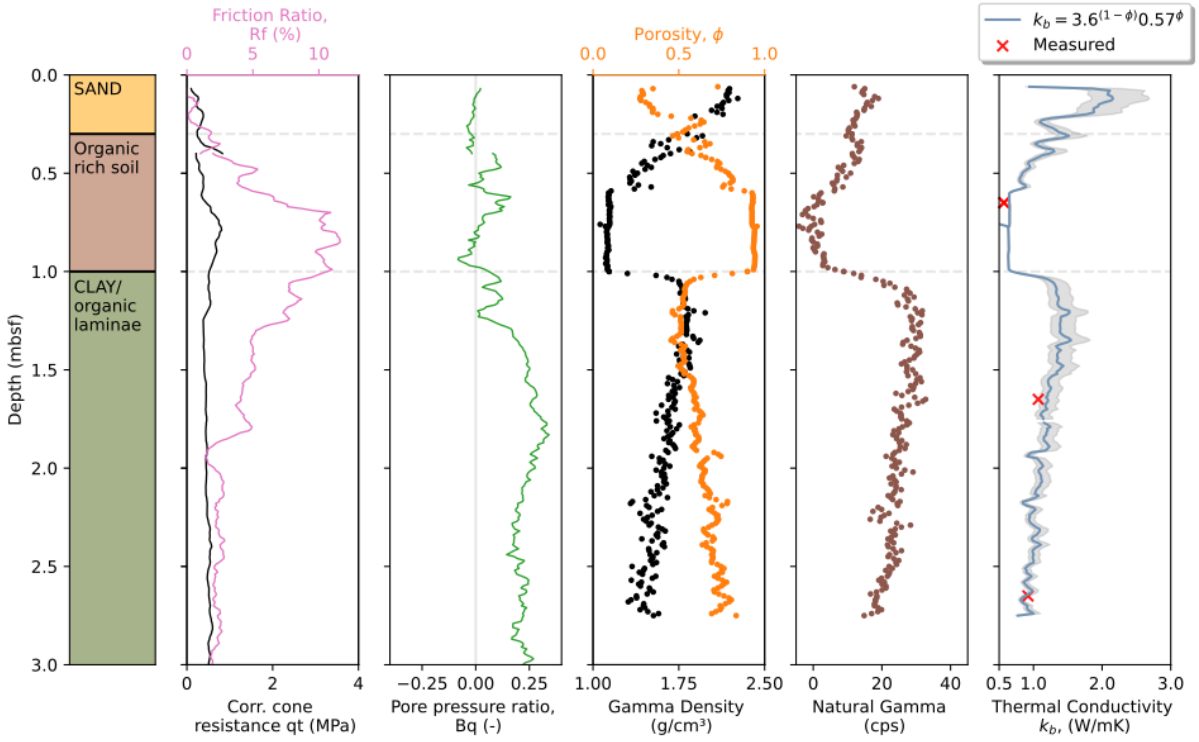


Figure 5.30. Organic rich sediments in multi-sensor core logging (MSCL) data. Soil type, CPTu, selected MSCL data and thermal conductivity profiles from the Central North Sea. The grey zone indicates low and high estimates at 15 and 85% confidence. The distance between adjacent Vibrocores and CPTu profiles is approximately 0.8 m. From Smith et al. (2024).

Engineering implications and associated geohazards

Peats and organic-rich soils are characterised by high compressibility and water (moisture) content of up to 1500% (examples of up to 2000% are known; M. Long – pers. comm.), low shear strength (S_u = 5 - 20 kPa), and can also be more laterally heterogeneous and more permeable than clays (Huat et al., 2014). These characteristics can pose problems for infrastructure design and installation. Foundation design may need to account for very high compressibility, where these soils occur in sufficient thicknesses, but also for extremely low strength, fine-grained material where other organic rich soils are present. The installation or maintenance of offshore structures must also take this into account, and

jacking operations need to consider the risk of punch through or hanging legs where peat "rafts" overlie lower strength materials. For the installation of pipelines or cables in the marine environment, but also in the nearshore and coastal environment, heavy plant such as trucks, horizontal drilling rigs, and trenching equipment may get stuck if not appropriately specified.

Organic- rich sediments are thermally insulating when compared to mineral deposits, with low thermal conductivity and high thermal resistivity. This means that design of thermally sensitive infrastructure, such as pipelines and cables, must properly consider the effects even small sections of peat or organic rich sediments may have on heat dissipation and thermal expansion during operation. As these soils do not allow for dissipation of heat generated by HVDC/AC cables, cables may encounter lower cable performance or, in extreme cases, in overheating and compromising an offshore transmission cable.

Due to being deposited in anoxic environment organic soils have the potential for further degradation if exposed to oxygen- rich environment and may undergo substantial change in their physical properties (Clare et al., 2023; Zhao et al., 2019; Zhao and Si, 2019). This could happen during installation of cables or pipelines, when peat beds may be disturbed in addition, the decomposition of organic matter results in highly acidic environments (Zhao et al., 2019; Zhao and Si, 2019; Blumenberg et al., 2022). This can cause issues with corrosion which may reduce the operational life of offshore infrastructure, particularly for foundations (e.g., Fugro, 2017).

The degradation of peat can also result in the modification of the overlying seabed, coastline or subsurface and release large amounts of inert, stored carbon to the ecosystem. Biogenic gas pockets associated with organic deposits can be a potential cause for blowouts, if disturbed, and pose a direct risk to life, health, and equipment.

During cable or pipeline installation process using a trenching plough presence of fibrous and woody elements above 1% were reported to cause issues requiring several re-runs of plough to achieve the desired depth of lowering (Brown et al., 2015).

Considering the potential issues associated with these soils, peats and organic soils are highly unfavourable from an engineering perspective. It is therefore important to utilise effective, fully integrated ground modelling techniques to identify locations and situations in which these soils might occur, and effective geophysical and geotechnical site investigation to ensure they are mapped and constrained appropriately.

5.10 Faults and fractures

The continental margins of Northern Europe are so called "passive margins" although the margins have been subjected to reiterative deformation since the opening of the North Atlantic Ocean ca. 55 Ma. Since then, the tectonic stress regime across the margins has evolved in time and space involving compression, transform faulting, extension, and even inversion (Gregersen et al., 1989; Mosar, 2003;

Roberts and Yielding, 1991, Faleide et al., 2025). Fracturing and faulting is widespread in the shallow subsurface along these continental margins. Large-scale Mesozoic faults can extend to the Quaternary strata and have a connection with the present-day seafloor as observed broadly in the Barents Sea (e.g., Faleide et al., 2019; Serov et al., 2023) and the Danish Basin in the North Sea (e.g., Ahlrichs et al., 2023). Polygonal faults, believed to be caused by dewatering of fine-grained saturated sediment, are also commonly observed along the continental margin since Miocene time (e.g., Berndt et al., 2003; Wrona et al., 2017). The Quaternary sequence is particularly prone to tensile fracturing in places where the crust is subjected to doming. In general, any discontinuity and weakness zone have the potential to accumulate stress leading to local alterations of the regional stress field. These stress concentrations can lead to fault reactivation and to the development of new fractures (Gudmundsson, 1999).

Stress changes associated with the advance and retreat of the large Quaternary ice sheets lead to the generation of glacially-induced seismicity and fracturing and deformation along continental margins at scales that are not easily identifiable due to their aseismic nature. In addition, periglacial areas (i.e., areas adjacent to contemporary or past ice-sheets) along continental margins have been exposed to reiterative ground freezing and thawing through glacial cycles (see also Section 5.8). These processes lead to a very specific type of deformation in near-surface poorly consolidated strata, referred to as involution (van Vliet-Lanoë et al., 2004). Tectonic (including glaciotectonics; see Section 5.12) and periglacial deformation are two different styles of deformation affecting the stability of Quaternary sediments at glaciated margins, but they interact and interfere with each other. For example, frost and ice wedges will exploit preexisting fractures and mechanical discontinuities in the sediment. Similarly, fresh water will circulate preferentially through dilated faults leading to pingo formation. In active hydrocarbon systems, fluid migration and associated gas-hydrate formation may lead to enhanced glacio-tectonism along faults (e.g., Bellwald et al., 2023a). Overall, the continental margins of northern Europe have been affected by faulting and fracturing associated with the following mechanisms: 1) lithospheric plate movements due to mid-ocean ridge spreading along the mid and north Atlantic mid-ocean ridges (ridge push); 2) glacial isostatic adjustments; 3) local neotectonics; 4) gravitational forcing due to large scale erosion and sedimentation; 4) salt and sill intrusion tectonics; and 5) periglacial deformation.

In compressional stress regimes on land (i.e., with reverse faults), high vertical stresses associated with the thick ice sheets (when present) tends to compensate the maximum, compressive horizontal background stress. This suppresses seismic activity (i.e., seismicity under Greenland and Antarctica is very low and the earthquakes that occur are relatively weak) (e.g., Johnston, 1987). However, crustal unloading following decay of the ice (i.e., reduction of the vertical stress) together with crustal strain accumulated under the ice sheets can lead to fault destabilization and strong seismicity occurring over a concentrated period of thousands of years (i.e., during deglaciation) (e.g., Brooks and Adams, 2020; Johnston, 1987).

Glacially induced seismicity accounts for most of the neotectonic phenomena at glaciated continental margins. It is a phenomenon that has been proved with numerous observations on land (Brooks and Adams, 2020; Olesen et al., 2004; Olesen et al., 2013; Brandes et al., 2015). Glacially-induced faulting and earthquakes activity in Fennoscandia is widely demonstrated (e.g., Olesen et al., 2004). In Norway there have been many claims and reports of neotectonic activity on land and offshore. Liquefaction, rock failure events, and submarine landslides have been associated with large magnitude recent as well as paleo-earthquakes and sub-seabed deformation (Olesen et al., 2004; Bellwald et al., 2019a; Eldholm and Bungum, 2021; Sørensen et al., 2023).

However, offshore evidence of glacially induced faulting and fracturing is less abundant. This could be due to 1) the fact that the stress regimes change significantly from the ice-sheet depocenter region to the forebulge regions. Glacially induced stress modelling for Fennoscandia shows that crust under a vanished ice sheet is currently experiencing uplift while the crust at the forebulge is experiencing present-day subsidence. These models also show that stress magnitude and orientations change more abruptly at the ice-sheet depocenters (Lund et al., 2009; Vachon et al., 2022); and/or 2) identifying fault propagation and near-surface seismicity is challenging due to thick Quaternary sediments covering relatively recent post-glacial faults and fractures. Nonetheless, theory shows that crustal doming associated with post-glacial uplift generates tensile stresses that are sufficiently large to generate tension fractures (e.g., Gudmundsson, 1999). Indeed, recent studies based on attribute analyses of high-resolution P-Cable 3D seismic data (3-5 m vertical resolution) off west-Svalbard reveal that certain chronological intervals are more severely fractured than others (Cooke et al., 2023; Figure 5.31).

Large-scale faults (i.e., planar features with detectable vertical throw in seismic data) are generally easy to identify even in 2D seismic lines given a favourable orientation of the surveys with respect to the fault strikes. The detection of small-scale fracture networks, however, is dependent on the availability of ultra-high-resolution 3D seismic data (Figure 5.31). In general, faults and fractures are commonly identified thanks to advanced multi-attribute analyses in 3D seismic data, often involving neural networks training. The quality of the data, data resolution and the methodology implemented, all impact the accuracy of fine-scale faults and fracture interpretation (e.g., Cunningham et al., 2020; Ligtenberg, 2005; Cooke et al., 2025).

The properties of faults and fractures in the shallow subsurface modulate the transport of fluids from deep to shallow sediments, and – in cases – into the ocean. Local changes in the stress field (i.e., given by stress focusing on small-scale features like fractures, fault segments, diagenetic depositions) can either enhance or hamper fluid migration, depending on whether permeability is increased (e.g., under tensile stress) or decreased (e.g., under compressive stresses) (e.g., Sibson, 1994) (Figure 5.31).

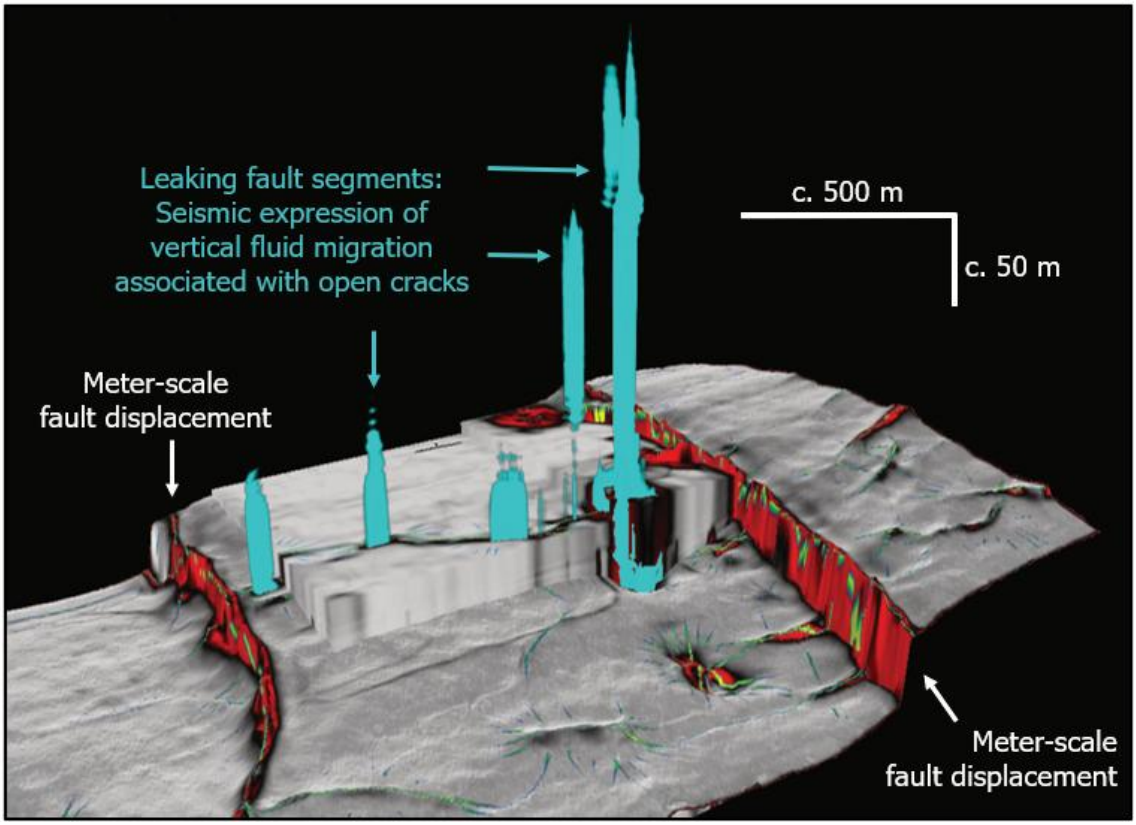


Figure 5.31. Example of vertical fluid migration (chimneys or pipes) through highly deformed strata offshore west-Svalbard imaged with high-resolution P-Cable 3D seismic data. The figure shows seismic variance extracted along a surface correlated with a ca. 1.2 Ma marker (close to the mid-Pleistocene transition (Cooke et al., 2023). The restricted location of gas chimneys (blue) indicates that leakage occurs exclusively through open segments along given deformation planes (Cooke et al., 2025). The figure was kindly provided by Frances Cooke.

Salt tectonics and polygonal faulting of dehydrated fine-grained sedimentary successions are geological mechanisms that promote fault-controlled fluid migration and leakage into Quaternary strata (Figure 5.32). The hydro-mechanical properties (e.g., porosity and permeability) of Quaternary strata (i.e., within the upper ~2 km below the seafloor) are mostly controlled by compaction processes and to some extent by diagenetic processes that contribute to volume changes (e.g., deposition of authigenic carbonate or gas hydrates). The vertical stress exerted on the shallow subsurface at continental margins is carried partly by the sediment matrix and partly by the fluid phase (e.g., Bjørlykke et al., 2015). Pore pressure measurements are therefore critical for constraining the effective stress (the vertical stress minus the fluid pressure) and assessing whether an area is critically pressured and is within the fracture failure/reactivation point or whether it is stable. Detailed studies on the orientation of pre-existing fractures in the shallow subsurface together with constraints on the regional stress regime are critical for predicting the fracturing behaviour of fluid saturated sediments (e.g., Zoback and Lund Snee, 2018).

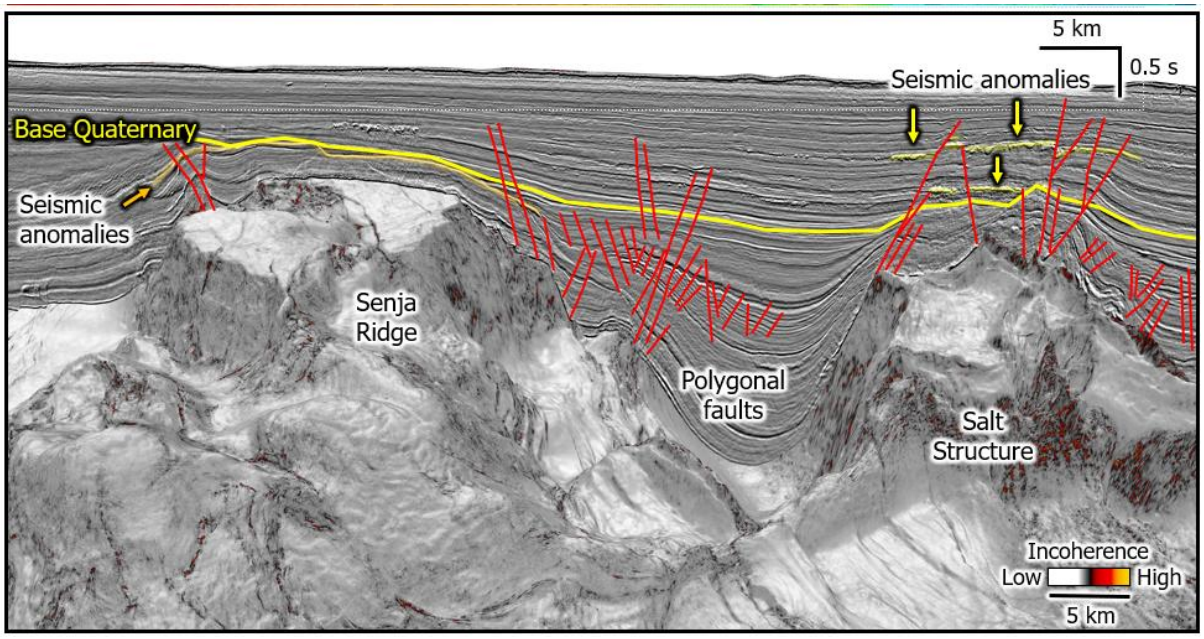


Figure 5.32. Chair view into Senja Ridge (basement high) and neighbouring salt structure with overlying stratigraphy, Southwestern Barents Sea. Shown are different types of faulting, and their implications on the Quaternary stratigraphy. Polygonal faulting mainly limited to the basin infill of Paleogene and Neogene age, while faulting related to basement and salt structures affecting the Quaternary stratigraphy. Example from SW Barents Sea. Data courtesy of TGS and VBER.

5.11 Glaciotectonic deformation

Glaciotectonic deformation refers to any kind of deformation within unconsolidated sediments and/or bedrock that is caused by the motion of glaciers and ice sheets or by differential loading caused by the ice mass. This includes faulting, folding, disturbance to pre-existing structure, or state of the sediments, but also quarrying and re-location of intact fragments of pre-existing strata i.e. glaciotectonic rafts (Aber, 1989, Aber and Ber 2011)

Glaciotectonic deformations can occur at multiple scales from ice sheet-scale glaciotectonic thrust sheets extending along the former ice margins for 10s of kilometres distorting 10s-100s of meters of strata, to outcrop-scale deformation where individual beds are folded or offset by small-scale reverse and normal faults on metre or cm scale (Figures 5.33 and 5.34) . The vast majority of glaciotectonic deformation occurs close to the ice margin either in the subglacial zone or a distance up to several km in front of it as the advancing ice mass loads, bulldozes and overrides sediments in front of it. On a regional scale, large glaciotectonic complexes are often related to major ice-sheet advances, re-advances, or stillstands of the ice sheet. Smaller glaciotectonic deformations are often present on more local scale (i.e. annual oscillations of the ice margin overriding and thrusting a recessional moraine), and are relatively common in former ice-marginal settings.

Some of the larger glaciotectonic thrust complexes offshore formed during or after the LGM can be observed as major shallow banks detached from land and are preferentially targeted for offshore wind farm development as they are suitable for fixed offshore wind turbine foundation design and offer a higher wind yield due to their distal location. Examples include Dogger Bank wind developments in the Southern North Sea (Philips et al., 2018; Emery et al., 2019) or Słupsk Bank and potentially Southern Middle Bank in the Baltic Sea (Figure 5.33). Despite being favourable from a bathymetric and wind yield point of view they are also associated with one of the most complex and variable glaciogenic deposits. It is also worth noting that not all glaciotectonic deformations, especially predating the LGM, are identifiable on bathymetric data (Figure 5.33). Evidence of former ice bulldozing and glaciotectonics is often only provided by seismic and borehole data (Figures 5.33 and 5.34).

Types of glaciotectonic deformations

The basic type of large-scale glaciotectonic deformation was readily described by Aber (1989) as 'Ice-scooped basin and ice-shoved hill' otherwise known as a glacial over deepening followed by thrust complex sometimes combined with a marginal push moraine or sediment / bedrock raft. Following ice retreat the 'hole' often accommodates a proglacial lake where fine-grained cohesive sediments are likely to be deposited. It is worth noting that glaciotectonic deformation or complexes do not form universally at all ice margins (Bennett, 2001).

Common characteristic of all glaciotectonic deformations is the presence of a detachment or decollement surface at the base of the glaciotectonically deformed zone (Lee and Phillips, 2013; Pedersen, 2014; Pedersen and Boldreel, 2015; Phillips et al., 2018; Vaughan-Hirsch and Phillips, 2017; Winsemann et al., 2020) (Figure 5.33). This surface typically forms along a strength anisotropy contrast within an undeformed sediment or rock package. The contrast may exist due to lithological differences (soft, weak clay under strong/stiff sand package), contrast between bedrock and unconsolidated sediments, fluid pore pressure gradient (e.g., permeable sands with high pore pressure under impermeable cohesive sediments) or the presence of permafrost horizon, or shallow gas and gas hydrates in the subsurface (Bellwald et al., 2023a; Huuse and Lykke-Andersen, 2000; Piotrowski et al., 2004; Winsemann et al., 2020 and references therein).

Glaciotectonic deformation is typically most severe close to the paleo-ice margin position and decreases in magnitude distally (radially) away from it (Figure 5.34). In many cases sediments in the most proximal, ice-contact zone are almost completely distorted and homogenized making it impossible to, for example, correlate them to their host unit or quantify the degree of shortening (Emery et al., 2019; Phillips et al., 2018; Vaughan-Hirsch and Phillips, 2017). In seismic data such sediments often appear acoustically chaotic without any coherent, traceable internal reflectors. The ice contact surface on top of the package will likely be a strong, positive kick due to compaction by ice. In borehole or outcrop

studies, the term 'glaciotectonite' is often used to describe sheared rocks or sediments with unrecognisable or highly distorted primary structures and widespread shear structures (Bayliss et al, 2015).

More distally to the ice margin, thrust faults form at +/-30° angle dipping towards the ice margin. These thrusts are often subsequently over-steepened if the ice margin continues to push the sediment pile in front of it and can ultimately be vertical to sub-vertical (for example Gehrmann, 2020). Subsurface examples from seismic data offshore indicate that the final thrust block moraine is often a product of multiple phases of ice advance and bulldozing (Emery et al., 2019b; Phillips et al., 2018). The resulting glaciotectonic deformation is often complex with multiple stacked thrust sheets, back thrusts and piggyback thrusts driven on top or cutting across the pre-existing deformed package. Imbricate stacks can be imaged and recognised from seismic data, but it can be very challenging to correlate the thrusts laterally and understand the orientation of thrust sheets unless 3D seismic data is available (Figure 5.34). Further away distally (radially) from the ice mass, the deformation of sediment/rock pile is transitioning from thrusting (due to breaching of the shear strength of sediments) to folding with decreasing amplitude and increasing wavelength until all of contraction is accommodated (Figure 5.34). It is worth mentioning that some glaciotectonic deformation can be caused by the loading by the ice mass alone and does not rely only on the 'push' component (Andersen et al., 2005).

Glaciotectonic deformation can be observed at all scales from outcrop and cm-scale reverse faults and folds, through medium-scale thrusting on the scale of 10s and 100s of meters to extensive regional thrust sheet complexes extending laterally and radially for 10s to 100s of kilometers (Figure 5.33 and 5.34; Cotterill et al., 2017; Emery et al., 2019b; Huuse and Lykke-Andersen, 2000; Phillips et al., 2018; Vaughan-Hirsch and Phillips, 2017). Glaciotectonic deformation has been demonstrated to extend for several to 10 km beyond the corresponding paleo ice extent (Andresen et al., 2005). The degree of shortening within glaciotectonic complexes is variable and often difficult to quantify. Examples of minimum shortenings of up to 50% are known from the North Sea.

Table 5.4. Types of glaciotectonic deformation.

Type	Variety	Description/ definition	Comment/dimensions
Large-scale glaciotectonic deformations	Thrust-block moraines	Formed proglacially by bulldozing of pre-existing sediments/rocks by advancing ice margin or by gravitational spreading under load	Also known as composite ridges. Imbricated stacks can be vertical or in the ice-proximal part. Multiple cross-cutting sets of thrusts could be present at the same margin. Individual thrust planes can be spaced very densely, even every 50-100 m. Laterally, thrust planes as short as 100 m were observed from seismic data.
	Cupola hills	A thrust-block moraine that was overridden by the ice resulting in partial erosion/scalping of the top of the thrust sheet and deposition of a till carapace on top	Many thrust block moraines have been at least partially overridden by the ice. They do not form a cupola hill *sensu stricte,* but their overridden parts can

			exhibit a very similar stratigraphic succession.
	Large-scale fold and thrust belts formed due to ice loading	Proglacial deformation driven by vertical load exerted by an ice mass on an unconsolidated sediment package	Thrusts will likely form at angles close to 30°. This deformation could affect large areas.
	Large push moraines	Push moraines are formed by a combination of ice push of unconsolidated loose material and melt out and plastering of basal sediments. Thrusts may be present but cannot be easily recognised due to the quasi-homogeneous nature of push moraine material.	Internal structure can be very chaotic and resemble glaciotectonite. Subglacial material, including boulders and till, could be incorporated in a push moraine. Slope failure and debris-flow sediments can often be expected with and on the flanks.
Small- and medium-scale glaciotectonic deformations	Recessional and de-Geer moraines.	Recessional moraines are formed by seasonal/ periodical re-advances of the ice margin during an overall retreat. Small volumes of sediments are bulldozed and deposited in linear mounds delineating the ice-margin position	De-Geer moraines are similar in their formation process but are characteristically formed when the ice margin is grounded in water. They are often very regular and evenly spaced. In general, recessional moraines can be composed of material similar to push moraines but their dimensions (meters high and 10s of meters wide) makes them difficult to observe in 2D seismic data)
	Ice-contact deformation of other landforms	In some cases, relatively minor ice-margin oscillations can cause glaciotectonic deformation of ice-contact parts of pre-existing sediments and landforms. Small, metre- to centimetre-scale faulting and folding can be readily observed in onshore outcrops.	This deformation may be too small to be imaged by UHRS data and difficult to identify from offshore sites. In such settings, it is crucial to understand whether the strength of the ground is reduced due to ice-contact deformation.
Glaciotectonic rafts	Sediment rafts	Sediment rafts form when portions of frozen but unconsolidated sediments are frozen onto the base of the moving ice or pushed in front of it without much disturbance to the primary internal structure.	Dimensions of glaciotectonic rafts can vary greatly from $<10m^2$ to $>10km^2$. Rafts are typically much thinner than their horizontal dimensions. They can be transported subglacially for a long distance away from their source area. Undeformed rafts can form a part of a thrust-block moraines or be isolated and form a flat-topped hill. Large rafts of chalk embedded in glacial tills are know from onshore exposures and offshore borehole and seismic data in the North Sea Basin.

	Bedrock rafts	Bedrock rafts are similar sediment rafts but composed pre-glacial, often fully consolidated strata. Bedrock rafts are typically detached along a zone/ plane of weakness within the rock (bedding plane, joint set, foliation fault, etc.).	Dimensions of glaciotectonic rafts can vary greatly from <10m^2 to >10km^2. Rafts are typically much thinner than their horizontal dimensions. They can be transported subglacially for a long distance away from their source area. Undeformed rafts can form a part of a thrust-block moraines or be isolated and form a flat-topped hill. Large rafts of chalk embedded in glacial tills are know from onshore exposures and offshore borehole and seismic data in the North Sea Basin.

2402

2403

2404 **Geohazards and offshore engineering implications:**

2405 Geohazard and geoengineering constrains linked to glaciotectonically deformed sediments and
2406 bedrock are described in Table 5.5.

2407 **Table 5.5.** Summary of geohazards and geo-engineering constraints related to glaciotectonics.

	Description	Comment
Weakened ground properties	Presence of pre-existing shear planes will likely change/weaken the geotechnical properties of the unit when compared to the undeformed state.	Representative and dense borehole sampling and subsequent laboratory tests
Sharp lithological changes over 10s-100s of metres	Variable and poorly predictable ground properties over short distances, repeated sequences of strata due to thrusting and varying degree of deformation	Design approach assuming the 'worst case ground conditions scenario' for foundations and anchors may be required
Variable thrust/shear plane density and orientation	Orientation of deformation planes can vary greatly (up to 120°) with respect to the regional ice-flow direction. Deformation density is non uniform along the ice margin, resulting in heterogeneities of geotechnical properties.	Lateral shear bands within glaciotectonic complexes can be orientated quasi parallel to the ice flow direction making them very difficult to image on 2D seismic data
Changing degree of deformation	In general, the degree of deformation is likely to decrease radially away from the ice margin, and gradually changing from thrusting to folding. This will affect the geotechnical properties.	Grouping all strata affected by glaciotectonic deformation into one soil unit may not be a suitable approach and could result in oversimplification of ground conditions if deformation affects differing lithological units with variable intensity
Presence of boulders	Boulders in highest density are likely to be present in the ice-contact part of glaciotectonic complexes where ice-marginal and subglacial lithologies are deposited directly from the ice.	Boulders (and till) can be present on top a glaciotectonic complex if it was overridden by ice, or within it if a pre-existing boulder-rich lithology was deformed by glaciotectonics.
Potential fluid migration pathways	Thrust planes can provide preferential fluid (including shallow gas) migration pathways.	Small shallow gas accumulation can be difficult to detect due to often chaotic internal seismic reflection facies within glaciotectonic complexes

High uncertainty in seismic imaging	Steep thrust planes and a high degree of deformation often result in poor subsurface imaging, thereby increasing the uncertainty in the ground model.	Some glaciotectonic features can be easily missed or misinterpreted due to their complex nature. This is more likely to occur if 2D seismic lines are not orientated and processed optimally or widely spaced. 3D seismic data are required for a more confident interpretation.
Presence of isolated sediment accumulations	Topography generated by glaciotectonics often results in accumulations of isolated sediments within ponds and kettle holes, or development of local drainage networks. Such soil units are often very local and can be difficult to identify, yet they will likely represent distinctively different ground properties.	Fine-grained and organic-rich sediments formed in kettle-hole like depressions can often be found in similar settings onshore and are now being more frequently found offshore.
Presence of unexpected lithological units	Glaciotectonic rafts can be transported for long distances. In consequence, unexpected lithological units (i.e. rocks or sediment otherwise absent on the site) can be introduced.	Such units may not have the same geotechnical properties as their parent lithology due to a degree of deformation during quarrying and transport by ice sheets.

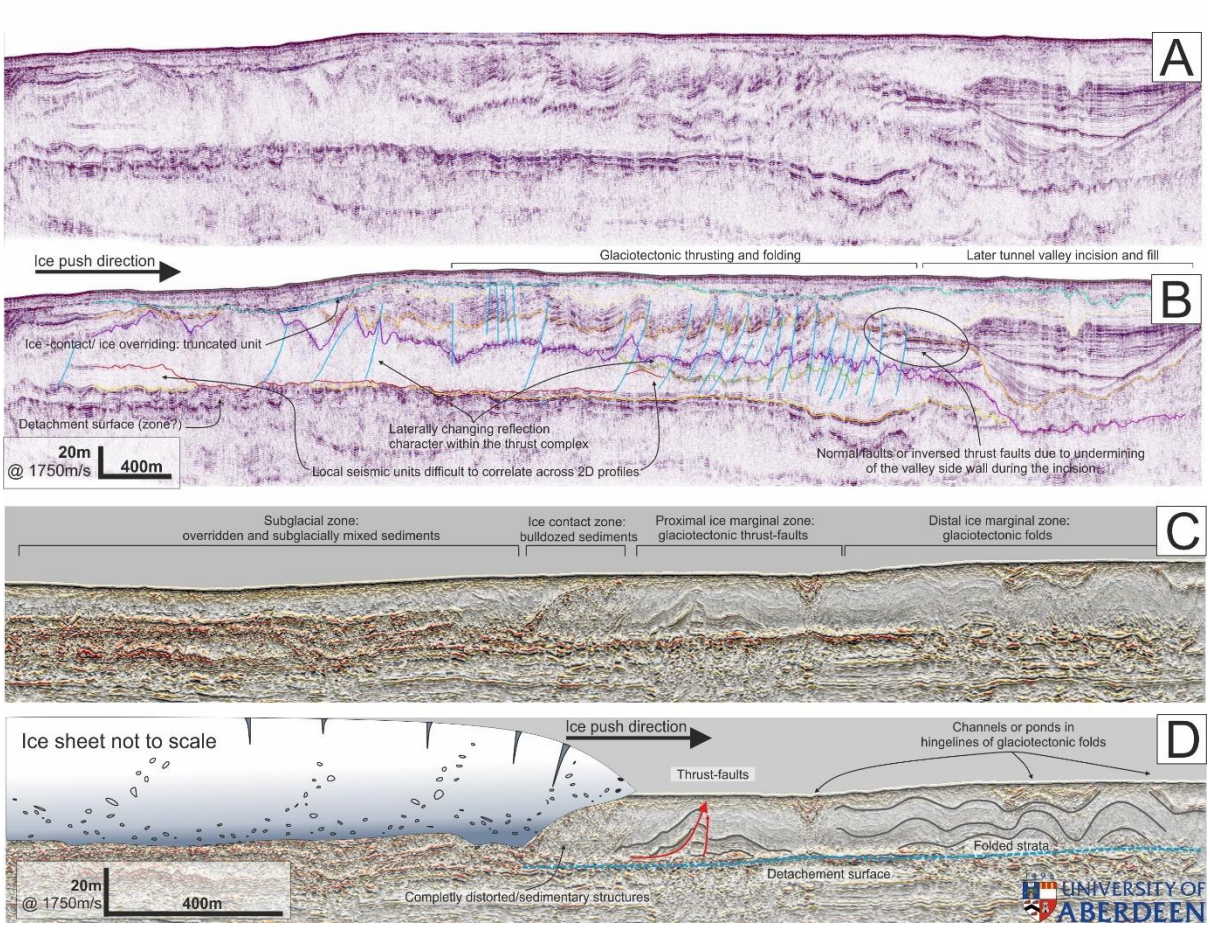


Figure 5.33. Complexes of glaciotectonic deformation. **a)** 2D UHR seismic profile from the North Sea. **b)** Interpreted seismic profile shown in Figure 5.33a. **c)** Seismic profile from the southern Baltic Sea.

d) Explaining sketch and interpreted seismic profile shown in Figure 5.33c. Note differences in thickness, style, complexity, and distribution of deformation between the examples that can be linked to differences in the ice-margin dynamics and position along the deformation front.

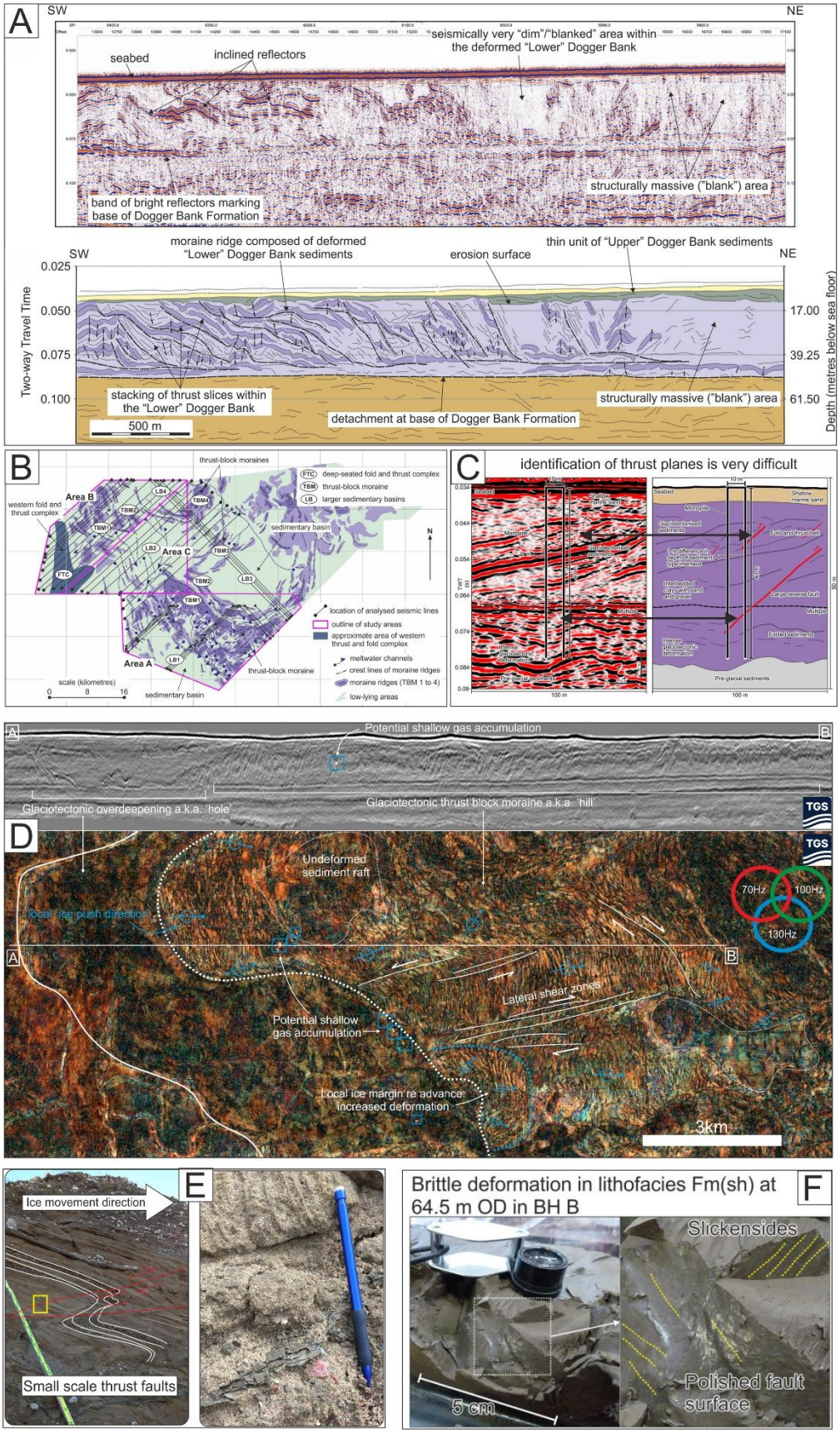


Figure 5.34. a) Uninterpreted and interpreted seismic cross section through a glaciotectonic complex of Dogger Bank from Phillips et al. (2018). **b)** Plan view example of an interpreter glaciotectonic

complex of Dogger Bank (Phillips et al., 2018). **c)**: Example of a projected monopile foundation penetrating glaciotectonised strata. Note several thrust planes intercepted by the foundation (modified from Velenturf et al. (2021). **d)** Regional cross section and corresponding spectral decomposition slice through a hill-hole pair. Note extensive thrusting with multiple lateral shear zones and variable local thrusting vector (blue circle with arrow) despite the general eastward palaeo ice push. Small gas accumulation can be observed as very bright spots (blue squares). HR data courtesy of TGS. **e)** Small scale thrusts in ice-contact setting in granular sediments. Note the presence of clay along the thrust plane possibly pointing to the tole of pressurised water in the thrust formation (Kurjański et al., 2021). **f)** Polished fault surfaces in cohesive sediments sampled from the Dogger Bank thrust complex (Emery et al., 2019b)

5.12 Salt tectonics

Salt of Late Palaeozoic age is present throughout much of the North Sea Basin whilst salt of Triassic, Jurassic and Cretaceous age is present along the Atlantic margins (Hudec and Jackson 2007). Salt tectonics refers to any kind of deformation caused by the movement of salt, typically halite, from early-stage deformation at surface, if deposited on a slope, to deformation during burial and tectonic re-activation. Salt is largely incompressible and weak on geological time scales, causing it to flow under differential loads (Hudec and Jackson 2007). Because of its incompressibility and low strength, salt, unlike other Earth materials, can remain unstable for hundreds of millions of years, often resulting in superimposed styles of deformation involving salt (Figure 5.35).

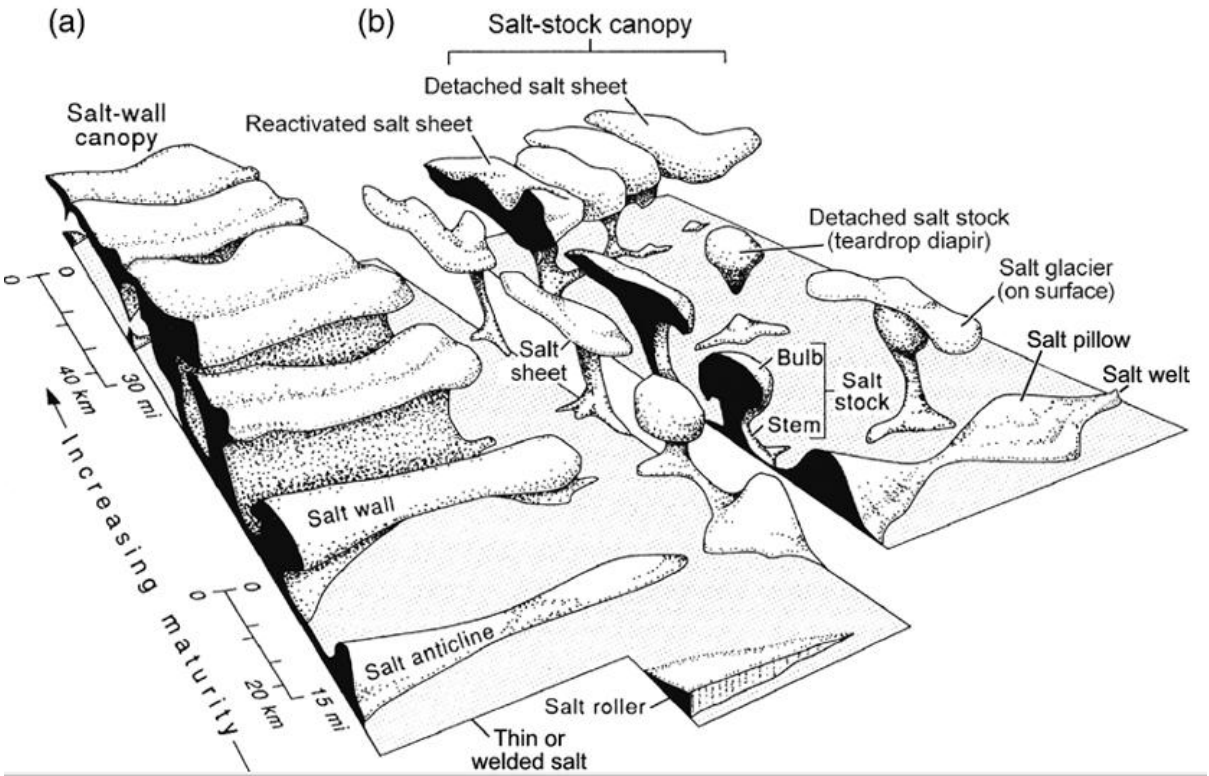


Figure 5.35. Schematic representation of salt structures. NW European examples (North Sea Basin and

Barents Sea) mainly comprise the low to middle maturity varieties, with the most mature structures mainly developing in continental margin or contractional basins with a strong slope (from Hudec and Jackson 2007: fig 6)

On a salt-tectonic timescale, the life span of an offshore installation (< 100 years) is relatively short, but salt structures can still affect offshore installation for a variety of reasons; a) Active deformation of the seabed; b) Triggering and reactivation by glacial loading; c) Providing juxtapositions of materials of different properties near the surface; d) Seismicity associated with salt tectonics adjusting to glacial loading/unloading; and e) by their strong control over subsurface fluid flow, often resulting in hydrocarbon seeps being located around the flanks or over the crests of salt bodies (e.g. Serie et al. 2017; Römer et al., 2021).

In the literature it has been suggested that salt structures may have controlled the location of glacial meltwater valleys (tunnel valleys). However, the evidence for this is sparse (see Huuse and Lykke-Andersen, 2000), and more recent compilations on regional and yet detailed scales using 3D seismic data show that any local controls are largely coincidental or second order with respect to regional ice-sheet hydrological controls (e.g. Kristensen et al. 2007; Ottesen et al. 2023). In terms of glaciotectonics, a similar second-order control is in place as the ice sheet is the primary driver imparting its load on substrate geo-mechanical properties, which can be affected by salt pushing up deeper layers or causing faults to propagate to the free land or sea-bed surface.

Given the often continuous deformation in a relatively low-stress, near-surface environment, the seismicity associated with salt tectonics is expected to be relatively low. Hence the main impacts to near-surface installations (upper 200 m) are expected to be faults propagating to the sediment surface and any lateral changes in the substrate conditions and fluid flow associated with salt-associated deformation of aquifers, seals and rupture by faulting (Figures 5.36, 5.37, and 5.38). Faulting can be due to salt rise and collapse as seen in the UK (Stewart, 2007), the Dutch North Sea (Harding and Huuse 2005), and elsewhere in the North Sea. Gravity sliding off buried highs, such as the Ringkobing-Fyn High, can lead to relatively long and linear faults (Huuse, 1999), but usually with small offsets and relatively little across-fault change in sediment properties, although across-fault changes in bathymetry could lead to peat accumulating in fault-controlled lows, with implications for high-voltage cable performance.

Types/scales of deformation and constraints affecting the geotechnical realm, also shown in Figure 5.37, are:

- Several km diameter of the diapir itself
- Several km radius around salt domes

- Tens to hundreds km long fault systems along buried highs and basin flanks (Figures 5.37 and 5.38)
- Vertical deformation can be several km in the case of diapirs, bringing salt or indurated bedrock into the geotechnical realm (Figures 5.36, 5.37, and 5.38)
- Vertical deformation along buried highs and basin flanks often limited to less than a few tens of metres offset in the upper few hundred metres (Figures 5.37 and 5.38)
- Fluid flow from overpressured strata or hydrocarbon reservoirs can connect over lateral scales of tens of km and vertical scales exceeding several km causing significant geotechnical constraints around any salt domes or deep salt-detached fault systems (Figure 5.38).

Identification criteria (e.g., in geophysics):

Salt domes are usually easily recognised by their concentric deformed layering (in case of preserved sedimentary overburden) or by near-surface chaotic facies characterised by an extremely high positive reflection coefficient in case of salt extending to the near-seabed environment. Figure 5.36 shows a hybrid case where the deformed sedimentary packages are seen dipping outward from a central diapir core where the exposure to circulating groundwater and perhaps glacial flushing has dissolved some of the evaporitic minerals leaving the anhydrite as a caprock with extreme acoustic impedance contrast and thus high-amplitude seismic reflection.

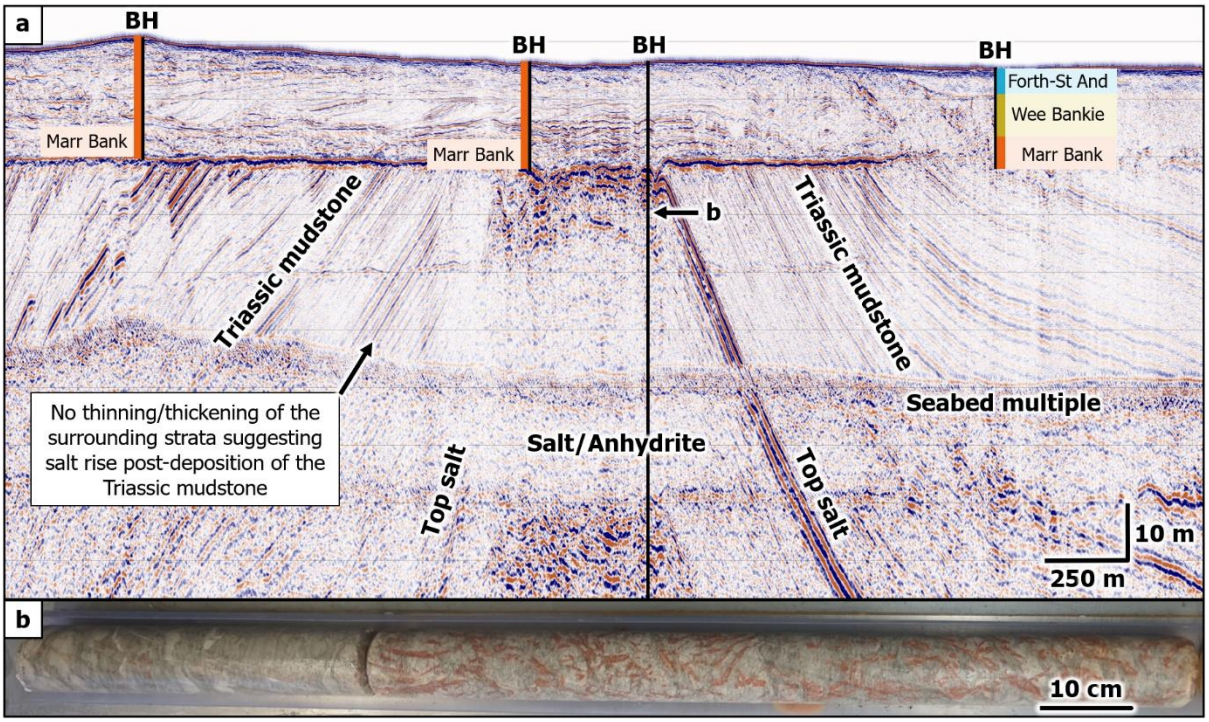


Figure 5.36. Salt dome example from the Berwick Bank wind farm development area in the Firth of Forth, UK North Sea. The seismic reflection character suggested possible salt dissolution and anhydrite

presence at a candidate wind turbine location (Figure 5.36a), which was confirmed by drilling (Figure 5.36b), causing the location to be moved. Data courtesy of SSE Renewables.

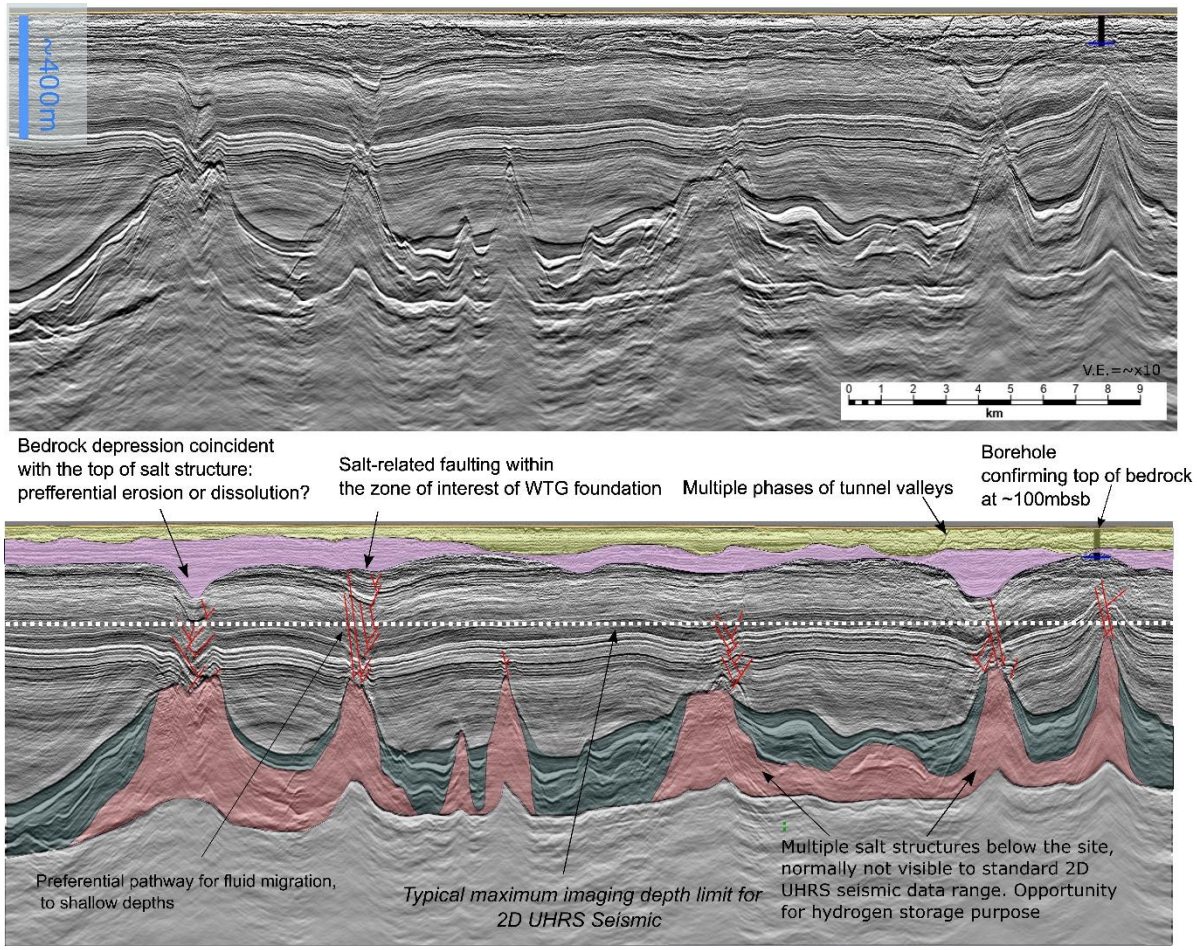


Figure 5.37. Repurposed 2D seismic line across the Mid North Sea High. The data was used for preliminary assessment of ground conditions across an OWF site prior to any commissioned site-specific survey. Note numerous salt structures and focused areas of salt- related faulting within the shallow subsurface within the dept of interest for WTG foundations. Thickened Quaternary sediments are present atop some of the salt structures potentially indicating salt dissolution or preferential erosion along the crests of structures. Figure modified from Tam (2023). Data courtesy of SSE Renewables.

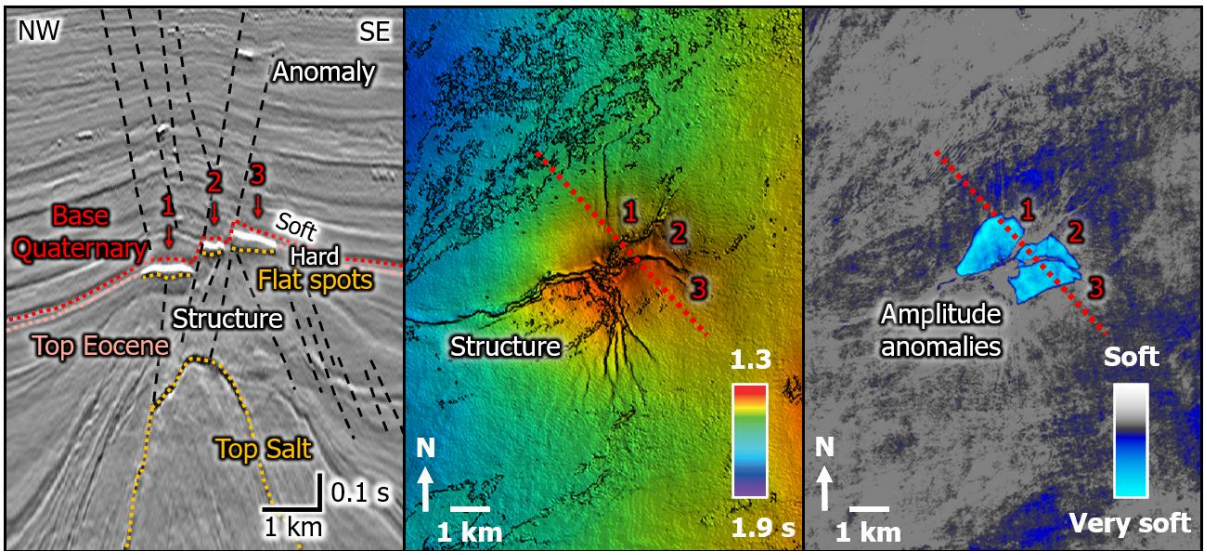


Figure 5.38. Salt tectonic deformation in Quaternary sediments above salt structure in the SW Barents Sea. **a)** Seismic profile indicating salt structure, Cenozoic overburden, and shallow gas trapped at the Quaternary-Neogene interface. Faults are associated with the salt structure, and still identified within the Quaternary stratigraphy. **b)** Structure map showing seismic geomorphology of the Base Quaternary reflection. **c)** Minimum amplitude map of the Base Quaternary surface, highlighting the distribution of the negative-amplitude anomalies along the fault segments of the salt structure. Potential shallow-gas accumulations in the lower Quaternary show as very soft 'bright spot' anomalies and flat spots in the faulted carapace to the salt dome. A 3D view into a salt structure is shown in Figure 5.32. Data courtesy of TGS and VBER.

5.13 Glacigenic landforms

A variety of glacigenic landforms shape the seafloor and shallow subsurface of glaciated margins (Figure 5.39; Dowdeswell et al., 2016). Along the glaciated European margins, these landforms are mainly formed by processes related to the dynamics of the Eurasian ice sheets, in particular subglacial, ice-marginal and proglacial deposition, reworking and erosion. Glacigenic landforms are often subject to later periglacial modification of reworking in marine environments by waves, tides and currents on continental shelves (Section 6.1), and submarine mass movements along the continental slopes (Section 6.2). The morphology of the present-day European margins is mainly caused by processes related to the ice-sheet activity during the Pleistocene glaciations. The presence of these glacigenic landforms and the deposits associated to the landforms have implications for geohazard assessments and marine engineering, which are summarized in Table 5.6.

Bathymetric, side-scan sonar and seismic data combined with sediment cores and boreholes are commonly used to study landforms located in the marine realm (Bryn et al., 2005a; Dowdeswell et al., 2016; Bellwald et al., 2019c; Newton et al., 2024). Over the last decade, developments of acquisition and interpretation of (ultra-)high-resolution 3D reflection seismic data and application of seismic

geomorphology allowed to image glacial landforms below the present seafloor on a meter-scale, establishing strong links between subsurface structures (e.g., faults, topographic highs) and landforms (Bellwald et al., 2023a).

Types of glacigenic landforms and deposits

Glacigenic landforms vary significantly depending on whether they were formed under the ice (subglacial landforms), at the margin of a glacier or an ice sheet (ice-marginal landforms), or formed distally to the ice margin lacking any glacial contact (proglacial landforms; Figure 5.40; Kurjanski et al., 2020). All of these types of glacigenic landforms have been documented along the glaciated European margin (Dowdeswell et al., 2016; Newton et al., 2024a).

Subglacial landforms can either be erosional (i.e. sliding of debris-rich basal ice abraded and eroded existing substratum), depositional (i.e. sediments were deposited from ice at the base of the ice sheet), or a combination of both. The resulting landforms also depend on their formation by a fast-flowing ice stream (i.e., mega-scale glacial lineations or drumlins), or a more slow-moving part of the ice sheet. Finally, the thermal regime at the base of the ice (i.e. whether the ice sheet is frozen to the ground or sliding at the interface) as well as presence and abundance of water at the ice-bed interface have an effect both on sliding velocities and types of landforms and sediments that are generated (Kurjanski et al., 2020; Bellwald et al., 2023a).

In the ice-marginal and proglacial zones, the landforms and sediments depend mainly on the environment in which the ice terminated. Different landforms are observed when ice sheets terminate in water (sea or lake, for example grounding zone wedge) to the ones associated with a land-terminating ice sheet (for example glaciofluvial fans and outwash plains; Figure 5.40). Landforms will also vary depending on the mode of their formation. Ice push and bulldozing in the ice marginal zone will result in the formation of frontal moraines, thrust block moraines, and morainal banks, whereas deposition from meltwater fill form ice contact fans or deltas in marine environment and vast outwash plains (or sandar) in terrestrial conditions (Figure 5.40; Kurjanski et al., 2020).

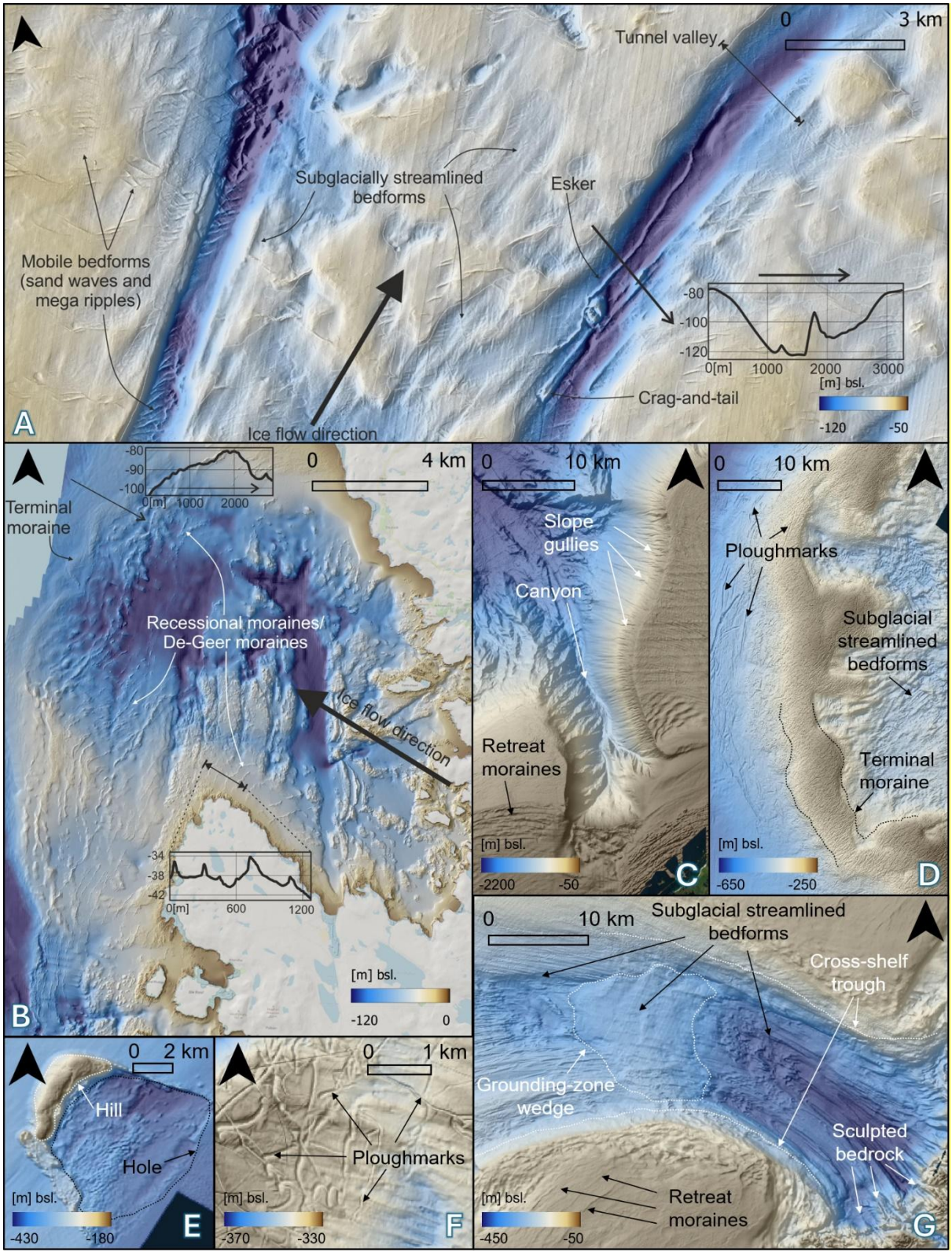
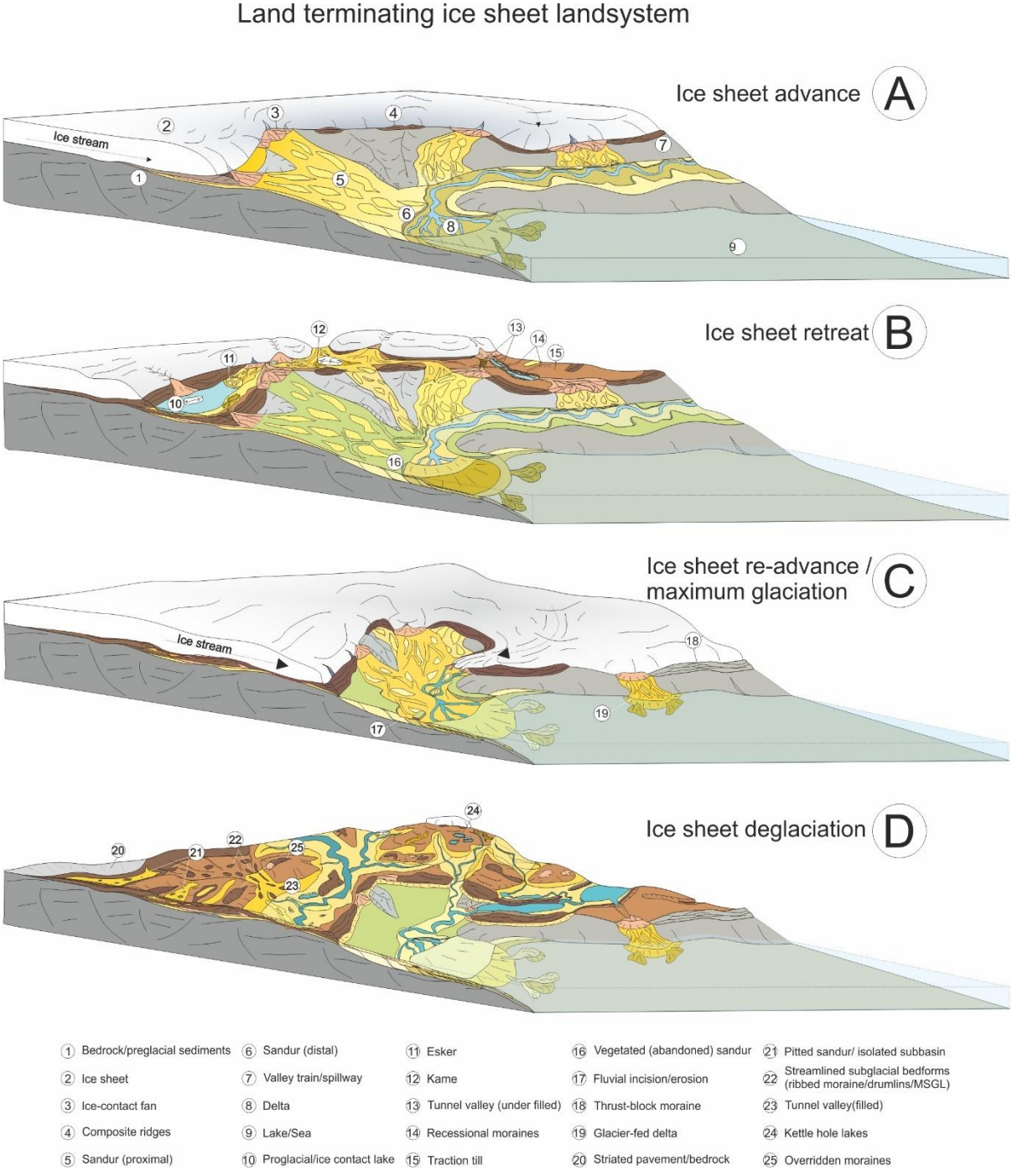
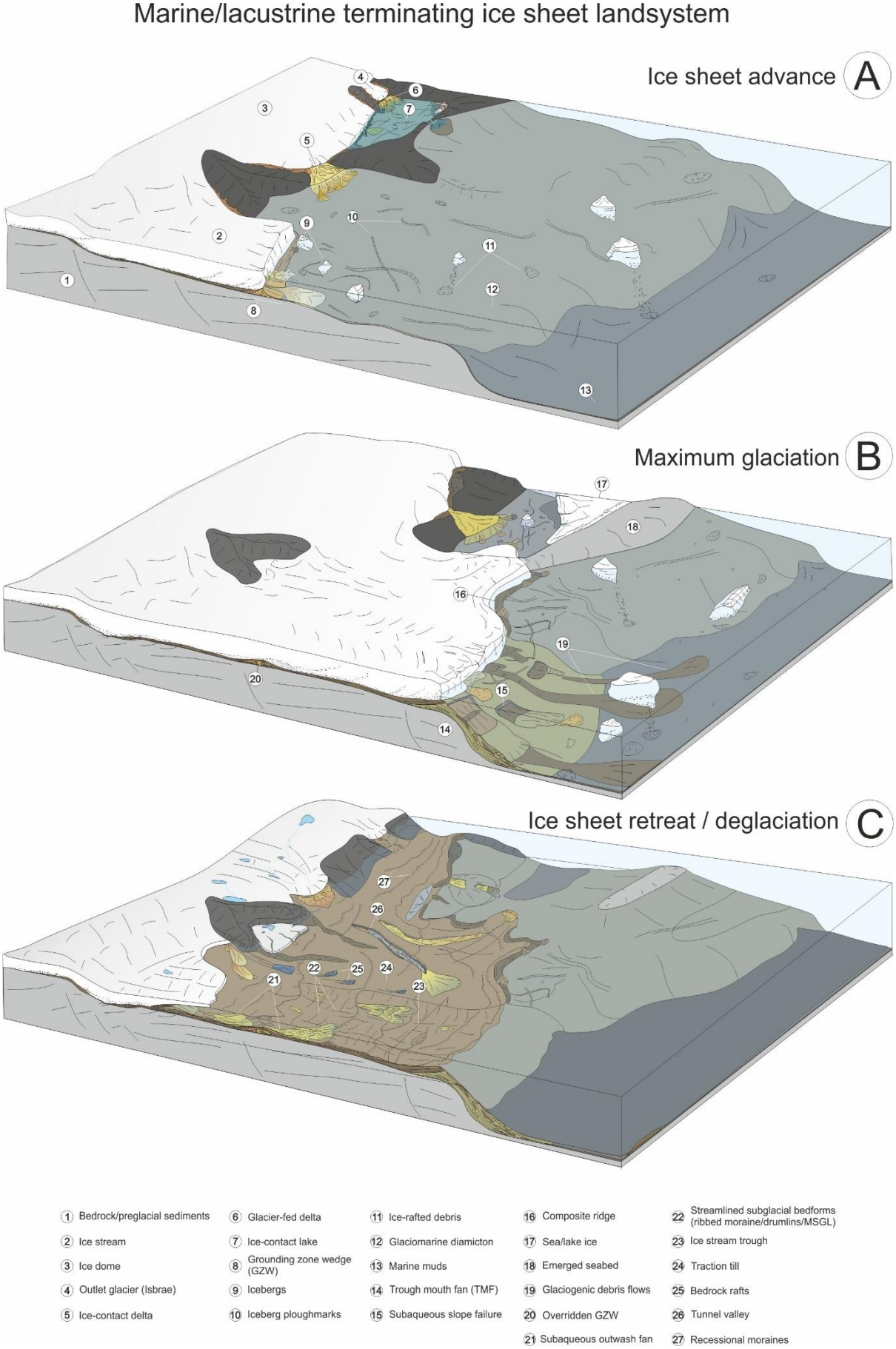


Figure 5.39. Examples of submarine glacial landforms observed along the European margin seafloor. Note that many of these same landforms can be observed buried in the shallow subsurface (see Newton et al., 2024a). **a)** Streamlined and glaciofluvial landforms, along with contemporary sediment waves observed offshore UK. **b)** Moraine features offshore UK showing former ice-margin positions. **c)** Retreat moraines, gullies, and a submarine canyon offshore Troms, northern Norway. **d)** The

Skjoldryggen terminal moraine on the outer mid-Norwegian shelf. **e)** A hill-hole pair observed on the mid-Norwegian shelf. **f)** Examples of iceberg ploughmarks. These landforms are observed extensively on the seafloor and within the subsurface. **g)** The Malangsdjupet cross-shelf trough offshore northern Norway with typical landforms associated in ice-stream and ice-stream proximal areas, such as moraines, streamlined bedforms, and a grounding-zone wedge. Data for the UK have been retrieved from the UK Hydrographic Office and data from Norway were provided by the MAREANO programme.


Land terminating ice sheet landsystem
Ice sheet advance A
Ice stream
Ice sheet retreat B
Ice sheet re-advance / maximum glaciation C
Ice stream
Ice sheet deglaciation D
1 Bedrock/preglacial sediments
2 Ice sheet
3 Ice-contact fan
4 Composite ridges
5 Sandur (proximal)
6 Sandur (distal)
7 Valley train/spillway
8 Delta
9 Lake/Sea
10 Proglacial/ice contact lake
11 Esker
12 Kame
13 Tunnel valley (under filled)
14 Recessional moraines
15 Traction till
16 Vegetated (abandoned) sandur
17 Fluvial incision/erosion
18 Thrust-block moraine
19 Glacier-fed delta
20 Striated pavement/bedrock
21 Pitted sandur/ isolated subbasin
22 Streamlined subglacial bedforms (ribbed moraine/drumlins/MSGL)
23 Tunnel valley(filled)
24 Kettle hole lakes
25 Overridden moraines

2566


Marine/lacustrine terminating ice sheet landsystem
Ice sheet advance A
Maximum glaciation B
Ice sheet retreat / deglaciation C
1 Bedrock/preglacial sediments
2 Ice stream
3 Ice dome
4 Outlet glacier (Isbrae)
5 Ice-contact delta
6 Glacier-fed delta
7 Ice-contact lake
8 Grounding zone wedge (GZW)
9 Icebergs
10 Iceberg ploughmarks
11 Ice-rafted debris
12 Glaciomarine diamicton
13 Marine muds
14 Trough mouth fan (TMF)
15 Subaqueous slope failure
16 Composite ridge
17 Sea/lake ice
18 Emerged seabed
19 Glaciogenic debris flows
20 Overridden GZW
21 Subaqueous outwash fan
22 Streamlined subglacial bedforms (ribbed moraine/drumlins/MSGL)
23 Ice stream trough
24 Traction till
25 Bedrock rafts
26 Tunnel valley
27 Recessional moraines

2567

Figure 5.40. Conceptual block diagrams showing the evolution of land terminating and marine terminating ice sheet ice landsystems over a glacial cycle. Vast areas of continental shelves in the Northern hemisphere that are currently submerged were hosting ice sheets that could be considered land-terminating due to the fact that the sea level was much lower than at present and parts of the present-day seabed were emergent. Note that multiple glacial cycles separated by warmer, interglacial conditions are likely to occur within an icehouse period. Landforms and sediments deposited during a glacial cycle are frequently eroded, transported and re-deposited during a subsequent ice-sheet advance leaving a mosaic-like patchy and highly discontinuous stratigraphic record. Nature of glacial deposition and erosion is responsible for the subsurface complexity of sediments on glaciated continental shelves. Figure modified from Kurjanski et al. (2020).

Implications

The deposits of the various glacigenic landforms can be very heterogenous vertically and laterally on 10s to 100s meter scales, and their grain size varies from large boulders in glacial moraines and subglacial tills to fine clay in glacial lakes and kettle holes (e.g., Figure 3.5). Due to these heterogeneities, glacigenic landforms always express strength variations (Section 5.4), and lateral variability on a meter-scale. Thus, the identification of glacigenic landforms allows prediction of geotechnical properties even before CPT or borehole sampling. In addition, these landforms can define fluid flow pathways (e.g., Mazzini et al., 2016; Tasianas et al., 2018; Bellwald et al., 2023a). The implications of the landforms are summarized in Table 5.6.

Subglacial landforms, typically composed of subglacial lodgement till, are often characterized by high undrained shear strength values (>400 MPa), heterogenous deposits (including boulders), sediment deformation, and overconsolidation due to ice loading (Clarke, 2018). Matrix of subglacial tills is variable and depends largely on the substratum that is cannibalised by overriding ice sheets. Clay-rich tills can be expected if fine-grained lithologies were present at the base whereas sandy tills could be anticipated if fresh bedrock or coarse-grained sediments were locally present under the ice. Some glacial tills are known to be highly reactive to HCl as the ice overrode and abraded carbonate lithologies (limestones, or chalk) incorporating them into till matrix. Such tills, depending on the carbonate content, can be prone to partial dissolution and volume loss if exposed to unfavourable geochemical conditions.

On formerly terrestrially exposed shelves, landforms and sediment formed by and deposited from glacial meltwaters, such as sandar, ice-contact deltas, tunnel valleys, eskers, and glaci-fluvial channels, are typically composed of better sorted, more permeable granular material. Eskers and topsets of ice-contact deltas are typically associated with boulder and cobble-sized deposits. The erosional nature of high-magnitude glacial meltwater flow, especially during deglaciation, implies that not all sediments are preserved, and erosional landforms or landscapes are formed. These landforms (i.e. tunnel valleys, meltwater corridors) are associated with steep slopes and a presence of very coarse fractions (up to

boulder size) towards the base of such features (channel lag; Figure 5.41). The channel infill can consist of well-sorted sand and gravel layers that can act as fluid reservoirs, resulting in shallow gas accumulations in the channel and valley infill (Bellwald et al., 2024c). In contrast, if shear strength of the valley infill is enhanced compared to the surroundings (e.g., subglacial till infilling valley), then those valleys might actually act as a seal for fluid migration (Figure 5.12). In terrestrial settings, proglacial lakes and kettle holes (depressions formed by meltout of buried dead ice blocks) are characterized as lower-energy sedimentary environments, and often dominated by interbedded sediments ranging from soft clays and till with subordinate coarser fractions. Downslope processes such as turbidites and debris flows, however, might contribute to more coarse-grained layers in these depocenters. Organic-rich sediments and peats have been previously reported from kettle hole settings offshore. Although the layering of lacustrine sediments is often indicating a homogenous infill, units within lake systems might still undergo gradual lateral changes (e.g., lateral fining within the same unit from delta to deep basin).

Pockmarks evidence shallow gas and gas hydrates in the subsurface, and occur in high densities in active hydrocarbon systems, such as the North Sea and Barents Sea (Figure 5.11; Forsberg et al., 2007; Mazzini et al., 2017; Tasianas et al., 2018). Pingos and hill-hole pairs might indicate shallow gas (Bellwald et al., 2023a), but are less common compared with pockmarks. Megaripples, sand waves, sand banks, and sediment scouring are distinct landforms that indicate a mobile seafloor (Passchier and Kleinhans, 2005; Stow et al., 2009; Bellec et al., 2019; Figure 6.3). Certain landforms, such as pockmarks, are important marine habitats (Figure 5.11). Interestingly, the Silver Pit Formation in the UK North Sea forming a prominent tunnel-valley infill unit, received its name due to its nature as good fishing ground.

The shelf break is the transition from shallow (<500 m, with deepest depths in the mouths of cross-shelf troughs) to deeper waters (>2 km) and associated with an increase of slope gradient. Signatures related to downslope and along slope sedimentation shape the slopes of these regions (Solheim et al., 2005a; Bryn et al., 2005a; Newton and Huuse, 2017; Barrett et al., 2021). Their deposits vary from boulders to sandy channel deposits to fine-grained contourite deposition (Bellwald et al., 2024a). The slope gradients of slide escarpments, fjord flanks, and canyons often incorporates slope instabilities (different types of mass movements) as an engineering constraint, and ultimately as a geohazard (Sections 6.2 and 6.3).

Identification of small landforms might be very relevant for offshore engineering: Pockmarks, for example, can generate problems for anchoring of seafloor infrastructure due to the soft-sediment infill during the Holocene (Bellwald et al., 2018), their correlation with sensitive benthic habitats (Revelas et al., 2020; Henkel et al., 2022; Webb et al., 2009; Mazzini et al., 2016; 2017), unconfined sediment gravity flows (Lundsten et al., 2024), and their link to the fluid release (Forsberg et al., 2007). The

identification of meter-scale pockmarks (also called unit pockmarks) is crucial, as they can reduce the foundation capacity, and are in consequence avoided for foundations.

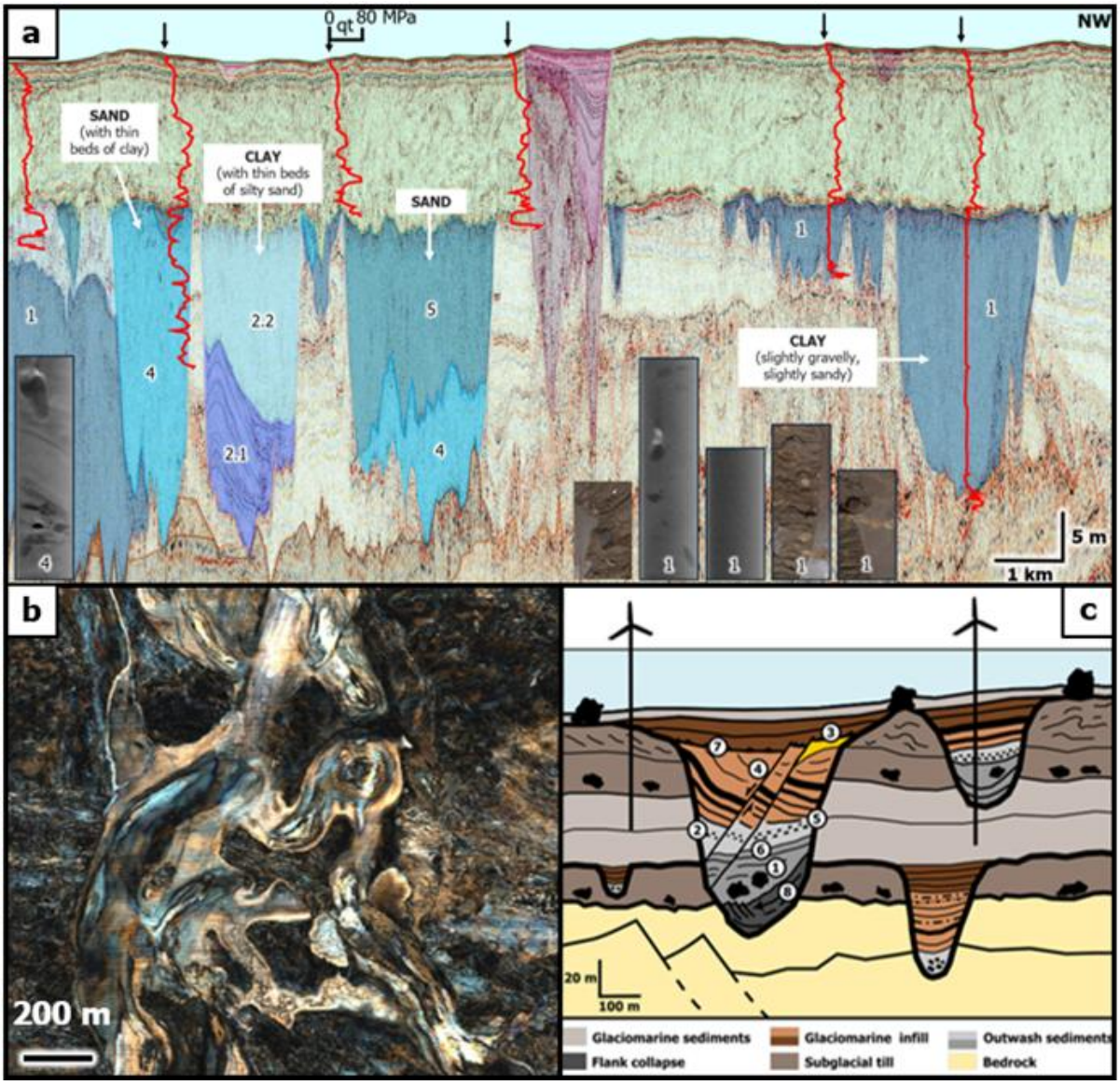


Figure. 5.41. Implications of tunnel valleys and their infill. **a)** Signatures of tunnel-valley infill in the Central North Sea. Ultra-high-resolution 2D seismic profile with cone penetration tests (black arrows and red lines). Although all tunnel valleys are formed during the Saalian glaciation, their infill is heterogeneous on short lateral distances. Different types of infill are labelled as 1-5, and shaded in different types of blue. X-ray scans and (black and white images) and core photography (images in brown) of the different infill are shown. Data courtesy of bp and EnBW. **b)** Geomorphologies within the tunnel valley infill identified in ultra-high-resolution 3D seismic data, Offshore Netherlands. Data courtesy of RVO. **c)** Sketch summarizing geo-engineering constraints and geohazards of tunnel valleys and their infill. 1: Boulders, 2: Gravel and pebble beds, 3: Shallow gas, 4: Faults and deformation structures, 5. Heterogeneities on small vertical and lateral scales, 6: Paleo-gas hydrates, 7: Low-strength

clays, 8: Peat and high-organic sediments, 9: Slope instability. Figures compiled from Bellwald et al. (2024c).

Table 5.6. Landforms shaping the seafloor of the glaciated European margins and their implications for offshore geohazard and geo-engineering.

Landform	*Boulders*	*Gravels and cobbles*	*Sands*	*Soft clay*	*Peat*	*Shallow gas*	*Gas hydrates*	*Mobile sediments*	*Steep slopes (>5°)*	*Slope instability*	*High-strength sediments*	*Overconsolidation*	*Deformation*	*Hotspot for marine life*
Mega-scale glacial lineations	X										X	X	X	
Iceberg ploughmarks			X						X				X	
Hill-hole pairs						X	X		X		X		X	
Glaciotectonic complexes	X	X	X	X					X		X	X	X	
Glacial moraines	X	X	X						X		X	X	X	
Grounding zone wedges	X	X	X								X	X		
Esker		X	X						X					
Drumlin	X	X	X											
Tunnel valleys and infill	?	X	X	X	X	X			X	X	X	X	X	
Fluvial channels and infill	X	X	X	X	X	X			X	X				
Ice-contact deltas/fans	?	X	X			?			X	?			?	
Glacial lakes		X	X	X	X	X			X	X	?			
Kettle holes		X	X	X	X	?			X					
Slide escarpment				X			?		X	X			X	
(Mega)slide		X	X	X		X			X	X	X		X	
Rock avalanche	X	X	X						X	X			X	
Turbidite channels	?	X	X	X		?				X				
Debris lobes	X	X	X	X						X				
Contourite sheets and mounds			X	X		X	X	X						
Pockmarks			X	X		X	X	X						X
Pingos				?		X	X		X					
Sandwaves		X	X					X						?
Megaripples		X	X					X						
Scouring marks	X	X		X				X						

6. Geohazards

This chapter is separated into geohazards characteristic for deglaciated continental margins related to sediment mobility (Section 6.1), slope instabilities and mass flow dynamics (Sections 6.2-6.3), glacio-isostatic rebound and sea-level changes (Section 6.4), seismicity (Section 6.5), and tsunamis (Section 6.6). A geohazard is here defined as a dynamic geo-event or process that is a risk to industry and/or society and/or marine life, and is addressed by project management frameworks. Geohazards can affect

the more static features, landforms, and deposits forming geo-engineering constraints (Figure 5.1; see also ISO 19901-10).

6.1 Sediment transportation and mobile bedforms

Sediment transport is broadly defined as the movement of particles by a fluid, which can be air or water (Collinson, 2005). The mechanism for transport depends principally on the grain size, the velocity, and viscosity of the fluid, together with gravity, but is also affected by grain angularity and grain-to-grain cohesion. Generally, the higher the velocity of the fluid and smaller the grain size, the more readily the particles are mobilized.

The Hjulström curve (Figure 6.1a) was initially developed in the early 20th century to predict the relationship between the size of sediment grains and the velocity required to erode (remove from the deposited state), transport (move, either in suspension or as bed load), and deposit (below the settling velocity) mineral grains in rivers (Ward, 2021). The Hjulström curve is a useful proxy for understanding expected sediment transport in any given system that is affected by constant directional current (e.g., ocean current circulation) or periodical changes in flow velocity (e.g., low and high tide flow). Generally, as grain size decreases, less energy is required to mobilize grains; however, in clay and silt-rich, cohesive soils, a larger flow speed is required to erode material due to grain-to-grain cohesion. As sediments are mobilised, they tend to self-organise into ridges, bands and furrows of different dimensions ranging from the i) small- cm-scale ripple marks through ii) sand dunes and sand waves that can reach several meters in height to iii) sand banks which can cover vast areas of seabed and be up to 10s of meters high. It is noteworthy that such bedforms are expressions within a relatively narrow spectrum of flow velocity and are dependent of the grain-size availability (Figure 6.1b; Boguchwal and Southard, 1989).

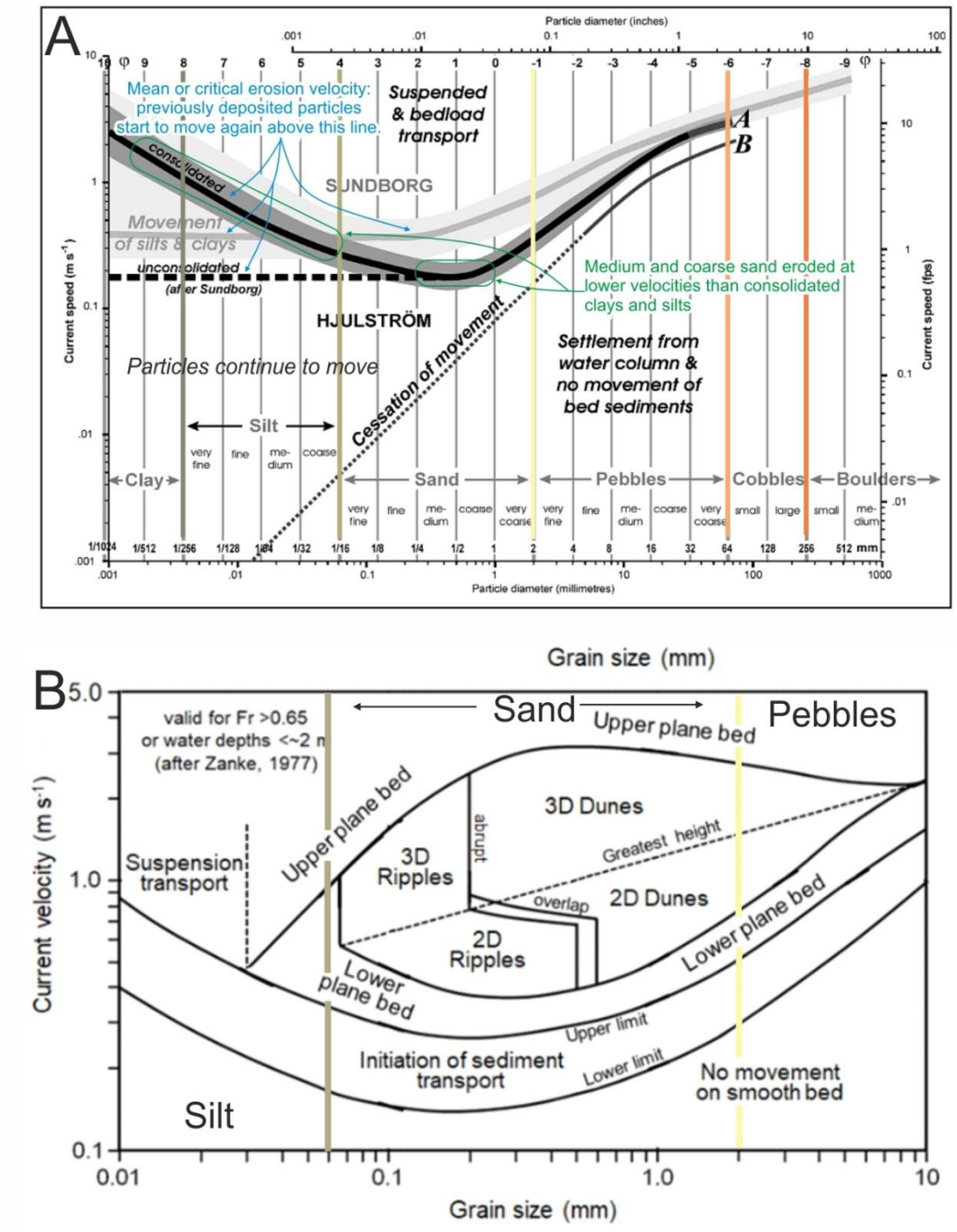


Figure 6.1. a) Hjulström-Sundborg diagram with Wentworth-Krumbein grade scale, showing sediment movement in flowing water as function of particle size and vertical-mean current (modified from Ward, 2021). **b)** Bedform phase diagram of North American researchers (modified from Boguchwal and Southard, 1989). Note that the biggest variety of bedforms forms within sand grain-size range but that does not exclude the possibility of sediment being mobile across a wider grain-size spectrum.

The Northwest European continental shelf is a dynamic and complex marine system where the interplay of waves, tides, and currents is having a substantial impact on the present-day seafloor landscape. With a large quantity of loose, glacially supplied clastic material on the seafloor and further input of material

from fluvial systems around the basin, conditions were and are optimal for the formation of a variety of mobile bedforms. The resulting seabed morphology can indicate both the processes active at present day, but also a record of relict seafloor processes during the marine transgression in the Late Pleistocene and Holocene. Key geological formations associated with mobile bedforms include the Naaldwijk Formation (offshore the Netherlands); the Bligh Bank Formation (offshore the UKS North Sea), and the Surface Sands Formation (offshore UKS Irish Sea), but there are many other and these are often locally subdivided or too small to be named.

Types of Bedforms

Features generated by sediment mobility vary greatly and these organised sediment accumulations are known collectively as bedforms (Figures 6.1b and 6.2). These bedforms vary in size, shape, formation processes and composition reflecting complex interactions between hydrodynamic conditions and seabed or coast topography. Any changes within the hydrodynamic conditions are likely going to be reflected as changes within seabed topography, including the effect of changes to flow and circulation introduced by offshore engineering projects. Figure 6.2 indicates a bedform velocity matrix, outlined by Stow et al. (2009), linking grain size and fluid velocity. It should be noted that Figure 6.2 was constructed with deepwater circulation in mind (i.e. beyond the shelf edge) and is only partially applicable to shallow continental margins.

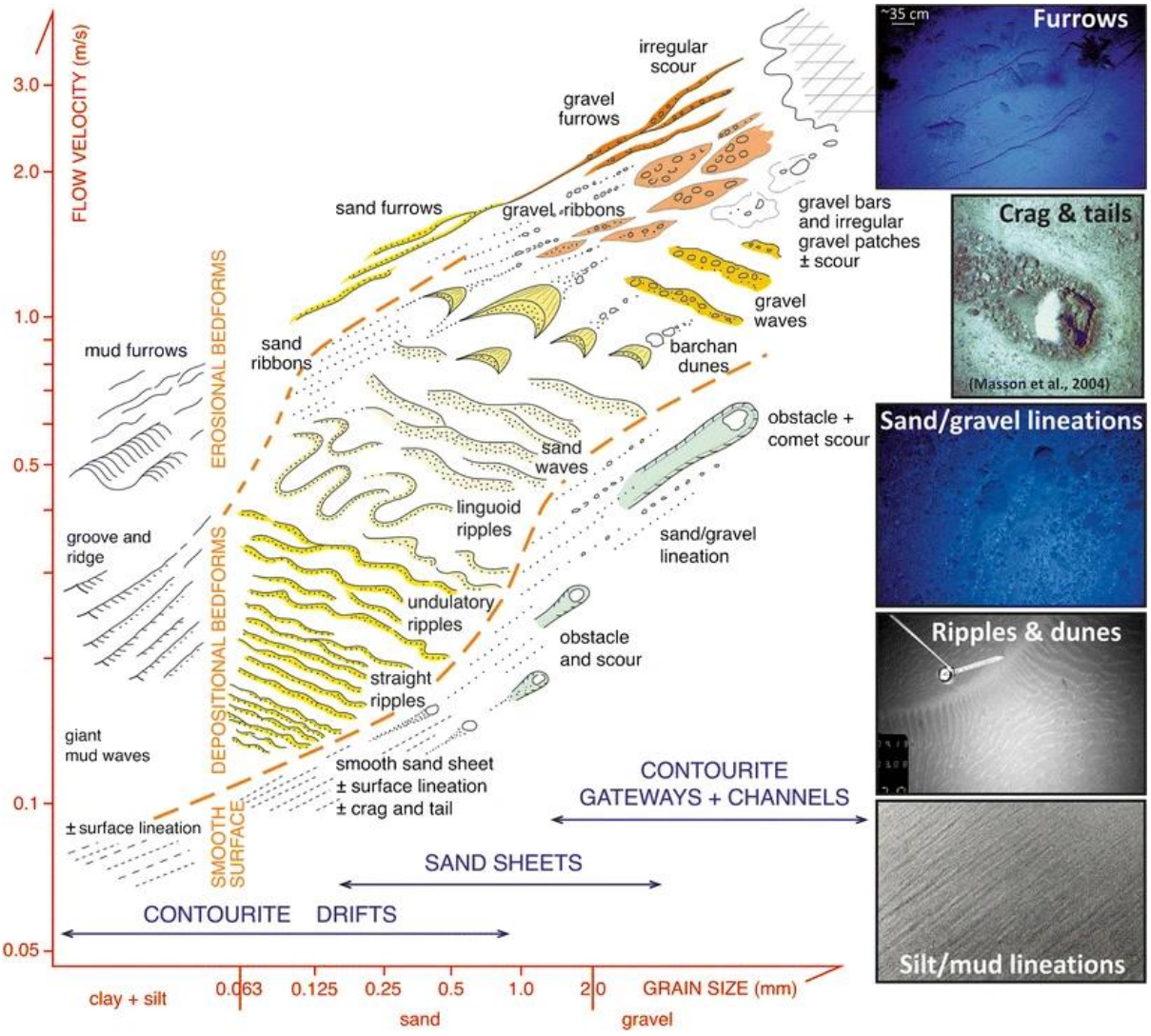


Figure 6.2 Bedform velocity matrix. From Hernandes-Molina et al. (2011) and modified from Stow et al. (2009).

On the continental shelves, mobile bedforms can be classified based on their orientation with respect to current direction, dimensions, and morphology as well as governing formation process (erosion, transport or accumulation). There are a number of bedform classification schemes, which attempt to categorize bedforms based on their wavelength and amplitude (e.g., Ashley, 1990). The truth is not so readily defined, and in complex marine environments, the local metocean regime of any given site can lead to a range of bedforms produced. An overview of some broad bedform types is included below.

Flow Transverse Bedforms

The crests of flow-transverse bedforms are perpendicular or quasi-perpendicular to the prevailing current direction. These types of bedforms can readily be subdivided by their amplitude (height) and wavelength (crest to crest distance).

Ripples are the smallest mobile bedforms with amplitudes of several centimetres and wavelengths not exceeding tens of centimetres. Ripples can be symmetrical when formed by oscillatory flows (wave action) or asymmetrical when directional current component is involved (Amos et al., 2017). They can migrate downstream or alongshore and are often observed superimposed on larger bedforms, such as sandwaves. The presence of ripples has no direct bearing and poses no threat to seabed or coastal infrastructure.

Megaripples are similar in shape to ripples but are significantly larger (tens of centimetres in height) and formed with longer wavelengths, with a crest-to-crest distance typically in the order of meters to tens of meters (Passchier and Kleinhans, 2005). Megaripples can also be symmetrical or asymmetrical. Their presence and migration across the site are unlikely to have a significant effect on seabed infrastructure.

Sediment waves (or sand waves, where material is confirmed) are morphologically similar to megaripples but have a much larger heights (metres to some >10m), and longer wavelength (crest-to-crest spacing) between them, in the order of tens to hundreds of metres (Bellec et al., 2019; Creane et al., 2022; Németh et al., 2002; van Dijk et al., 2021). They are large-scale rhythmic transverse bedforms composed chiefly of sand, although gravel waves may also form in very high current areas. Their formation is typically related to a predominant directional flow, but wave action (oscillatory flows) can also affect their morphology. The heights of sand waves can grow up to 30% of the average water depth and may migrate with speeds of up to several metres per year (Adnyani et al., 2024). Distinction between megaripples and sand waves is often arbitrary and based on site specific size (height/wavelength) criterium rather than a difference in physical process of their formation. Sand waves have been extensively studied in the North Sea, as they are a navigational hazard and can be considered a constraint and geohazard for offshore infrastructure due to their migration across the shelf in shallow seas (Schmitt et al., 2007). While they are often formed in groups or sets, single, isolated, large scale sediment waves are also known to occur.

Flow-Parallel Bedforms

Flow-parallel bedforms such as sediment streaks, linear sediment banks, sediment ribbons, banner/ headland banks are elongated parallel to the prevailing current direction, especially in tidally influenced waters and close to river mouth (Dyer and Huntley, 1999). Flow-parallel bedforms are often indicative of high current velocities associated with large tidal ranges; in macro- and mega-scale tidal environments, such banks can be re-shaped and migrate laterally during diurnal tidal cycles (Li et al., 2014). In extreme cases, when the current energy is high, the bedforms can be separated by erosional furrows. The banks are often quasi-stable and commonly have an anticlockwise migration of smaller bedforms on their flanks. In many cases, modern sand banks are anchored on older banks or glacial features.

These large banks can pose a substantial constraint to development as a result of the strong tidal currents that form and maintain them and shallow waters along bank crests. Site characterisation of these areas can be challenging with vessel crabbing and potential collision issues while towing equipment near to seabed. Additionally, varying water depths due to the presence of mobile bedforms can also cause difficulties with seismic data acquisition due to source energy scattering, as well as problems with streamer positioning. Therefore, the site investigation must be carefully planned in these areas to capture site conditions appropriately. Similarly, design and installation of infrastructure will be constrained by current velocities and water depths, so developers in these areas need to work effectively across technical disciplines to ensure all infrastructure can be designed and installed appropriately for the site conditions.

Sand banks, particularly where they occur within 20 m water depth, are often considered by Annex 1 habitat under the JNCC Designated Special Areas of Conservation due to the range of invertebrate species they support, including Sabellaria spinulosa (Ross worm). They are therefore important to characterise correctly to ensure that the impact of offshore projects on these habitats is minimised during and following construction.

Non-Directional and Sorted Bedforms

Currents and waves can move sediment without organizing it into well-defined bedforms. Sand patches, sheets or drifts are frequently described from bathymetric data (Fenster, 2018; Dyer and Huntley, 1999). Their formation and mechanisms of mobility are poorly constrained, yet they can be significant in extent and thickness. The largest accumulations of unconsolidated sediments that are mobilised by currents and waves are often described as sand banks, which differs from the flow-parallel sand-bank definition. Although these non-directional sand banks are generally large, their migration rates are low, which allows for siting that limits the potential effect of sand bank migration on offshore infrastructure.

Sand sheets and banks in this form are often associated with the nearshore area and thought to be a result of seasonal removal of beach material during winter storms (Fenster, 2018). These features require consideration for engineering such as horizontal directional drilling, as they may cover exit pits if their movement has not been accounted for.

Discrete accumulations of isolated, often rippled or patchy coarser sediments on otherwise fine-grained substrate are referred to as sorted bedforms (Coco et al., 2007a; 2007b; Murray and Thieler, 2004). Such bedforms are typically re-generated as a consequence of interaction of waves and currents with poorly sorted bed material. These features are characterised by slight depressions (often <1m) composed of sequences of coarse-to-very coarse sand, gravel and/or shell debris, that is arranged into large wave-generated ripples, with wavelengths in the order of a metre (Murray and Thieler, 2004).

Two scales of sorted bedforms are noted – Very large runnels 100s-1000s m wide and many kilometres in length (known as runnels) and smaller 10s-500s m more regular or circular depressions known as rippled scoured depression with relief <1.5m ((Dix et al., 2023.; Riera et al., 2023). Although individual features are relatively small, they can cover large areas with many 10s or 100s of such features close by.

Bedforms in Equilibrium

Bedforms are mobile and dynamically change morphology in response to hydrodynamic conditions until they achieve a hydraulically stable state when changes become more subtle. Such bedforms are considered in equilibrium and may not migrate or be modified by waves and or currents despite their appearance. Bedform equilibrium state is transient and specific to hydrodynamic conditions at a given time. Any changes to current direction or velocity, sediment supply, or topography and water depth, may disturb that equilibrium upon which sediments will re-organise to achieve a different hydraulically stable morphology. An example of such a disturbance is the formation of scour around a seafloor object or feature, which does not scour infinitely but becomes stable based on the size of the object after a period or duration of tidal cycling.

Similarly, understanding the effects of sea level change is an important factor for assessing how climate change may impact the mobility of a site throughout the life of offshore assets.

Sediment availability, erosion and by-pass

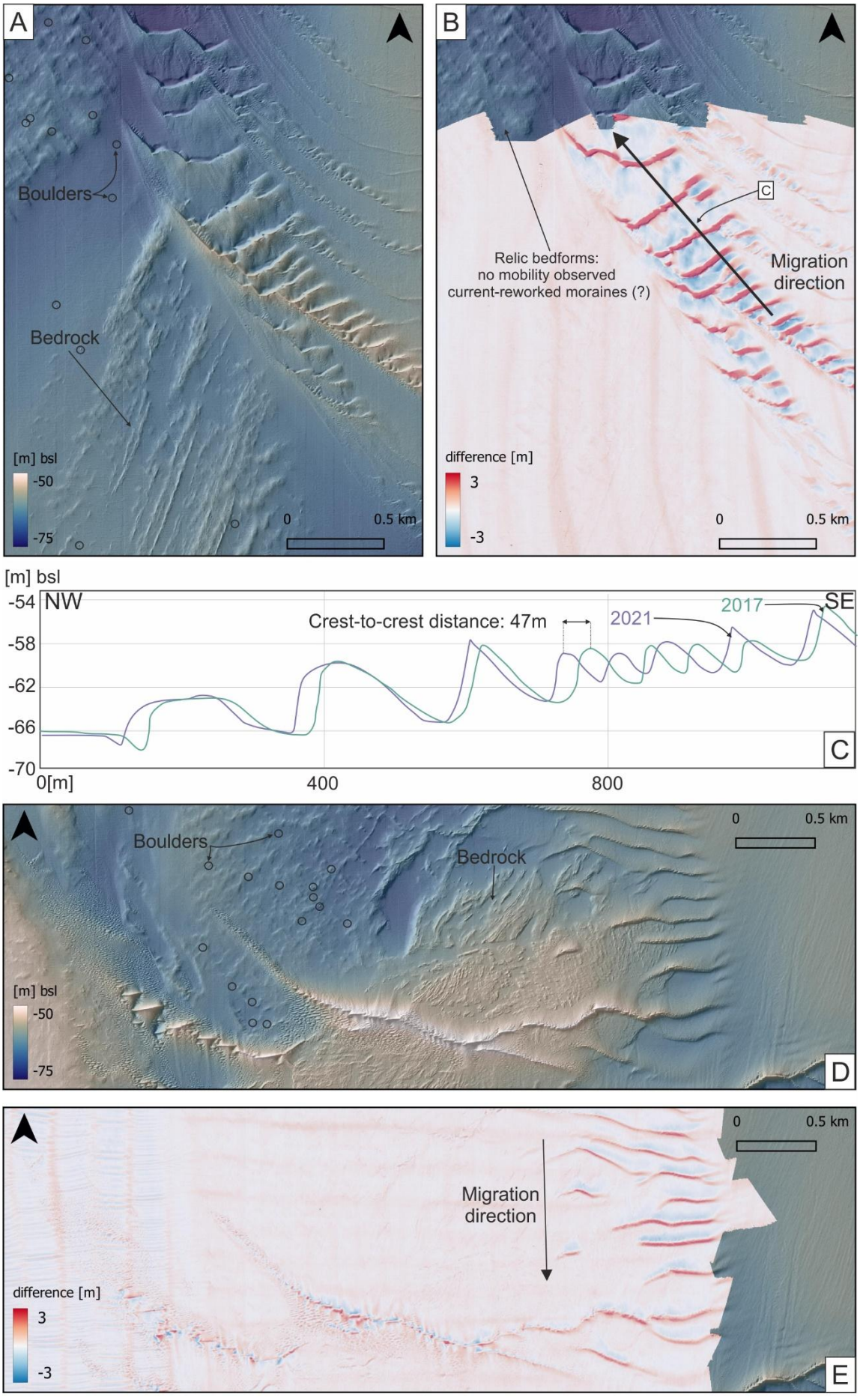
Sediment mobility is prevailing where granular material is available, typically in nearshore areas where sediment supply by rivers is continuous, and areas where the substrate contains sufficient granular material, such as glaciated areas. In areas where sediment supply is scarce, mobile bedforms may be absent, despite sufficient current or wave energy, or may exist as 'starved' bedforms that bypass the seabed with minimal interaction and exchange of material with substrate. It is worth noting that the availability and distribution of granular material is broader on glaciated continental shelves that underwent dynamic changes in sediment supply and sea level. In consequence, (1) mobile bedforms may form further offshore and away from modern-day sediment input sources, (2) relict mobile bedforms active in the past due to different palaeoceanographic conditions not mobile at present, may be preserved at seabed, (3) the presence of steep glacial topography and reworking of glacial landforms at the seabed (moraines, lineations and iceberg ploughmarks) can result in complex seabed morphology and, consequently, challenges in identifying and quantifying sediment mobility.

Characterising and Monitoring Bedforms and Seabed Mobility

Several methods and approaches can be utilised to understand and quantify sediment mobility across an area of interest. These methods have been detailed in the Table 6.1 below:

2824 **Table 6.1.** Methods used for sediment mobility assessment.

Approach or method	Data and information obtained	Application to sediment mobility analysis
Met-ocean data acquisition – site specific	Wave, wind and current data Seabed shear stress Suspended sediment concentration	• To identify sediment mobility threshold based on oceanographic conditions and seabed sediment information • To provide input for hydrodynamic modelling of sediment mobility (for example computational fluid dynamics)
Bathymetric surveys (MBES) including repeated bathymetric surveys	Bathymetry and geomorphology of the seabed Multi-beam bathymetric surveys conducted at appropriate time intervals allow to trace the changes in seabed morphology	• To identify and map mobile bedforms • To map other geomorphic features (glacial landforms, submerged coastlines etc.) • To distinguish between relict and active bedforms • To model seabed changes and compute difference over time, evaluate bedform migration speed and direction, • To identify areas of sediment erosion and accumulation
Seabed lithology mapping	Sidescan sonar or acoustic backscatter data combined with sediment sampling (grab samples or box coring)	• To distinguish between mobile bedforms active at present and relict ones. • To identify and map the distribution of sediment types and grain size across the AoI. • To delineate areas of sediments likely to be remobilised. • To identify changes in acoustic response and texture of the seabed due to sediment mobility (repeated surveys required)
Sub-bottom profiler/ single channel seismic surveys	Imaging of the shallow subsurface in extremely high vertical resolution (2D)	• To identify the internal structure of mobile bedforms and confirm their formation process • To delineate a 'base level' defined as the base of a mobile sediment unit beyond which the seabed is unlikely to be lowered/eroded.
LiDAR surveys	High resolution topography in coastal areas.	• To identify areas of material loss and movement due to erosion, deposition and transport in the coastal environment.


A
Boulders
Bedrock
[m] bsl
-50
-75
0
0.5 km
B
Relic bedforms:
no mobility observed
current-reworked moraines (?)
C
Migration
direction
difference [m]
3
-3
0
0.5 km
[m] bsl
-54
-58
-62
-66
-70
NW
SE
Crest-to-crest distance: 47m
2021
2017
0[m]
400
800
C
Boulders
Bedrock
0
0.5 km
[m] bsl
-50
-75
D
0
0.5 km
Migration
direction
difference [m]
3
-3
E

2825

Figure 6.3 Mobile bedforms offshore on the seabed near Wick (NE Scotland). **a)** Bedforms at the seabed as imaged in 2017. **b)** Difference map showing the migration of bedforms between 2017 and 2021. Note that bedforms in the northwestern corner of the map did not move and are likely relic glacial features (moraines or crevasse-squeeze ridges). **c)** Bathymetric profile showing the morphological change along the profile in Figure 6.3b. Note the difference between smaller and bigger bedforms. **d+e)** Morphological expression of linear dunes in 2017 and the difference map showing the bedform migration between 2017 and 2021. Note that the migration direction is now to the South despite "site d" being ~ 4 km away from site "site a". All bedforms are in water depths exceeding 50 m and there is no active terrestrial sediment supply. The bedforms are likely composed of current-reworked glacial material and migrate on top of a glacial substratum as evidenced by the presence of boulders at the seabed.

Implications and Considerations for Engineering

Sediment mobility has several engineering implications, depending on sediment erosion or sediment accumulation. It is therefore important to understand sediment mobility and bedform migration rates effectively to ensure continued integrity of the asset through their design life (Table 6.2).

Table 6.2. Types of sediment mobility and implications for offshore assets.

Type of sediment mobility	Description	Engineering implication
Scouring around a foundation/ anchor	Removal of material around foundations due to localised flow acceleration and development of turbulent eddies	• Uncovering of buried parts of piles can affect their lateral stiffness, load bearing capacity and resonance frequency. In worst case scenario this can lead to inclination and failure of the structure • Removal of material around the anchor or chai may reduce overall mooring holding strength. In extreme cases this may lead to mooring failure.
Accumulation of sediment around a foundation	Buildup of sediment around a structure	• Considerations for the operation and maintenance stages of design life, restricting access to the structure by vessels and jack-ups • Changes of resonance frequency and lateral stiffness
Burial of linear assets (cables and pipelines)	Migration of mobile bedforms across a section of a cable/pipeline or accumulation of a continuous sand bank/sand sheet	• Negative effect on high-voltage direct current (HVDC) and high voltage alternating current cables (HVAC) as thicker sediments reduce dissipation of heat generated during transmission. This can result in reduced power transmission capacity or, in extreme cases, cable 'cooking' and breakage. • Burial can exert excessive loading of an asset which can cause structural damage. • Over-burial may prevent an asset from moving as it should under thermal expansion and contraction during operation, which could cause fatigue and stress points elsewhere in the structure.
Uncovering of linear assets (cables and pipelines)	Winnowing of sand sheets, migration of sand waves and sand banks away from	• Uncovering buried linear assets leading to free spanning, where pipelines or cables can 'hang' in water column. Uncovered cables and pipelines are more susceptible to anchor striking and snagging by, for example fishing vessels.

	the asset. Scouring around a linear asset	• Alternating burial and free spanning (for example by migrating sand waves) may cause sections of cables and pipelines to become over stiffened which in turn may lead to breakage as the asset thermally expands and contracts.
Nearshore and coastal sediment mobility	Accumulation or removal of coastal material and migration of coastline-attached sand banks	• Short migration timescales need to be accounted for while designing HHD solution or trenching as the seabed level may change by several meters on seasonal/annual basis due to migration. • Erosion of coast can put structural integrity of asset landfall at risk. Transition joint Bays (TJBs) need to be located sufficiently inland to mitigate the eventual erosion.

There are also several additional aspects related to sediment mobility that are important to mention: (1) During decommissioning, substantial increase in material may be a significant consideration; it is commonly required to remove all trace of a turbine foundation to prevent future hazards to shipping once turbines are removed. (2) Landfalls for cables and pipelines are some of the most challenging areas of any offshore development and most sensitive to the effects of future climate change. A robust understanding of sediment mobility under different climate scenarios is needed to ensure suitability of the landfall throughout the design life of the offshore assets. (3) An important secondary consideration is the burial and emergence of potential unexploded ordnance on the seafloor where sediments are mobile. In such settings, magnetometric surveys provide only a snapshot of a site, and items may be buried or move depending on seafloor mobility levels. This means that data acquired has a "shelf life" which must be aligned with project development timelines and on-site activities to ensure maximum efficiency in data acquisition, analysis, and safe removal where required.

6.2 Slope instabilities

During the repetitive Quaternary EIS glaciations an up to 4500 m thick sedimentary package, comprising trough mouth fans (TMFs) and prograding wedges, was deposited along the Western European continental margin, from Ireland to Svalbard (Figure 6.4; Hjelstuen and Sejrup, 2021). Various types of mass movements, from large submarine landslides remobilizing sediment volumes in the order of 10^6 km^3, to turbidity currents resulting in deposition of cm-to-meter-scale thick turbidite layers, were important sedimentary processes during the Western European margin development (e.g., Nygård et al., 2005).

6.2.1 Submarine landslides

Around 20 larger-sized Quaternary submarine landslides have been mapped along the Western European margin (Table 6.3; Figure 6.4) (e.g., Berg et al., 2005; Evans et al., 2005). These landslides have, commonly, been identified by using 2D and 3D seismic data (Figure 6.5a) or bathymetric surveys. Indicators of mass movement events include vertical slide scars, acoustically chaotic seismic facies and the deep erosion of sediment layers stratigraphically beneath the interpreted landslide debrites (e.g., Bryn et al., 2005a; Barrett et al., 2021).

Along the Western European continental margin, the largest submarine landslides are located in the TMF systems (Figure 6.4). Furthermore, it seems that submarine landslides along this margin segment tend to occur recurrently at the same locations (Nygård et al., 2005). It has been estimated that the largest landslides remobilized a sediment volume of 25 x 10^3 km^3 and affected an area of up to 120 x 10^3 km^2 (Hjelstuen et al., 2007). However, more commonly, such failure events involved sediment volumes of 2-5 x 10^3 km^3, where the sediment remobilization areas are around 10-15 x 10^3 km^2 in size.

The slope failures along the Western European continental margin seem to be restricted to the Quaternary time period (Figure 6.6). This restriction might partly be related to enhanced sedimentation rates associated with the Pleistocene glaciations (Bellwald et al., 2019b). Even though the chronological constraints in the region still are rather poor, it seems that most of the landslides occurred in the Middle and Late Pleistocene, i.e. over the last 0.78 million years (Figure 6.6; Solheim et al., 2005a; Nygård et al., 2005; Hjelstuen et al., 2007). Preconditioning factors and trigger mechanisms have been thoroughly studied within the region (e.g., Kvalstad et al., 2005a), and it is commonly accepted that high sedimentation rates, weak layers, abrupt lithological changes, and excess pore pressure are needed precondition factors for the slides to fail and that earthquakes resulting from isostatic uplift are the main trigger mechanism (e.g., Leynaud et al., 2009; Bellwald et al., 2019b; Llopart et al., 2019; Gatter et al., 2020).

6.2.2 Turbidity currents

Turbidity currents are commonly initiated in association with the larger-sized submarine landslides, as for instance the 8200 ka BP Storegga Slide event (e.g., Haflidason et al., 2005). Such mass movements are frequently occurring in fjord systems along the Western European continental margin, and it is also in such depositional environments that data, such as high-resolution seismic profiles and sediment cores, exist that allow for detailed studies of this mass movement process (Bøe et al., 2004; Bellwald et al., 2019a).

In Norwegian fjord systems, turbidity currents have resulted in up to nearly 15 m thick turbidite layers (e.g., Bellwald et al., 2019a), which commonly are identified as acoustic transparent units in high resolution seismic data (Figure 6.5b). These turbidite layers have an erosive base and can be divided into two sub-units (Bellwald et al., 2016). Commonly, the lower sub-unit is fining upward, from fine sand to clay, having a shear strength of 10-55 kPa, whereas the upper sub-unit, representing the tail of the turbidity current, consists of homogeneous clay with a shear strength of 7-10 kPa. The potential trigger mechanisms considered for turbidity currents include climatic changes, variations in sedimentation rates, ocean and tsunami currents (such as the Storegga Slide tsunami), and earthquakes.

6.2.3 Glacigenic debris flows

Glacigenic Debris Flows (GDFs) (Figure 6.5c) are important building blocks of the TMF systems along the Western European continental margin (Laberg and Vorren, 1996; Dimakis et al., 2000; Nygård et

al., 2002; Elverhøi et al., 2010; Beaten et al., 2014) and are also considered to represent an important precondition factor for landslide failures. In seismic data, GDFs are identified as hundreds of kilometres long lobate-shaped features, that are lensoid in cross section, 2–40 km wide and 15–60 m thick (Nygård et al., 2005; Garcia et al., 2024) (Figure 6.5c). The GDFs are only deposited when ice streams that occupied cross-shelf troughs during maximum glaciations transported huge amounts of sediments to the shelf edges (King et al., 1996). Shallow cores, penetrating into such flows, show that they are characterised by a complete lack of structure and that they are fine grained (1% gravel, 29% sand, 36% silt, and 34% clay) (King et al., 1998). GDFs are commonly stacked on top of each other, defining thick sedimentary units. During one shelf edge glaciation GDF units as thick as 400 m can be deposited, as evidenced from the North Sea TMF (Nygård et al., 2005). As the GDF units may be rapidly deposited stratigraphically above fine-grained thin deglacial and/or interglacial sediment layers (so-called "weak" layers) the TMFs complexes are prone to fail if a trigger mechanism such as e.g., an earthquake (Bellwald et al., 2019b), occurs.

6.2.4 Slope instability as a modern geohazard: Spatio-temporal patterns

Submarine landslides remobilized large sediment volumes along the Western European continental margin (e.g., Hjelstuen et al., 2007), and are commonly associated to major Mid- and Late Pleistocene glaciations (e.g., Nygård et al., 2005; Figure 6.6). However, studies along the Møre and Northern North Sea margins have concluded that another shelf-edge glaciation (with stratified sedimentation introducing weak layers exposed to earthquakes resulting from the glacio-isostatic uplift) is needed for large-scale submarine landslides to be initiated (Bryn et al., 2005a). As there is a lack of direct observations of megaslides occurring in historic times, the development and hazard potential for future events is mainly based on the study of the morphology of paleo-slide deposits (e.g., Barrett et al., 2021). Given thoughtful placement of infrastructure, seafloor stability in the form of a megaslide is not a big issue over the timeframe of the life of a producing oil and gas field (10-40 years; Shipp, 2017). However, the relief shaping the top surface of a megaslide still expressed on the seafloor might be a big challenge for seafloor infrastructure (e.g., pipelines or cable routes).

Ocean and wave currents as well as extratropical cyclones and storm surges may affect seabed stability. Hence, one should expect that global warming affecting the patterns (likelihood/frequency, intensity) of the environmental impacts will also influence slope stability. Global warming may further be followed by increased seismicity around the present-day ice sheets (in particular Greenland), sea-level rise, hydrate melting, and ice loading alterations, thus triggering slope instability (Berndt et al., 2009; British Geological Survey, 2009; Huhn et al., 2020). However, Urlaub et al. (2013) show that there is no strong global correlation of landslide frequency with sea-level changes or increases in local sedimentation rate. A recent study on the Afen Slide suggests that lithological interfaces, particularly a sandy contourite layer overlying silty clay, can significantly influence slope instability in contourite

drifts, and climate change may further precondition these failures, emphasising the need for multi-scale analysis to understand submarine landslide hazards (Gatter et al, 2020; 2021).

Turbidite layers are commonly identified in deglacial and interglacial sequences in fjord environment, and for Norwegian fjord systems it has been indicated that mass movements related to turbidity currents may have been in the order of one event every 80 years, even for the Late Holocene (Bellwald et al., 2019a). Turbidity currents and smaller sub-marine landslides in fjords should thus be evaluated carefully in geohazard assessments (Carlton et al., 2019b), as they are a major threat for submarine infrastructure and coastal societies.

Table 6.3. Major submarine landslides in the study area, listed from north to south. References to those papers that identified the submarine landslides first.

Slide	Age	Area	Reference
Slide Body A	Ca. 2.7 Ma	Northern Svalbard Margin	Lasabuda et al., 2018
Hinlopen/Yermak	MIS3	Northern Svalbard Margin	Winkelmann et al., 2007
Fram Slide Complex	5-0.068 Ma	Western Svalbard Margin	Elger et al., 2017
Slide B	0.5–0.6	Western Barents Sea margin	Laberg and Vorren, 1996
Slide A	0.5–0.6 Ma	Western Barents Sea margin	Laberg and Vorren, 1996
Bear Island Fan Slide Complex III	0.2–0.5 Ma	Western Barents Sea margin	Hjelstuen et al., 2007
Bear Island Fan Slide Complex II	0.5–0.78 Ma	Western Barents Sea margin	Hjelstuen et al., 2007
Bear Island Fan Slide Complex I	0.78–1.0 Ma	Western Barents Sea margin	Hjelstuen et al., 2007
Bjørnøya Slide	0.2–0.3 Ma	Western Barents Sea margin	Laberg and Vorren, 1993; 1996
Andøya Slide	Holocene	Lofoten-Vesterålen margin	Laberg et al., 2000
Trænadjupet Slide	4 ka	Mid-Norwegian margin	Laberg et al., 2002
Nyk Slide	16.3 ka	Mid-Norwegian margin	Lindberg et al., 2004
Vigrid Slide	> 0.2 Ma	Mid-Norwegian margin	Solheim et al., 2005a
Sklinnadjupet Slide	0.3 Ma	Mid-Norwegian margin	Solheim et al., 2005a
Slide R	0.3 Ma	Mid-Norwegian margin	Solheim et al., 2005a
Slide W	> 1.7 Ma	Mid-Norwegian margin	Solheim et al., 2005a
Storegga Slide	8.2 ka	Norwegian Sea	Haflidason et al., 2005

Slide S	0.5 Ma	Mid-Norwegian margin	Solheim et al., 2005a
Tampen Slide	0.13 Ma	Mid-Norwegian margin	Nygård et al, 2005
Møre Slide	0.38–0.4 Ma	Mid-Norwegian margin	Nygård et al, 2005
Stad Slide	MIS12	Mid-Norwegian margin	Hjelstuen and Grinde, 2016
Solsikke Slide	MIS3	Mid-Norwegian margin	Barrett et al., 2025
Norway Basin Slide A	2.7-1.7 Ma	Norway Basin	Hjelstuen and Andreassen, 2015
Norway Basin Slide B	1.7-1.1 Ma	Norway Basin	Hjelstuen and Andreassen, 2015
Norway Basin Slide C	Ca. 0.5 Ma	Norway Basin	Hjelstuen and Andreassen, 2015
Miller Slide	pre-MIS7		Long et al., 2011
Faroe	9.9 ka	Faroe slope	Lee, 2009 (and refs therein)
Afen Slide	58 ka <2.9 ka	Faroe—Shetland Channel	Wilson et al., 2004; Long et al., 2011
Palaeo-Afen Slide	Mid-Pleistocene	Faroe—Shetland Channel	Long et al., 2003 (and refs therein)
Walker Slide	?	Faroe—Shetland Channel	Long et al., 2003 (and refs therein)
Fugloy Slide	?	Faroe—Shetland Channel	Long et al., 2011
GEM Raft	Late Pleistocene-Holocene	Faroe—Shetland Channel	Long et al., 2011
NE Sula Sgeir Slide	Early Weichselian	Hebrides Slope	Baltzer et al., 1998 (and refs therein)
Geikie Slide	Early Weichselian	Hebrides Slope	Evans et al., 2005 (and refs therein)
3B Slump, offshore Ireland	?	Rockall Trough	EMODnet Map Viewer ("X Monteys (GSI) pers. comm (2011)")
Peach Slide	10.5 ka	Rockall Trough	Lee, 2009 (and refs therein)
Rockall Bank Slide	15-16 ka		Lee, 2009 (and refs therein)
West Porcupine Bank	Pliocene-Pleistocene	Porcupine Bank	Unnithan et al., 2001 (and refs therein)
West Porcupine Bank Debris Slide	?	Porcupine Bank	Weaver et al., 2000 (and refs therein)

2950

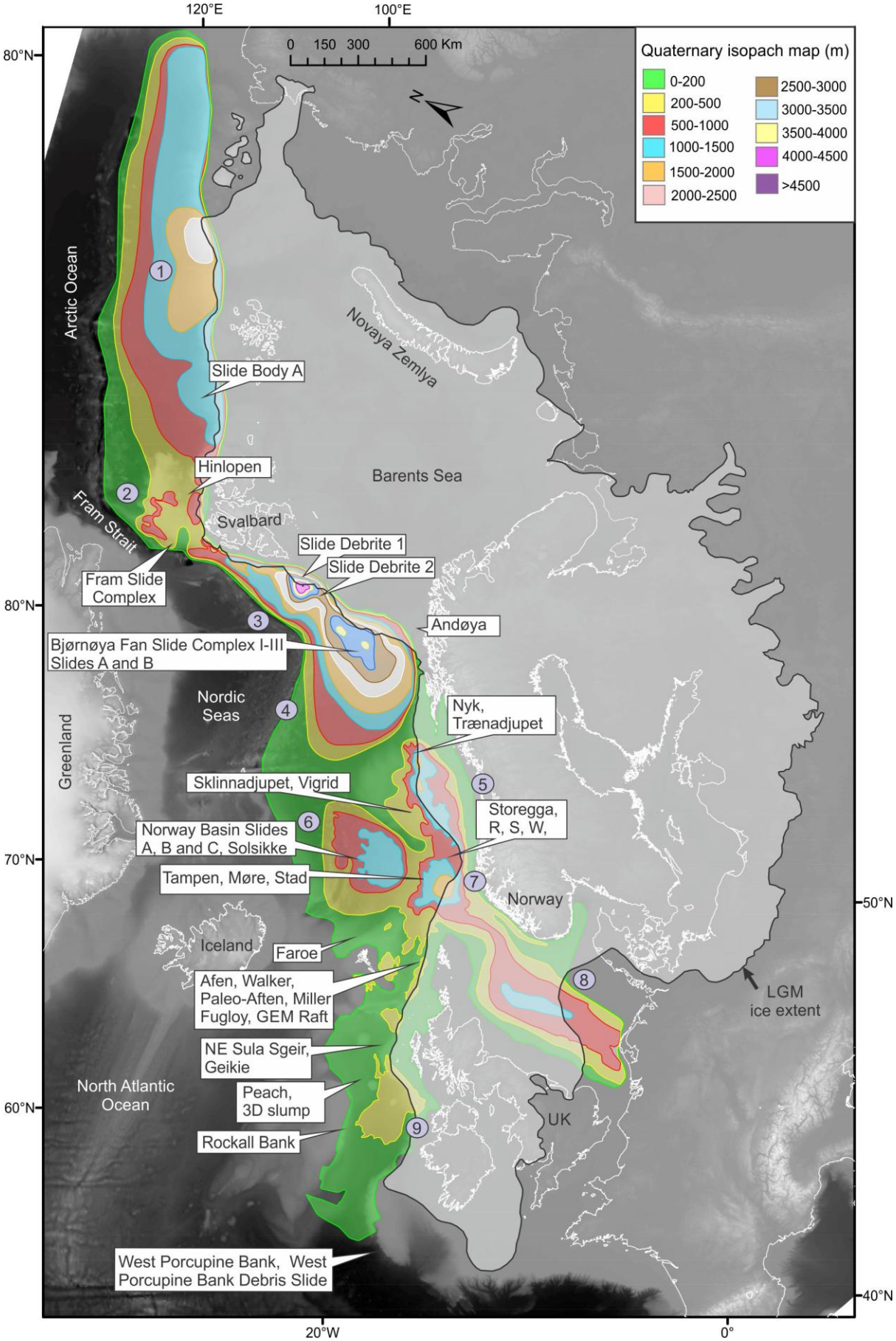
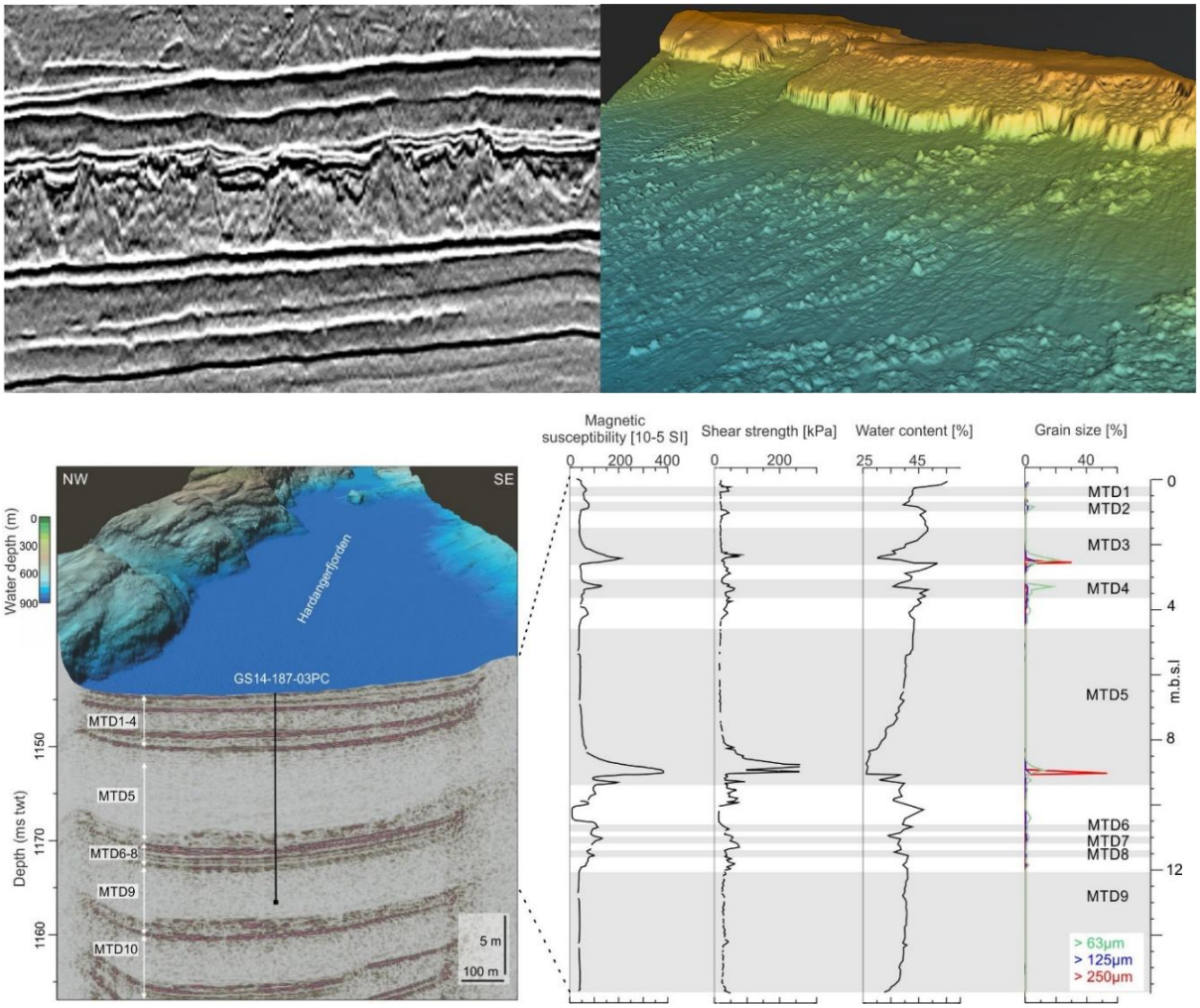

120°E
100°E
80°N
70°N
60°N
50°N
40°N
20°W
0°
0 150 300 600 Km
N
Quaternary isopach map (m)
0-200
200-500
500-1000
1000-1500
1500-2000
2000-2500
2500-3000
3000-3500
3500-4000
4000-4500
>4500
Arctic Ocean
Novaya Zemlya
Barents Sea
Svalbard
Fram Strait
Greenland
Nordic Seas
Iceland
Norway
UK
North Atlantic Ocean
LGM ice extent
1
2
3
4
5
6
7
8
9
Slide Body A
Hinlopen
Slide Debrite 1
Slide Debrite 2
Fram Slide Complex
Andøya
Bjørnøya Fan Slide Complex I-III Slides A and B
Nyk, Trænadjupet
Sklinnadjupet, Vigrid
Storegga, R, S, W,
Norway Basin Slides A, B and C, Solsikke
Tampen, Møre, Stad
Faroe
Afen, Walker, Paleo-Aften, Miller Fugloy, GEM Raft
NE Sula Sgeir, Geikie
Peach, 3D slump
Rockall Bank
West Porcupine Bank, West Porcupine Bank Debris Slide

Figure 6.4. Location of major landslides along the NE Atlantic margin (based on Lasabuda et al. (2018), Vanneste et al. (2006), Winkelmann et al. (2008), Elger et al. (2017), Safronova et al. (2015), Laberg and Vorren (1993; 1996), Knutsen et al. (1993), Hjelstuen et al. (2007), Hjelstuen and Andreassen (2015), Laberg et al. (2000; 2002), Lindberg et al. (2004), Rise et al. (2006), Nygård et al. (2005), Haflidason et al. (2005), Solheim et al. (2005a)). The Quaternary thickness map is from Hjelstuen and Sejrup (2021) and is clearly delineating the main sedimentary depocenters, i.e., trough mouth fans (TMFs) and prograding wedge systems, that have developed along the margin. (1) Nansen Basin, (2) Yermak Plateau, (3) Storfjorden TMF, (4) Bjørnøya TMF, (5) Mid-Norwegian Margin, (6) Norway Basin, (7) North Sea TMF, (8) North Sea, (9) Donegal Fan. LGM: Last Glacial Maximum (based on Patton et al., 2017).



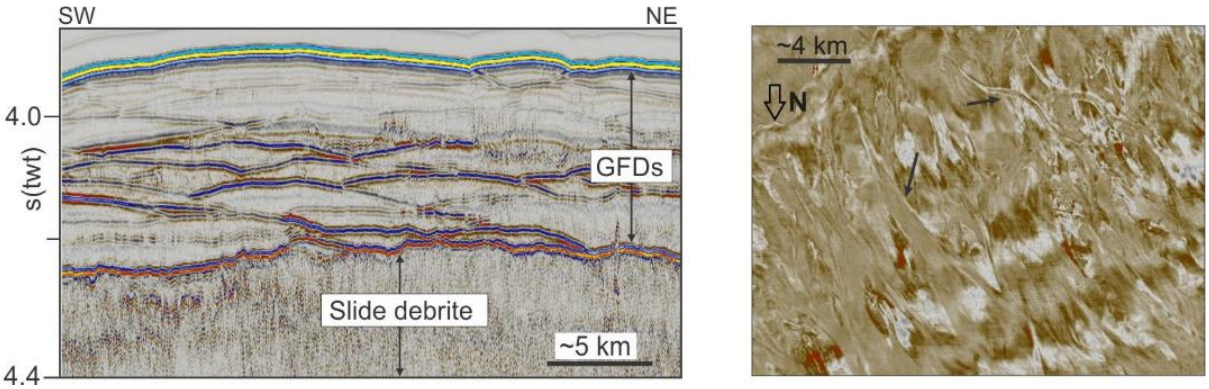


Figure 6.5. Expressions of different types of submarine mass movements. **a) Left panel:** Seismic expression of the buried Tampen Slide. **Right panel:** Top surface of the buried Tampen Slide on the North Sea Fan (modified after Barrett et al. (2021)). **b) Left panel**: High resolution TOPAS profile from Hardangerfjorden, western Norway, showing typical acoustic character of mass transport deposits (MTD 1-9), mostly interpreted as turbidite layers. **Right panel**: Analyze results from a c. 15-m-long sediment core showing typical lithological and geotechnical character of the identified MTDs. Modified from Bellwald et al. (2016). **c) Left panel**: 2D Multichannel seismic profile from the distal part of the North Sea TMF, showing the characteristic lensoid shape of Glacigenic Debris Flows (GDFs). Figure modified from Hjelstuen and Andreassen (2015). **Right panel**: Time slice, at approximately 300 metres below the seabed, from a 3D seismic cube located at the uppermost part of the North Sea TMF. Some of the GDFs observed are indicated by arrows. Figure modified from Hjelstuen and Grinde (2016).

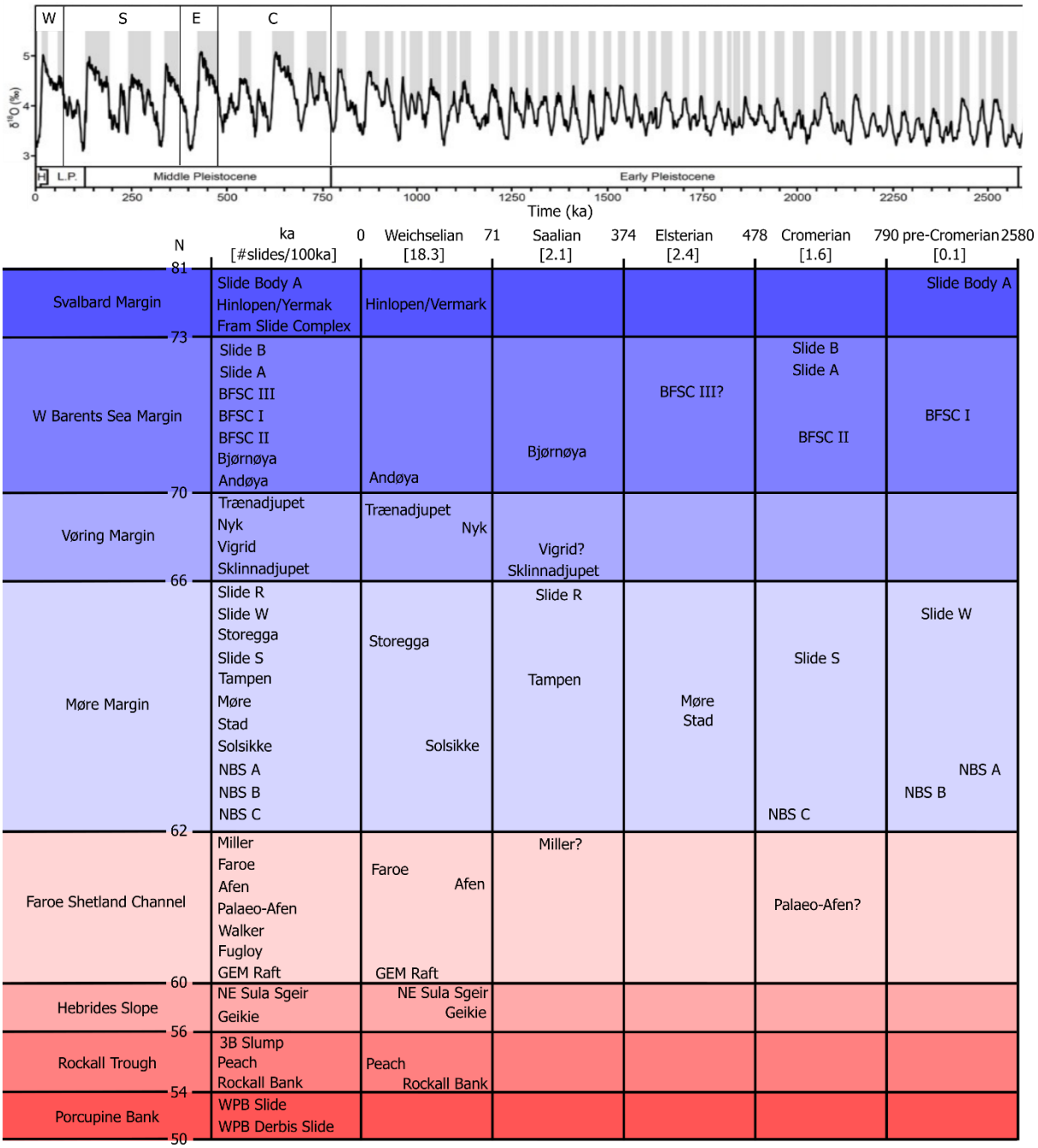


Figure 6.6. Spatio-temporal distribution of major submarine landslides along the NE European margin. See Table 6.3 for details. BFSC: Bear Island Fan Slide Complex, WPG: West Porcupine Bank. Ages of landslides indicated with ? are weakly constrained; Ages for Fugloy and Fram Slides are excluded due to lacking (precise) age suggestions. Global oxygen isotope curve after Lisiecki and Raymo (2005). W: Weichselian (MIS4-2), S: Saalian and Eemian (MIS10-5), E: Elsterian and Holsteinian (MIS12-11), C: Cromerian (MIS19-11).

6.3 Gravity mass flow dynamics

Understanding the dynamics of gravity mass flows (GMFs) both on land and in the water is a fascinating scientific problem that has attracted the attention of many researchers over more than a century. At the same time, it is of eminent practical importance in hazard mitigation. From a risk perspective, one needs

to estimate the occurrence probability of such events (i.e., the probabilities of release – discussed in the preceding section – and of reaching specific points of interest), their intensity (typically characterized by the depth, velocity, density and possibly particle hardness and size), and their effect on living beings and material assets.

Along the passive glaciated margins, two circumstances must be kept in mind: First, GMFs can originate not only in the sea but also on land, which means that their dynamics must be studied in both environments, with the transition from air to water posing specific challenges in connection with tsunamigenesis (see Section 6.6). Second, the moving particulate mass can range from huge rock fragments to highly sensitive clay, spanning an extremely wide range of rheological properties that translate into many different flow regimes. This section cannot cover them all but tries to highlight the physical phenomena that are most important in practical matters of hazard assessment and mitigation. One consequence of this variety of GMFs is that substantial events can originate in steep mountainous terrain (rock avalanches in fjords or flank collapses of volcanoes on islands) or gentle slopes on land (quick-clay landslides) or in almost flat areas of the continental shelf (submarine debris flows or landslides).

6.3.1 Rheology

A central step in assessing the dynamics of both submarine and onshore GMFs is to estimate the mass involved as well as to understand the physical properties of the sliding or flowing mass, the substrate, and the ambient fluid. These properties are decisive for the flow regime, run-out distance, velocity, and interaction of GMFs with obstacles.

The ambient fluid plays a subordinate role in many GMFs on land because of the large density difference between air (1–1.3 kg m^{-3}) and soil (typically 1500–2500 kg m^{-3}), but the turbulent entrainment of ambient air is the major resistive force in suspension flows like powder snow avalanches and pyroclastic suspension flows (nuées ardentes) with typical densities below 50 kg m^{-3}. In the marine environment, the ambient fluid density is much closer to the density of the mass flow so that ambient-water entrainment into turbidity currents as well as viscous drag (pressure drag and skin friction) and added mass are important, especially at high velocities or accelerations. The rheology of the ambient fluid is simple – it is a Newtonian fluid; however, near a GMF, the Reynolds number is very high, the fluid is in the turbulent regime and viscous drag typically grows as the square of velocity.

Many numerical models of dense GMFs describe the shear stress, τ (Pa), inside the flow and at the bed–flow interface with the Coulomb failure criterion,

$$\tau = \sigma_n \tan\phi = \mu\sigma_n. \quad (1)$$

Here, σ_n (Pa) is the normal stress on the shear plane, ϕ is the friction angle (which may be different inside the flow and at its bottom); $\mu = \tan\phi$ (–) denotes the friction coefficient. In very rapid flows

like rock or snow avalanches, where the shear rates at the bottom of the flow are very high, the bed shear stress is sometimes formulated as the Voellmy friction law (Voellmy, 1955),

$$\tau = \mu\sigma_n + k\rho_f u^2, \tag{2}$$

with ρ_f (kg m^{-3}) the flow density, u (m s^{-1}) the mean flow velocity, and k a dimensionless drag coefficient (often expressed as g/ξ in the literature, where ξ has the dimensions of the gravitational acceleration g). The Coulomb law expresses the experimental observation that the shear strength of a granular material is proportional to the overburden under quasi-static deformation. The Voellmy friction law, inspired by open-channel hydraulics, accounts for the increase in shear stress at increasing shear rates.

A great many laboratory experiments (e.g., Pouliquen, 1999; GdR MiDi, 2004; Forterre and Pouliquen, 2009) have shown that the $\mu(I)$ rheology (Jop et al., 2006) provides a much better approximation of the behaviour of granular matter than the Coulomb or Voellmy friction laws that are used in most models in practical use. If the soil consists of dry sand or coarser grains, the shear stress can be expressed as

$$\tau = \mu_{\text{eff}}(I)\sigma_e = \left(\mu_1 + \frac{\mu_2 - \mu_1}{I_0/I + 1}\right)\sigma_e, \tag{3}$$

where the so-called inertial number, I, is the non-dimensionalized shear rate (s^{-1}) and defined as

$$I = \frac{\dot{\gamma} d}{\sqrt{\sigma_n/\rho_f}}, \tag{4}$$

with $\dot{\gamma} = \partial_z u$ the dimensional shear rate and d (m) the mean particle diameter. The effective friction coefficient $\mu_{\text{eff}}(I)$ grows from a minimum value μ_1 at $I = 0$ to a maximum value μ_2 as $I \to \infty$, the parameters $\mu_{1,2}$ and I_0 depending mainly on the shape and size distribution of the granular material. At very low and high values of I, deviations from this behaviour have been found and parameterized (Barker et al., 2017). GdR MiDi (2004) in addition showed that the volumetric concentration (–) in steady flow also changes with I, according to

$$c(I) = c_0 - \beta I, \tag{5}$$

at least up to moderate values of $I \ll c_0/\beta$..

An important discovery was that the $\mu(I)$-rheology also describes water-saturated or submerged granular materials quite well, where fluid pore pressure is intimately coupled with granular dynamics. This requires, however, redefining I in a way that accounts for the modified time scales of intergranular processes due to the pore fluid (Cassar et al., 2005; Boyer et al., 2011; Guazzelli and Pouliquen, 2018). In steady flows, the excess pore pressure is also controlled by this modified I. Perhaps not surprisingly, the modified form of I depends on the fluid viscosity, the particle concentration and the ratio of particle

to fluid density; moreover, it distinguishes between the viscous and inertial regime of particle motion in the fluid. Further generalizations consider transition from geotechnical plasticity formulations (soil behavior) to granular flow behavior, unifying cohesive and granular suspended fluids (Si et al., 2018; Rauter et al., 2021). Most of the submarine landslides along the glaciated margins involve clayey material, which shows rather different rheological behaviour from sandy materials. Clays are shear-thinning visco-plastic fluids with a yield strength, τ_y (Pa), and are well described by the Herschel–Bulkley rheology or flow rule,

$$\tau = \tau_y + \eta\dot{\gamma}^n \,, \tag{6}$$

where n (–) is the flow exponent (typically in the range 0.1–0.5 for clays) and η the generalized viscosity (units Pa·s^n). τ_y, η and, to some degree, n depend on the water content (or liquidity index) of the material. This is of particular significance in the submarine realm, where ambient water can easily be mixed into sandy flows but not into clay-rich flows because of their very low permeability.

The amount and the type of clay is especially important for the cohesive (high clay-content) landslide dynamics (Ilstad et al. 2004a,b,c; Elverhøi et al. 2005, 2010; Breien et al. 2007, 2010), from a modelling perspective approximated by the Herschel–Bulkley rheology (e.g., Huang and Garcia 1998; Elverhøi et al. 2005, Kim et al. 2019).

Figure 6.7 compares the flow rules, i.e., the dependence of the shear stress on the shear rate, schematically for these rheologies. For the Coulomb yield criterion, the $\mu(I)$-rheology and the Voellmy friction law, the offset of the curves at $\dot{\gamma} = 0$ is proportional to the effective normal stress. Here, it was drawn equal to the one of the Herschel–Bulkley fluid to highlight the differences in the flow rules as $\dot{\gamma} \to 0$ and $\dot{\gamma} \to \infty$.

Yet another highly relevant property of clays is that they can lose a fraction of their original yield strength and viscosity as a function of accumulated shear, which destroys the bonds between clay platelets and frees the large amount of water that was trapped between them. This remoulding effect is quantified by the sensitivity S (–) of the clay, which is the ratio of non-remoulded to fully remoulded yield strength. In the case of quick clays, values of S up to 400 have been measured, i.e., the yield strength may disappear almost completely. The development of a slide in sensitive clay depends critically on how quickly the remoulding takes place. Some dynamical slide models attempt to capture this by assuming τ_y and η to be empirical functions of the accumulated shear $\Gamma(t) = \int_0^t \dot{\gamma}(x(t'), t')\mathrm{d}t'$, e.g., $\tau_y(\Gamma) = \tau_{y,0} - \left(\tau_{y,0} - \tau_{y,\infty}\right)\exp(-\lambda\Gamma)$, $\tau_{y,0}$ the non-remoulded and $\tau_{y,\infty}$ the fully remoulded yield strength (De Blasio et al., 2003). Toorman (1997) showed that a physical and accurate constitutive equation for clayey muds as thixotropic fluids can be derived from structural kinetics theory, which describes the competition between the formation (flocculation) and break-up of inter-particle bonds under shear. This process-based approach deserves to be explored further.

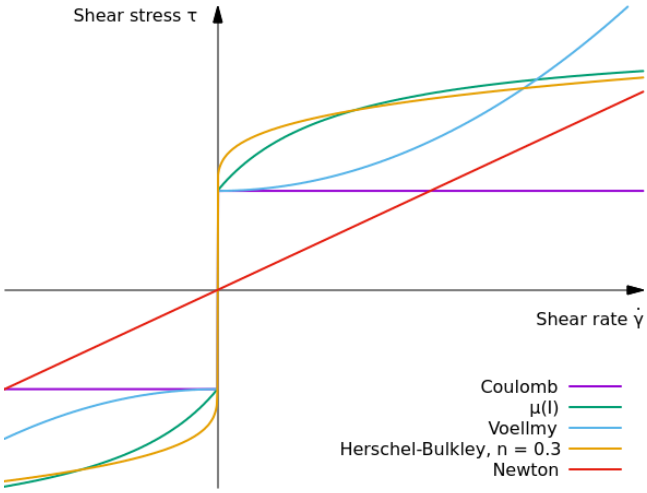


Figure 6.7. Schematic representation of the flow rules mentioned in Section 6.3.1 *Rheology*

6.3.2 Flow Regimes

Like GMFs on land, submarine GMFs exhibit a wide variety of flow regimes; they may pass through different regimes along their path, and the flow regime may vary spatially at a given instant. In dry granular materials without cohesion, the flow regime is determined by the shear rate and the density. It is crucial that subaerial GMFs are free-surface flows, i.e., they can adjust their density to the flow conditions. At high density and very low shear rates, in the quasi-static regime, persistent contacts between grains dominate and the concepts of critical-state soil mechanics can be applied: depending on the initial volumetric particle concentration, the soil contracts or dilates until it reaches the critical-state density. If one increases the shear rate, the density decreases and the contacts between particles become more collisional than frictional. At high shear rates, the concentration diminishes to the point where grains interact with each other only through collisions and the flow is fully fluidized. If the shear rate is increased further, the mean free path of a particle between collisions exceeds a few particle diameters; this is the inertial regime of a granular gas.

In the submarine environment, the incompressibility and large mass of the water above do not allow the flow to expand easily. Instead, the particle concentration can decrease only if ambient water penetrates the soil. In sandy, non-cohesive flows, the stagnation pressure at the flow front leads to seepage and dilution of the head (Figure 6.8b); this intermediate-density flow regime appears to be similar to the fluidized or intermittency regime of dry-snow avalanches (Sovilla et al., 2015) and may be what is often called a high-density turbidity current in the literature (Shanmugam, 1996). In rapid non-cohesive flows, Kelvin–Helmholtz instabilities tend to develop along the upper surface of the flow, leading to intensive mixing with ambient water and turbulent suspension of the soil particles. This is a different, much more dilute flow regime, in which particle collisions are infrequent; it corresponds to the macro-viscous regime in suspensions (Bagnold, 1954) except for the dominant role of turbulence.

In the late 1990s, laboratory experiments comparing clay-rich and sandy mixtures showed that the flow behaviour of these mixtures depends critically on the sand–clay ratio besides the water content. These flows could be described quite well with a visco-plastic rheology of the Bingham or the more general Herschel–Bulkley type (Imran et al., 2001). Mixtures with relatively high water and/or sand content had higher velocity and longer run-out in air than in water, as expected. In contrast, clay-rich mixtures ran out much farther and faster under water than in air. The reason is hydroplaning, i.e., ambient water penetrating underneath the front of clay-rich flows is trapped and lubricates the flow when the velocity becomes sufficiently high (Figures 6.8a and 6.9). The onset of hydroplaning is controlled by the densimetric Froude number $\mathrm{Fr} = u_f/\sqrt{g'h_f}$, with u_f and h_f the front velocity and depth of the flow and $g' = \left(1 - \rho_w/\rho_f\right)g$ the gravitational acceleration (m s^{-2}) reduced for buoyancy. The critical value of Fr is of the order of 0.4 (Harbitz et al., 2003). This result is confirmed by numerical simulations (Gauer, 2006).

As it is almost impossible to observe submarine debris flows when they occur, there is only circumstantial evidence for this phenomenon occurring in Nature. One indication could be the absence of bed erosion because the thin water layer underneath the flow reduces the bed shear stress dramatically (Mohrig et al., 1999), as illustrated in Figure 6.8a and demonstrated in the laboratory (Figure 6.9). However, hydroplaning occurs typically only in the head of the flow and the flow body may erode the bed. Outrunner blocks that travelled much farther than the main body—observed in many medium-size to very large events—can be explained by frontal hydroplaning leading to block detachment and enhanced run-out (Ilstad et al., 2004c). A particularly intriguing example is the relatively small 1996 Finneidfjord landslide in northern Norway, where the distal-most outrunner block is of substantial size and was stopped by a mound more than 1 km beyond the deposits of the main body. Along its path, there are no signs of erosion on the fjord bottom except for a very shallow depression.

In suspension flows, turbulent eddies can maintain particles in suspension, with the concentration gradient in the quasi-steady state directly coupled to the difference between mean eddy velocity and mean particle settling velocity. Along the upper surface of the suspension layer, entrained ambient fluid is imparted not only momentum from the flow body but also turbulent kinetic energy (TKE); moreover, lifting particles against gravity throughout the flow also dissipates TKE (Figure 6.11). This implies that the balance between creation and dissipation of TKE is of prime importance for the evolution of the flow (Parker et al., 1986).

Laboratory experiments including particle tracking and pressure measurements indicate that the dynamics of the body of sandy debris flows is complex (Ilstad et al., 2004a,b,c; Breien et al., 2010). The cohesive clay creates a matrix supporting the sand particles to some degree, but it is progressively elutriated from the top of the dense flow. Water progressively penetrates the sand and fluidizes it, but as the matrix strength diminishes, they settle progressively and form a deposit. Figure 6.11 illustrates

these processes schematically. The velocity and runout of the flow body depend sensitively on the clay type and content, the grain size distribution of the sand, the depth of the flow and the slope angle. These effects are only partially analysed and mathematically modelled at present.

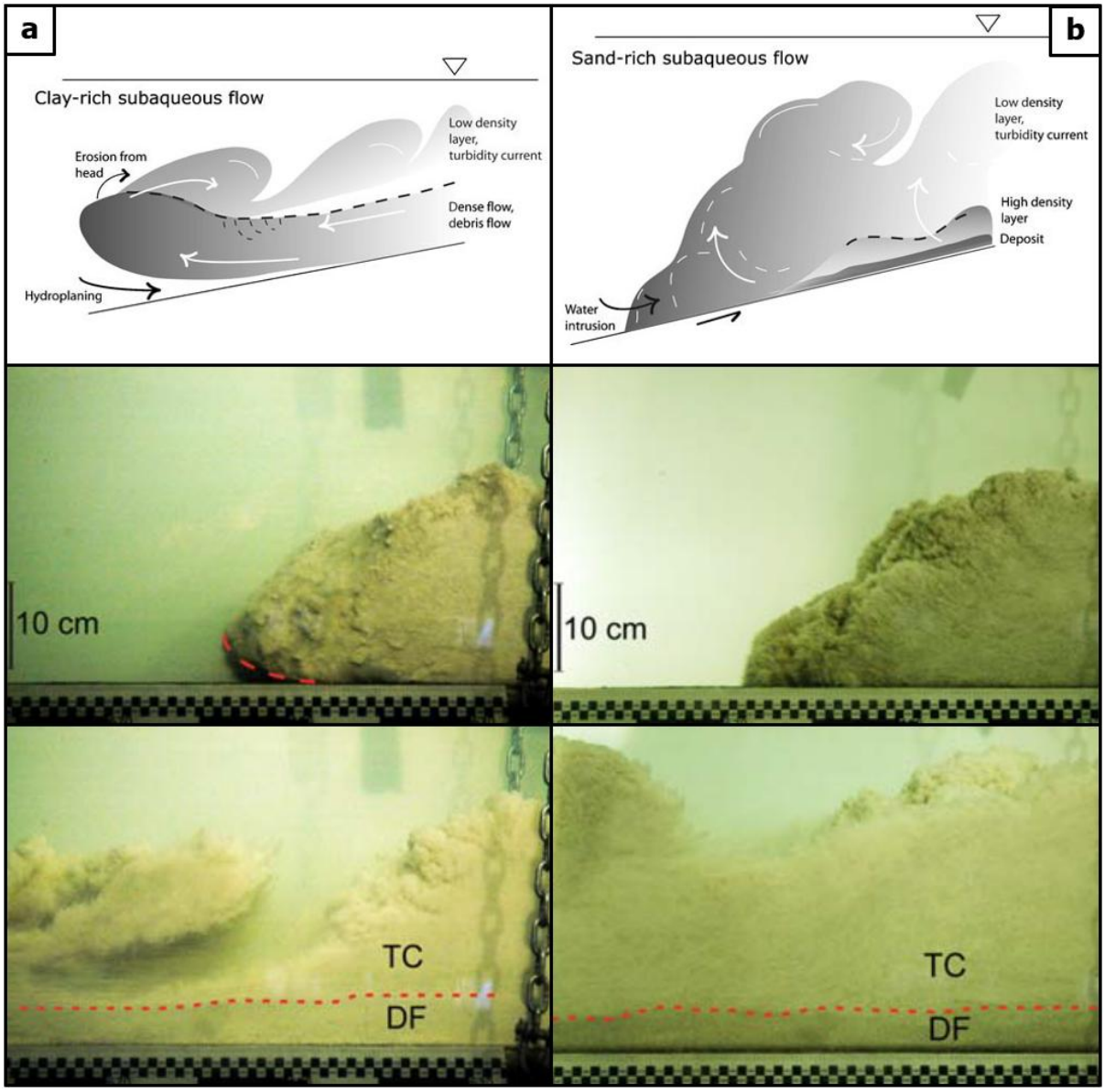


Figure 6.8. Illustration of the difference between the flow regimes of (a) clay-rich and (b) sand-rich sub-aqueous debris flows. The high cohesion of clay-rich flows prevents ambient water from penetrating the head; instead, the stagnation pressure exceeds the weight of the snout above a critical velocity (corresponding to a Froude number of approximately 0.4) and lifts it from the bed, leading to hydroplaning. In clay-rich flows, the turbidity current consists mainly of elutriated clay and is usually less developed. Clay and sand are more easily suspended from sand-rich flows, but keeping the sand in suspension requires a strong and sustained production of turbulence. Figure from Elverhøi et al. (2010). Photographs show comparison of the fronts and bodies of sand-rich (5% clay, upper images) and clay-rich (20% clay, lower images) debris flows in the laboratory. In the sand-rich flow, the head is

progressively diluted by water penetrating it while in the clay-rich, cohesive flow the head is lifted from the bed.by the water that is pressed underneath. TC: Turbidity current; DF: Debris flow. From Breien et al. (2007).

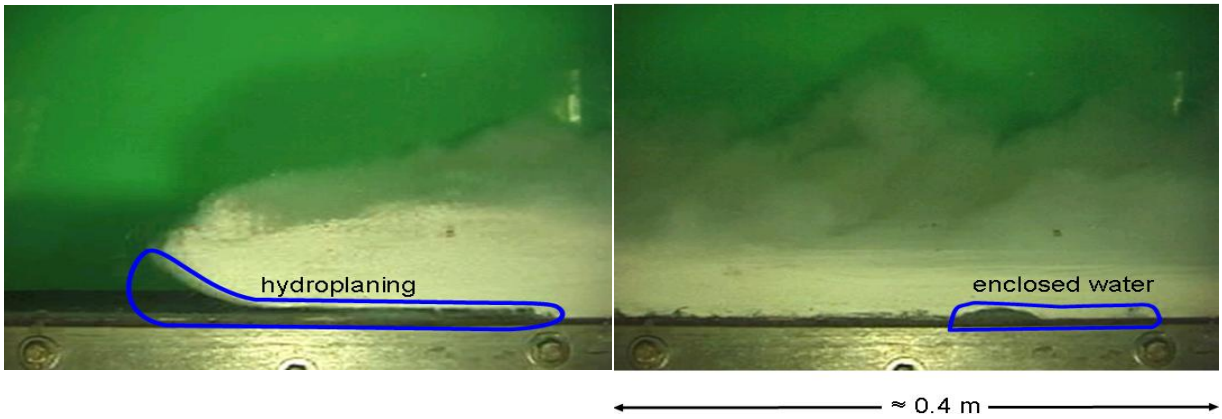


Figure 6.9. Side view of a highly cohesive laboratory flow at the St. Anthony Falls Laboratory. Except on the flow surface, there is very little internal shear in the flow. One can clearly see that a water layer lifts the front of the bed, dramatically reducing the bed friction of the head. In some experiments, auto-acephalation occurred, i.e., the velocity difference between the head and the body stretched and thinned the "neck" of the flow to the point where it broke. In sufficiently cohesive and thin flows, the head could be flipped back over the non-hydroplaning body. As the right image shows, a turbulent suspension layer is formed, but its density remains low, and it moves more slowly than the dense underflow. Figure from Gauer et al. (2006).

This brief discussion of the flow behaviour of sub-aqueous GMFs shows that, if one wishes to model them in some detail, accounting for flow-regime transitions is crucial. The most pressing knowledge gaps, given their practical consequences, are (i) the question whether hydroplaning indeed occurs in full-size debris or mud flows, (ii) how quickly water can be mixed into the shear layer of dense flows, and (iii) how quickly the suspension layer is formed.

6.3.3 Erosion and Deposition

The very existence of submarine canyons of enormous dimensions testifies to the erosive power of GMFs in water. Entrainment of bed material can play a decisive role in the development of turbidity currents (TCs), as pointed out and modelled by Parker et al. (1986): To maintain their speed despite continuously mixing in ambient water, turbidity currents must be able to entrain the right amount of bed material. Various possible erosion mechanisms have been observed or hypothesized (Gauer and Issler, 2004). In the context of TCs, scour along the base of the flow is presumably dominant, but in non-cohesive beds, eruption currents at the front of large TCs, where the excess pore pressure in the bed generated by the approaching GMF may overcome soil cohesion and eject mass, might contribute significantly (Louge et al., 2011).

Several experiments have studied the dependence of the entrainment rate, q_e, on the bed particle size and the flow parameters for TCs over sandy beds, e.g., (Parker et al., 1987). Despite significant differences between experiments and theoretical analyses, the general trends appear to be established. For cohesive beds, the functional form of q_e does not appear to be well established; many analyses are inconsistent with certain mechanical principles or are empirical to a degree that makes them highly questionable outside the specific context in which they were developed. It is generally recognized that pore pressure in the bed plays an important role in erosion, but the mechanisms of pore pressure generation in rapid GMFs are still a topic of active research.

Modelling erosion and entrainment in a mathematical model that resolves the structure of the bed and flow in the bed-normal direction is, in principle, fairly straightforward: the response of the bed to the extra normal load and shear stress of the approaching or overriding flow can be calculated in detail and the assumed failure criterion can be applied to decide whether and how a portion of the bed is eroded and entrained. However, in the frequently used, much more efficient depth-averaged flow models (Section 6.3.4), this detailed information is not available and additional modelling assumptions must be made to determine the entrainment rate. For non-cohesive granular beds, detailed theoretical analyses (e.g. Gray, 2001) have elucidated much of the phenomenon and yielded erosion rate formulas that appear to describe experiments well. If the bed material can be characterized as brittle with a clear yield strength, a simple formula of the type

$$q_e \approx \Theta(\tau_b - \tau_c)\frac{\tau_b(h,u) - \tau_c}{u}\,, \tag{7}$$

has been proposed (Fraccarollo and Capart, 2002; Issler, 2014). The step function $\Theta(x)$, which is 0 if $x \leq 0$ and 1 otherwise, imposes a threshold τ_c on the bed shear stress τ_b for the onset of entrainment; the fraction limits the entrainment rate so that the excess shear stress $\tau_b - \tau_c$ suffices to accelerate the eroded mass to the flow velocity u. It remains to test this simple concept against carefully designed laboratory experiments and evidence from field observations of different types of GMFs. Incidentally, a similar approach can be applied at the interface between a dense flow and the suspension layer developing above it. Observations on wet-snow avalanches, laboratory experiments on granular flows (Barbolini et al., 2005) and numerical simulations (Li et al., 2022; Ligneau et al., 2024) point to the importance of frontal entrainment by ploughing in relatively slow, dense flows. This mechanism was already included in the first "modern" numerical model for snow avalanches in the 1960s (see Eglit et al. (2020) for a summary and references).

Many authors have assumed that deposition is simply the opposite process of entrainment; one could then simply omit the step function in Eq. (7) and interpret negative q_e as the deposition rate. Up to hysteresis effects, this works for dry, non-cohesive granular materials, but in general there is an asymmetry between entrainment and deposition: Entropy increases in the transition from a solid to a

(granular) fluid, but it must decrease during deposition. Entropy having the tendency to increase in a closed system, deposition cannot simply be time-mirrored entrainment. Rauter and Köhler (2020) analysed the velocity profiles of decelerating flows and found pronounced differences near the bed, which led them to suggest the following expression for the deposition rate:

$$q_d = \Theta\left(u_{\mathrm{dep}} - \|\boldsymbol{u}\|\right) \cdot \Theta\left(-\boldsymbol{u} \cdot \left(\boldsymbol{F}_g - \boldsymbol{F}_b - \boldsymbol{F}_p\right)\right) \cdot \left(1 - \frac{\|\boldsymbol{u}\|}{u_{\mathrm{dep}}}\right) \cdot \frac{\left\|\boldsymbol{F}_g - \boldsymbol{F}_b - \boldsymbol{F}_p\right\|}{\|\boldsymbol{u}\|} \,. \tag{8}$$

It captures that deposition only occurs (i) below some (material-dependent) maximum velocity u_{dep} and (ii) if the flow decelerates, i.e., if the resultant of the gravitational force $\boldsymbol{F}_g$, the shear force $\boldsymbol{F}_b$ at the bed and the pressure-gradient force $\boldsymbol{F}_p$ opposes the velocity $\boldsymbol{u}$. Moreover, (iii) q_d is assumed to increase linearly with the difference between u_{dep} and $\|\boldsymbol{u}\|$. This assumption is theoretically less well founded than the rest of Eq. (8), but it is simple and can be tested.

6.3.4 Physical and Numerical Modelling

Laboratory experiments on sub-aqueous GMFs have been carried out for more than 70 years (Kuenen, 1937) and have yielded many important insights about flow regimes, run-out distance, velocity, erosion and deposition. There have been a few attempts to use physical modelling in a water tank to estimate the path and run-out of full-scale debris flows or even the pressure distribution from powder-snow avalanches, but the effort of constructing a scale model of the terrain, running the experiments and analysing the data is too large in most practical problems. In addition, fulfilling all relevant scaling requirements may be difficult or even impossible.

Another approach—at least for estimating the run-out length of a potential future slide—makes use of data aggregated from the entire world or, more specifically, from multiple events in a specific setting. The run-out angle or the effective friction coefficient of sub-aerial landslides diminishes with increasing volume, V; Scheidegger (1973) found the relation

$$\mu_{\mathrm{eff}} = 4.2 \cdot \left(V / 1\,\mathrm{m}^3\right)^{-0.16} \tag{9}$$

for rock avalanches, which corresponds to run-out angles of 35° for $V = 10^5$ m^3 and 9° for $V = 10^9$ m^3. (This does not apply to quick-clay slides, which typically have much higher mobility.) Landslides and debris flows in the marine environment seem to obey a similar correlation up to volumes of about 10^9 m^3. Beyond that threshold, events dominated by very large rock fragments appear to follow the same trend, but the effective friction of large debris and mud flows decreases with a power close to −1/3 instead of −1/6, indicating the emergence of a different flow regime (Figure 6.10; Elverhøi et al., 2002; De Blasio et al., 2006). The wide scatter in the global data set is not surprising, given the wide range of geotechnical conditions. The single slide events identified in the extremely large Storegga slide complex

(Haflidason et al., 2005) follow the same trend over the volume range 10^7–10^{11} m^3 but have considerably lower scatter due to their highly similar soil compositions (Issler et al., 2005).

These empirical scaling relations can be used to test theoretical concepts on GMF dynamics (Issler et al., 2005), but they are only useful in practical problems if one may assume that the exponent is about −1/6 for smaller slides and near −1/3 for large, clay-rich debris flows, and they do not give information about velocity, scour and impact pressure. Developing analogous correlations for these quantities—with traditional statistical methods or with machine learning—is hardly possible because measurements are too scarce.

At this point, dynamical models based on the principle of conservation of mass, momentum and total energy come to the rescue. However, developing accurate yet practically useful models is a highly non-trivial task. There is a bewildering range of modelling approaches that can be useful under specific conditions with regard to the questions that must be answered, the required level of accuracy, the available computational resources, the size of the study area, the seascape, and the soil composition. At one end of this spectrum are extensions of the concept of mass-point models. At the other extreme, discrete element models (DEM) simulate the movement and interaction of large numbers of "particles" in 3D and may require weeks on a super-computer for a single simulation. The middle ground consists mostly of continuum models, which are solved numerically by discretizing the space–time continuum as finite time intervals and spatial cells; this turns the partial differential equations into algebraic ones. The models solve an appropriately simplified set of balance equations for mass, momentum and, possibly, different forms of energy, employing model-specific constitutive equations (describing material properties) for closure. In the following, only a few remarks on the merits and problems of a few selected modelling approaches can be given. Interested readers are referred to review papers (e.g., Trujillo-Vela et al., 2022, and references contained therein).

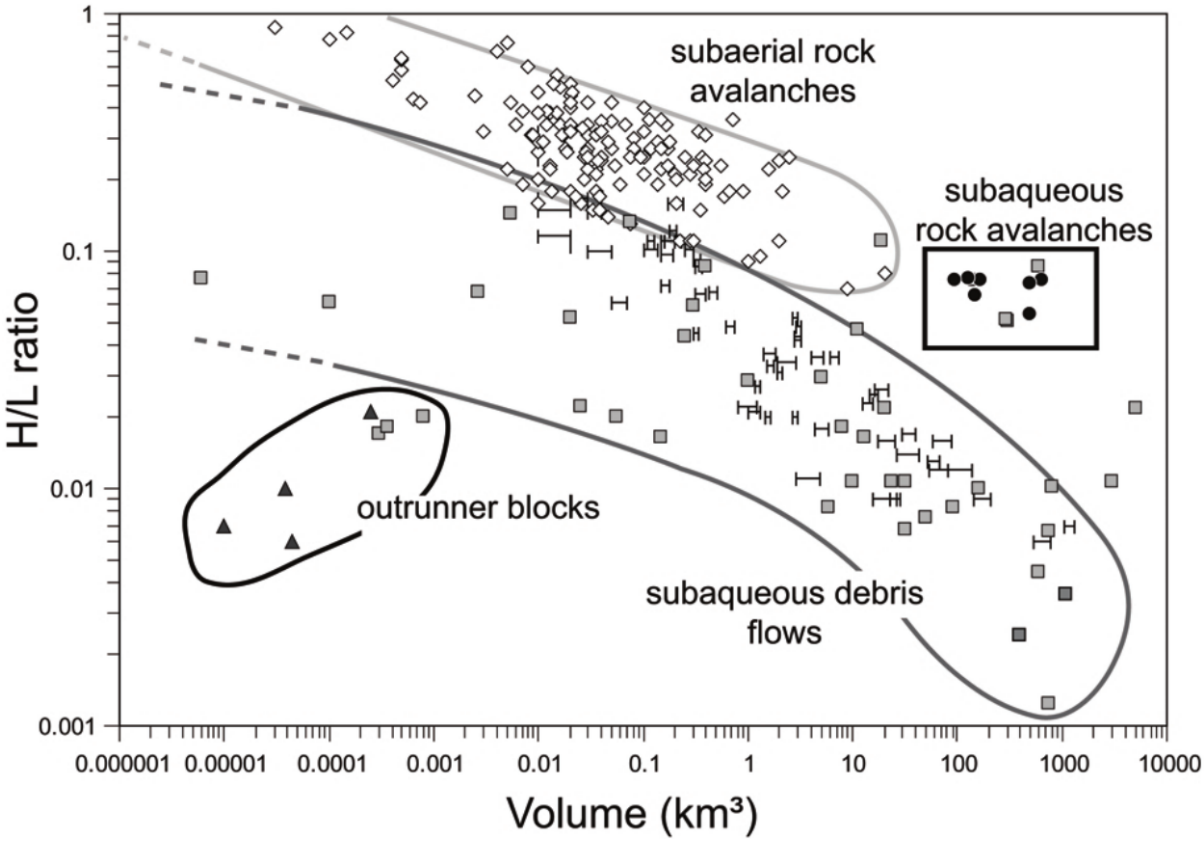


Figure 6.10. Diagram showing the distribution of runout ratios H/L of subaqueous and subaerial landslide deposits as a function of deposit volume. The plot is reproduced from De Blasio et al. (2006), where the sources of the different data points are reported.

Mass-point models solve the equation of motion of the centre of mass of the slide,

$$\frac{\mathrm{d}v}{\mathrm{d}t} = g' \sin\theta(s) - \frac{F_r}{M} - \frac{Q_{e/d}v}{M}, \tag{10}$$

together with the mass balance equation,

$$\frac{\mathrm{d}M}{\mathrm{d}t} = Q_{e/d}\,. \tag{11}$$

Here, t is the time, s the distance along the slope, $\theta(s)$ the spatially varying slope angle, $v = \mathrm{d}s/\mathrm{d}t$ the velocity, $g' = g\left(1 - \rho_f/\rho_s\right)$ the effective gravitational acceleration accounting for buoyancy, with ρ_f and ρ_s the densities of the ambient water and the flowing mass, respectively. F_r is the resistive force, M the total mass of the slide, and $Q_{e/d}$ the net mass gain or loss per unit time interval.

Huppert and co-workers chose a slightly different concept, modelling turbidity currents as elongating and widening boxes or pie slices and obtained analytical solutions for the run-out distance and the asymptotic behaviour of velocity and deposition depth on a plane, which correspond well with observed turbidites (Dade and Huppert, 1994). These models are simplified to the most essential features yet capture a surprising wealth of phenomena with very few adjustable parameters, and there are additional

processes that could be built into them to describe more specific properties of these flows with modest computational effort—albeit at the cost of introducing additional parameters that must be calibrated.

However, if one requires more detailed modelling and better spatio-temporal resolution, one may idealize the GMF as a continuum at a scale between the typical particle sizes and the typical flow depth and describe the relevant fluid properties (density, velocity, etc.) in terms of fields $\rho(\boldsymbol{x}, t)$, $\boldsymbol{u}(\boldsymbol{x}, t)$, etc. These fields must obey the mass conservation equation for a single-component fluid,

$$\partial_t \rho + \boldsymbol{\nabla} \cdot (\rho \boldsymbol{u}) = 0, \tag{12}$$

and the Navier–Stokes (momentum balance) equation,

$$\partial_t (\rho \boldsymbol{u}) + \boldsymbol{\nabla} \cdot (\rho \boldsymbol{u}\boldsymbol{u}) = \boldsymbol{f} - \boldsymbol{\nabla} p + \boldsymbol{\nabla} \cdot \boldsymbol{\sigma}. \tag{13}$$

$\boldsymbol{f} = \rho \boldsymbol{g}'$ is the body force per unit volume, i.e., the buoyant gravity in GMFs, while p is the pressure and $\boldsymbol{\sigma}$ the deviator of the stress tensor. As indicated in Section 6.3.1 on rheology, the constitutive equations expressing p and $\boldsymbol{\sigma}$ in terms of ρ and $\boldsymbol{u}$ (and other fields if additional variables are included) are much more complex than those for ideal fluids or gases. If they are formulated in a sufficiently general way, they can encompass both solid and fluid phases so that the transition between these phases during the release and stopping of a slide as well as erosion and deposition during the flow can be modelled, as demonstrated, e.g., by Gaume et al. (2019). However, if the constitutive relations are not smooth, as in the case of a yield-strength fluid, there can be significant numerical challenges.

At any rate, solving these equations in 3D in a large area typical of submarine landslides requires an enormous computational effort. It can be reduced by some three orders of magnitude if one simulates only a longitudinal section of the flow (i.e., two dimensions in a vertical plane or 2DV), but essential information about the sideways spreading of the slide is lost. An alternative simplification is to formally integrate the Eqs. (12) and (13) over the flow depth to reduce them to two-dimensional (2DH) equations for $h\rho$ (or h if the density is constant) and $h\rho\boldsymbol{u}$ (or $h\boldsymbol{u}$). One thereby loses information about the variation of the fields in the bed-normal or vertical dimension but can reduce the computational effort typically by six orders of magnitude or more, which makes simulation practical in many cases. If the sideways spreading is not essential (e.g. when scanning the parameter space for a specific flow), a speed-up by another two orders of magnitude can be achieved by also integrating the equations over the flow width. Many variants of 1D or 2D depth-averaged continuum models for all types of GMFs have been developed over the past 60 years (Eglit et al., 2020) and have become indispensable tools in research as well as practical hazard management.

In contrast to the Saint-Venant or shallow-water equations, depth-averaged models of GMFs necessarily include several source terms to describe the down-slope gravitational force, bed friction, and erosion/deposition. Extra conservation or constitutive equations are needed if the flow density is variable, if segregation must be accounted for, or if two or more different layers are present. Examples

of the latter are turbidity currents with a dense underflow, coupled landslide–tsunami models and flows of visco-plastic materials like clay with a plug layer riding on a basal shear layer, both of which have variable thickness. We illustrate the complexity and wealth of options of such models with a minimal two-layer formulation for (non-hydroplaning) debris flows developing a turbidity current, as schematically depicted in Figure 6.11. It comprises three mass-conservation equations for the bed (index 0), the dense underflow (index 1) and the suspension flow layer (index 2) layers but not the ambient water layer (index 3),

$$\partial_t b = -q_{01} + q_{10} - q_{02} + q_{20}, \tag{1}$$

$$\partial_t(h_1\rho_1) + \boldsymbol{\nabla}\cdot(h_1\rho_1\boldsymbol{u}_1) = q_{01} - q_{10} - q_{12} + q_{21}, \tag{2}$$

$$\partial_t(h_2\rho_2) + \boldsymbol{\nabla}\cdot(h_2\rho_2\boldsymbol{u}_2) = q_{02} - q_{20} + q_{12} - q_{21} + q_{32}, \tag{3}$$

two volume-conservation equations for layers 1 and 2 because the particle concentration in these layers can change,

$$\partial_t h_1 + \boldsymbol{\nabla}\cdot(h_1\boldsymbol{u}_1) = \frac{q_{01} - q_{10} - q_{12} + q_{21}}{\rho_1} \tag{4}$$

$$\partial_t h_2 + \boldsymbol{\nabla}\cdot(h_2\boldsymbol{u}_2) = \frac{q_{02} - q_{20} + q_{12} - q_{21} + q_{32}}{\rho_2} \tag{5}$$

and two vectorial momentum-balance equations,

$$\begin{aligned}\partial_t(h_1\rho_1\boldsymbol{u}_1) + \boldsymbol{\nabla}\cdot(k_{1u}h_1\rho_1\boldsymbol{u}_1\boldsymbol{u}_1)\\ = \boldsymbol{f}_1 + \boldsymbol{\nabla}\cdot(h_1\overline{\boldsymbol{\sigma}}_1) - \boldsymbol{\tau}_{10} + \boldsymbol{\tau}_{21} - (q_{10} + q_{12})\,\boldsymbol{u}_1 + q_{21}\boldsymbol{u}_2,\end{aligned} \tag{6}$$

$$\begin{aligned}\partial_t(h_2\rho_2\boldsymbol{u}_2) + \boldsymbol{\nabla}\cdot(k_{2u}h_2\rho_2\boldsymbol{u}_2\boldsymbol{u}_2)\\ = \boldsymbol{f}_2 + \boldsymbol{\nabla}\cdot(h_2\overline{\boldsymbol{\sigma}}_2) - \boldsymbol{\tau}_{20} - \boldsymbol{\tau}_{21} - \boldsymbol{\tau}_{23} - (q_{10} + q_{21})\,\boldsymbol{u}_2 + q_{12}\boldsymbol{u}_1.\end{aligned} \tag{7}$$

These nine partial differential equations must be supplemented by closure relations for the six mass exchange rates $q_{ij}, i,j = 0,1,2,\ i \neq j$, between layers and with the ambient fluid (q_{32}), the interfacial shear stresses $\boldsymbol{\tau}_{10}$, $\boldsymbol{\tau}_{20}$, $\boldsymbol{\tau}_{21}$, $\boldsymbol{\tau}_{23}$ as well as the depth-averaged stress tensors $\overline{\boldsymbol{\sigma}}_1$, $\overline{\boldsymbol{\sigma}}_2$ and the pressure in the ambient fluid. There is considerable freedom in modelling these relations, and the simulation results depend crucially on these choices.

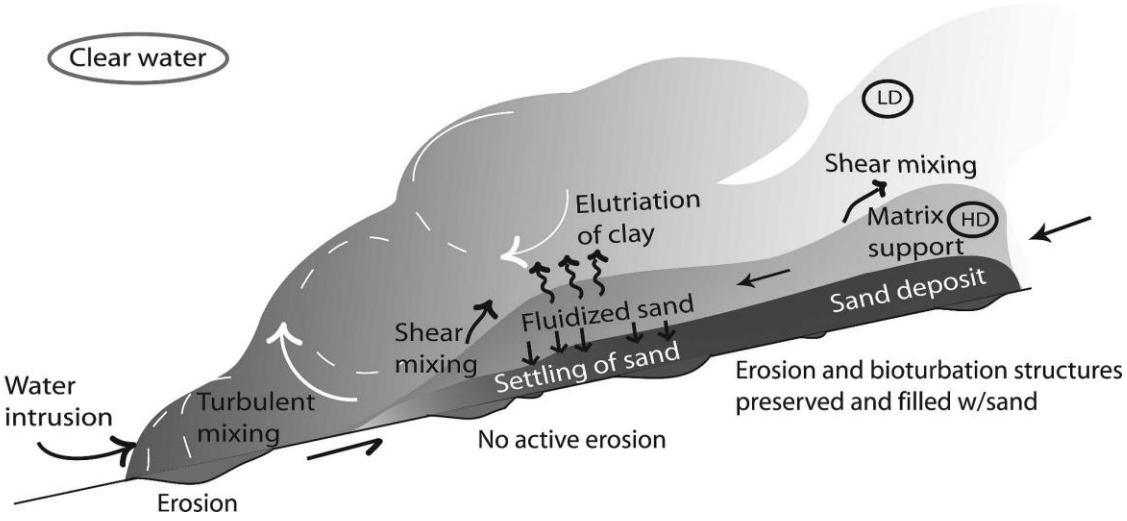


Figure 6.11. Schematic illustration of the structure and mass fluxes in a sand-rich subaqueous debris flow. Through the front, water intrudes into the head and dilutes it, thus generating a sizeable turbidity current if the velocity and the shear rate are high enough to produce enough turbulence to keep the sand particles in suspension. On an easily erodible sea floor, entrainment can make up for the mass loss of the head due to shedding wakes and maintain the flow over very long distances. The dynamics of the main body of the debris flow is governed by the interplay of clay elutriation, sand supported by the matrix of residual clay, fluidization of the sand by penetrating water, and settling of sand particles leading to deposition. The balance of these processes depends dynamically on the sediment composition, flow size, and stage of the flow. LD: Low density; HD: High density. From Breien et al. (2010).

Simple one-layer models with constant density are described by hyperbolic equations; in contrast, depth-averaged variable-density and/or two-layer models may not be hyperbolic in their entire parameter ranges (Nazarov, 1991), which may pose challenges for numerical codes. The proposed mathematical models have been implemented with finite-difference, finite-volume, finite-element and meshless discretization techniques like Smoothed Particle Hydrodynamics (SPH), or with a combination thereof in the case of the Material Point Method (MPM). Choosing the most suitable method for a given situation is challenging because increased flexibility or accuracy usually comes with higher program complexity and lower speed. While Eulerian finite-volume codes have been dominant for some decades, SPH and MPM codes have caught centre-stage recently (e.g., Pastor et al., 2024; Guillet et al., 2023).

Assuming a code correctly solves the model equations, one must verify that these equations describe the target phenomenon sufficiently well for the purpose at hand. In this process, laboratory experiments play an important role because one can control the initial and boundary conditions and measure the flow

variables during the flow. One can test whether a model correctly simulates the dependence of velocity and run-out on the soil composition. However, detailed laboratory studies of bed entrainment (Barbolini et al., 2005) and turbidity-current formation (Mohrig and Marr, 2003) are scarce. It would be equally important to validate and calibrate models against real-scale GMFs, but there are almost no measurements of the dynamics of sub-aqueous GMFs besides the recent exceptional data sets on turbidity currents, e.g., (Paull et al., 2018). Moreover, comprehensive geotechnical data from actual subaqueous landslides and their surroundings are available only for a few sites, where detailed assessment of the GMF risk was crucial (e.g., Solheim et al., 2005b; Carlton et al., 2018). Such geotechnical data have recently been used as input to an advanced 2DV model, which uses MPM for simulating the solid constituents and computational fluid dynamics (CFD) for the interstitial and ambient water (Tran et al., 2024). The good agreement with the observed longitudinal deposit section and erosion depth suggests that satisfactory Class-A predictions can indeed be achieved, albeit at a staggering computational cost. At present, therefore, one may use such advanced models primarily to improve the closure relations in depth-averaged models, which will continue to be the workhorse in practical applications in the foreseeable future.

6.3.5 Implications and Considerations for Engineering

In practice, GMF dynamics is mainly relevant for estimating the key parameters of the tsunami that a given mass flow will generate (see Sections 6.6.2) and for determining whether sub-sea installations are potentially endangered and, if so, how large the impact forces may be. The run-out distance can often be estimated with relatively simple empirical models if the latter can be calibrated from observed nearby landslides with the same soil conditions, as was done, e.g., for the Ormen Lange gas field within the Storegga slide area (De Blasio et al., 2003). If not enough data for calibrating is available, models that incorporate more of the relevant physics and have been validated against observed GMFs with similar characteristics should be used.

The interaction of GMFs with man-made sub-sea structures depends not only on the impact velocity and depth of the mass flow but also on its composition (notably its content of clay and/or hard rocks), the erodibility of the sea floor in the immediate surrounding of the structure, as well as the shape and exposed surface of the structure. In simple configurations like those in laboratory experiments, 2DV simulations with computational fluid dynamics (CFD) software have been carried out with rather satisfactory results (Zakeri et al., 2009). It is often assumed that the interaction of a GMF with an obstacle can only be modelled with a 3D simulation, and this is certainly true when studying the impact of a debris flow or turbidity current on a pipeline, where scour underneath the pipe is a critical effect. To make this practically feasible, one may carry out a depth-integrated simulation (in two horizontal dimensions) of the slide from release to the vicinity of the object and use the depth-integrated values to initialize the 3D simulation some distance upstream of the object. However, experience has shown that depth-averaged GMF models for granular flows are unexpectedly adept at simulating the main features

of the flow interaction with obstacles like dams or mounds (Gray et al., 2003; Tregaskis, 2020). If the vertical velocity and density profiles can be estimated, one may obtain an approximate vertical distribution of the impact forces, which may be sufficient in many cases—especially for turbidity currents. However, the case of soil flows with considerable yield strength has not been extensively studied with such models so far, thus there is a large amount of uncertainty connected with clay-rich debris flows or mudflows and it is advisable to use a 3D model.

Salmanidou et al. (2017) discussed uncertainty in landslide material parameter values by running multiple, simple granular (frictional-collisional) landslide-dynamics simulations for a statistical study. By comparing the results with observed landslide run-out distance for a large landslide at the Rockall Bank offshore Ireland, they found wide uncertainty distributions. However, this uncertainty can be reduced by also applying tsunami data (Løvholt et al., 2020) and measurements of geotechnical soil parameters, even though there is large epistemic uncertainty in the material behaviour that cannot be measured effectively in the laboratory (Vanneste et al., 2019).

An additional complication arises for flows of sensitive clays because the yield strength varies from an initial to a final remoulded value as a function of the shear strain accumulated during the flow (De Blasio et al., 2005). The final yield strength normally has the strongest influence on the run-out distance (Marr et al., 2002; Løvholt et al., 2017, 2019; Kim et al., 2019; Vanneste et al., 2019). In hazard studies, yield strength parameter values are often tuned to match modelling results with observations of run-out distance and are typically found to be much lower than the corresponding values measured in the laboratory, as it to some extent represents different effects that reduce friction, such as hydroplaning, weak layers, pore overpressure, etc. Owing to consolidation, the yield strength measured today may also be higher than when the landslide took place. A combination of strain-softening clay with high sensitivity together with anisotropic strength properties also enables a retrogressive failure (Kvalstad et al. 2005b), which can take place as a fairly slow process mobilizing the blocks one-by-one or a much faster process involving several blocks at the same time (Gauer et al. 2005; Løvholt et al. 2016).

In summary, numerical modelling of the release, propagation and impact of submarine GMFs still requires use of all available information on the geological setting of the area, the geotechnical properties of the soils, and the landslide history for calibration of the model(s). Based on this and the project requirements, the most suitable models must be chosen and their results critically appraised. Despite best efforts, the remaining uncertainty with regard to release probability, runout distance and impact on structures will often remain considerable. However, recent work (Tran et al., 2024) on highly sophisticated models holds promise of making numerical simulation of the entire process including slide release and impact possible, allowing so-called class-A predictions based on measured soil properties instead of calibrated empirical parameters. However, the computational cost for 3D simulations is prohibitive at present. As Figure 6.12 shows, even relatively simple models may be able

to capture the main features of an event if they adequately capture the key flow mechanisms (in this case, hydroplaning)

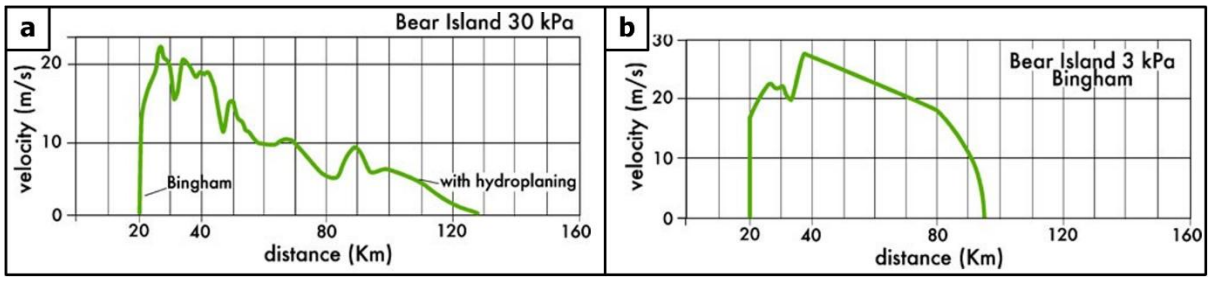


Figure 6.12. Illustrative example of numerical simulations of a subaqueous debris flow on the Bear Island Fan with the models BING (Imran et al., 2001) and W-BING (De Blasio et al., 2004). The observed runout exceeds 150 km, amounting to an effective friction coefficient of only 0.012. With the visco-plastic rheology implemented in BING, the observations cannot be reproduced even if the yield strength of the flowing material is set as low as 3 kPa. In contrast, W-BING includes hydroplaning at Froude numbers above 0.4 and almost reaches the observed runout with a yield strength of 30 kPa, which is realistic for over-consolidated clay deposits. Figure from Elverhøi et al. (2010).

6.4 Glacio-isostatic adjustment and sea-level changes

Generally, during the Pleistocene, global sea level varied from between approximately 10 m above present day to up to approximately 130 m below present levels (e.g., MIS2; Hansen et al, 2013; Lambeck et al., 2014). On glaciated continental margins the relative sea level is a combination of global sea level changes due to sequestration of water in ice sheets, and the viscos-elastic response of the crust and mantle to loading by growing and melting of continental-scale ice mass known as glacio-isostasy or glacio-isostatic adjustment (GIA; Shennan et al., 2011). Apart from the two primary mechanisms the relative sea level is also influenced by: (1) gravitational attraction of the water in the vicinity of the ice mass, (2) location and migration of a forebulge in front of the ice sheet as it grows and decays, and (3) thermal contraction and expansion of water due to changes in water temperature.

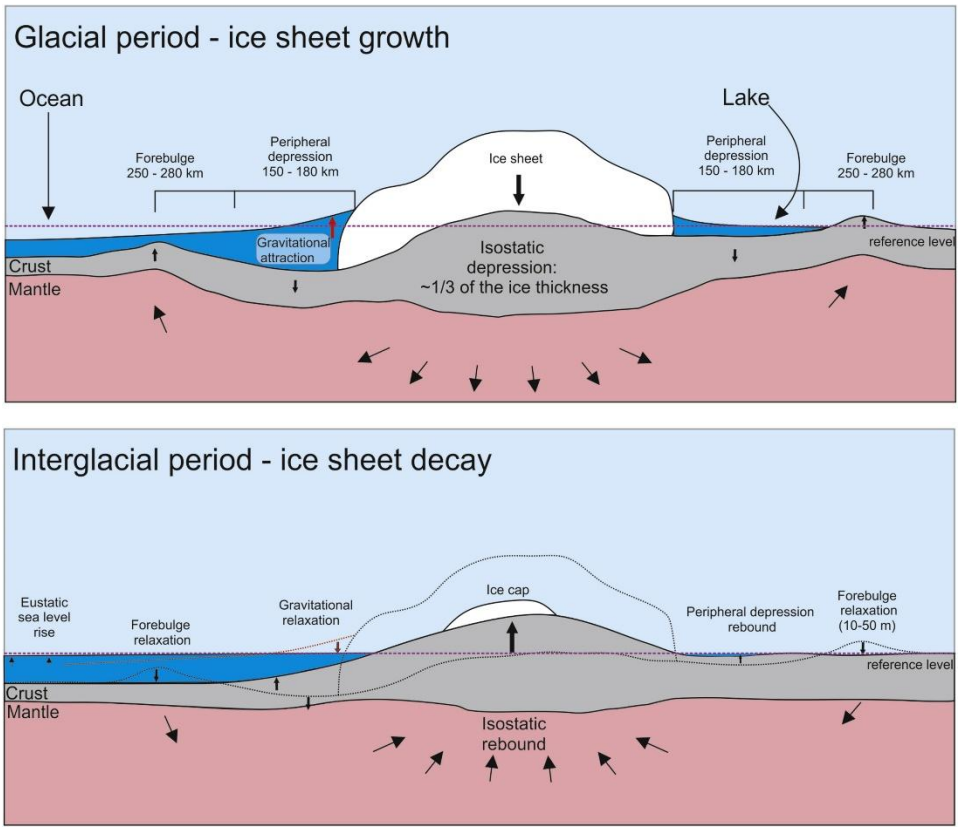


Figure 6.13. Behaviour of crust and mantle in response to loading by ice mass during ice-sheet growth and subsequent ice-sheet decay. Note the changes of relative sea level between the vicinity of the ice sheet (near field) and areas further afield (far field).

The global sea level was generally lower during Pleistocene glaciations and rose following ice demise (Figure 6.13). In the proximity of the ice sheet, the crustal rebound after deglaciation resulted in the relative sea level fall (not rise) as the land uplift outpaced the rise in the global ocean (Figure 6.13).

This can be described as a near-field relative sea-level trend where sea level generally is observed to fall after deglaciation (Figure 6.14). The opposite trend is observed for sites further away from the palaeo-ice sheet margins where only a sea-level rise is observed. Between the near-field and far-field sites, there is a wide zone where the interplay of eustatic sea-level rise and isostatic rebound results on a complex, undulating sea-level curve. This is referred to as a mid-field effect (Figure 6.14). This see-saw behaviour repeated itself between glacial and interglacial periods and was further complicated by spatiotemporal differences in ice extent, advance and decay rates (Figure 6.14).

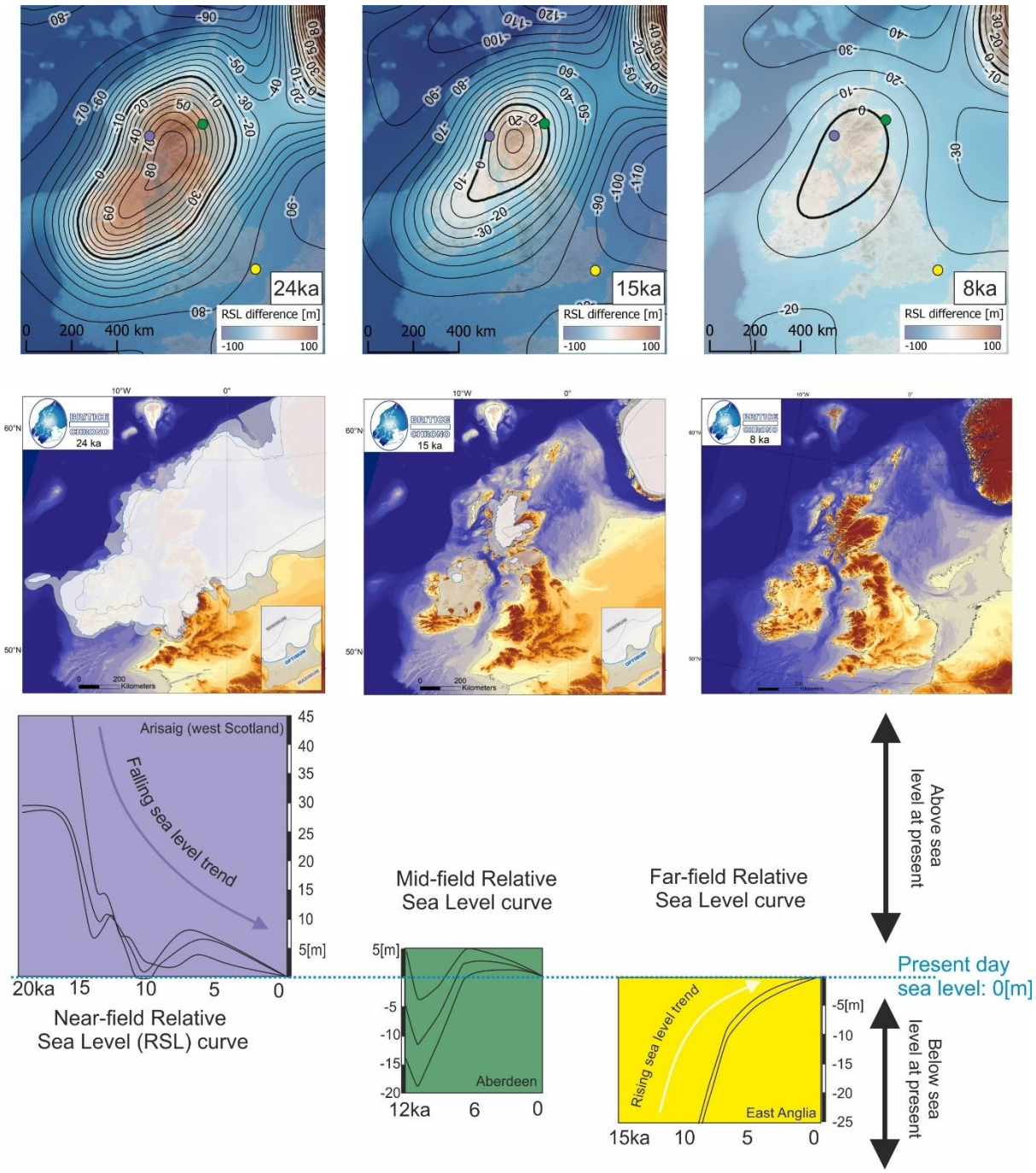


Figure 6.14. Top row: distribution of the relative sea level (RSL) difference between present day and respective time in the past due to the combined effect of ice loading and changes in the global ocean water volume due to sequestration within ice sheets and glaciers. Positive values indicate areas where sea level was higher than at present whereas negative values show areas of lower sea level. Bold contour indicates a 'hinge line' where sea level was the same as at present. Points on the map correspond to colour-coded RSL curves at the bottom. Middle row: Paleogeographic reconstruction by Clark et al., (2022) showing the differences in the coastline position and ice-sheet coverage for respective time steps.

Note for 24 ka that the land was still covered by thick ice sheets, and it was not submerged. Bottom: Relative sea-level (RSL) curves showing the difference of sea-level history depending on the region/distance in relation to the centre of the ice sheet. Purple curves are typical for regions close to the ice sheet where crustal rebound response dominates and RSL falls during and following deglaciation. Green curves show the mid-field response where the interplay of crustal response and changes of water volume in the global ocean interact dynamically resulting in a complex RSL curve. Yellow curves are typical for far-field where the effect of release of water from ice sheets dominates over the crustal rebound and the RSL rises.

Understanding the complex interplay between eustatic sea-level rise and GIA is important for the constraint of relative sea-level history, migration of coastlines and depositional environments, and associated geohazards and engineering constraints during ground modelling (Section 5.9), which in turn influence the design of offshore infrastructure. From a geohazard perspective, ongoing GIA is further relevant in terms of post-glacial faulting (Section 5.10). Glacio-isostatic uplift of former marine clays to elevations of >200 m asl (e.g., 220 m asl in SE Norway; NGU, 2025) resulted in pronounced marine limits in some fjord systems, below which quick clay (the formerly-deposited marine clay) can be located and acts as a serious geohazard for infrastructure projects and settlements (Figure 1.1; Section 5.7; NGU, 2025) Calculated remaining uplift due to the melting of the Weichselian ice sheet is modelled to ~40 m in Central Fennoscandia (Fjeldskaar and Amantov, 2018).

The load of large volumes of glacial sediments, in particular in trough mouth fans and thick progrades along the margins (Figure 6.4), resulted in local subsidence of neighboring regions, such as the North Sea Basin and the Northern North Sea (Sejrup et al., 2004). This subsidence, again, generates accommodation space for sediments on the shelves (e.g., North Sea; Lamb et al., 2018).

Sea-level changes are additionally important when it comes to archaeology and assessment of submerged paleolandscape evolution (e.g. Andresen et al., 2022; Figure 6.15). For the southern North Sea, the exposed continental shelf constituted an attractive habitat for hunter-gatherer populations before it was flooded during the late glacial and early Holocene (Bailey et al., 2020). Findings of well-preserved archaeological artefacts in the shallow waters (< 10 m) of the inner Danish waters and southern Baltic Sea, document early human occupation in these areas (Bailey et al., 2020). In the southern North Sea and generally at deeper water depths, the archaeological potential remains uncertain. Cultural heritage and screening for marine archaeology (including wrecks and UXOs) are however in any cases, critical and costly elements of pre-investigation surveys for offshore windfarms and other offshore developments in areas such as the southern North Sea.

Local GIA can vary considerably and in combination with global sea-level change can result in unique relative sea-level curves depending on location. For example, studies around the UK and Ireland show significantly different sea-level curves across a relatively short lateral distance (Shennan et al., 2018;

Figure 6.14). The growth in offshore development size, including wind farms and large interconnector projects, increasing amounts of pre-investigation data can mean that geo-evolutionary models and relative sea-level curves can be varied across the breadth of a site area: some projects can have relative sea-level curves that differ from one end of a route or site to the other. This needs to be appropriately captured to fully appreciate geo-engineering constraints across a development area. Together with the progression to deeper water settings, the current approach for archaeological screening requires revision to better capture the archaeological potential. Machine learning approaches and automated identification of geo-archaeological potential in prospect areas, need to be developed to ensure a fast and efficient construction phase.

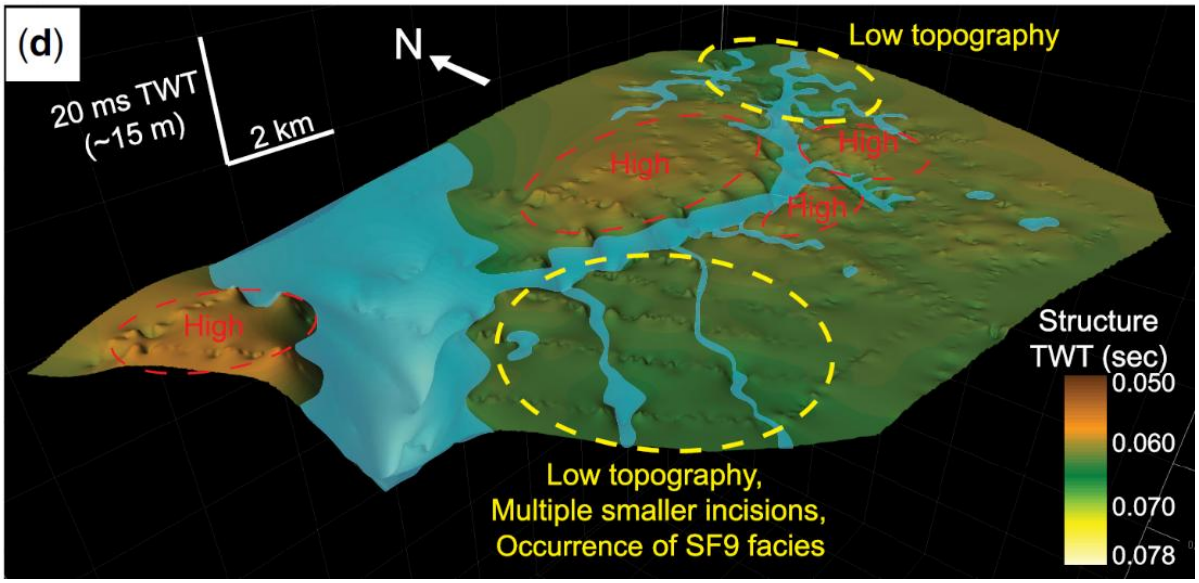


Figure 6.15. 3D perspective view of a mapped former late glacial to early Holocene terrestrial surface in the central North Sea, rivers and indications of topographical highs and lows added for visualization purposes. Mapping based on sub-bottom profiles and sediment cores. From Andresen et al. (2022).

6.5 Seismicity

The seismic hazard in northern Europe is relatively low on a global scale. Figure 6.16 shows the peak ground acceleration (PGA) on bedrock (Vs_{30} = 800 m/s) for a return period of 475 years estimated by the SHARP storage project (Carlton et al. 2024). The values along the coasts of the UK, Norway, Denmark and Germany are consistent with the corresponding values from the most recent onshore national studies (Mosca et al., 2024; Lindholm et al., 2025; Voss et al., 2015; Grünthal et al, 2018, respectively). The highest PGA values occur off the west coast of Norway in the Tampen Area (62°N, 4°E), between Norway and Denmark along the Tornquist Zone (57.5°N, 7.5°E), and at the Dover Straight (51°N, 1.5°E). This follows roughly the same pattern as the observed seismicity (Figure 6.17).

Figure 6.17 displays seismicity in Northwestern Europe, Scandinavia, and the surrounding seas since 1900. The most seismic activity in the region is along the spreading mid-Atlantic ridge (e.g. Engen et al., 2003), which is a divergent boundary formed by the separation of the North American Plate and the

Eurasian Plate. Earthquakes along the ridge are frequent, moderate in size (M<6), and mainly caused by the movement of the tectonic plates. The rest of the study area is a stable continental region characterised by lower seismicity. The three main hypotheses for the occurrence of earthquakes in this region are the release of stresses built up and propagated from the spreading of the mid-Atlantic ridge, stress adjustments caused by isostatic rebound related to deglaciation, and sediment loading/unloading (Fejerskov and Lindholm, 2000; Olesen et al., 2013). The completeness and accuracy of earthquake catalogues are continually advancing through improved instrumental coverage, better exploitation of historical data, and better location algorithms, with the current state of the art in regional seismic monitoring described by Ottemöller et al. (2021). The most recent update to the seismicity catalogue for the North Sea is provided by Kettlety et al. (2024) as part of the SHARP storage project.

The largest earthquake onshore Norway in historical times was the 31. August 1819 Lurøy event (Muir Wood, 1989; Mäntyniemi et al., 2020), estimated at M5.9, and the Nordland coastline is host to relatively frequent earthquake swarms with events up to M4.5 (e.g. Bungum et al., 1979; Gibbons et al., 2007; Bungum et al., 2010). The earthquake of October 23, 1904, that caused significant damage in the city of Oslo, was attributed to a magnitude of 5.4 and located in the eastern Oslofjord by Bungum et al. (2009). There is evidence for paleoearthquakes of magnitude over 7 in Scandinavia (e.g. Arvidsson, 1996; Olesen et al., 2021), and Olesen et al. (2013) believe there is a possibility of magnitude 6+ earthquakes along the coastal parts of western Norway, Nordland and the Oslo rift zone.

Although the largest earthquakes are located along the mid-Atlantic ridge, there are notable exceptions such as the 1931 Mw 5.9 Dogger Bank earthquake off the east coast of England. More recent North Sea earthquakes, such as the 30 June 2017 (Mw 4.5, Jerkins et al., 2020) and 21 March 2022 (Mw 5.1, Jerkins et al., 2023) events, have been located and characterized with unprecedented accuracy with both global and regional seismic networks and using offshore permanent reservoir monitoring networks.

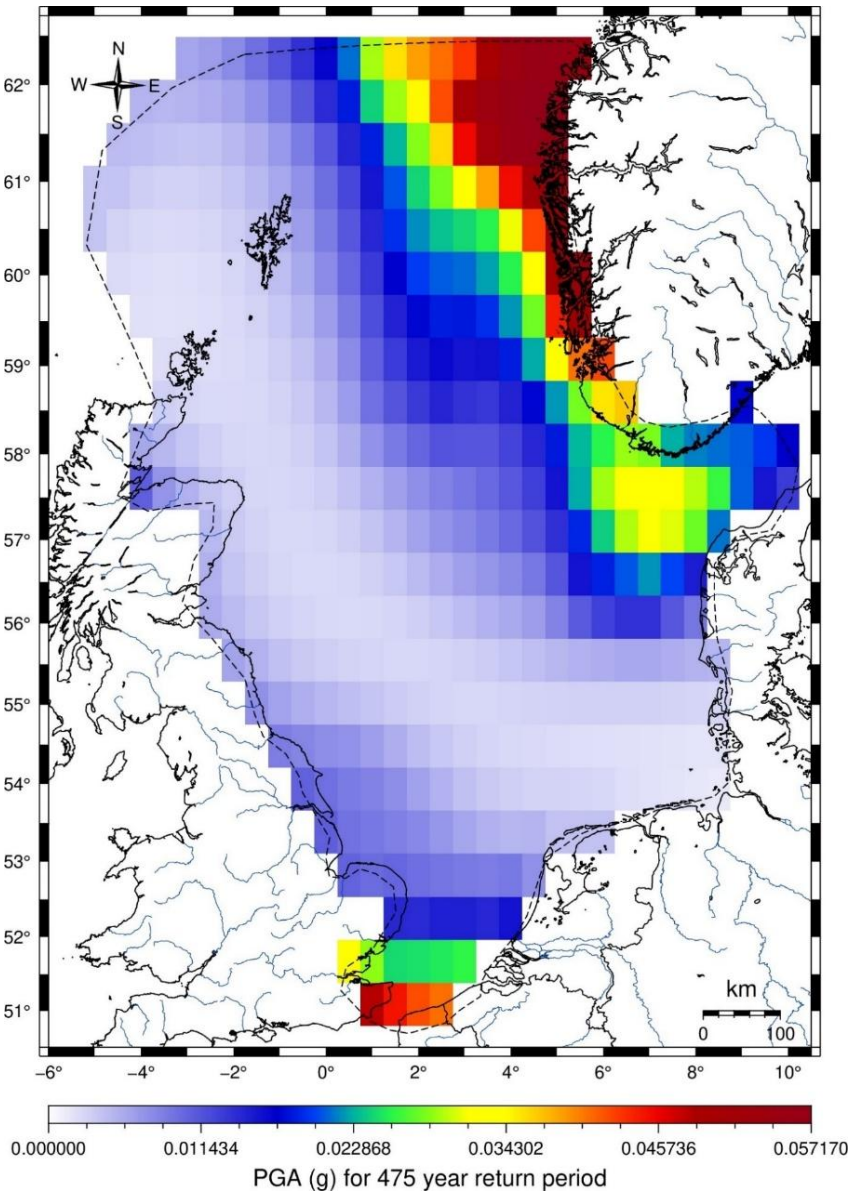
Despite the relatively low seismic hazard, earthquakes can still pose a threat to offshore industries. Earthquake shaking in the horizontal direction is strongest between frequencies of 1-20 Hz. Offshore wind turbines (OWT) have low natural frequencies (0.25-0.5Hz), which means that they are generally not vulnerable to horizontal earthquake shaking in low-to-moderately seismic areas (Hovind et al. 2014). However, OWTs are vulnerable to earthquake shaking in the vertical direction due to their low damping and similar natural frequencies in the vertical direction as earthquakes (Kjørlaug and Kaynia, 2015). In addition, OWTs have strict performance requirements (e.g. less than one-degree allowable tilt), which means that even small deformations caused by earthquake shaking or liquefaction are not desired. Therefore, the seismic design of offshore wind turbines in low to moderately seismic areas is governed by performance-based considerations (Kaynia, 2019).

CCS facilities are generally located shallower than most earthquakes. However, even small magnitude earthquakes, if they occur in the cap rock, could cause enough fault deformation to threaten the seal

integrity (Zoback and Gorelick, 2012). This, along with the necessity to identify structural traps suitable for large-scale CO_2 storage in the North Sea (e.g. Osmond et al., 2022), has reinforced the need for robust monitoring of low-magnitude offshore seismicity (e.g. Zarifi et al., 2022). It is also important to remember that CCS and Oil and Gas activities may result in induced seismicity. For example, on May 7, 2001, there was an Mw 4.3 vertical dip-slip seismic event in the Ekofisk field, resulting from an unintentional fluid injection (Selby et al., 2005; Ottemöller et al., 2005; Cesca et al., 2011; Dahm et al., 2015).

The geological record is often used for the identification of paleoseismic events (e.g., Goldfinger, 2011; Kremer et al., 2017; Ojala et al., 2019), which commonly lacks historic documentation (Figure 6.18a). In passive continental margins such as our study area, this evidence is off-fault and considered as indirect evidence. Bellwald et al. (2019a) suggest based on marine sediments that over the last 11,000 years, 33 earthquakes have simultaneously triggered submarine slides in different Norwegian fjords (Figure 6.18b), with a seismic activity highest during deglaciation, at around 8 ka, and in the past 4 ka (Figure 6.18c). The observations from the Norwegian sediment records match with the Swedish and Finish paleoseismic records (Figure 6.18c and 6.18d; Mörner, 2013; Bellwald et al., 2019a; Ojala et al., 2019). A higher seismic activity in the Late Holocene at around 4 ka is further supported by modelling of the reactivation potential of faults due to ice unloading in Northern Germany (Brandes et al., 2015), an area also affected by the Fennoscandian Ice Sheet. Sørensen et al. (2023) identified 22 landslides caused by eight earthquakes with M4.5-5.9 over the past 200 years in Norway, demonstrating that even in moderately seismic areas, earthquake induced landslides can occur with regularity. Along the glaciated European margins, several submarine mega-paleoslides have been identified (Table 6.1 and Figure 6.4). The most likely final trigger mechanism for these slides are earthquakes (Bellwald et al., 2019b; Eldholm and Bungum, 2021). For the Tampen Slide on the North Sea Fan, an earthquake of approximately Mw 6.9 or larger at a short distance from the headwall has been modelled to be the most likely triggering mechanism (Bellwald et al., 2019b).

The main geohazards related to earthquakes include primary effects such as shaking, fault displacement, and liquefaction, and secondary effects such as slope instabilities (Section 6.2), tsunami initiation (Section 6.6), and fluid release (Section 5.3) (Eldholm and Bungum, 2021), all of which can affect both society and infrastructure (e.g., Piper et al., 1988). Increased seismicity during deglaciation may have aided the escape of hydrocarbons from their source rocks through gas chimneys to produce pockmarks on the seafloor on the continental margins off Norway, the Barents Sea and Svalbard (Muir Wood and King, 1993; Olesen et al. 2004; Olesen et al., 2013, Eldholm and Bungum; 2021).



3614

3615 **Figure 6.16.** Peak ground acceleration (PGA) for Vs_{30} = 800 m/s (soft rock) for a return period of 475
3616 years from the SHARP project (Carlton et al. 2024).

3617

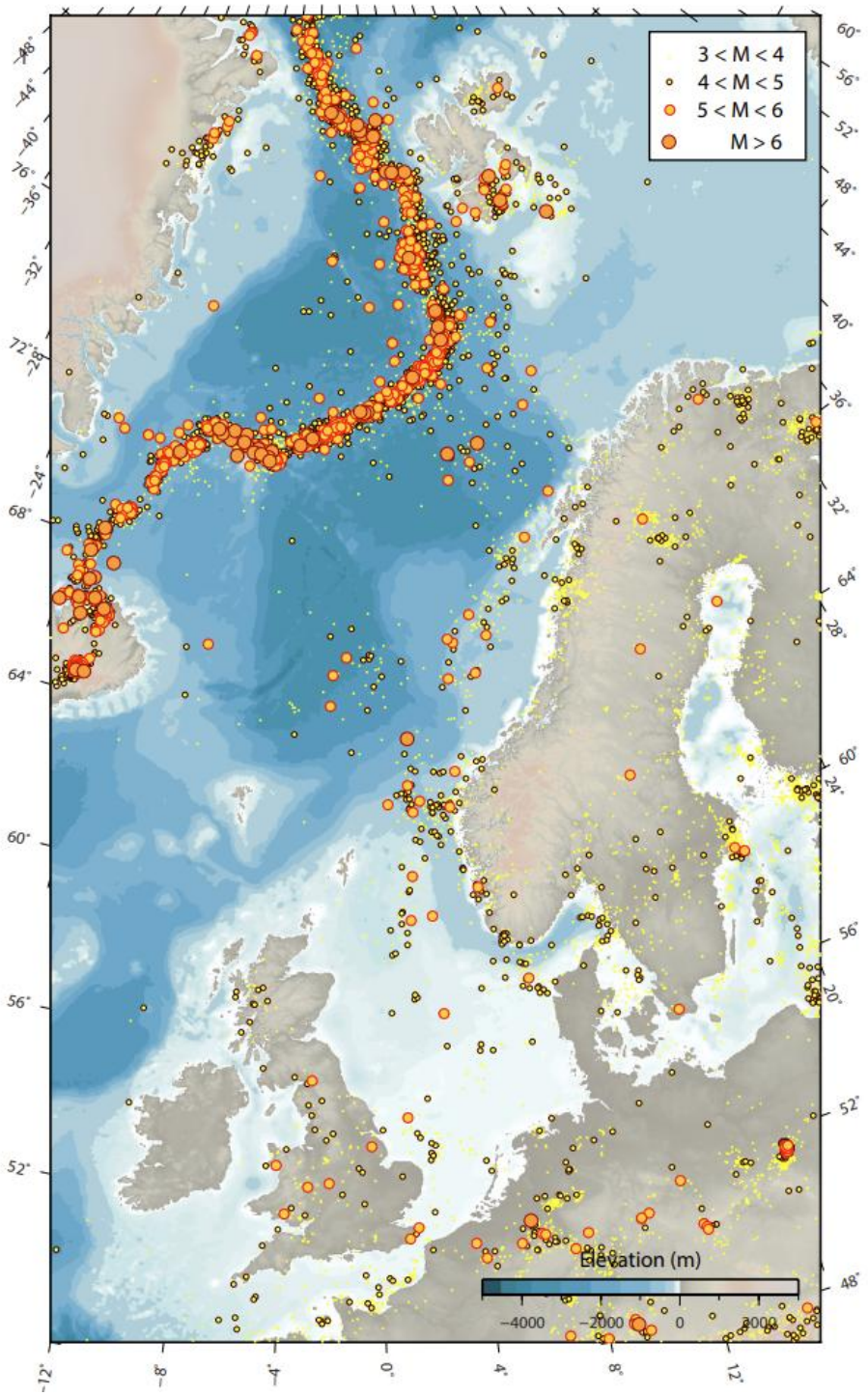


Figure 6.17. Seismicity in Northwestern Europe, Scandinavia, and the surrounding seas from 1900 to 2022 as provided by the bulletin of the International Seismological Center (ISC, 2022). Events below magnitude 3 are not displayed. Event clusters in Germany, the Netherlands, Poland, the Baltic Sea, northern Sweden, and the Kola Peninsula are associated with mining and military operations and are seldom natural earthquakes. The completeness of the underlying earthquake catalogue improves dramatically in the most recent 30 years with the deployment and development of today's digital

broadband seismic network (reference: ISC, 2022. International Seismological Center Online Bulletin [WWW Document]. https://doi.org/10.31905/D808B830)

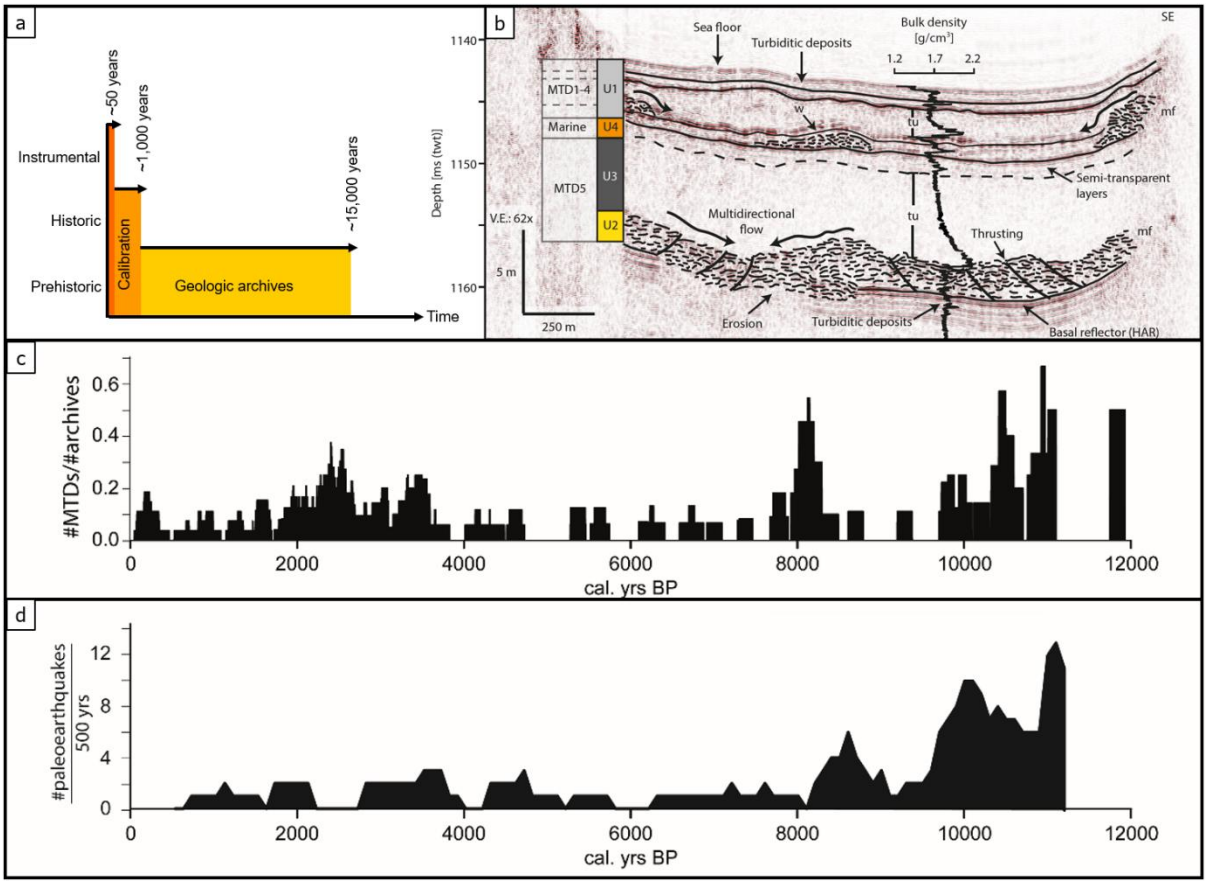


Figure 6.18. Paleoseismic events in Fennoscandia. **a)** Geological archives as a tool for paleoseismic events. **b)** Multiple, coevally-triggered mass movements as proxy for paleoseismic event. Interpreted TOPAS seismic profile of the uppermost part of the infill of Hardangerfjorden. MTD5 indicates basin-wide, bi-directional mass flow (black arrows) and thrusting (black lines) of mass flow deposits, whereas multiple local wedges have been identified for MTD4, one wedge for MTD3, and no wedges for MTD1 and MTD2 in this profile. Bulk density values shown are from the analyzed Calypso core. V.E.: Vertical exaggeration. Figure from Bellwald et al. (2016). **c)** Submarine mass movement activity in Norwegian fjords and lakes in the last 11,000 years (Bellwald et al., 2019a). **d)** Swedish paleoearthquake catalogue, with number of earthquakes within 500 years (from Mörner, 2013, and references therein).

6.6 Tsunamis

6.6.1 Introduction

Globally, earthquakes are the most frequent source of tsunamis. However, for the glaciated and currently passive European margin, gravity mass flows are the only significant source of tsunamis. For an extensive review of submarine landslide tsunamis, see Løvholt et al. (2022).

Gravity mass-flow (GMF) tsunami sources in the glaciated European margin encompass submarine landslides (high-density flows like slides, slumps, debris flows, mud flows, and granular flows), and slides originating from onshore (or along the shoreline), including clay and quick-clay slides, debris flows, mud flows, rockslides, snow avalanches, and glacier calving. Depending on the material properties and speed of these mass flows, most of them (except rock, snow, and ice) can evolve into low-density turbidity currents of grains in turbulent suspension in the water (see Chapter 6.3.2).

The Euro-Mediterranean tsunami catalogue (EMTC, https://doi.org/10.13127/tsunami/emtc.2.0; Maramai et al., 2019) presently comprises 64 tsunami events in the Nordic Seas (Figure 6.19) spanning from an ancient 9000 BP Boknafjorden event inferred from archaeological interpretations (Bøe et al., 2007), via the well-documented 8150 BP Storegga slide and tsunami (Figure 6.20; Bryn et al., 2005a; Bondevik et al., 2005a; Kim et al., 2019), to recent rockslide (Harbitz et al., 2014; Løvholt et al., 2020) and coastal (often quick-clay) landslide (L'Heureux et al. 2011, 2013b, 2014, 2017; Liu et al., 2021) tsunami events in the Norwegian fjords (events in lakes excluded). Out of these 64 events, we note that there are three small to moderately sized tsunami events caused by earthquakes in the region, four seiches events triggered by distant earthquakes, while the remaining 57 are caused by various kinds of mass flows. However, some tsunamigenic landslides may have been triggered by earthquakes, in particular during intensive periods of isostatic uplift following the final deglaciation. In this period, rockslide activity was also especially high (Blikra et al., 2006; NGU, 2009, Bellwald et al., 2016; Hermanns et al., 2017), likely due to stronger isostatic uplift, more earthquakes, steeper reliefs, and permafrost melting (Bøe et al., 2004; Vorren et al., 2008; Bellwald et al., 2019a). The number of fatalities from fjord tsunamis is typically limited by the relatively local impact and sparsely populated settlements along the exposed coastlines; the event in historical times with the greatest number of fatalities (40) is the 1934 Tafjord rockslide tsunami (the 1905 and 1936 Lake Loen events with 61 and 73 fatalities, respectively, are here excluded; Harbitz et al., 2014).

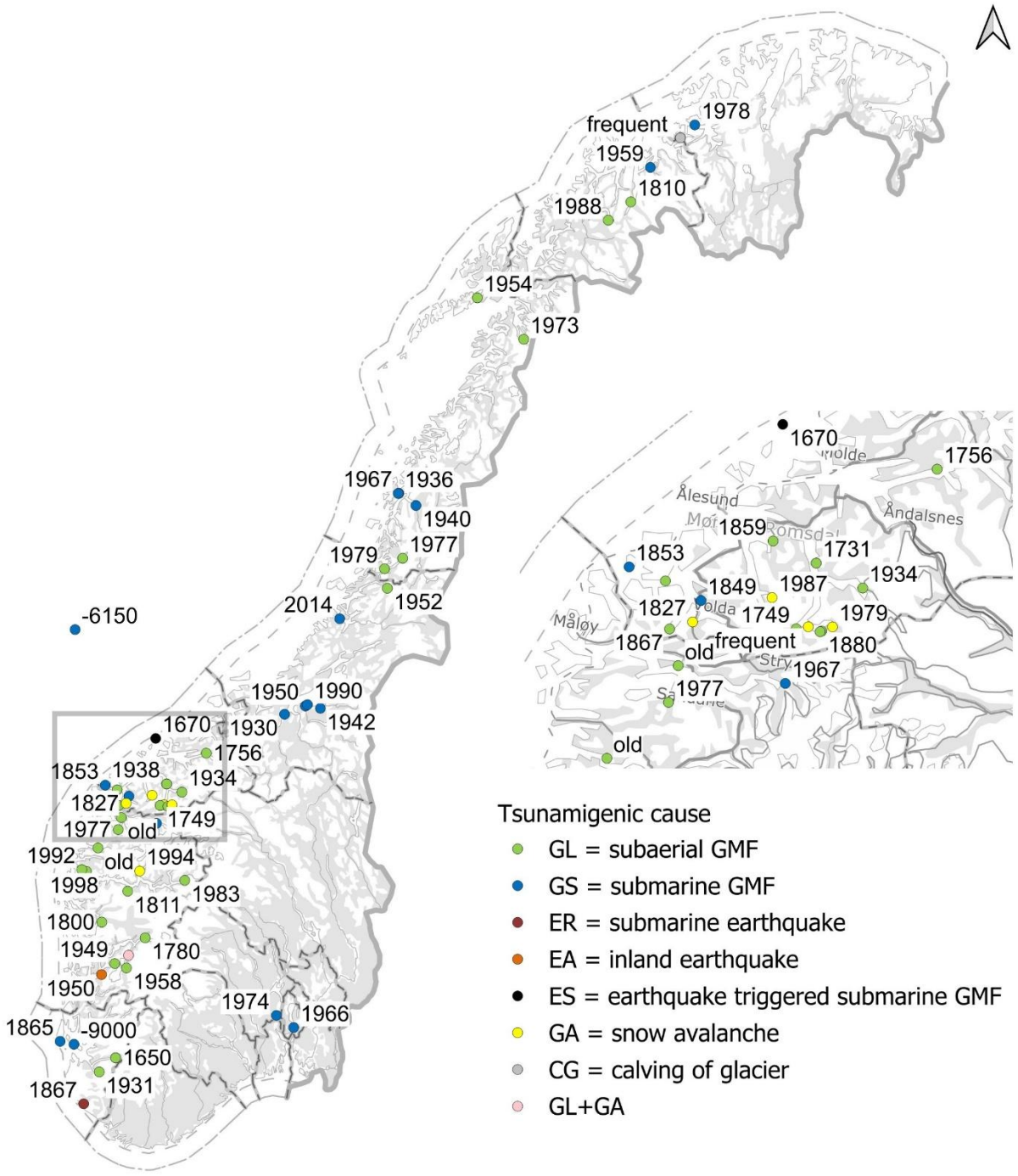


Figure 6.19. Registered tsunami events in the Nordic Seas (with year of event). GMF = Gravity Mass Flow. Seiche events triggered by distant earthquakes as well as all tsunami events in lakes are here excluded.

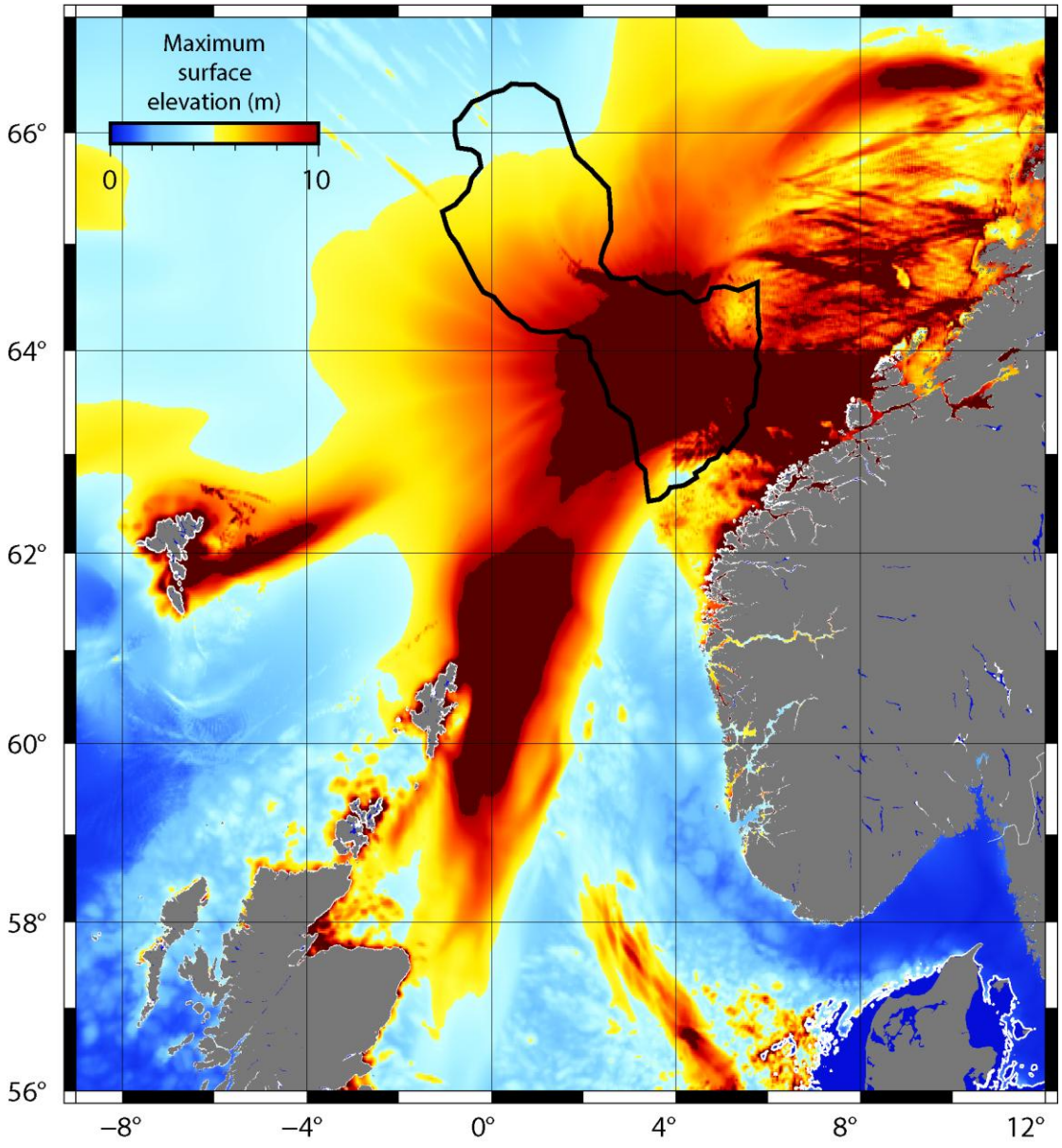


Figure 6.20. "Wave directivity plot" showing maximum surface elevation in meters obtained during a numerical simulation of the 8150 BP Storegga landslide and tsunami (using paleo-bathymetry). Surface elevations greater than 10 m are shown in dark red. The thick black line indicates the outline of the landslide runout area. Present-day land is shaded in grey, and the coastline of the paleo-bathymetry is marked with a thin white line. Parameters for the numerical simulation are found in Bondevik et al. (2024) and a new simulation of 20 hours following the slide was performed using the 8000 BP bathymetric model of Clark et al. (2022).

6.6.2 Basic mechanisms in tsunami generation

Different types of GMFs have different tsunamigenic properties. The tsunamigenesis is primarily controlled by the volume (length, height, width; for subaerial mass flows rather the frontal area) and the dynamics of the mass flow (velocity u, acceleration a), as well as the water depth. The factors controlling the landslide dynamics are primarily the slope angle, the volume and the rheological

properties of the landslide material (which in turn depend on the geological setting), as well as the external forces from the ambient water acting on the landslide. Submarine landslides with high clay content are more mobile than their subaerial counterparts and can reach high velocities (and long run-out distances) even on very gentle slopes. The mass flows go through various flow regimes from solid to fluid when evolving from failure to disintegration, remolding, erosion, and entrainment forming higher-density debris flows or lower-density suspension flows. The largest landslide volumes show the greatest mobility (De Blasio et al. 2006), while out-runner blocks being detached from the front of the slide due to hydroplaning can reach even longer run-out distances than the main body (Harbitz et al. 2003; see also Section 6.3)

Because of the strong influence of the complex topo-bathymetry on the dynamics, numerical models are needed to model the tsunami generation with sufficient accuracy (see e.g. Løvholt et al., 2015; Yavari-Ramshe and Ataie-Ashtiani, 2016; Behrens et al., 2021). Yet, simplified expressions relating either landslide geometry, friction, or ambient fluid resistance (e.g. Watts et al., 2005) or landslide kinematics (e.g. Zengaffinen et al., 2020) can offer hints regarding the parameter values governing tsunamigenesis.

Submarine landslides are most often clearly sub-critical, implying that the Froude number (the ratio of the landslide velocity u to the linear shallow water wave celerity c), is much less than one. This implies that the tsunami will race away from the wave-generating landslide, limiting the build-up of the wave. Under such conditions, the maximum surface elevation increases with the landslide volume and acceleration but is inversely proportional to the wave speed (Løvholt et al. 2005; Figure 6.21). This scaling behaviour was explained through analytical models in simplified geometries by Haugen et al. (2005) but is also supported by earlier pioneering studies of Honda and Nakamura (1951) and Hammack (1973). This simplified analysis was performed assuming a very gentle slope and a non-deformable slide with a prescribed motion. With these assumptions it can be demonstrated that for debris flows, the related acceleration and deceleration phases may produce two sets of spatially and temporally shifted tsunami dipoles, each consisting of a positive and a negative surface elevation, that together form a quadrupole. For slumps, the surface elevation can be shown also to scale with the rotational dynamics (angular momentum; Zengaffinen et al., 2020). Slump acceleration processes may further happen so quickly that only one dipole is generated (see Løvholt et al., 2015). The tendency of submarine landslides to produce such an initial quadrupole-like tsunami shape, implies that landslide tsunamis are attenuated (radially) more efficiently compared with tsunamis from an earthquake dipole source that is distributed over a longer distance azimuthally along the fault. In addition, landslide tsunamis often produce shorter waves more subject to frequency dispersion, which may further reduce the potential for efficient far-field propagation (Glimsdal et al., 2013; Løvholt et al., 2015). However, landslides can generate larger vertical displacements than earthquakes and thus generate higher waves locally (e.g.,

Okal and Synolakis, 2004). The commonly shorter waves are also more prone to amplification due to shoaling (and possible wave breaking).

For sensitive clay materials, the landslide can evolve like a series of blocks failing retrogressively Kvalstad et al, 2005). A retrogressive failure normally reduces associated tsunami heights, but block-wise retrogression might increase the height of the landward propagating wave for unfavourable time lags between release of individual elements of the total landslide mass (e.g., Haugen et al., 2005; Løvholt et al., 2016). Yet, Løvholt et al. (2017) showed that for large landslides a more rapid mass mobilisation of a larger part of the slide body may follow even with a retrogressive failure initiating the landslide, this may likely have been the case for the 8150 BP Storegga Slide. On the other hand, if the retrogressive process is retained across the entire slide, or if there are major delays between the release of individual slide blocks, the process is likely less tsunamigenic, which may have been the case for the ~4000 BP Trænadjupet Slide.

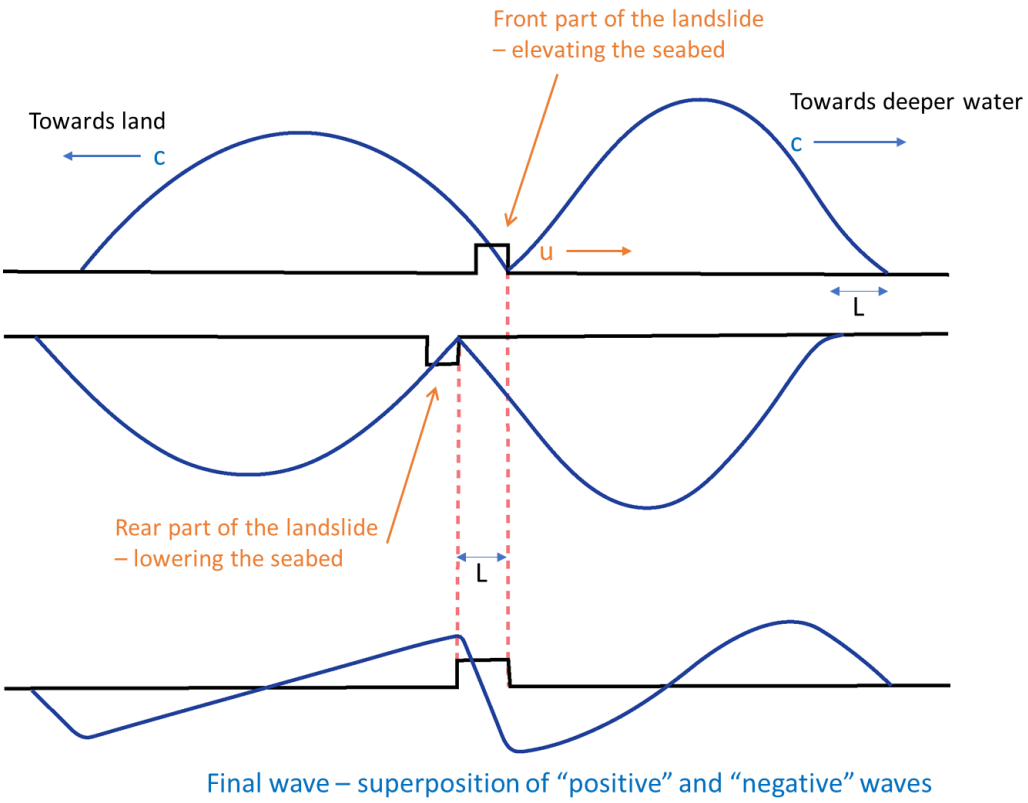


Figure 6.21. Illustration of how a landslide with length *L* and velocity u builds up a positive wave (with celerity *c*) above its front where water is elevated (upper part of figure) until the build-up is cut off by the negative wave formed above its rear end, where water is lowered and trailing a distance *L* behind (mid part of figure). The two wave components combine to a dipole with a landward depression and a seaward elevation (lower part of figure).

Subaerial mass flows impacting the water body always give rise to super-critical wave generation in the beginning, and they often produce an impact crater and ejection of the water body. Hence, the preceding

tsunami propagation is therefore strongly affected by nonlinear effects in the initial stages. The generation, as studied in a high number of experimental analyses (see e.g. the analysis by Rauter et al., (2021), or the review by Heller and Ruffini (2023)), is determined mainly by the frontal area, the impact velocity when plunging into the water body, and the water depth. As demonstrated by these studies, there is also a clear heterogeneity in the analytical expressions obtained from the experimental analysis. Hence, despite the large resources put into studies of gravity mass flow tsunamis in the laboratory, they have failed to produce predictive equations that are generally applicable. There has not been a similar number of numerical studies. This is partly due to the computational complexity needed to resolve the three-dimensional nature of the phenomenon, and partly due to the complex mechanics of rockslides. Yet, recent studies (e.g., Si et al., 2018; Macias et al., 2021; Esposti Ongaro et al., 2021; Rauter et al., 2022) show promise that improved predictive skills can be brought into numerical modelling of rockslide tsunamis, validated by both full-scale field observations and laboratory-scale studies. To this end, we note that also a set of benchmark studies for both submarine and subaerial landslides have been developed to improve model validation (Kirby et al., 2022).

6.6.3 Tsunami deposits

When tsunamis flood the land, they may deposit sediments that over time may be well preserved, and along the coastlines of the North Atlantic these sediments are found along the coasts of Norway, Greenland, the Faroe Islands, and northern Britain (Figure 6.22; Bondevik and Svendsen, 1993; Bondevik et al., 1997a; Dawson et al., 1988; Dawson et al., 1993; Smith et al., 2004; Wagner et al., 2007; Bondevik, 2019). Failure of the most recent large-volume submarine landslides, the Storegga and Trænadjupet slides offshore Norway, would be expected to generate significant tsunamis, but the deposits identified so far have only been generated by the Storegga Slide, at 8150 BP, except for some, on the Shetland Islands, which are much younger, as they have been dated at 5,500 and 1,500 BP (Bondevik et al., 2005b). The origin of the younger deposits is unknown.

The most prominent event deposits in the study area are the tsunami deposits triggered by the Storegga Slide (Figure 6.22): These deposits indicate that the runup height, of the tsunami varies between 10-11 m along the Norwegian coast, 5 metres in eastern Scotland, to more than 20 m on the Shetland islands and in northern Britain (Figure 6.22a; Bondevik et al., 1998; 2019). The absence of sedimentary traces from the Trænadjupet Slide is supported by numerical modelling of the megaslide and its resulting (small) tsunami (Løvholt et al., 2017).

Tsunamis are a large geohazard in modern fjord systems (Harbitz et al., 2014), but evidence on paleo-tsunamis is rather sparse, much due to a low preservation potential due to subsequent erosive processes and topography. In Boknafjorden, SW Norway, flint artefacts that are embedded in beach sediments are interpreted to be derived from near-shoreline sediments that were flooded and eroded by a slide-generated tsunami at approximately 10-9.7 ^{14}C yr BP (Bøe et al., 2007).

In 1580, an earthquake in the Dover Strait is proposed as triggering a cliff fall in the Chalk on the southeast coast of England that triggered a tsunami that struck the coast of France with considerable destruction to Calais and Boulogne (Neilson et al., 1984).

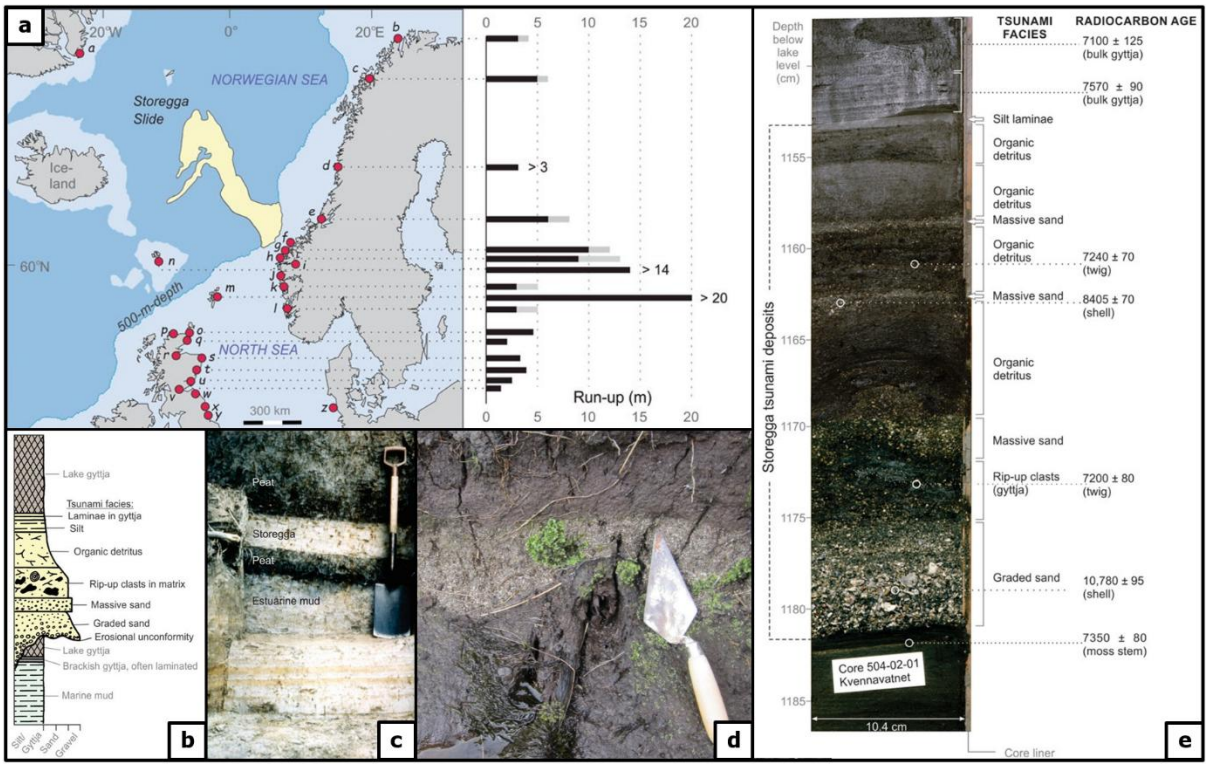


Figure 6.22. Tsunami deposits of the Storegga Slide. **a)** Map of the Storegga Slide and tsunami deposits. Red dots show locations of Storegga tsunami deposits; Run-up estimates, inferred from deposits, are given to the right; black columns show minimum estimates, and gray columns give maximum estimates (from Bondevik, 2019). **b)** Description of the Storegga tsunami deposits (in yellow) presented as an idealized, complete facies sequence of tsunami deposits in nearshore lakes (from Bondevik, 2019). **c)** Outcrop at Maryton in the Montrose Basin, Eastern Scotland, shows the Storegga tsunami as a 25 cm thick silty sand deposit between peats. The estuarine mud is laminated silt and clay (Photo D. Smith, shown in Bondevik, 2019). **d)** Storegga tsunami sand, at Sullom Voe, Shetland. Note the underlying birch branch (trowel blade 12 cm long; Photo D.R. Tappin). **e)** Tsunami deposits in Kvennavatnet, Bjugn, Western Norway. Depth is cm below lake level. To the right is the description of deposits and radiocarbon ages (in ^{14}C years BP). From Bondevik (2019).

More broadly, tsunami deposits vary from laminated, graded to massive, depending on their sediment composition and depositional mechanism (Figure 6.22b). The tsunami sediments in Norway are preserved in coastal lakes located in uplifted basins, and deposited within marine or lacustrine gyttja (peat) overlying an erosional unconformity surface (Figure 6.22e; Bondevik et al., 1998; Bondevik et al., 1997b; Vasskog et al., 2013). In Scotland within subaerial peat layers, on which their dating is based, and which allows their provenance to be ascertained by correlation with the source landslide (Figure

6.22c). The lowermost sands are graded or massive and locally contain marine fossils. The sands thin and decrease in grain size in a landward direction. Overlying the sands is coarse organic detritus with rip-up clasts and finer organic detritus. The sands generally fine and thin upwards. In the higher basins (6-11 m above the 7000-year shoreline) there is one sand bed, whereas basins closer to the sea level 7000 years ago, may show several sand beds separated by organic detritus. In basins that were some few metres below sea level at 7000 years BP, the tsunami deposit is more minerogenic and commonly present as graded sand beds. In some of these shallow marine basins, however, organic-rich facies occur between the sand beds. The total thickness of the tsunami deposit is 20-100 cm in most studied sites. Dating of organic matter in the tsunami deposits allowed their origin from the Storegga submarine landslide to be established (Figure 6.22e; Harbitz, 1992; Bondevik et al., 1998; Bondevik et al., 2005a).

In Britain, the Storegga deposits extend from northeast England to the Shetland islands (Figure 6.22a). On Shetland, where they are best preserved, they are as follows (Smith et al., 2004). At the base, there is a sand and gravel surface, overlain to seaward by a grey silty clay which thins out landward and forms a gently sloping surface. Above the silty clay is a widespread layer of grey micaceous sand, up to 0.75 m thick, containing fragments of vegetation (roots, stems and twigs) (Figure 6.22d).

The Storegga tsunami deposits may contain fragments or intraclasts of organic material and intraclasts of silt (Figure 6.22b; 6.22e); there are rip-up clasts of peat. Above the sand, peat with horizons of organic silt and sand extends to the surface. The sand shows high values for corroded pollen and spores and the top, Chenopodiaceae. Plantago maritima in the sand layer, support a marine origin. No diatoms could be found in the fine sand, but the silty clay contains a few broken and eroded pennate forms, mainly Pinnularia viridis. The presence of Pinnularia fragments in the bottom silty clay is thought to indicate reworking of underlying freshwater (possibly peaty) sediments (Dawson et al., 1996). In eastern Scotland the tsunami deposits comprise a thin (centimetres) fine or fine-medium sand, sometimes with some silt and clay and very occasionally containing gravel or stones in the basal layers preserved within estuarine sediments or subaerial peats (Figure 6.22c; Smith et al., 2004). The high proportion of tychopelagic diatoms (i.e., those found living on bottom marine sediments), notably Paralia sulcata (Ehrenberg) Cleve, and some evidence of erosion of underlying sediments, originally led Smith et al. (1985) to interpret the sediments as deposits from a storm surge, but their continuous extent and height (15 metres) above sea level led to their reinterpretation as a tsunami deposit (Dawson et al., 1988).

The evidence for the two younger tsunamis dated at 5,500 and 1,500 BP is from Shetland (Bondevik et al., 2005b). The sediment deposit of the 5,500 BP deposit is similar to that of the Storegga tsunami—rip-up clasts, sand layers, re-deposited material and marine diatoms. Runup was probably more than 10 m. The 1,500 BP deposit is preserved in peat at two sites 40 km apart. The sand layer thins and fines inland and traced to ca 5–6 m above present high tide.

Evidence on the Dover Strait 1580 tsunami, triggered by a cliff fall, is limited. Effects on water were noticeable, especially since all accounts agree that at the time of the earthquake the weather was fine and calm. The agitation of the Thames is reported by Churchyard (1580) and others. In the English Channel, it was worse. At Sandwich, "the sea so foamed, that the ships tottered" (Stow, 1601). One contemporary account suggests that marine effects were more severe on the other side of the Channel. "In Calais ...there was such a horrible and fearful trembling that a great part of the houses collapsed and even the sea flooded into the town . . . In Boulogne there was a similar earthquake and flooding by the sea" (Coquerel, 1580). This may be a seismic sea-wave, but unfortunately there is some doubt about the time, and therefore about the actual relationship between earthquake and marine incursion. Elsewhere in the same document we find it stated that on the 7th of April between 4 and 5 a.m. (which coincidentally is the time of the third Kent aftershock) "there occurred in these places great signs of floods".

6.6.4 Tsunamis as a geohazard on the glaciated European margins

Both near-field and far-field potential tsunamigenic sources have been assessed for a first screening of regional tsunami hazard for the Northeast Atlantic (Harbitz et al., 2009). Trough mouth fans are locations with reoccurring megaslides (Nygård et al., 2005; Hjelstuen et al., 2007), and deserve specific attention (see Figure 6.3). Rapid sediment deposition on the North Sea Fan (location of the Storegga, Tampen, Møre, and Stad Slides) potentially builds up quite high pore pressures. However, preliminary studies of slope stability and the potential to develop new landslides concluded that the pore pressures in the North Sea Fan have been dissipating since the ice age (Bellwald et al., 2019b).

Based on the present soil conditions and slope stability analysis, it is found that most of the unstable volumes are already released, and the stability of the offshore slopes is generally good. Hence, the present potential for large-scale tsunamigenic landslides in the Storegga/Ormen Lange area is also small (Kvalstad et al., 2005b; Nadim et al., 2005; Harbitz et al., 2009). It should be noted that global warming affecting the environmental impact might also influence slope stability (see Section 6.2.4).

In conclusion, potential rockslides in the fjords of Norway and Greenland are considered the only high-risk tsunamigenic sources in the NE Atlantic (Harbitz et al., 2014). Figure 6.23 shows an example of a tsunami hazard analysis (based on long-wave equations) for the potential 54 Mm^3 Åkerneset rockslide, western Norway. Future climate changes with global warming (implying more freezing–thawing situations and a potential role of permafrost melting) combined with more frequent and extreme situations of intense precipitation (leading to increased pore pressures) may increase the rockslide tsunami potential along the glaciated European margins (Hilger, 2019; Magnin et al. 2019). For Norway, the Norwegian Planning and Building Act has been altered to open for further development in exposed areas under given conditions. Probabilistic analyses of rockslide tsunamis are applied in hazard zoning and areal planning (Løvholt et al., 2020). Glacial debuttressing is the probable cause of a 25 Mm^3 rock-ice avalanche in a Greenland fjord in September 2023 that resulted in a tsunami with 200 m run-up (Svennevig et al., 2024).

It should be noted that important segments of the continental margins surrounding the northern North Atlantic and Arctic Ocean are still not mapped in sufficient detail. Moreover, both submarine landslides and rockslides may cause potentially extreme tsunami run-up heights and dominate the (local) risk, which may be important for location and design of critical infrastructure often based on very long return periods (generally carrying the largest uncertainties).

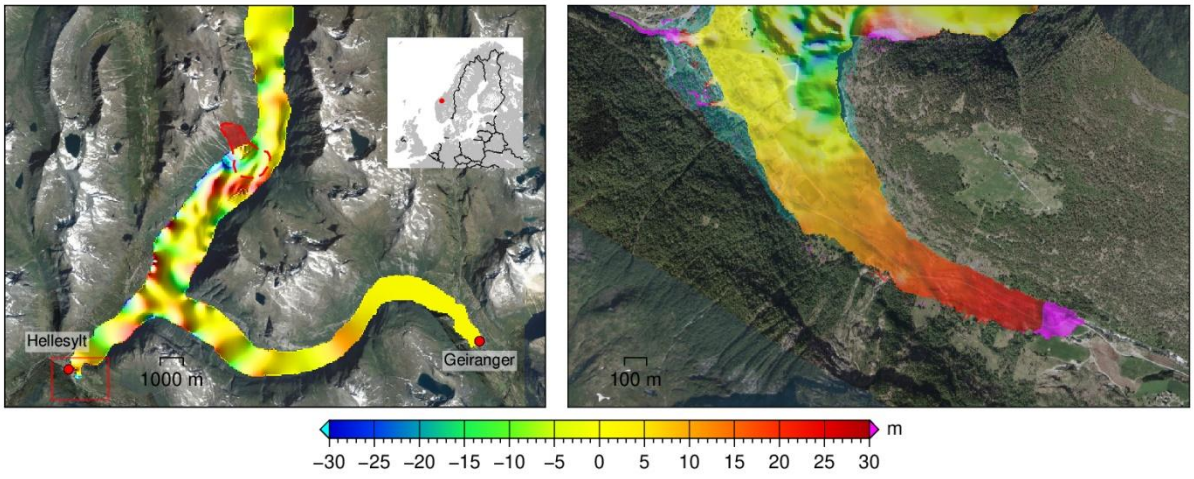


Figure 6.23. Example of tsunami hazard analysis; numerical tsunami simulation snapshots 400 s after a potential 54 Mm^3 rockslide impacting the fjord at Åkerneset (area marked red), western Norway. Left panel: Tsunami propagation in Sunnylvsfjorden (linear dispersive equations). Right: High-resolution simulation of tsunami inundation at Hellesylt (nonlinear shallow-water equations). Figure based on simulations for the Åknes/Tafjord Beredskap IKS project.

7. Implications

Growth of near-shore population and increased scale of activities offshore due to energy transition and growth of blue economies, combined with the effects of climate change and geopolitical instabilities, mean that marine, especially continental shelf, areas are becoming more and more important. In the following chapter, we discuss the potential implications of geohazards and geo-engineering constraints on society and environment, offshore energy industries, and scientific drilling. We further summarize how the challenges vary in a regional context.

7.1 Society and environment

Marine geohazards and constraints related to marine geo-engineering can have a distinct societal impact:

i) **Tsunami hazard**: Improved and advanced assessments – and particularly early warning systems – can save lives in urban centres along the coasts.

ii) **Sites with cultural heritage**: The early identification of cultural heritage sites reduces the costs of the offshore infrastructure development.

iii) **Environmental impact**: The environmental impact of anthropogenic actions can be reduced by detailed assessments. Keywords are shallow gas seepage, sediment remobilization, the presence of (cold-water) corals and benthic communities, but also anthropogenic features such as UXO (unexploded ordnance: mines, bombs, ammunition dumps).

iv) **Geoscience mindset**: Specific skills are required for acquisition and interpretation of required datasets, in particular for the renewable energy transition. Working in a multi-disciplinary team, often consisting of geologists, geophysicists, geotechnical engineers, laboratory analysts, and numerical modellers (and as of late data scientists), is another requirement.

7.2 Offshore energy industry

The different sectors of the offshore energy industry have different needs (Table 7.1), and the ongoing energy transition may require a different focus on geohazard assessment and their importance (e.g., Velenturf et al., 2021): The offshore wind industry typically targets much larger geographical areas and will require more densely spaced infrastructure compared to the infrastructure required by the hydrocarbon industry. Thus, certain hazards and particularly engineering constraints might be more frequent and not avoidable in offshore wind compared to the smaller acreage required for seafloor infrastructure in the hydrocarbon industry. However, the wells and deviated wells planned in the hydrocarbon industry require some planning and dedicated efforts too, covering several kilometers in depth.

The different types of offshore energy technologies are affected by ecological, societal, and economic factors: Although costs of offshore wind and other renewable technologies have rapidly decreased in the last years (e.g., Taylor et al., 2020), these energy sources have currently very low profit margins compared with oil and gas, and incorporate challenging financial conditions (Table 7.1; Virtanen et al., 2022). Despite the lower profitability, renewable energies have often a high societal acceptability (Karakosta et al., 2013; Ahsan and Pedersen 2018).

Table 7.1. Comparison of different offshore-energy branches. HC: Hydrocarbon (oil and gas), CCS: Carbon capture and storage. Conv: Conventional. MBES: Multi-beam echosounder, MSCL: Multi-sensor core logger, SSS: Side-scan sonar. *seabed infrastructure, **exploration

	HC and CCS	**Offshore wind**	**Cable routes**
Budget	High	Moderate	Low
Schedule	Wide	Tight (cycles are shorter)	Very tight
Profit margin/Profitability of project	High for HC; low for CCS	Moderate	Moderate
Areal extent (km^2)	1*-10,000**	100-1000	10-100
Subsurface depth of investigation (m)	1000-6000	<200	<10
Subsurface complexity	Moderate (as area of interest is smaller due to site investigations and often in deeper waters)	Very high (uppermost c. 100 m of large areas)	High (uppermost 6 m are of interest over very long distances, sometimes >100 km)
Geology	(Un-)Consolidated sediments*, bedrock**	Mobile sediments, (un-)consolidated sediments, bedrock	Mobile sediments, (un-)consolidated sediments, bedrock outcrops, soft sediments
Geophysical dataset	Conv3D (sometimes bottom nodes), HR2D/3D (reservoir and overburden); Foundation -> see offshore wind	2DUHRS, 3DUHRS, SBP, SSS, MBES, magnetometer, metocean, seismic CPTs, MSCL	SBP, (Repeated) MBES, SSS, magnetometer
Geotechnical dataset	10s of CPTs	100s-1000s of CPTs; 10s-100s of BHs	Vibrocores (c. 1/km); Shallow CPTs (c. 1/km)
Resources for data interpretation	High	Moderate	Low
Amount of data	High	Very high	High
Data accessibility	Partly accessible after some years	Full access depending on national regulations	Full access depending on national regulations

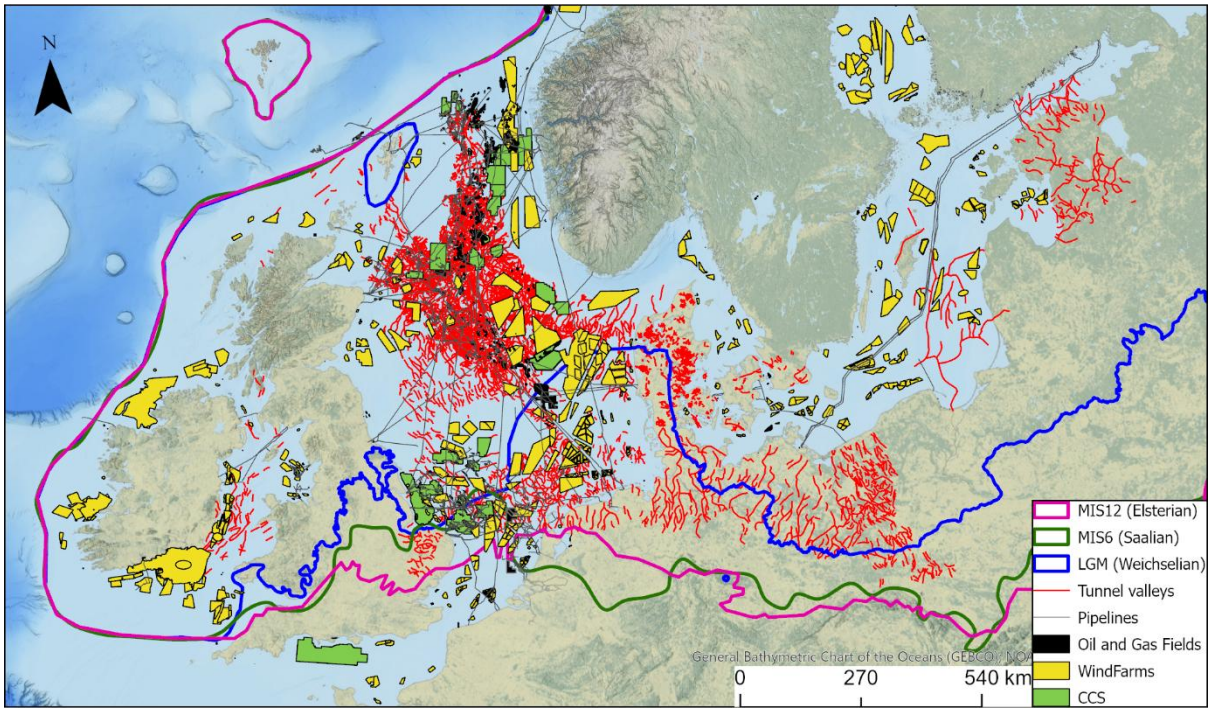


Figure 7.1. The presence of tunnel valleys and their overlap with the different sectors of offshore energy as shown for the southern part of the study area. Windfarms shapes include blocks defined as suitable for future application rounds.

7.2.1 Offshore wind

By 2024, 37 GW of offshore wind have been installed in Europe (WindEurope, 2024). The global demand for renewable energy is on the rise, and Europe could deploy up to 450 GW of offshore wind by 2050 (Ramirez et al., 2020; WindEurope, 2024). Most of this energy is produced by windfarms located on the formerly glaciated European margins, with the UK and Germany currently leading the deployment.

Depending on water depths and soil-rock conditions, a range of offshore foundations are used in offshore wind. Most of the windfarms are located in regions with water depths of <40 m, some up to 80 m, with fixed foundations (e.g., monopiles, suction caisson jackets or piled jackets). These areas with shallow water depths were terrestrially exposed platforms during the Quaternary glaciations and sea level oscillations, and include a multitude of glacigenic landforms.

Many glacigenic landforms incorporate complexities (e.g., changing soil conditions); the best examples for lateral variability are arguably glacial channels and tunnel valleys (Figure 5.41; Bellwald et al., 2024c). The acreage defined for offshore wind (e.g., in the North Sea Basin) often coincides with mapped tunnel valleys (Figure 7.1). These channels can have formed in several generations and be located at multiple stratigraphic levels. Their infill, in addition, can be vertically changing on small scales, thus requiring a proper subsurface characterization (Figure 5.41). This has implications for any offshore energy business.

Centimeter- to meter-scale lateral and vertical variability are important in offshore wind (Figure 7.2): The widths of existing monopiles vary from 4-15 m, and the footprint for certain foundation designs reaches 50 m with an engineering zone of influence around these considerably larger. Within such distances, the subsurface might change drastically (Figure 7.2).

It is also important to consider the operations and maintenance of offshore wind farms, particularly in shallower water where jack-up vessels are the vessel of choice for many operators. Jack-up activities are sensitive to a range of risks associated with vertical and lateral variability and a suitable footprint around foundation locations should also be considered to de-risk these activities.

However, offshore wind turbines become larger and are gradually moving into deeper waters. Different foundation types are designed and installed in these deeper waters. Additional hazards or geo-constraints for floating wind (compared to fixed foundations) are deep-ocean currents, deepwater geohazards such as landslides and turbidity currents, gas hydrates (if occurring in foundation zone), and possible free gas trapped in the subsurface. Floating wind anchor solutions also have a wide footprint, and more contact points with the seabed than fixed bottom solutions, meaning characterising lateral variability is just as important for these sites.

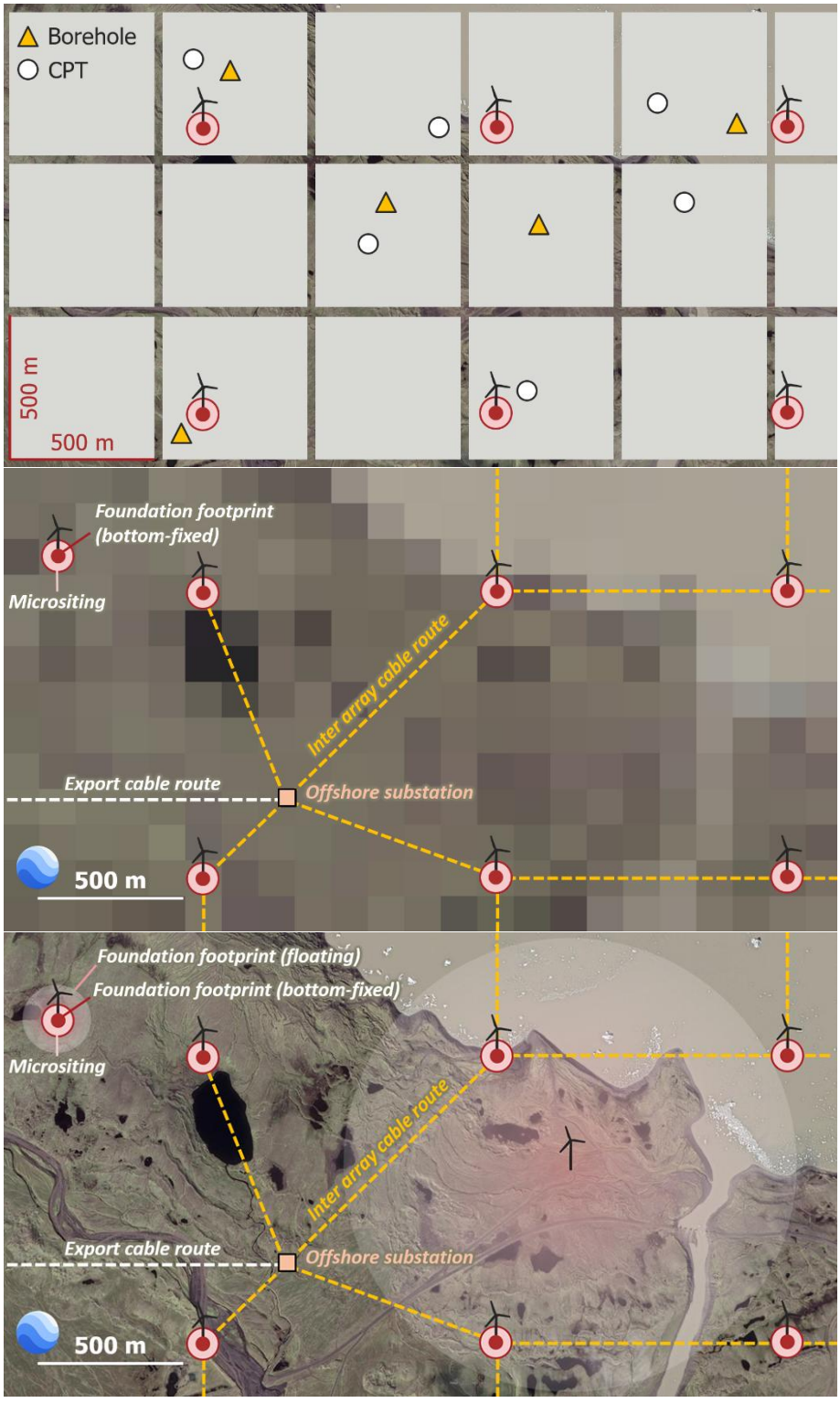


Figure 7.2. Glacial landscapes with extremely complex lateral changes (Fjallsárlón, SE Iceland). Circles around WTGs have 25 m radius for foundation footprint and 50 m radius for micro-siting. Upper panel: Early-phase offshore wind setup, with CPTs and boreholes away from the 2D seismic grid. Central panel: Planar view of interpreting a densely-spaced 2D seismic grid (here 125 m bin size). Lower panel: Planar view of interpreting a EHR3D seismic grid (here 1 m bin size). Satellite imagery from 9/2019 CNES Airbus.

7.2.2 Cable routes

The transfer of energy from the offshore windfarm to the national power grids occurs via export cables. The export cable routes (ECR) are 10s to 100s of kilometres in length and may cross highly variable lithologies in commonly changing Quaternary terrains (Figures 7.2 and 5.19). Cable-route surveys are thus shaped as very long but narrow corridors, often limited to c. 100-400 m on either side of the cable allowing for flexibility in exact cable location within the corridor. The uppermost meters (e.g., 6 m) are usually of interest for cable burial risk assessment (Carbon Trust, 2016). In addition, inter-array cables (IAC) link individual wind turbines and deliver power to the offshore substation (OSS) or offshore converter platform (OCP). The OSS collects the power of the wind turbines and prepares it for transmission to shore. The OSS or OCP structures can be very large, with a footprint substantially exceeding that of the turbine foundation solutions. The goal of a cable-run setup is to define and derisk an effective route. Apart from cabling for offshore wind, submarine interconnector cables, supplying power between two land locations, or telecommunication cables, providing data links, are also frequently placed at and below the seabed on glaciated continental margins. Major challenges for most cable projects include:

i) Complex geological settings: Physical material is commonly sampled in vibrocores combined with shallow CPTs, with an arbitrary spacing of c. 1 core per few hundreds of m to few kilometers (DNV, 2014). However, even within one kilometre, geospatial variability can be significant, and potentially affecting the operations (e.g., trenching, jetting). Sampling locations should be carefully considered in conjunction with ultra-high-resolution seismics (sub-bottom profiling) and geological data to optimize sampling in different soil types to ensure representative sampling.

ii) Seafloor and sub-seafloor obstructions: The cable-route layouts are defined to avoid boulders or boulder fields, as moving or relocating boulders can be challenging, particularly if they are partially embedded in dense sand or high strength clay. Depending on the selected trenching technique, the critical boulder size can vary as well. Other obstructions could include environmentally sensitive habitats or archaeologically significant features.

iii) Thermal conductivity: The transfer of electricity in cables causes the cables to heat up, and heat will dissipate into the surrounding soil or water medium. When heat dissipation is limited (e.g., cable in resistive materials), the transmission capacity reduces and can cause cable failure. Identification of thermally insulating materials within the ground from seismic data and geotechnical boreholes and testing (for example clays or organic-rich sediments and ashes), as well as in situ and laboratory thermal conductivity measurements are therefore crucial.

iv) Steep slopes and high-angle gradients, associated with seabed morphology including mobile bedforms, outcropping geology or channel incisions, can present considerable

challenges to installation vehicles and would normally be routed around. In areas of seabed mobility, pre-dredging may occur to create a suitable route through, with natural reburial.

v) Rockhead or hard substrate present a considerable difficulty to cable installation, and it is often preferred to route to avoid having to install within those materials. However, closer to shore such conditions may be unavoidable, and a balance must be struck between costly installation methods and costly protection methods such as imported rock armour. It is therefore important to identify and map potential rock outcrop or subcrop along cable routes, and geotechnically characterise them sufficiently to understand the correct approach to take.

vi) Also important is the potential for free-span, i.e., the cable becomes suspended between two points on the seafloor, which needs careful attention in the design. Free-span can be caused by uneven or undulating seafloor, current-induced erosion, scouring or seabed mobility, or hard seabed features. Free-span may result in fatigue, increased stress on the cable connections, higher likelihood of mechanical failures, and as indicated above, potential for overheating due to poor heat dissipation.

7.2.3 CCS and hydrocarbon industry

Capture and storage of CO_2 in geological formations represent an important measure with a large potential to reduce global greenhouse gas emissions (NPD, 2014). On the glaciated European margin, the CO_2 storage projects in operation are Sleipner, Greensand, Longship (all North Sea) as well as Snøhvit (Barents Sea). Approximately 1 Mt of CO_2 have per year been stored in Sleipner since 1996, and approximately 0.7 Mt of CO_2 have been safely injected and stored in the Snøhvit CCS project since 2008 (NPD, 2014). 28 of the 43 European CCS projects are located within the glaciated European margins (IOGP, 2024; Figure 7.1). Until 2030, the annual CO_2 storage capacity of projects planned in Norway, the UK, Denmark, and the Netherlands account for approximately 87 $MtCO_2/yr$ (compared to the approximately 4.7 $MtCO_2/yr$ in operation in 2024; IOGP, 2024). This development shows that geohazard assessments and geo-engineering constraints in these glaciated settings will have to be analysed and monitored on larger scales in near future. Understanding the engineering properties of the Quaternary sediments are key to guarantee a safe and sustainable storage of CO_2.

Several oil and gas fields are in operation from the mid-20 century onwards on the glaciated European margin, particularly on the UK Continental Shelf and the Norwegian Continental Shelf (Figure 7.1; 5.41). Reservoir rocks commonly are of Paleozoic, Mesozoic, or Paleogene age. However, unconventional hydrocarbon models include Quaternary deposits for gas reservoirs (Huuse et al., 2012; Bellwald et al., 2022b). Structures and processes related to these deeper stratigraphic levels, such as salt tectonics and sill intrusions, can impact the Quaternary systems and deposits (see Figures 5.32 and 5.38). The most prominent discoveries of Quaternary hydrocarbon reservoirs include the Peon field in the Northern North Sea (Figure 2.6) and the Aviat field in the Central North Sea.

Quaternary sands might be charged with gas, as proven by the Peon discovery in the Northern North Sea. Despite proven as a gas discovery, the Peon field has not been developed yet. This might change with Norway's ambition to supply gas to Europe with the current geopolitical outlook, and it was stated that more wells are planned to be drilled around Peon (Upstreamonline, 2025).

More commonly, Quaternary sediments act as the seal for the underlying pre-Quaternary reservoir rocks. Knowhow on the Quaternary (e.g., lateral heterogeneities) is important to properly image CCS and O&G reservoirs. Landforms identified in the overburden, such as tunnel valleys and their infill, might result in wrong conclusions when imaging the deeper reservoirs.

The uppermost meters of the Quaternary stratigraphy are in addition very important for platform foundation, well placement, and well stability. Data collected for hydrocarbon exploration are commercially highly sensitive, compared to the less sensitive data collected for windfarm projects.

Hydrocarbon exploration may extend into frontier areas, such as the Arctic waters of the Barents Sea, which is not yet seriously considered for offshore wind. However, there is serious public debate and concern over such developments. A safe assessment in these frontier areas, with additional geohazards and geo-engineering challenges, is key to convince society and stakeholders.

7.2.4 Cable and pipeline landfalls

The interface between land and sea is a complex juncture of physical processes (marine, terrestrial and atmospheric), anthropogenic use, and industry development. Bringing cables or pipelines ashore means crossing this boundary, and to do so conditions in all systems should be understood to engineer a suitable solution. Due to sea-level change and glacio-isostatic adjustment (Section 6.4), the coastline is dynamically evolving and, in some places, continues to respond to local and global changes. Therefore, consideration must be made not only to current conditions but past and future conditions as well when engineering the ocean-land interface.

The geology and geomorphology of the landfall will often dictate the method of installation and subsequently how to investigate it. The two main options for landfalls are open cut and Horizontal Directional Drilling (HDD). The most common option for offshore wind is HDD, as it is less disruptive and obtrusive than an open cut. Drillers often prefer soils with good consistency, and so previously glaciated soils can present a particular challenge to HDD, which can encounter issues with:

- Variable soils, which affect drilling pressures and progression if incorrectly characterised, for example beds of sand within stiff clays which can be washed out by drilling fluids;
- Cemented layers, or beds of cobbles or boulders, which can alter the course of the drilling head away from the desired course;
- Large individual very hard boulders, particularly stiff soils which cannot be drilled through or moved aside by the drill-head and directly obstruct or slow down drilling progression.

It is therefore critical to correctly investigate the site to fully characterise ground conditions ahead of HDD works. However, the methods of geophysical, geotechnical and metocean investigation techniques in these areas can be variable and challenging. For example, restrictions on vessel size during geophysical surveys may restrict what equipment can be used compared to a "normal" offshore survey, and data types used in the nearshore zone need to be compatible with both onshore and deeper-water surveys.

In addition to engineering for the current coastline, offshore energy developers need to be conscious of future changes to sea-levels, coastal position and erosion rates. Cable landfall HDD positions in areas with high erosion will need to be suitable for the future lifetime of the offshore project, so predictions of sea-level change and erosion rates/future positions need to be predicted for 30 to 50 years into the future to be correctly designed. Previously glaciated soils, such as those on the East Riding of Yorkshire, are associated with some of the highest erosion rates in the world and also home to many of the North Sea wind farm cables coming into shore.

7.3 Scientific drilling

Drilling for scientific research is of crucial importance as it provides direct access to the geological records beneath the Earth's surface in very-high (vertical) resolution, which sheds light on our understanding of the Earth systems, climate changes, oceanography and natural hazard assessments. The International Ocean Discovery Program (IODP), and its previous iterations, have been the main vehicle for this type of academic research, collecting up to ~500 km of core from across the globe since the late 1960s (IODP, 2024). From a drilling perspective, the documentation of geohazards, such as submarine landslides, methane hydrates, and fault zones, are all crucial for ensuring safe drilling operations and limiting the potential for wellbore collapse and the loss or damage of equipment. In order to drill through such features requires advanced geotechnical assessments and engineering protocols that are largely unaffordable outside of the energy industry. Thus, in such instances, scientific drilling, like that by IODP, must prioritise more cost-effective solutions. Often this will mean that drill-site planning deliberately avoids these strata entirely, requiring geohazard workflows for avoiding problematic features (Cox et al., 2020). The documentation of geohazards is not restricted to just drilling operations, but are themselves an area of scientific research. This is because of the potential to extract profound insights into Earth's dynamic processes, such as earthquakes, landslides, and tsunamis from the analyses of rock, sediment, and fluid samples that make up these hazards (IODP, 2020). These records can yield information on past climate changes and natural disasters, providing important information on the timing, the magnitude, and the nature of how these geohazards evolved in the first place, their initiation points, and the characteristics of potential preconditioning (IODP, 2020). All of this research is crucial for developing predictive models and risk mitigation strategies for natural hazards, as well as the development of engineering strategies for disaster preparedness and response.

As outlined in this review paper, the northwest European margin has a wide range of geohazard features at a variety of different scales. Scientific drilling plays an important role in understanding the nature of these geohazards, while the geohazards and geo-engineering constraints themselves can provide a limiting factor on what can be drilled – i.e., it can be a bi-directional relationship. As such, there are several proposals currently under consideration that seek to target the Quaternary stratigraphy offshore northwest Europe and the potential insights that they may hold (e.g., Newton et al. (2024b) that seeks to drill in the North Sea). These proposals have required a detailed understanding of the nature and distribution of geohazards in the region. Knowledge on the geohazards on northwest Europe also have an increased relevance for the energy transition, where geohazards impact not just the initial drilling operations, but also the subsequent efficacy of potential sites to achieve their aims. For example, how subsurface geohazard features may have a positive or negative effect on the migration of greenhouse gases in potential sequestration aquifers (e.g., Lloyd et al., 2021). Documenting the distribution of geohazards on the northwest European margin is going to continue to be crucial for understanding climatic changes of the past and mitigating climate changes of the future.

7.4 Implications for different regions of the glaciated European glaciated margin

The importance of geohazards and geo-engineering constraints depends on the region within the glaciated European margin. In the following table, we summarize the likelihood of the different geohazards and geo-engineering constraints depending on the location in the study area (see Chapter 2).

Table 7.2. Summary of geo-engineering constraints and geohazards in the different regions of the study area. Traffic-light system is relative, with red: high potential of constraint/hazard, orange: moderate, yellow: low.

		Barents Sea	Mid-Norway	Northern North Sea	Central North Sea	Southern North Sea	Baltic Sea and Gulf of Bothnia	Irish Sea and Celtic Sea	Outer Hebrides and Rockall	West of Shetland
Geo-engineering constraints	Shallow gas									
	Gas hydrates									
	Fluid flow									
	Strength variability									
	Boulders									
	Gravel and pebble beds									
	Soft marine sediments									
	Weathered and unweathered bedrock (<200m)									
	Organic materials and peat									
	Faults and fractures									
	Glaciotectonic deformation									
	Salt tectonics									
	Glacigenic landforms									
Geohazards	Sediment transportation and mobility									
	Slope instabilities (at slopes; not fjords)									
	Glacio-isostatic adjustment; sea-level changes									
	Seismicity									
	Tsunamis									

8. Summary

Processes related to glaciations and sea-level changes have defined sediment deposition in glaciated regions over the last 2.58 million years, the time period called the Quaternary. The Quaternary sediments along the glaciated European margin form a complex subsurface with thicknesses of some 10s to 100s of meters on the shelves, and 100s to 1000s of meters on the upper slopes and the central North Sea. Changing sedimentary environments resulted in extreme geospatial variability, from basin scale (e.g., instanced of large-scale instabilities) to local scale (e.g., specific glacial landforms like moraines, eskers, etc.) as well as micro-scale (composition, porosity, permeability). As a consequence, these deposits can host static geo-engineering constraints, which have different complexities: i) changes

in grain sizes from fine clay to boulders, ii) accumulations of shallow gas, gas hydrates, and overpressured layers potentially resulting in fluid flow and fluid seepage, iii) composition and strength variability in particular related to glacigenic landforms, iv) faulted, fractured, and deformed packages, and v) high-organic-content sediments (e.g., presence of peat).

Dynamic Earth processes affect and interfere with the Quaternary sediments, and form a variety of potential geohazards: i) seabed mobility, ii) slope instabilities, iii) earthquakes, iv) tsunamis, v) sea-level changes, and vi) glacio-isostatic adjustments. Some of these geohazards are challenging to identify and forecast (e.g., earthquakes, tsunamis); they affect large areas, and occur on short time scales. Other geohazards act on longer time scales, and have an easier predictability, such as glacio-isostacy and sea-level change. A proper identification and characterization of these geo-engineering constraints and geohazards, as well as understanding the processes and behaviour over time, allow a safe mitigation of the risks.

Acknowledgements

We acknowledge the following companies for access of geophysical, geotechnical, and geological data: bp, Eliis, EnBW, Equinor, Fugro, GEO, Geo Marine Survey Systems, RVO, SSE Renewables, TGS, Vattenfall, VBER, and Viridien.

Lina Jakaite and Strike-dip.com are thanked for their artistic drawing of the sketch summarizing the geohazards and geo-engineering constraints. Sylfest Glimsdal is acknowledged for producing the figure on the tsunami model from Åknes/Tafjord, and Clement Tam for providing the figure on the salt in the North Sea. Elisabeth Hoffstad Reutz and Sigrid Esmeralda Arnestad are thanked for supporting GIS activities. Stein Bondevik is acknowledged for the fruitful feedback on the tsunami deposits. GeoSurveys is thanked for supporting our requests with figures on boulders and peat.

Contributions to this paper were supported by the EU project “A Digital Twin for Geophysical Extremes” (DT-GEO) and has received funding from Horizon Europe under Grant Agreement No 101058129. Documentation of landslide tsunami events was prepared under the “Geosphere INfrastructures for QUestions into Integrated REsearch” (Geo-INQUIRE) project, funded by the European Commission under project No. 101058518 within the HORIZON-INFRA-2021-SERV-01 call. Both projects have also received funding from NGI’s internal R&D programme supported by the Research Council of Norway. David R. Tappin publishes with permission of the British Geological Survey, United Kingdom Research and Innovation.

References

Aber, J. S., & Ber, A. (2011). Glaciotectonic structures, landforms, and processes. Encyclopedia of Earth Sciences Series, Part 3, 444–458. https://doi.org/10.1007/978-90-481-2642-2_217/FIGURES/7102

Aber, J. S., Croot, D. G., & Fenton, M. M. (1989). Nature of Glaciotectonism. In Glaciotectonic Landforms and Structures (pp. 1–12). https://doi.org/10.1007/978-94-015-6841-8_

Adnyani, L. P., Draper, S., An, H. W., & Cheng, L. (2024). Modelling Sand Wave Evolution and Migration in North Sea Using ROMS. Applied Mechanics and Materials, 924, 139–152. https://doi.org/10.4028/p-E52NOj

Ahlrichs, N., Hübscher, C., Andersen, T. R., Preine, J., Bogner, L., and Schäfer, W., 2023, The Langeland Fault System unravelled: Quaternary fault reactivation along an elevated basement block between the North German and Norwegian–Danish basins: Boreas, v. 52, no. 3, p. 381-401.

Ahsan, D., & Pedersen, S. (2018). The influence of stakeholder groups in operation and maintenance services of offshore wind farms: Lesson from Denmark. Renewable Energy, 125, 819-828.

Alexandropoulou, N., Winsborrow, M., Andreassen, K., Plaza-Faverola, A., Dessandier, P. A., Mattingsdal, R., ... & Knies, J. (2021). A continuous seismostratigraphic framework for the Western Svalbard-Barents sea margin over the last 2.7 Ma: implications for the late Cenozoic glacial history of the Svalbard-Barents sea ice sheet. Frontiers in Earth Science, 9, 656732.

Amos, C. L., Kassem, H., & Friend, P. L. (2017). Ripple Marks (pp. 1–8). https://doi.org/10.1007/978-3-319-48657-4_262-2

Andersen, L. T., Hansen, D. L., & Huuse, M. (2005). Numerical modelling of thrust structures in unconsolidated sediments: Implications for glaciotectonic deformation. Journal of Structural Geology, 27(4), 587–596. https://doi.org/10.1016/J.JSG.2005.01.005

Andersen, K.H., Lunne, T., Kvalstad, T.J., Forsberg, C.F., 2008. Deep water geotechnical engineering, in: XXIV National Conference of the Mexican Society of Soil Mechanics. Norwegian Geotechnical Institute (NGI), Aguascalientes, Mexico, pp. 1–57.

Andersen, K.H., Engin, H.K., D'Ignazio, M., Yang, S., 2023. Determination of cyclic soil parameters for offshore foundation design from an existing data base. Ocean Eng. 267, 113180. https://doi.org/10.1016/j.oceaneng.2022.113180

Andreassen, K., Hubbard, A., Winsborrow, M., Patton, H., Vadakkepuliyambatta, S., Plaza-Faverola, A., Gudlaugsson, E., Serov, P., Deryabin, A., and Mattingsdal, R., 2017, Massive blow-out craters

formed by hydrate-controlled methane expulsion from the Arctic seafloor: Science, v. 356, no. 6341, p. 948-953.

Andresen, K. J. (2012). Fluid flow features in hydrocarbon plumbing systems: What do they tell us about the basin evolution?. Marine Geology, 332, 89-108.

Andersen, L. T., Hansen, D. L., & Huuse, M. (2005). Numerical modelling of thrust structures in unconsolidated sediments: implications for glaciotectonic deformation. Journal of Structural Geology, 27(4), 587-596.

Andresen, K.J., Hepp, D.A., Keil, H., Spiess, V. (2022): Seismic morphologies of submerged late glacial to early Holocene landscapes at the eastern Dogger Bank, central North Sea Basin - implications for geo-archaeological potential. Geological Society London, Special Publication 525. doi.org/10.1144/SP525-2021-155

Andrews, I.J., Long, D., Richards, P.C., Thomson, A.R., Brown, S., Chesher, J.A., McCormac, M. (1990). United Kingdom offshore regional report: the geology of the Moray Firth. London: HMSO for the British Geological Survey.

Arfai, J., Kuhlmann, G., Ladage, S., Lutz, R., Gaedicke, C. (2018). Iceberg scour marks in the Southern North Sea - Indications for iceberg transport at the beginning of Northern Hemispher. 80th EAGE Conference and Exhibition 2018: Opportunities Presented by the Energy Transition, 2018, 1–5, https://doi.org/10.3997/2214-4609.201801642.

Arosio, R., Dove, D., Ó Cofaigh, C., & Howe, J. A. (2018). Submarine deglacial sediment and geomorphological record of southwestern Scotland after the Last Glacial Maximum. Marine Geology, 403, 62-79.

Arosio, R., Wheeler, A.J., Sacchetti, F., Guinan, J., Benetti, S., O'Keeffe, E., van Landeghem, K.J.J., Conti, L.A., Furey, T., Lim, A., 2023. The geomorphology of Ireland's continental shelf. J. Maps 19. https://doi.org/10.1080/17445647.2023.2283192

Arvidsson, R., 1996. Fennoscandian Earthquakes: Whole Crustal Rupturing Related to Postglacial Rebound. Science 274, 744–746. https://doi.org/10.1126/science.274.5288.744

Ashley, G. (1990). Classification of Large-Scale Subaqueous Bedforms: A New Look at an Old Problem-SEPM Bedforms and Bedding Structures. SEPM Journal of Sedimentary Research. Vol. 60. 10.1306/212F9138-2B24-11D7-8648000102C1865D.

ASTM (2010). D2487: Standard practice for classification of soils for engineering purposes (unified soil classification system). In ASTM.

Audsley, A., Bradwell, T., Howe, J., Baxter, J. (2021). Spatial Relationships between Pockmarks and Sub-Seabed Gas in Fjordic Settings: Evidence from Loch Linnhe, West Scotland. Geosciences, v. 11, 283. https://doi.org/10.3390/geosciences11070283

Baeten, N. J., Laberg, J. S., Vanneste, M., Forsberg, C. F., Kvalstad, T. J., Forwick, M., ... & Haflidason, H. (2014). Origin of shallow submarine mass movements and their glide planes—Sedimentological and geotechnical analyses from the continental slope off northern Norway. Journal of Geophysical Research: Earth Surface, 119(11), 2335-2360.

Bagnold, R. A. (1954). Experiments on a gravity-free dispersion of large solid spheres in a Newtonian fluid under shear. Philosophical Transactions of the Royal Society London, Series A 225, 49–63, DOI 10.1098/rspa.1954.0186.

Baig, I., Faleide, J.I., Mondol, N.H., Jahren, J., 2019. Burial and exhumation history controls on shale compaction and thermal maturity along the Norwegian North Sea basin margin areas. Mar. Petrol. Geol. 104, 61–85.

Bailey, G., Galanidou, N., Peeters, H., Jöns, H. and Mennenga, M. (eds). 2020. The Archaeology of Europe's Drowned Landscapes. Springer Open, Coastal Research Library, 35.

Ballantyne, C.K., Small, D., 2019. The Last Scottish Ice Sheet. Earth and Environmental Science Transactions of the Royal Society of Edinburgh, 110, pp. 93–131.

Baltzer, A., Holmes, R., & Evans, D. (1998). Debris flows on the Sula Sgeir Fan, NW of Scotland. Geological Society, London, Special Publications, 129(1), 105-115.

Barbolini, M.; Biancardi, A.; Cappabianca, F.; Natale, L. and Pagliardi, M. (2005). Laboratory study of erosion processes in snow avalanches, Cold Regions Science and Technology 43: 1–9, DOI 10.1016/j.coldregions.2005.01.007.

Barker, T.; Schaeffer, D. G.; Shearer, M. and Gray, J. M. N. T. (2017). Well-posed continuum equations for granular flow with compressibility and μ(I)-rheology. Proceedings of the Royal Society, London, Ser. A 473: 20160846, DOI 10.1098/rspa.2016.0846.

Barrett, R. S., Bellwald, B., Talling, P. J., Micallef, A., Gross, F., Berndt, C., ... & Krastel, S. (2021). Does retrogression always account for the large volume of submarine megaslides? Evidence to the contrary from the Tampen Slide, offshore Norway. Journal of Geophysical Research: Solid Earth, 126(2), e2020JB020655.

Barrett, R., Bellwald, B., Talling, P. J., Sokolkova, E., Grob, H., Lenz, K. F., ... & Krastel, S. (2025). Deep Secrets: Discovery of a giant mega-slide in the North Sea Fan, offshore Norway. Marine Geology, 107554.

Batchelor, C.L., Margold, M., Krapp, M., Murton, D.K., Dalton, A.S., Gibbard, P.L., Stokes, C.R., Murton, J.B., Manica, A. 2019. The configuration of Northern Hemisphere ice sheets through the Quaternary. Nature Communications. 10:3713, 10pp.

Batchelor, C. L., Bellwald, B., Planke, S., Ottesen, D., Henriksen, S., Myklebust, R., ... & Dowdeswell, J. A. (2021). Glacial, fluvial and contour-current-derived sedimentation along the northern North Sea margin through the Quaternary. Earth and Planetary Science Letters, 566, 116966.

Batchelor, C.L., Christie, F.D.W., Ottesen, D. et al. Rapid, buoyancy-driven ice-sheet retreat of hundreds of metres per day. Nature 617, 105–110 (2023). https://doi.org/10.1038/s41586-023-05876-1

Bayliss, A. I. (2015). Geotechnical characterization and performance of Glaciotectonites for earth structures and natural slopes.

Behrens J, Løvholt F, Jalayer F, Lorito S, Salgado-Gálvez M, et al. (2021) Probabilistic tsunami hazard and risk analysis—A review of research gaps. Frontiers in Earth Science 9: 114. https://doi.org/10.3389/feart.2021.628772.

Belderson, R.H., 1964. Holocene sedimentation in the western half of the Irish Sea. Mar. Geol. 2, 147–163.

Bellec, V. K., Bøe, R., Bjarnadóttir, L. R., Albretsen, J., Dolan, M., Chand, S., Thorsnes, T., Jakobsen, F. W., Nixon, C., Plassen, L., Jensen, H., Baeten, N., Olsen, H., & Elvenes, S. (2019). Sandbanks, sandwaves and megaripples on Spitsbergenbanken, Barents Sea. Marine Geology, 416, 105998. https://doi.org/10.1016/j.margeo.2019.105998

Bellwald, B., Hjelstuen, B.O., Sejrup, H.P., Haflidason, H., 2016. Postglacial mass movements and depositional environments in a high-latitude fjord system – Hardangerfjorden, Western Norway. Marine Geology 379, 157-175.

Bellwald, B., Waage, M., Planke, S., Lebedeva-Ivanova, N., Polteau, S., Tasianas, A., ... & Myklebust, R. (2018, November). Monitoring Of CO2 Leakage Using High-Resolution 3D Seismic Data–Examples From Snøhvit, Vestnesa Ridge And The Western Barents Sea. In Fifth CO2 Geological Storage Workshop (Vol. 2018, No. 1, pp. 1-5). European Association of Geoscientists & Engineers.

Bellwald, B., & Planke, S. (2019). Shear margin moraine, mass transport deposits and soft beds revealed by high-resolution P-Cable three-dimensional seismic data in the Hoop area, Barents Sea. Geological Society, London, Special Publications, 477(1), 537-548.

Bellwald, B., Hjelstuen, B. O., Sejrup, H. P., Stokowy, T., & Kuvås, J. (2019a). Holocene mass movements in west and mid-Norwegian fjords and lakes. Marine Geology, 407, 192-212.

Bellwald, B., Urlaub, M., Hjelstuen, B.O., Sejrup, H.P., Sørensen, M.B., Forsberg, C.F., and Vanneste, M., 2019b, NE Atlantic continental slope stability from a numerical modelling perspective: Quaternary Science Reviews, v. 203, p. 248-265, https://doi.org/10.1016/j.quascirev.2018.11.019.

Bellwald, B., Planke, S., Lebedeva-Ivanova, N., Piasecka, E. D., & Andreassen, K. (2019c). High-resolution landform assemblage along a buried glacio-erosive surface in the SW Barents Sea revealed by P-Cable 3D seismic data. Geomorphology, 332, 33-50.2020

Bellwald, B., Planke, S., Polteau, S., Lebedeva-Ivanova, N., Faleide, J. I., Morris, S. M., ... & Castelltort, S. (2021). Characterization of a glacial paleo-outburst flood using high-resolution 3-D seismic data: Bjørnelva River Valley, SW Barents Sea. Journal of Glaciology, 67(263), 404-420.

B. Bellwald, C. Batchelor, A. Garcia, R. Barrett, M. Rosenqvist, S. Planke, I. Midtkandal, R. Myklebust, B. Kjølhamar, 2022a. Contourites of the Northern North Sea, North Sea Fan, and Mid-Norwegian Margin. 83rd EAGE Annual Conference & Exhibition, Volume 2022, p.1 – 5 DOI: https://doi.org/10.3997/2214-4609.202210247

Bellwald, B., Planke, S., Vadakkepuliyambatta, S., Buenz, S., Batchelor, C., Manton, B., ... & Kjølhamar, B. (2022b). Quaternary and Neogene Reservoirs of the Norwegian continental shelf and the Faroe-Shetland basin. First Break, 40(6), 43-54.

Bellwald, B., Stokke, H., Winsborrow, M., Planke, S., Sættem, J., Lebedeva-Ivanova, N., ... & Polteau, S. (2023a). Structural and fluid-migration control on hill-hole pair formation: Evidence from high-resolution 3D seismic data from the SW Barents Sea. Geomorphology, 420, 108502.

Bellwald, B., Griffiths, L., Hansen, R. C., Dujardin, J., Forsberg, C., De Gail, M., ... & Piotrowski, J. A. (2023b, September). Multi-disciplinary Characterization of Sedimentary Environments on Glaciated Margins: Implications for Engineering of Offshore Windfarm Sites. In NSG2023 1st Conference on Sub-surface Characterisation for Offshore Wind (Vol. 2023, No. 1, pp. 1-5). European Association of Geoscientists & Engineers.

Bellwald, B., Maharjan, D., Planke, S., Winsborrow, M., Rydningen, T.A., Alexandropoulou, N. and Myklebust, R., 2024a. Major tunnel valleys and sedimentation changes document extensive Early Pleistocene glaciations of the Barents Sea. Communications Earth & Environment, 5(1), p.551.

Bellwald, B., Manton, B., Lebedeva-Ivanova, N., Zastrozhnov, D., Myklebust, R., Planke, S., ... & Locat, J. (2024b). Rapid glacial sedimentation and overpressure in oozes causing large craters on the mid-Norwegian margin: integrated interpretation of the Naust, Kai and Brygge formations.

Bellwald, B., Kurjanski, B., Wood, G., Carter, G., Stokke, H. H., Planke, S., ... & Vanneste, M. (2024c, June). Resolution requirements for characterization of sedimentary environments in glaciated margins: a geomorphological perspective. In 85th EAGE Annual Conference & Exhibition (including the

Workshop Programme) (Vol. 2024, No. 1, pp. 1-5). European Association of Geoscientists & Engineers.

Benetti, S., Chiverrell, R.C., Cofaigh, C.Ó., Burke, M., Medialdea, A., Small, D., Ballantyne, C., Bateman, M.D., Callard, S.L., Wilson, P., Fabel, D., Clark, C.D., Arosio, R., Bradley, S., Dunlop, P., Ely, J.C., Gales, J., Livingstone, S.J., Moreton, S.G., Purcell, C., Saher, M., Schiele, K., Van Landeghem, K., Weilbach, K. (2021). Exploring controls of the early and stepped deglaciation on the western margin of the British Irish Ice Sheet. Journal of Quaternary Science, v. 36: 833-870. https://doi.org/10.1002/jqs.3315

Bennett, M. R. (2001). The morphology, structural evolution and significance of push moraines. Earth Science Reviews, 53(3–4), 197–236. https://doi.org/10.1016/S0012-8252(00)00039-8

Benvenuti, A., Kombrink, H., Veen, J.H. ten, Munsterman, D.K., Bardi, F., Benvenuti, M., 2012. Late Cenozoic shelf delta development and Mass Transport Deposits in the Dutch offshore area – results of 3D seismic interpretation. Netherlands Journal of Geosciences - Geologie en Mijnbouw 91, 591–608.

Berg, K., Solheim, A., and Bryn, P., 2005, The Pleistocene to recent geological development of the Ormen Lange area: Marine and Petroleum Geology, v. 22, p. 45-56, https://doi.org/10.1016/j.marpetgeo.2004.10.009.

Berndt, C., Bünz, S., & Mienert, J. (2003). Polygonal fault systems on the mid-Norwegian margin: a long-term source for fluid flow.

Berndt, C., Brune, S., Nisbet, E., Zschau, J., Sobolev, S.V., 2009. Tsunami modeling of a submarine landslide in the Fram Strait, Geochem. Geophys. Geosyst., 10, Q04009, doi:10.1029/2008GC002292.

Bienen, B., Qiu, G., & Pucker, T. (2015). CPT correlation developed from numerical analysis to predict jack-up foundation penetration into sand overlying clay. Ocean Engineering, 108, 216-226.

Bjørlykke, K., Høeg, K., and Mondol, N. H., 2015, Introduction to Geomechanics: stress and strain in sedimentary basins: Petroleum Geoscience: from sedimentary environments to rock physics, p. 301-318.

Blikra, L.H., Longva, O., Braathen, A., Anda, E., Dehls, J., and Stalsberg, K. (2006). Rock-slope failures in Norwegian fjord areas: examples, spatial distribution and temporal pattern. In: Evans, S.G., Scarawcia Mugnozza, G., Strom, A.L., Hermanns, R.L. (Eds.), Landslides from Massive Rock Slope Failure. Nato Science Series IV, Earth and Environmental Sciences, 49, 475–496.

Blumenberg, M., Schlömer, S., Reinhardt, L., Scheeder, G., Pape, T., & Römer, M. (2022). Biomarker insights into a methane-enriched Holocene peat-setting from “Doggerland”(central North Sea). The Holocene, 32(10), 1015-1025.

Boguchwal, L. A., & Southard, J. B. (1990). Bed configurations in steady unidirectional water flows; Part 1, Scale model study using fine sands. Journal of Sedimentary Research, 60(5), 649–657. https://doi.org/10.1306/212F923C-2B24-11D7-8648000102C1865D

Bondevik, S., Svendsen, J.I., 1993. Palaeotsunamis in the Norwegian Sea and the North Sea, in: Tinti, S. (Ed.), Genesis and Impact of Tsunamis on the European Coasts -- GITEC. Mid-Term Scientific Report, Contract EV5F-CT92-0175, 7.2-7.27.

Bondevik, S., Svendsen, J.I., Johnsen, G., Mangerud, J.A.N., Kaland, P.E., 1997a. The Storegga tsunami along the Norwegian coast, its age and run up. Boreas 26, 29-53.

Bondevik, S., Svendsen, J.I., Mangerud, J.A.N., 1997b. Tsunami sedimentary facies deposited by the Storegga tsunami in shallow marine basins and coastal lakes, western Norway. Sedimentology 44, 1115-1131.

Bondevik, S., Svendsen, J.I., Mangerud, J., 1998. Distinction between the Storegga tsunami and the holocene marine transgression in coastal basin deposits of western Norway. Journal of Quaternary Science 13, 529-537.

Bondevik, S., Løvholt, F., Harbitz, C., Mangerud, J., Dawson, A., and Svendsen, J. I. (2005a). The Storegga Slide tsunami – comparing field observations with numerical simulations. In Ormen Lange – An integrated study for safe field development in the Storegga submarine area, 195-208. Elsevier.

Bondevik, S., Mangerud, J., Dawson, S., Dawson, A., Lohne, Ø., 2005b. Evidence for three North Sea tsunamis at the Shetland Islands between 8000 and 1500 years ago. Quaternary Science Reviews 24, 1757-1775.

Bondevik, S., Risebrobakken, B., Gibbons, S.J., Rasmussen, T.L., and Løvholt, F. (2024) Contamination of 8.2 ka cold climate records by the Storegga tsunami in the Nordic Seas. Nat. Comm. 15, 2904.

Boulton, G. S. (1986). Push-moraines and glacier-contact fans in marine and terrestrial environments. Sedimentology, 33(5), 677-698.

Boyer, F., Guazzelli, É. And Pouliquen, O. (2011). Dense suspensions in rotating-rod flows: normal stresses and particle migration. Journal of Fluid Mechanics 686: 5–25, DOI 10.1017/jfm.2011.272.

Braathen, A., Blikra, L.H., Berg, S.S. & Karlsen, F.: Rock-slope failures in Norway; type, geometry and hazard. Norwegian Journal of Geology, Vol. 84, pp. 67-88. Trondheim 2004. ISSN 029-196X. https://www.geologi.no/images/NJG_articles/NJG_84_67-88.pdf

Bradwell, T., Fabel, D., Clark, C.D., Chiverrell, R.C., Small, D., Smedley, R.K., Saher, M.H., Moreton, S.G., Dove, D., Callard, S.L., Duller, G.A.T., Madialdea, A., Bateman, D., Burke, M.J., McDonald, N.,

Gilgannon, S., Morgan, S., Roberts, D.H., Ó Cofaigh, C. (2021) Pattern, style and timing of British–Irish Ice Sheet advance and retreat over the last 45,000 years: evidence from NW Scotland and the adjacent continental shelf. Journal of Quaternary Science. 1–63. DOI: 10.1002/jqs.3296

Bradwell, T., Small, S., Fabel, D., Clark, C.D., Chiverrell, R.C., Saher, M.H., Dove, D., Callard, S.L., Burke, M.J., Moreton, S.G., Madialdea, A., Bateman, D., Roberts, D.H., Golledge, N.R., Finlayson, A., Morgan, S., Ó Cofaigh, C. (2019a). Pattern, style and timing of British–Irish Ice Sheet retreat: Shetland and northern North Sea sector. Journal of Quaternary Science. 1–42. https://doi.org/10.1002/jqs.3163.

Bradwell, T., Small, S., Fabel, D., Smedley, R.K., Clark, C.D., Saher, M.H., Callard, S.L., Chiverrell, R.C., Dove, D., Moreton, S.G., Roberts, D.H., Duller, G.A.T., Ó Cofaigh, C. (2019b) Ice-stream demise dynamically conditioned by trough shape and bed strength. Science Advances, 5:eaau1380.

Bradwell, T., Stoker, M.S., Golledge, N.R., Wilson, C.K., Merritt, J.W., Long, D., Everest, J. D., Hestvik, O.B., Stevenson, A.G., Hubbard, A.L., Finlayson, A.G., Mathers, H.E. (2008). The northern sector of the last British Ice Sheet: Maximum extent and demise. Earth-Science Reviews, v. 88, 207–226.

Brandes, C., Steffen, H., Steffen, R., Wu, P. (2015). Intraplate seismicity in northern Central Europe is induced by the last glaciation. Geology, 43(7), 611-614.

Breien H, Pagliardi M, De Blasio FV, Issler D, and Elverhøi A (2007). Experimental studies of subaqueous vs. subaerial debris flows–velocity characteristics as a function of the ambient fluid. In: Submarine Mass Movements and Their Consequences, pp. 101–110. Dordrecht: Springer.

Breien H, De Blasio FV, Elverhøi A, Nystuen JP, and Harbitz CB (2010). Transport mechanisms of sand in deep-marine environments—Insights based on laboratory experiments. Journal of Sedimentary Research 80(11): 975–990.

British Geological Survey. (2009) TRANSFER project deliverable D3.1–D3.5: An examination of non-seismic sources of tsunamis and their impacts on European coastlines – WP3 of EU project TRANSFER http://www.transferproject.eu

Brooks, G. R., Adams, J. (2020). A review of evidence of glacially-induced faulting and seismic shaking in eastern Canada: Quaternary Science Reviews, v. 228, p. 106070.

Brown, M. J., Bransby, M. F., Knappett, J., Tovey, S., Lauder, K. D., & Pyrah, J. (2015). The effect of buried fibres on offshore pipeline plough performance. Ocean Engineering, 108, 760–768. https://doi.org/10.1016/j.oceaneng.2015.08.022

Brown, A., Russell, J., Scaife, R. G., Tizzard, L., Whittaker, J., and Wyles, S. F. (2018). "Late glacial / early Holocene palaeoenvironments in the southern North Sea Basin: new data from the Dudgeon offshore wind farm." Quaternary Science, 33, 597 - 610.

Bryn, P., Berg, K., Forsberg, C.F., Solheim, A., Kvalstad, T.J. (2005a). Explaining the Storegga Slide. Marine and Petroleum Geology, Volume 22, 11-19, https://doi.org/10.1016/j.marpetgeo.2004.12.003.

Bryn, P., Berg, K., Stoker, M.S., Haflidason, H. Solheim, A. (2005b). Contourites and their relevance for mass wasting along the Mid-Norwegian Margin. Marine and Petroleum Geology, 22, 85–96, https://doi.org/10.1016/j.marpetgeo.2004.10.012

BS 5930: 2015—The Code of Practice for Site Investigations. British Standards Institute, Milton Keynes.

BS 5930:1981—The Code of Practice for Site Investigations. British Standards Institute, Milton Keynes.

BS 5930:1981—The Code of Practice for Site Investigations. British Standards Institute, Milton Keynes.

BSH. (2023). Geological Report of the Preliminary Investigation of FEP Site N-9.1 Investigation Area: N-09. Published by Bundesamt für Seeschifffahrt und Hydrographie, Hamburg, Germany. https://pinta.bsh.de/N-9.1

Buckley, F.A. (2017). A glaciogenic sequence from the Early Pleistocene of the Central North Sea. Journal of Quaternary Science, 32(2), pp.145-168.

Bulat, J., Long, D. (2001). Images of the seabed in the Faroe-Shetland Channel from commercial 3D seismic data. Marine Geophysical Researches, v. 22, 345–367.

Bull, S., Cartwright, J., Huuse, M. (2009). A subsurface evacuation model for submarine slope failure. Basin Research, 21(4), 433-443.

Bungum, H., Hokland, B.K., Husebye, E.S., Ringdal, F. (1979). An exceptional intraplate earthquake sequence in Meloy, Northern Norway. Nature 280, 32–35. https://doi.org/10.1038/280032a0

Bungum, H., Alsaker, A., Kvamme, L.B., Hansen, R.A. (1991). Seismicity and seismotectonics of Norway and nearby continental shelf areas. J Geophys Res 96, 2249–2265. https://doi.org/10.1029/90jb02010

Bungum, H., Lindholm, C.D., Dahle, A., Woo, G., Nadim, F., Holme, J.K., Gudmestad, O.T., Hagberg, T., Karthigeyan, K. (2000). New seismic zoning maps for Norway, the North Sea, and the United Kingdom. Seismological research letters, 71, 687-697.

Bungum, H., Pettenati, F., Schweitzer, J., Sirovich, L., Faleide, J.I. (2009). The 23 October 1904 MS 5.4 Oslofjord Earthquake: Reanalysis Based on Macroseismic and Instrumental Data. Bull. Seismol. Soc. Am. 99, 2836–2854. https://doi.org/10.1785/0120080357

Bungum, H., Olesen, O., Pascal, C., Gibbons, S., Lindholm, C., VestØl, O. (2010). To what extent is the present seismicity of Norway driven by post-glacial rebound? J. Geol. Soc. 167, 373–384. https://doi.org/10.1144/0016-76492009-009

Bunkholt, H. S., Oftedal, B. T., Hansen, J. A., Løseth, H., Kløvjan, O. S. (2024). Trøndelag Platform and Halten–Dønna Terraces Composite Tectono-Sedimentary Element, Norwegian Rifted Margin, Norwegian Sea. Geological Society, London, Memoirs, 57(1), M57-2017.

Butt, F. A., Elverhøi, A., Solheim, A., & Forsberg, C. F. (2000). Deciphering Late Cenozoic development of the western Svalbard Margin from ODP Site 986 results. Marine Geology, 169(3-4), 373-390.

Butt, F. A., Drange, H., Elverhøi, A., Otterå, O. H., & Solheim, A. (2002). Modelling Late Cenozoic isostatic elevation changes in the Barents Sea and their implications for oceanic and climatic regimes: preliminary results. Quaternary Science Reviews, 21(14-15), 1643-1660.

Böttner, C., Berndt, C., Reinardy, B.T.I., Geersen, J., Karstens, J., Bull, J.M., Callow, B.J., Lichtschlag, A., Schmidt, M., Elger, J., Schramm, B., Haeckel, M. (2019). Pockmarks in the Witch Ground Basin, Central North Sea. Geochemistry, Geophys. Geosystems 20, 1698–1719. https://doi.org/https://doi.org/10.1029/2018GC008068

Böttner, C., Hoffmann, J. J., Unverricht, D., Schmidt, M., Spiegel, T., Geersen, J., ... & Schmidt, C. (2024). The enigmatic pockmarks of the sandy southeastern North Sea. Geochemistry, Geophysics, Geosystems, 25(11), e2024GC011837.

Bøe, R., Longva, O., Lepland, A., Blikra, L.H., Sønstegaard, E., Haflidason, H., Bryn, P., Lien, R. (2004) Postglacial mass movements and their causes in fjords and lakes in western Norway. Nor J Geol 84: 35-55.

Bøe, R., Prøsch-Danielsen, L., Lepland, A., Harbitz, C.B., Gauer, P., Løvholt, F., and Høgestøl, M. (2007). An early Holocene submarine slide in Boknafjorden and the effect of a slide-triggered tsunami on the Stone Age settlement at Rennesøy, SW Norway. Marine Geology, Vol. 243, 157-168.

Bünz, S., Mienert, J. (2004). Acoustic imaging of gas hydrate and free gas at the Storegga Slide, J. Geophys. Res., 109, B04102, doi:10.1029/2003JB002863.

Callard, S.L., Ó Cofaigh, C., Benetti, S., Chiverrell, R.C., Van Landeghem, K.J.J., Saher, M.H., Livingstone, S.J., Clark, C.D., Small, D., Fabel, D., Moreton, S.G. (2020). Oscillating retreat of the last

British-Irish Ice Sheet on the continental shelf offshore Galway Bay, western Ireland. Marine Geology, v. 420. https://doi.org/10.1016/j.margeo.2019.106087.

Callard, S.L., Ó Cofaigh, C., Benetti, S., Chiverrell, R.C., Van Landeghem, K.J.J., Saher, M.H., Gales, J.A., Small, D., Clark, C.D., Livingstone, S.J., Fabel, D., Moreton, S.G. (2018). Extent and retreat history of the Barra Fan Ice Stream offshore western Scotland and northern Ireland during the last glaciation. Quaternary Science Reviews, v. 201, 280-302. https://doi.org/10.1016/j.quascirev.2018.10.002

Callaway, A., Smyth, J., Brown, C.J., Quinn, R., Service, M., Long, D. (2009). The impact of scour processes on a smothered reef system in the Irish Sea. Estuar. Coast. Shelf Sci. 84, 409–418. https://doi.org/http://dx.doi.org/10.1016/j.ecss.2009.07.011

Callaway, A., Quinn, R., Brown, C.J., Service, M., Long, D., Benetti, S. (2011). The formation and evolution of an isolated submarine valley in the North Channel, Irish Sea: an investigation of Beaufort's Dyke. J. Quat. Sci. 26, 362–373. https://doi.org/10.1002/jqs.1460

Cameron, T.D.J., Stoker, M.S., Long, D. (1987) The history of Quaternary sedimentation in the UK sector of the North Sea Basin. Journal of the Geological Society of London, v. 144, 43–58.

Carbon Trust. (2016). Application Guide for the specification of the Depth of Lowering using the Cable Burial Risk Assessment (CBRA) methodology. Report. 51pp.

Carlsten, P. (2000). "Geotechnical properties of some Swedish peats." 13th Nordic Geotechnical Meeting (Nordiska Geoteknikermötet) NGM-2000, H. Rathmayer, ed., Finnish Geotechnical Society, Helsinki, Finland, Helsinki, Finland, 51-60.

Carlton, B.D., Skurtveit, E., Atakan, K., Kaynia, A.M. (2019a). Probabilistic seismic hazard analysis of a CO2 storage prospect using the NGA East ground motion models. In Proceedings of the SECED 2019 Conference, Greenwich, London, 9–10 September.

Carlton, B., Vanneste, M., Forsberg, C. F., Knudsen, S., Løvholt, F., Kvalstad, T., ... & Haflidason, H. (2019b). Geohazard assessment related to submarine instabilities in Bjørnafjorden, Norway. Geological Society, London, Special Publications, 477(1), 549–566.

Carlton, B., Shin, Y., Leoncino, V., Kaynia, A.M., (2021). Seismic Hazard Assessment for TNW Wind Farm Zone. NGI Report 20190798-03-TN. https://offshorewind.rvo.nl/files/view/629c2998-6429-4f85-86d6-767c680e0ad0/1638781502tnw_20211202_gm_ngi_seismic%20hazard%20assessment_rev0-f.pdf.

Carlton B., Barwise A., Kaynia A.M. (2022). Seismic Hazard Assessment for a Wind Farm Offshore England. Geotechnics 2(1):14-31. https://doi.org/10.3390/geotechnics2010002

Carlton B., Huang, C., Kettlety, T., Larsen, T. (2024). Development of a ground motion model and probabilistic seismic hazard analysis for the North Sea. SHARP Storage project deliverable 5.5.

Carr, S. (1999). The micromorphology of Last Glacial Maximum sediments in the Southern North Sea. Catena, Vol. 35, 123–145.

Cartelle, V., Barlow, N.L.M., Hodgson, D.M., Busschers, F.S., Cohen, K.M., Meijninger, B.M.L., van Kesteren, W.P. (2021). Sedimentary architecture and landforms of the late Saalian (MIS 6) ice sheet margin offshore of the Netherlands. Earth Surface Dynamics 9, 1399–1421. https://doi.org/10.5194/esurf-9-1399-2021

Carter, G.D.O., Birchall, R., Flint, A., Rose, M., Bellwald, B., Cotterill, C., Arlott, L., Wood, G. (2025). Formation and implications of glacially-derived gravel lag deposits; mapping a geo-constraint to shallow offshore infrastructure. 5th International Symposium on Frontiers in Offshore Geotechnics (ISFOG), Nantes, France.

Caruso, S., Maselli V., Rea, B., Spagnolo, M. (2022). Deep-water sedimentation processes on a glaciated margin: The Foula Wedge trough mouth fan, West of Shetland. Marine Geology 446, 106769. https://doi.org/10.1016/j.margeo.2022.106769.

Cassar, C.; Nicolas, M. Pouliquen, O. (2005). Submarine granular flows down inclined planes. Physics of Fluids 17: 103301, DOI 10.1063/1.2069864.

Castelltort, S., & Van Den Driessche, J. (2003). How plausible are high-frequency sediment supply-driven cycles in the stratigraphic record?. Sedimentary Geology, 157(1-2), 3-13.

Cesca, S., Dahm, T., Juretzek, C., Kühn, D. (2011). Rupture process of the 2001 May 7 Mw 4.3 Ekofisk induced earthquake: The Ekofisk induced earthquake. Geophys. J. Int. 187, 407–413. https://doi.org/10.1111/j.1365-246X.2011.05151.x

Chand, S., Mienert, J., Andreassen, K., Knies, J., Plassen, L., Fotland, B. (2008). Gas hydrate stability zone modelling in areas of salt tectonics and pockmarks of the Barents Sea suggests an active hydrocarbon venting system. Marine and Petroleum Geology, 25(7), 625-636.

Chand, S., Rise, L., Knies, J., Haflidason, H., Hjelstuen, B.O., Bøe, L. (2011). Stratigraphic development of the south Vøring Margin (Mid-Norway) since early Cenozoic time and its influence on subsurface fluid flow. Marine and Petreoleum Geology, 28(7), 1350-1363.

Chiverrell, R.C., Thrasher, I.M., Thomas, G.S.P., Lang, A., Scourse, J.D., van Landeghem, K.J.J., McCarroll, D., Clark, C.D., Ó Cofaigh, C., Evans, D.J.A., Ballantyne, C.K., 2013. Bayesian modelling the retreat of the Irish Sea Ice Stream. J. Quat. Sci. 28, 200–209. https://doi.org/10.1002/jqs.2616

Chiverrell, R.C., Smedley, R.K., Small, D., Ballantyne, C.K., Burke, M.J., Callard, S.L., Clark, C.D., Duller, G.A.T., Evans, D.J.A., Fabel, D., van Landeghem, K., Livingstone, S., Ó Cofaigh, C., Thomas, G.S.P., Roberts, D.H., Saher, M., Scourse, J.D., Wilson, P., 2018. Ice margin oscillations during deglaciation of the northern Irish Sea Basin. J. Quat. Sci. https://doi.org/10.1002/jqs.3057

Chiverrell, R.C., Thomas, G.S.P., Burke, M., Medialdea, A., Smedley, R., Bateman, M., Clark, C., Duller, G.A.T., Fabel, D., Jenkins, G., Ou, X., Roberts, H.M., Scourse, J., 2021. The evolution of the terrestrial-terminating Irish Sea glacier during the last glaciation. J. Quat. Sci. 36, 752–779. https://doi.org/https://doi.org/10.1002/jqs.3229

Churchyard, T., 1580. A warning for the wise. J, Allde and N. Ling, London.

Clare, M. A., Lichtschlag, A., Paradis, S., & Barlow, N. L. M. (2023). Assessing the impact of the global subsea telecommunications network on sedimentary organic carbon stocks. Nature Communications, 14(1), 2080. https://doi.org/10.1038/s41467-023-37854-6.

Clark, C. D., Hughes, A. L. C., Greenwood, S. L., Jordan, C. J., and Sejrup, H.P. (2012) Pattern and timing of retreat of the last British–Irish Ice Sheet. Quaternary Science Reviews, v. 44, 112–149.

Clark, C. D., Ely, J. C., Greenwood, S. L., Hughes, A. L. C., Meehan, R., Barr, I. D., Bateman, M. D., Bradwell, T., Doole, J., Evans, D. J. A., Jordan, C. J., Monteys, X., Pellicer, X. M., Sheehy, M. (2017). BRITICE Glacial Map, version 2: a map and GIS database of glacial landforms of the last British–Irish Ice Sheet. Boreas, Vol. 47,11–27.

Clark, C. D., Ely, J. C., Hindmarsh, R. C. A., Bradley, S., Ign´eczi, A., Fabel, D., Ó Cofaigh, C., Chiverrell, R. C., Scourse, J., Benetti, S., Bradwell, T., Evans, D. J. A., Roberts, D. H., Burke, M., Callard, S. L., Medialdea, A., Saher,M., Small, D., Smedley, R. K., Gasson, E., Gregoire, L., Gandy, N., Hughes, A. L. C., Ballantyne, C., Bateman, M. D., Bigg, G. R., Doole, J., Dove, D., Duller, G. A. T., Jenkins, G. T. H., Livingstone, S. L., McCarron, S., Moreton, S., Pollard, D., Praeg, D., Sejrup, H. P., van Landeghem, K. J. J. & Wilson, P. 2022 (October): Growth and retreat of the last British–Irish Ice Sheet, 31 000 to 15 000 years ago: the BRITICE-CHRONO reconstruction. Boreas, Vol. 51, pp.699–758. https://doi.org/10.1111/bor.12594. ISSN 0300-9483

Clarke, B. G. (2018). The engineering properties of glacial tills. Geotechnical Research, 5(4), 262–277. https://doi.org/10.1680/jgere.18.00020

Coco, G., Murray, A. B., & Green, M. O. (2007a). Sorted bed forms as self-organized patterns: 1. Model development. Journal of Geophysical Research: Earth Surface, 112(F3), 3015. https://doi.org/10.1029/2006JF000665

Coco, G., Murray, A. B., Green, M. O., Thieler, E. R., & Hume, T. M. (2007b). Sorted bed forms as self-organized patterns: 2. Complex forcing scenarios. Journal of Geophysical Research: Earth Surface, 112(F3). https://doi.org/10.1029/2006JF000666

Collinson, J. (2005). SEDIMENTARY PROCESSES | Depositional Sedimentary Structures. Encyclopedia of Geology, 593–602. https://doi.org/10.1016/B0-12-369396-9/00466-4

Cooke, F., Plaza-Faverola, A., Bünz, S., Sultan, N., Ramachandran, H., Bedle, H., ... & Knies, J. (2023). Sedimentary deformation relating to episodic seepage in the last 1.2 million years: a multi-scale seismic study from the Vestnesa Ridge, eastern Fram Strait. Frontiers in Earth Science, 11, 1188737.

Cooke, F., Plaza-Faverola, A., Bünz, S., De Groot, P., & Peacock, D. C. (2025). Semiautomated analysis of faults with meter-scale displacements and networks of planar features using high-resolution 3D seismic data to investigate gas leakage at the Vestnesa Ridge, Eastern Fram Strait. Interpretation, 13(1), B1-B23.

Coquerel, J., (1580). Discours d'une merveilleuse et veritable copie du grand deluge et debordemēt de la mer, avec le nom des lieux et places qui ont esté submergez et le nombre des navires qui ont esté peris entre Douvre&Calais,&autres lieux, le vi. et vii. jour d'Avril, 1580, Paris.

Cotterill, C. J., Phillips, E., James, L., Forsberg, C. F., Tjelta, T. I., Carter, G., & Dove, D. (2017). The evolution of the Dogger Bank, North Sea: A complex history of terrestrial, glacial and marine environmental change. Quaternary Science Reviews, 171, 136–153. https://doi.org/10.1016/j.quascirev.2017.07.006

Coughlan, M., Fleischer, M., Wheeler, A.J., Hepp, D.A., Hebbeln, D., Mörz, T., 2018. A revised stratigraphical framework for the Quaternary deposits of the German North Sea sector: a geological-geotechnical approach. Boreas 47. https://doi.org/10.1111/bor.12253

Coughlan, M., Tóth, Z., Van Landeghem, K.J.J., McCarron, S., Wheeler, A.J., 2020a. Formational history of the Wicklow Trough: a marine-transgressed tunnel valley revealing ice flow velocity and retreat rates for the largest ice stream draining the late-Devensian British–Irish Ice Sheet. J. Quat. Sci. 00, 1–13. https://doi.org/10.1002/jqs.3234

Coughlan, M, Long, M., Doherty, P., 2020b. Geological and geotechnical constraints in the Irish Sea for offshore renewable energy. Journal of Maps, v. 16, 420–431. https://doi.org/10.1080/17445647.2020.1758811

Coughlan, M, Guerrini, M., Creane, S., O'Shea, M., Ward, S.L., Van Landeghem, K.J.J., Murphy, J., Doherty, P., 2021a. A new seabed mobility index for the Irish Sea: Modelling seabed shear stress and classifying sediment mobilisation to help predict erosion, deposition, and sediment distribution. Cont. Shelf Res. 229, 104574. https://doi.org/10.1016/j.csr.2021.104574

Coughlan, M., Roy, S., O'Sullivan, C., Clements, A., O'Toole, R., Plets, R., 2021. Geological settings and controls of fluid migration and associated seafloor seepage features in the north Irish Sea. Mar. Pet. Geol. 123. https://doi.org/10.1016/j.marpetgeo.2020.104762

Coughlan, M., Trafford, A., Corrales, S., Donohue, S., Wheeler, A.J., Long, M., 2023. Geological and geotechnical characterisation of soft Holocene marine sediments: A case study from the north Irish Sea. Eng. Geol. 313, 106980. https://doi.org/10.1016/j.enggeo.2022.106980

Cox, D.R., Knutz, P.C., Campbell, D.C., Hopper, J.R., Newton, A.M.W, Huuse, M. and Gohl, K., 2020. Geohazard detection using 3D seismic data to enhance offshore scientific drilling site selection. Scientific Drilling, 28, pp.1-27.

Creane, S., Coughlan, M., O'Shea, M., & Murphy, J. (2022). Development and Dynamics of Sediment Waves in a Complex Morphological and Tidal Dominant System: Southern Irish Sea. Geosciences, 12(12), 431. https://doi.org/10.3390/geosciences12120431

Creane, S., O'Shea, M., Coughlan, M., Murphy, J., 2023a. Hydrodynamic Processes Controlling Sand Bank Mobility and Long-Term Base Stability: A Case Study of Arklow Bank. Geosci. 13. https://doi.org/10.3390/geosciences13020060

Creane, S., O'Shea, M., Coughlan, M., Murphy, J., 2023b. Morphological Modelling to Investigate the Role of External Sediment Sources and Wind and Wave-Induced Flow on Sand Bank Sustainability: An Arklow Bank Case Study. J. Mar. Sci. Eng. 11. https://doi.org/10.3390/jmse11102027

Croker, P.F., Kozachenko, M., Wheeler, A.J., 2005. Gas-Related Seabed Structures in the Western Irish Sea (IRL-SEA6).

Cunningham, J., Cardozo, N., Townsend, C., and Callow, R., 2020, The impact of seismic interpretation methods on the analysis of faults: a case study from the Snøhvit field, Barents Sea: Solid Earth Discussions, v. 2020, p. 1-48.

Dade, W. B. and Huppert, H. E. (1994). Predicting the geometry of channelized deep-sea turbidites, Geol. 22: 645–648, DOI 10.1130/0091-7613(1994)022<0645:ptgocd>2.3.co;2.

Dahm, T., Cesca, S., Hainzl, S., Braun, T., Krüger, F., 2015. Discrimination between induced, triggered, and natural earthquakes close to hydrocarbon reservoirs: A probabilistic approach based on the modeling of depletion-induced stress changes and seismological source parameters. J. Geophys. Res. Solid Earth 120, 2491–2509. https://doi.org/10.1002/2014JB011778

Danish Maritime Authority (2023). Maritime spatial plan. https://www.dma.dk/growth-and-framework-conditions/maritime-spatial-plan . Accessed April 2025.

Davies, R. J., Swarbrick, R. E., Evans, R. J. & Huuse, M., 2007. Birth of a mud volcano: East Java, 29 May 2006. GSA Today: v. 17, no. 2, doi: 10.1130/GSAT01702A.1

Davis, A. M. (1992). Shallow gas: an overview. Continental shelf research, 12(10), 1077-1079.

Davison, S., 2004. Reconstructing the Last Pleistocene (Late Devensian) Glaciation on the Continental Margin of Northwest Britain. Ph.D. Thesis. The University of Edinburgh.

Dawson, A.G., Long, D., Smith, D.E., 1988. The Storegga Slides: evidence from eastern Scotland for a possible tsunami. Marine Geology 82, 271–276.

Dawson, A.G., Long, D., Smith, D.E., Shi, S., Foster, I.D.L., 1993. Tsunamis in the Norwegian Sca and North Sea caused by the Storegga submarine landslides, in: Tinti, S. (Ed.), Tsunamis in the World. Kluwer Academic Publishers, The Netherlands, pp. 31 -42.

Dawson, S., Smith, D.E., Ruffman, A., Shi, S., 1996. The diatom biostratigraphy of tsunami sediments: Examples from recent and middle holocene events. Physics and Chemistry of the Earth 21, 87-92.

De Blasio, F. V.; Issler, D.; Elverhøi, A.; Harbitz, C. B.; Ilstad, T.; Bryn, P.; Lien, R. and Løvholt, F. (2003). Dynamics, velocity and run-out of the giant Storegga slide. In: Submarine Mass Movements and Their Consequences, Locat, J. and Mienert, J. (eds.), Adv. Natural Technol. Hazards Res. 19 : 223–230, DOI 10.1007/978-94-010-0093-2_25.

De Blasio, F. V., Engvik, L.,Harbitz, C. B. and Elverhøi, A. (2004). Hydroplaning and submarine debris flows. Journal of Geophysical Research 109, C01002, DOI 10.1029/2002JC001714.

De Blasio F. V., Elverhøi A., Issler D., Harbitz C. B., Bryn P,, and Lien R. (2005) On the dynamics of subaqueous clay rich gravity mass flows—the giant Storegga slide, Norway. In: Ormen Lange –– an Integrated Study for Safe Field Development in the Storegga Submarine Area, pp. 179–186. Elsevier.

De Blasio, F.V., Elverhøi, A., Engvik, L., Issler, D., Gauer, P., and Harbitz, C. B. (2006). Understanding the high mobility of subaqueous debris flows. Norwegian Journal of Geology 86, 275–284.

De Falco, G., Budillon, F., Conforti, A., Di Bitetto, M., Di Martino, G., Innangi, S., Simeone, S., & Tonielli, R. (2015). Sorted bedforms over transgressive deposits along the continental shelf of western Sardinia (Mediterranean Sea). Marine Geology, 359, 75–88. https://doi.org/10.1016/j.margeo.2014.11.008

de Jonge-Anderson, I., & Underhill, J. R. (2022). Use of subsurface geology in assessing the optimal co-location of CO2 storage and wind energy sites. Earth Science, Systems and Society, 2(1), 10055.

Den Haan, E. J., and Kruse, G. A. M. (2007). "Characterisation and engineering properties of Dutch peats." Characterisation and Engineering Properties of Natural Soils, T. S. Tan, K. K. Phoon, D. W. Hight, and S. Leroueil, eds., Taylor and Francis Group, London, Singapore, 2101-2133.

Diesing, M., Ware, S., Foster-Smith, R., Stewart, H., Long, D., Vanstaen, K., Forster, R., & Morando, A. (2009). Understanding the marine environment – seabed habitat investigations of the Dogger Bank offshore draft SAC. Joint Nature Conservation Committee, Peterborough. JNCC Report No. 429, 89pp., 5 Appendices.

Diesing, M., Kröger, S., Parker, R., Jenkins, C., Mason, C., Weston, K., 2017. Predicting the standing stock of organic carbon in surface sediments of the North–West European continental shelf. Biogeochemistry 135, 183–200. https://doi.org/10.1007/s10533-017-0310-4

Dimakis, P., Braathen, B. I., Faleide, J. I., Elverhøi, A., & Gudlaugsson, S. T. (1998). Cenozoic erosion and the preglacial uplift of the Svalbard–Barents Sea region. Tectonophysics, 300(1-4), 311-327.

Dimakis, P., Elverhøi, A., Høeg, K., Solheim, A., Harbitz, C.B., Laberg, J.S., Vorren, T., and Marr, J. (2000). Submarine slope stability on high-latitude glaciated Svalbard–Barents Sea margin. Marine Geology, Vol. 162, No. 2–4, 303–316.

Dimmock, P. S., Riera, R., Tam, T. A., & Boylan, N. (2023, January). Geohazard or Geo-engineering constraint?. In Offshore Site Investigation Geotechnics 9th International Conference Proceeding (Vol. 2067, No. 2071, pp. 2067-2071). Society for Underwater Technology.

Dix, J. K., Riera, R., Dimmock, P., Barwise, A., & Arlott, L. (n.d.). Sorted bedforms implications for offshore renewable infrastructure. 9th International SUT Offshore Site Investigation Geotechnics Conference Proceedings "Innovative Geotechnologies for Energy Transition," 643–650. https://doi.org/10.3723/MLPJ7639

DNV, D. N. V. (2014). DNV-RP-J301: Subsea power cables in shallow water renewable energy applications. Høvik, Oslo, Norway.

Donovan, S.K., Pickerill, R.K., 1997. Dropstones: their origin and significance: a comment. Palaeogeography, Palaeoclimatology, Palaeoecology 131, 175–178. https://doi.org/10.1016/S0031-0182(96)00150-2

Dove, D., Evans, D.J.A., Lee, J.R., Roberts, D.H., Tappin, D.R., Mellett, C.L., Long, D., Callard, S.L. (2017). Phased occupation and retreat of the last British–Irish Ice Sheet in the southern North Sea; geomorphic and seismostratigraphic evidence of a dynamic ice lobe. Quaternary Science Reviews, v. 163, 114–134.

Dowdeswell, J.A., Ottesen, D., and Rise, L., 2010, Rates of sediment delivery from the Fennoscandian Ice Sheet through an ice age: Geology, v. 38, p. 3–6, https://doi.org/10.1130/G25523.1.

Dowdeswell, J. A., & Ottesen, D. (2013). Buried iceberg ploughmarks in the early Quaternary sediments of the central North Sea: a two-million year record of glacial influence from 3D seismic data. Marine Geology, 344, 1-9.

Dowdeswell, J. A., Canals, M., Jakobsson, M., Todd, B. J., Dowdeswell, E. K., & Hogan, K. A. (2016). The variety and distribution of submarine glacial landforms and implications for ice-sheet reconstruction. Geological Society, London, Memoirs, 46(1), 519-552.

Durán, R., Guillén, J., Muñoz, A., Durán, R., Guillén, Á. J., & Muñoz, A. (2017). Sorted Bedforms Developed on Sandy Deposits Derived from Small Ephemeral Streams (Catalan Continental Shelf). Atlas of Bedforms in the Western Mediterranean, 127–133. https://doi.org/10.1007/978-3-319-33940-5_21

Dyer, K. R., & Huntley, D. A. (1999). The origin, classification and modelling of sand banks and ridges. Continental Shelf Research, 19(10), 1285–1330. https://doi.org/10.1016/S0278-4343(99)00028-X

Dyer, J. M. (2011). Geohazard identification: the gap between the possible and reality in geophysical surveys for the engineering industry. Marine Geophysical Researches, Vol. 32, 37–47.

Dück, Y., Lorke, A., Jokiel, C., Gierse, J., 2019. Laboratory and field investigations on freeze and gravity core sampling and assessment of coring disturbances with implications on gas bubble characterization. Limnol. Oceanogr. Methods 17, 585–606. https://doi.org/10.1002/lom3.10335

Eaton, S.J., Hodgson, D.M., Barlow, N.L.M., Mortimer, E.E.J., Mellett, C.L., 2020. Palaeogeographical changes in response to glacial–interglacial cycles, as recorded in Middle and Late Pleistocene seismic stratigraphy, southern North Sea. Journal of Quaternary Science 35, 760–775. https://doi.org/10.1002/jqs.3230

Eaton, S., N. L. M. Barlow, D. M. Hodgson, C. L. Mellet, and A. R. Emery (2024). Landscape evolution during Holocene transgression of a mid-latitude low-relief coastal plain: The southern North Sea, Earth Surface Processes and Landforms, 49, 3139–3157, doi:https://doi.org/10.1002/esp.5880.

Eglit, M. E.; Yakubenko, A. and Zayko, J. (2020). A review of Russian snow avalanche models — from analytical solutions to novel 3D models, Geosciences 10: 77, DOI 10.3390/geosciences10020077.

Eidvin, T., Bugge, T. & Smelror, M., 2007: The Molo Formation, deposited by coastal progradation on the inner Mid-Norwegian continental shelf, coeval with the Kai Formation to the west and the Utsira Formation in the North Sea. Norwegian Journal of Geology 87, 75–142.

Eigaard, O.R., Bastardie, F., Hintzen, N.T., Buhl-Mortensen, L., Buhl-Mortensen, P., Catarino, R., Dinesen, G.E., Egekvist, J., Fock, H.O., Geitner, K., Gerritsen, H.D., González, M.M., Jonsson, P., Kavadas, S., Laffargue, P., Lundy, M., Gonzalez-Mirelis, G., Nielsen, J.R., Papadopoulou, N., Posen,

4741 P.E., Pulcinella, J., Russo, T., Sala, A., Silva, C., Smith, C.J., Vanelslander, B., Rijnsdorp, A.D., 2017.
4742 The footprint of bottom trawling in European waters: distribution, intensity, and seabed integrity. ICES
4743 J. Mar. Sci. 74, 847–865. https://doi.org/10.1093/icesjms/fsw194

4744 Ekman, S.R., Scourse, J.D. (1993) Early and Middle Pleistocene pollen stratigraphy from British
4745 Geological Survey Borehole 81/26, Fladen Ground, central North Sea. Review of Palaeobotany and
4746 Palynology, v. 79, 285–295.

4747 Eldholm, O., and Bungum, H. (2021). Potential secondary events caused by early Holocene
4748 paleoearthquakes in Fennoscandia – a climate-related review. Norwegian Journal of Geology 101,
4749 202108. https://dx.doi.org/10.17850/njg101-2-3

4750 Elger, J., Berndt, C., Krastel, S., Piper, D.J.W., Gross, F., Geissler, W.H., 2017. Chronology of the Fram
4751 Slide Complex offshore NW Svalbard and its implications for local and regional slope stability, Marine
4752 Geology, Volume 393, 141-155, https://doi.org/10.1016/j.margeo.2016.11.003.

4753 Ellis, J.R., Milligan, S.P., Readdy, L., Taylor, N. and Brown, M.J. 2012. Spawning and nursery grounds
4754 of selected fish species in UK waters. Sci. Ser. Tech. Rep., Cefas Lowestoft, 147: 56pp

4755 Elverhøi, A., & Solheim, A. (1983). The Barents Sea ice sheet – a sedimentological discussion. Polar
4756 Research, 1(1), 23-42.

4757 Elverhøi, A.; De Blasio, F. V.; Butt, F. A.; Issler, D.; Harbitz, C. B.; Engvik, L.; Solheim A. and Marr,
4758 J. (2002). Submarine mass-wasting on glacially influenced continental slopes—processes and
4759 dynamics. In: Glacier-Influenced Sedimentation on High-Latitude Continental Margins, Dowdeswell,
4760 J. A. and Ó Cofaigh, C. (eds.), Special Publications, No. 203, Geological Society of London: London,
4761 U.K., pp. 73–87, DOI 10.1144/gsl.sp.2002.203.01.05.

4762 Elverhøi A, Issler D, De Blasio FV, Ilstad T, Harbitz CB, and Gauer P (2005). Emerging insights into
4763 the dynamics of submarine debris flows. Natural Hazards and Earth System Sciences 5(5): 633–648,
4764 DOI 10.5194/nhess-5-633-2005.

4765 Elverhøi, A., Breien, H., De Blasio, F.V., Harbitz, C.B., and Pagliardi, M. (2010). Submarine landslides
4766 and the importance of the initial sediment composition for run-out length and final deposit. 70th
4767 anniversary of Prof. B. N. Gjevik. Ocean Dynamics Special Issue 60(4): 1027–1046, DOI
4768 10.1007/s10236-010-0317-z.

4769 Emery, A. R., Hodgson, D. M., Barlow, N. L. M., Carrivick, J. L., Cotterill, C. J., Mellett, C. L., &
4770 Booth, A. D. (2019). Topographic and hydrodynamic controls on barrier retreat and preservation: An
4771 example from Dogger Bank, North Sea. Marine Geology, 416.
4772 https://doi.org/10.1016/j.margeo.2019.105981

Engen, Ø., Eldholm, O., Bungum, H., 2003. The Arctic plate boundary. J. Geophys. Res. - Solid Earth 108, 2075+. https://doi.org/10.1029/2002jb001809

Esposti Ongaro, T., de'Michieli Vitturi, M., Cerminara, M., Fornaciai, A., Nannipieri, L., Favalli, M., Calusi, B., Macías, J., Castro, M.J., Ortega, S., González-Vida, J.M., and Escalante, C. (2021). Modeling tsunamis generated by submarine landslides at Stromboli Volcano (Aeolian Islands, Italy): A numerical benchmark study. Frontiers in Earth Science, 9, 628652.

Evans, D., Graham, C., Armour, A. & Bathurst, P. (editors) 2003. The Millennium Atlas: Petroleum Geology of the Central and Northern North Sea. 389 pp. London, Bath: Geological Society of London. ISBN 1 86239 119 X.

Evans, D., Harrison, Z., Shannon, P.M., Laberg, J.S., Nielsen, T., Ayers, S., Holmes, R., Hoult, R.J., Lindberg, B., Haflidason, H., Long, D., Kuijpers, A., Andersen, E.S., and Bryn, P., 2005, Palaeoslides and other mass failures of Pliocene to Pleistocene age along the Atlantic continental margin of NW Europe: Marine and Petroleum Geology, v. 22, p. 1131-1148. https://doi.org/10.1016/j.marpetgeo.2005.01.010.

Evans, D.J.A., Roberts, D.H., Bateman, M.D., Clark, C.D., Medialdea, A., Callard, S.L., Grimoldi, E., Chiverrell, R.C., Ely, J.C., Dove, D., O' Cofaigh, C., Saher, M., Bradwell, T., Moreton, S.G., Fabel, D., Bradley S.L. (2021) Retreat dynamics of the eastern sector of the British–Irish Ice Sheet during the last glaciation. Journal of Quaternary Science, 1-29.

Eyles, N. (Ed.). (2013). Glacial geology: an introduction for engineers and earth scientists. Elsevier.

Eyles, C.H., Eyles, N., 2010. Glacial Deposits, in: Facies Models 4. The Geological Association of Canada, Ontario, pp. 73–104.

Faleide, J. I., Solheim, A., Fiedler, A., Hjelstuen, B. O., Andersen, E. S., & Vanneste, K. (1996). Late Cenozoic evolution of the western Barents Sea-Svalbard continental margin. Global and Planetary Change, 12(1-4), 53-74.

Faleide, J. I., P. W. Wong, M. Hassaan, R. H. Gabrielsen, M. M. Abdelmalak, S. Planke, F. Tsikalas, B. Manton, and R. Myklebust (2025), West Barents Sheared Margin Composite Tectono-Sedimentary Element, Norwegian–Greenland Sea and Fram Strait, Geological Society, London, Memoirs, 57(1), M57-2023-2019.

Faleide, T. S., Midtkandal, I., Planke, S., Corseri, R., Faleide, J. I., Serck, C. S., and Nystuen, J. P., 2019, Characterisation and development of Early Cretaceous shelf platform deposition and faulting in the Hoop area, southwestern Barents Sea—constrained by high-resolution seismic data: Norwegian Journal of Geology, v. 99, no. 3, p. 1-20.

Fejerskov, M., and Lindholm, C. (2000). Crustal stress in and around Norway: an evaluation of stress generating mechanisms. Geological Society, London, Special Publications, 167, 451–467.

Fenster, M.S. (2018). Offshore Sand Sheets. In: Finkl, C., Makowski, C. (eds) Encyclopedia of Coastal Science . Encyclopedia of Earth Sciences Series. Springer, Cham. https://doi.org/10.1007/978-3-319-48657-4_236-2

Fjeldskaar, W., & Amantov, A. (2018). Effects of glaciations on sedimentary basins. Journal of Geodynamics, 118, 66-81.

Fleischer, M., Abegunrin, A., Hepp, D.A., Kreiter, S., Coughlan, M., Mörz, T., 2023. Stratigraphic and geotechnical characterization of regionally extensive and highly competent shallow sand units in the southern North Sea. Boreas 52, 78–98. https://doi.org/10.1111/bor.12595

Forterre, Y. and Pouliquen, O. (2009). Granular flows. Sémin. Poincaré XIII: 69–100, DOI 10.1007/978-3-0348-0084-6_4.

Forsberg, C. F., Plank, S., Tjelta, T. I., Svano, G., Strout, J. M., & Svensen, H. (2007, September). Formation of pockmarks in the Norwegian Channel. In SUT Offshore Site Investigation and Geotechnics (pp. SUT-OSIG). SUT.

Forterre, Y. and Pouliquen, O., 2009. Granular flows. Séminaire Poincaré XIII: 69–100. DOI 10.1007/978-3-0348-0084-6_4.

Fraccarollo, L. and Capart, H. (2002). Riemann wave description of erosional dam-break flows. Journal of Fluid Mechanics 461: 183–228, DOI 10.1017/S0022112002008455.

Fugro Engineering Services. (2013). Burbo Bank Extension Offshore Wind Farm; Geotechnical Site Investigation. C1516/G2667/N1220016U. 2078pp.

Fugro, 2017. Microbial Influenced Corrosion. Hollandse Kust (zuid) Wind Farm Zone. Technical Note for Rijksdienst voor Ondernemend Nederland (RVO). 24 pp.

Fugro, 2024. Report no 2, 2D UHRS Survey Geomodel Integrated with CPT Data, Full Site, Danish Offshore Wind 2030, North Sea 1, Denmark, F217715-REP-002 [03], 222 pp.

Fyfe, J. A., Long, D., Evans, D. (1993). United Kingdom offshore regional report: the geology of the Malin-Hebrides sea area. London: HMSO for the British Geological Survey.

Garcia, A. M., Bellwald, B., Planke, S., Anell, I., Myklebust, R., Sternai, P., & Midtkandal, I. (2024). Sedimentation record of a complete glacial-interglacial cycle: Down-slope deposits, contourites and plumites of the North Sea trough mouth fan. Quaternary Science Reviews, 339, 108839.

Gatliff, R.W., Richards, P.C., Smith, K., Graham, C.C., McCormac, M., Smith, N.J.P., Long, D., Cameron, T.D.J., Evans, D., Stevenson, A.G., Bulat, J., Ritchie, J.D. (1994) UK Offshore Regional Report: the Geology of the Central North Sea. London: HMSO for the British Geological Survey.

Gatter, R., et al., 2020. A multi-disciplinary investigation of the AFEN Slide: the relationship between contourites and submarine landslides. From: Georgiopoulou, A., Amy, L. A., Benetti, S., Chaytor, J. D., Clare, M. A., Gamboa, D., Haughton, P. D. W., Moernaut, J. and Mountjoy, J. J. (eds) 2020. Subaqueous Mass Movements and their Consequences: Advances in Process Understanding, Monitoring and Hazard Assessments. Geological Society, London, Special Publications, 500, https://doi.org/10.1144/SP500-2019-184.

Gatter, R., Clare, M. A., Kuhlmann, J., & Huhn, K. (2021). Characterisation of weak layers, physical controls on their global distribution and their role in submarine landslide formation. Earth-Science Reviews, 223, 103845.

Gauer, P. and Issler, D. (2004). Possible erosion mechanisms in snow avalanches. Annals of Glaciology 32: 384–392, DOI 10.3189/172756404781815068.

Gauer P, Kvalstad TJ, Forsberg CF, Bryn P, and Berg K (2005). The last phase of the Storegga slide: Simulation of retrogressive slide dynamics and comparison with slide-scar morphology. Marine and Petroleum Geology 22(1–2): 171–178. DOI 10.1016/j.marpetgeo.2004.10.004.

Gauer, P.; Elverhøi, A.; Issler, D. and De Blasio, F. V. (2006). On numerical simulations of subaqueous slides: Back-calculations of laboratory experiments of clay-rich slides. Norwegian Journal of Geology 86(3): 295–300.

Gaume, J.; van Herwijnen, A.; Gast, T.; Teranc, J. and Jiang, C. (2019). Investigating the release and flow of snow avalanches at the slope-scale using a unified model based on the material point method. Cold Regions Science and Technology 168: 102847, DOI 10.1016/j.coldregions.2019.102847.

GdR MiDi (Groupement de Recherche Milieux Divisés), 2004. On dense granular flows. The European Physical Journal E 14:340–365. DOI 10.1140/epje/i2003-10153-0.

GEBCO Compilation Group (2024) GEBCO 2024 Grid (doi:10.5285/1c44ce99-0a0d-5f4f-e063-7086abc0ea0f)

Gibbons, S.J., Bøttger Sørensen, M., Harris, D.B., Ringdal, F., 2007. The detection and location of low magnitude earthquakes in northern Norway using multi-channel waveform correlation at regional distances. Phys. Earth Planet. Inter. 160, 285–309. https://doi.org/10.1016/j.pepi.2006.11.008

Giglio, C., Benetti, S., Sacchetti, F., Lockhart, E., Hughes Clarke, J., Plets, R., Van Landeghem, K., Ó Cofaigh, C., Scourse, J., Dunlop, P., 2021. A Late Pleistocene channelized subglacial meltwater system

on the Atlantic continental shelf south of Ireland. Boreas 51, 118–135. https://doi.org/10.1111/bor.12536

Giglio, C., Benetti, S., Plets, R.M.K., Dunlop, P., Ó Cofaigh, C., Sacchetti, F., Salomon, E., 2022a. Character of advance and retreat of the southwest sector of the British-Irish Ice Sheet during the last glaciation. Quat. Sci. Rev. 291, 107655. https://doi.org/10.1016/j.quascirev.2022.107655

Giles, D.P., (2020a). Introduction to Geological Hazards in the UK: Their Occurrence, Monitoring and Mitigation. Geological Society, London, Engineering Geology Special Publications, 29, 1-41.

Giles, D. P. (2020b). Quick clay behaviour in sensitive Quaternary marine clays–a UK perspective.

Glimsdal, S., Pedersen, G.K., Harbitz, C.B., and Løvholt, F. (2013). Dispersion of tsunamis: does it really matter? Nat. Hazards Earth Syst. Sci., 13, 1507-1526, doi: 10.5194/nhess-13-1507-2013.

Goldfinger, C. (2011). Submarine paleoseismology based on turbidite records. Annual Review of Marine Science, 3(1), 35-66.

Goldstein, E. B., Murray, A. B., & Coco, G. (2011). Sorted bedform pattern evolution: Persistence, destruction and self-organized intermittency. Geophysical Research Letters, 38(24). https://doi.org/10.1029/2011GL049732

Golledge, N.R., Stoker, M.S. (2006) A palaeo-ice stream of the British Ice Sheet in eastern Scotland. Boreas, v. 35, 231–243.

Goswami, B. K., Weitemeyer, K. A., Minshull, T. A., Sinha, M. C., Westbrook, G. K., Chabert, A., ... & Ker, S. (2015). A joint electromagnetic and seismic study of an active pockmark within the hydrate stability field at the Vestnesa Ridge, West Svalbard margin. Journal of Geophysical Research: Solid Earth, 120(10), 6797-6822.

Graham, A.G.C., Lonergan, L., Stoker, M.S. (2009) Seafloor glacial features reveal the extent and decay of the last British Ice Sheet, east of Scotland. Journal of Quaternary Science, v. 24, 117–138.

Graham, A.G.C. Stoker, M.S., Lonergan, L., Bradwell, T. & Stewart, M.A,. 2011. Chapter 21-ThePleistocene Glaciations of the North Sea Basin. Developments of Quaternary Science, Vol 15, 261-278.

Gray, J. M. N. T. (2001). Granular flow in partially filled slowly rotating drums. Journal of Fluid Mechanics 441: 1–29, DOI 10.1017/S0022112001004736.

Gray, J. M. N. T.; Tai, Y.-C. and Noelle, S. (2003). Shock waves, dead-zones and particle-free regions in rapid granular free surface flows. Journal of Fluid Mechanics 491: 161–181, DOI 10.1017/s0022112003005317.

Greenwood, S. L., Clason, C. C., Nyberg, J., Jakobsson, M., & Holmlund, P. (2017). The Bothnian Sea ice stream: early Holocene retreat dynamics of the south-central Fennoscandian Ice Sheet. Boreas, 46(2), 346-362.

Greenwood, S. L., Avery, R. S., Gyllencreutz, R., Regnéll, C., & Tylmann, K. (2024). Footprint of the Baltic Ice Stream: geomorphic evidence for shifting ice stream pathways. Boreas, 53(1), 4-26.

Gregersen, S., Basham, P. W., and Wood, R. M., 1989, Fifty million years of 'passive margin'deformation in North West Europe: Earthquakes at North-Atlantic passive margins: neotectonics and postglacial rebound, p. 7-36.

Griffiths, J. S., & Martin, C. J. (Eds.). 2017. Engineering Geology and Geomorphology of Glaciated and Periglaciated Terrains. London, UK: Geological Society of London.

Grimstad E, Nesdal S (1990) The Loen rockslides—a historical review. In: Barton M, Stephanson W (eds) Rock joints. Balkema, Rotterdam, pp 1–6

Groupement de Recherche Milieux Divisés (2004). On dense granular flows. Eur. J. Phys. E 14(4) : 340–365, DOI 10.1140/epje/i2003-10153-0.

Grünthal, G., Stromeyer, D., Bosse, C. Cotton, F. & Bindi, D. (2018). The probabilistic seismic hazard assessment of Germany — version 2016, considering the range of epistemic uncertainties and aleatory variability. Bulletin of Earthquake Engineering, 16, p. 4339-4395.

Guazzelli, É. and Pouliquen, O. (2018). Rheology of dense granular suspensions. Journal of Fluid Mechanics 852: P1, DOI 10.1017/jfm.2018.548.

Gudmundsson, A., 1999, Postglacial crustal doming, stresses and fracture formation with application to Norway: Tectonophysics, v. 307, no. 3-4, p. 407-419.

Guillet, L.; Blatny, L.; Trottet, B.; Steffen, D. and Gaume, J. (2023). A depth-averaged Material Point Method for shallow landslides: Applications to snow slab avalanche release. Journal of Geophysical Research – Earth Surface 128: e2023JF007092, DOI 10.1029/2023JF007092.

Guinan, J., McKeon, C., O'Keeffe, E., Monteys, X., Sacchetti, F., Coughlan, M., Nic Aonghusa, C., 2020. INFOMAR data supports offshore energy development and marine spatial planning in the Irish offshore via the EMODnet Geology portal. Q. J. Eng. Geol. Hydrogeol. 54, qjegh2020-033. https://doi.org/10.1144/qjegh2020-033

Gupta, S., Collier, J. S., Palmer-Felgate, A., & Potter, G. (2007). Catastrophic flooding origin of shelf valley systems in the English Channel. Nature, 448(7151), 342-345.

Haflidason, H., Sejrup, H. P., Berstad, I. M., Nygård, A., Richter, T., Bryn, P., ... & Berg, K. (2003). A weak layer feature on the Northern Storegga Slide escarpment. European Margin Sediment Dynamics: side-scan sonar and seismic images, 55-62.

Haflidason, H., Lien, R., Sejrup, H.P., Forsberg, C.F., Bryn, P., 2005. The dating and morphometry of the Storegga Slide. Marine and Petroleum Geology 22, 123–136, DOI 10.1016/j.marpetgeo.2004.10.008.

Hall, A., & van Boeckel, M. (2020). Origin of the Baltic Sea basin by Pleistocene glacial erosion. Gff, 142(3), 237-252.

Hall, A. M., Merritt, J., W., Connel, E. R., Hubbard, A., 2019. Early and Middle Pleistocene environments, landforms and sediments in Scotland. Earth and Environmental Science Transactions of the Royal Society of Edinburgh, 110, 5–37, https://doi.org/10.1017/S1755691018000713.

Hammack JL (1973) A note on tsunamis: Their generation and propagation in an ocean of uniform depth. Journal of Fluid Mechanics 60(4): 769–799.

Hanebuth, T.J.J., Lantzsch, H., Nizou, J., 2015. Mud depocenters on continental shelves—appearance, initiation times, and growth dynamics. Geo-Marine Lett. 35, 487–503. https://doi.org/10.1007/s00367-015-0422-6

Hansen, J., Sato, M., Russell, G., & Kharecha, P. (2013). Climate sensitivity, sea level and atmospheric carbon dioxide. Philosophical Transactions of the Royal Society A: Mathematical, Physical and Engineering Sciences, 371(2001), 20120294.

Harbitz, C. (1992). Model Simulations of Tsunamis Generated by the Storegga Slides. Marine Geology, Vol. 104.

Harbitz, C., Pedersen, G. and Gjevik, B. (1993). Numerical Simulations of Large Water Waves Due to Landslides. Jour. of Hydr. Eng., Vol. 119, No. 12.

Harbitz, C. B., Parker, G., Elverhøi, A., Marr, J.G., Mohrig, D., and Harff, P.A. (2003). Hydroplaning of subaqueous debris flows and glide blocks: Analytical solutions and discussion. Journal of Geophysical Research 108(B7), 2349–2366, DOI:10.1029/2001JB001454.

Harbitz, C.B., Glimsdal, S., Løvholt, F., Pedersen, G.K., Vanneste, M., Eidsvig, U.M.K, and Bungum, H. (2009). Tsunami hazard assessment and early warning systems for the North East Atlantic. Proceedings of the DEWS Midterm Conference 2009, Potsdam, Germany, 7-8 July 2009.

Harbitz, C. B., Glimsdal, S., Løvholt, F., Kveldsvik, V., Pedersen, G. K., and Jensen, A. (2014). Rockslide tsunamis in complex fjords: From an unstable rock slope at Åkerneset to tsunami risk in western Norway. Coastal engineering, 88, 101-122.

Harding, R., & Huuse, M. (2015). Salt on the move: Multi stage evolution of salt diapirs in the Netherlands North Sea. Marine and Petroleum Geology, 61, 39-55.

Haugen, K.B., Løvholt, F., and Harbitz, C.B. (2005). Fundamental mechanisms for tsunami generation by submarine mass flows in idealised geometries. Ormen Lange Special Issue, Marine and Petroleum Geology 22, 209-217, doi: 10.1016/j.marpetgeo.2004.10.016.

Hazell, Z. J. (2008). Offshore and intertidal peat deposits, England—a resource assessment and development of a database. Environmental Archaeology, 13(2), 101-110.

Heller, V. and Ruffini, G., 2023. A critical review about generic subaerial landslide-tsunami experiments and options for a needed step change Earth-Science Reviews.

Henkel, S.K., Revelas, E.C., Wodzicki, S., and Chapman, J. 2022. Discovery of a large offshore population of the northeast Pacific burrowing shrimp Neotrypaea sp.(Decapoda: Axiidea). Estuarine, Coastal and Shelf Science. doi.org/10.1016/j.ecss.2022.107936

Henriksen, S. & Weimer, P. 1996: High-frequency depositional sequences and stratal stacking patterns in lower Pliocene coastal deltas, mid-Norwegian continental shelf. American Association of Petroleum Geologists Bulletin 80, 1867–1895. https://doi.org/10.1306/64EDA226-1724-11D7-8645000102C1865D

Hepp, D. A., Romero, O. E., Mörz, T., DE POL-HOLZ, R., & Hebbeln, D. (2019). How a river submerges into the sea: a geological record of changing a fluvial to a marine paleoenvironment during early Holocene sea level rise. Journal of Quaternary Science, 34(7), 581-592.

Hermanns, R. L., Schleier, M., Böhme, M., Blikra, L. H., Gosse, J., Ivy-Ochs, S., & Hilger, P. (2017). Rock-avalanche activity in W and S Norway peaks after the retreat of the Scandinavian ice sheet. In Advancing Culture of Living with Landslides: Volume 5 Landslides in Different Environments (pp. 331-338). Springer International Publishing.

Hernández-Molina, F. J., Stow, D. A. V., Llave, E., Rebesco, M., Ercilla, G., van Rooij, D., Mena, A., Vázquez, J. T., & Voelker, A. H. L. (2011). Deep-water Circulation: Processes & Products (16-18 June 2010, Baiona): Introduction and future challenges. Geo-Marine Letters, 31(5–6), 285–300. https://doi.org/10.1007/S00367-011-0261-Z/FIGURES/10

Hilger, P. (2019). Rock-slope failures in Norway - temporal development and climatic conditioning. Doctoral thesis University of Oslo, Dept. of Geosciences.
https://www.duo.uio.no/bitstream/handle/10852/70806/1/PhD-Hilger-2019.pdf

Hill, J., Collins, G. S., Avdis, A., Kramer, S. C., & Piggott, M. D. (2014). How does multiscale modelling and inclusion of realistic palaeobathymetry affect numerical simulation of the Storegga Slide tsunami?. Ocean Modelling, 83, 11-25.

Hill, A. W., Nicol, G., & Cook, M. R. (2024). A Proposed Standard Seismic Frequency Nomenclature for Geophysical Site Investigation Surveys in the Offshore Energy Sector. First Break, 42(11), 37-41.

Hitchen, K., Johnson, J., Gatliff, R.W. (2013). Geology of the Rockall Basin and adjacent areas. British Geological Survey Research Report, RR/12/03.

Hjelstuen, B.O., Eldholm, O. & Faleide, J.I. 2007: Recurrent Pleistocene mega-failures on the SW Barents Sea Margin. Earth and Planetary Science Letters 258, 605–618. https://doi.org/10.1016/j.epsl.2007.04.025.

Hjelstuen, B.O., and Andreassen, E.V., 2015, North Atlantic Ocean deep-water processes and depositional environments: A study of the Cenozoic Norway Basin: Marine and Petroleum Geology, v. 59, p. 429-441, https://doi.org/10.1016/j.marpetgeo.2014.09.011.

Hjelstuen, B.O., Grinde, S., 2016. 3D seismic investigation of Pleistocene Mass Transport Deposits and Glacigenic Debris Flows on the North Sea Fan, NE Atlantic Margin. In: Lamarche, G et al. (eds) Submarine Mass Movements and Their Consequences, Advances in Natural and Technological Hazard Research, pp 265-272.

Hjelstuen, B. O., Sejrup, H. P., Valvik, E., & Becker, L. W. (2018). Evidence of an ice-dammed lake outburst in the North Sea during the last deglaciation. Marine Geology, 402, 118-130.

Hjelstuen, B.O., Sejrup, H.P., 2021. Latitudinal variability in the Quaternary development of the Eurasian ice sheets—Evidence from the marine domain. Geology 49, 356-351.

Hjelstuen B.O., Sejrup, H.P., 2023. The North Sea and Mid-Norwegian Continental Margin: glacial landforms during deglaciation, the Bølling-Allerød Interstadial and the Younger Dryas. In: Palacios et al. (eds) European Glacial Landscapes: Last Deglaciation. Elsevier. Part III, Section 1, Chapter14, pp 119-127.

Hjelstuen, B.O., Eldholm, O. and Skogseid, J., 1997. Vøring Plateau diapir fields and their structural and depositional settings. Marine Geology 144: 33-57.

Holeyman, A., Peralta, P., Charue, N., 2015. Boulder-soil-pile dynamic interaction, in: Meyer, V. (Ed.), Frontiers in Offshore Geotechnics III. CRC Press, London, pp. 563–568.

Honda, H. and Nakamura, K. (1951). The waves caused by one-dimensional deformation of the bottom of shallow sea of uniform depth, Sci. Rep. Tohoku Univ. Ser., Geophysics, 3, 133-137.

Hornbach, M. J., Saffer, D. M., and Steven Holbrook, W., 2004, Critically pressured free-gas reservoirs below gas-hydrate provinces: Nature, v. 427, no. 6970, p. 142-144.

Hovind E, Kaynia AM. Earthquake response of wind turbine with non-linear soil-structure interaction. In: Proceedings of the 9th international conference on structural dynamics EURODYN2014. Porto; 2014. p. 623–30.

Hovland, M., Gardner, J.V. and Judd, A.G., 2002. The significance of pockmarks to understanding fluid flow processes and geohazards. Geofluids, 2(2), 127-136.

Howe, J. A., Stoker, M. S., & Woolfe, K. J. (2001). Deep-marine seabed erosion, and gravel lags in the northwestern Rockall Trough, North Atlantic Ocean. Journal of the Geological Society of London, Vol. 158, 427–438.

Huang, X. and García, M. H. (1998). A Herschel–Bulkley model for mud flow down a slope. Journal of Fluid Mechanics 374: 305–333, DOI 10.1017/S0022112098002845.

Huat, B. B. K., Prasad, A., Asadi, A., & Kazemian, S. (2014). Geotechnics of Organic Soils and Peat. CRC Press. https://doi.org/10.1201/b15627

Hudec, M. R., & Jackson, M. P. (2007). Terra infirma: Understanding salt tectonics. Earth-Science Reviews, 82(1-2), 1-28.

Hughes, A. L., Gyllencreutz, R., Lohne, Ø. S., Mangerud, J., & Svendsen, J. I. (2016). The last Eurasian ice sheets–a chronological database and time-slice reconstruction, DATED-1. Boreas, 45(1), 1-45.

Huhn, K., Arroyo, M., Cattaneo, A., Clare, M.A., Gràcia, E., Harbitz, C.B., Krastel, S., Kopf, A., Løvholt, F., Rovere, M., Strasser, M., Talling, P.J., and Urgeles, R. (2020). Modern Submarine Landslide Complexes: A Short Review. In: Ogata, K., Festa, A., and Pini, G.A. (eds.). Submarine Landslides – Subaqueous Mass Transport Deposits from Outcrops to Seismic Profiles. Geophysical Monograph 246. John Wiley & Sons, NJ 07030 and the American Geophysical Union, Washington, D.C. 20009.

Hustoft, S., Bünz, S., Mienert, J., & Chand, S. (2009). Gas hydrate reservoir and active methane-venting province in sediments on< 20 Ma young oceanic crust in the Fram Strait, offshore NW-Svalbard. Earth and Planetary Science Letters, 284(1-2), 12-24.

Huuse, M., Jackson, C.A.L., Van Rensbergen, P., Davies, R.J., Flemings, P.B. and Dixon, R.J., 2010. Subsurface sediment remobilization and fluid flow in sedimentary basins: an overview. Basin Research, 22(4), 342-360.

Huuse, M. (1999). Detailed morphology of the Top Chalk surface in the eastern Danish North Sea. Petroleum Geoscience, 5(3), 303-314.

Huuse, M., & Lykke-Andersen, H. (2000). Large-scale glaciotectonic thrust structures in the eastern Danish North Sea. Geological Society, London, Special Publications, 176(1), 293–305. https://doi.org/10.1144/GSL.SP.2000.176.01.22Huuse, M., Lykke-Andersen, H. and Michelsen, O., 2001. Cenozoic evolution of the eastern Danish North Sea. Marine Geology, 177(3-4), pp.243-269.

Huuse, M., Le Heron, D. P., Dixon, R., Redfern, J., Moscariello, A., & Craig, J. (2012). Glaciogenic reservoirs and hydrocarbon systems: an introduction.

Hyndman, R., and Spence, G., 1992, A seismic study of methane hydrate marine bottom simulating reflectors: Journal of Geophysical Research: Solid Earth, v. 97, no. B5, p. 6683-6698.

Høgaas, F., & Longva, O. (2016). Mega deposits and erosive features related to the glacial lake Nedre Glomsjø outburst flood, southeastern Norway. Quaternary Science Reviews, 151, 273-291.

IHO (2020). IHO standards for hydrographic surveys 6th Edition special publication No.44

Ilstad T, Elverhøi A, Issler D, and Marr JG (2004a). Subaqueous debris flow behaviour and its dependence on the sand/clay ratio: A laboratory study using particle tracking. Marine Geology 213(1–4): 415–438.

Ilstad T, Marr JG, Elverhøi A, and Harbitz CB (2004b). Laboratory studies of subaqueous debris flows by measurements of pore-fluid pressure and total stress. Marine Geology 213(1–4): 403–414.

Ilstad T, De Blasio FV, Elverhøi A, Harbitz CB, Engvik L, Longva O, and Marr JG (2004c). On the frontal dynamics and morphology of submarine debris flows. Marine Geology 213(1–4): 481–497.

Imran, J.; Parker, G.; Locat, J. and Lee, H. (2001). 1D numerical model of muddy subaqueous and subaerial debris flows. J. Hydr. Eng. 127(11): 959–968, DOI 10.1061/(asce)0733-9429(2001)127:11(959).

IODP, 2020. International Ocean Discovery Program (IODP), 2020. 2050 Science Framework: Exploring Earth by Scientific Ocean Drilling. Available at: https://www.iodp.org/2050-science-framework

IODP, 2024. International Ocean Discovery Program (IODP), 2024. Core Repositories. https://www.iodp.org/resources/core-repositories

IOGP, 2024. CO2 storage projects in Europe. International Association of Oil and Gas Producers. October 2024. https://iogpeurope.org/wp-content/uploads/2024/10/CO2-Storage-Projects-in-Europe-map.pdf. Accessed 05 May 2025.

Ismail-Meyer, K., Stolt, M. H., & Lindbo, D. L. (2018). Soil Organic Matter. Interpretation of Micromorphological Features of Soils and Regoliths, 471–512. https://doi.org/10.1016/B978-0-444-63522-8.00017-6

ISO 14688-2:2018. Geotechnical investigation and testing. Identification and classification of soil. British Standard Institute.

ISO 14688-1:2017. Geotechnical investigation and testing. Identification and classification of soil - Part 1: Identification and description. .

ISO 14688-2:2017. Geotechnical investigation and testing. Identification and classification of soil - Part 2: Principles for a classification.

ISO 19901-10: 2018(E), 2018. Petroleum and natural gas industries — Specific requirements for offshore structures — Part 8: Marine geophysical investigations. ISO/TC 67/SC 7/WG 10

Issler, D.; De Blasio, F. V.; Elverhøi, A.; Bryn, P. and Lien, R. (2005). Scaling behaviour of clay-rich submarine debris flows. Marine and Petroleum Geology 22: 187–194, DOI 10.1016/j.marpetgeo.2004.10.015.

Issler, D. (2014). Dynamically consistent entrainment laws for depth-averaged avalanche models. Journal of Fluid Mechanics 759: 701–738, DOI 10.1017/jfm.2014.584.

Jackson, D.I., Jackson, A.A., Evans, D., Wingfield, R.T.R., Barnes, R.P., Arthur, M.J., 1995. United Kingdom offshore regional report: the geology of the Irish Sea. British Geological Survey, London.

Jakobsson, M., Stranne, C., O'Regan, M., Greenwood, S. L., Gustafsson, B., Humborg, C., & Weidner, E. (2019). Bathymetric properties of the Baltic Sea. Ocean Science, 15(4), 905-924.

Jensen, J.B. and Bennike, O. (2022). Geological screening of Kattegat Area A and B. Geological seabed screening in relation to possible location of windfarm areas. Client Danish Energy Agency. GEUS, Copenhagen. Danmarks og Grønlands Geologiske Undersøgelse Rapport 2021(64). https://doi.org/10.22008/gpub/34624

Jerkins, A.E., Shiddiqi, H.A., Kværna, T., Gibbons, S.J., Schweitzer, J., Ottemöller, L., Bungum, H., 2020. The 30 June 2017 North Sea Earthquake: Location, Characteristics, and Context. Bull. Seismol. Soc. Am. 110, 937–952. https://doi.org/10.1785/0120190181

Jerkins, A.E., Oye, V., Alvizuri, C., Halpaap, F., Kværna, T., 2023. The 21 March 2022 Mw 5.1 Tampen Spur Earthquake, North Sea: Location, Moment Tensor, and Context. Bull. Seismol. Soc. Am. https://doi.org/10.1785/0120230163

Johnson, H., Richards, P.C., Long, D., Graham, C.C. (1993). United Kingdom offshore regional report: the geology of the northern North Sea. London: HMSO for the British Geological Survey.

Johnson, K. R., Dakin, N., Carter, G. D. O., Phillips, E. R. P. (2023). Geo-challenges for ground model development in previously glaciated and periglaciated terrains. In 9th International SUT Offshore Site

Investigation and Geotechnics Conference, Innovative Geotechnologies for Energy Transition. 12-14 September 2023, London, UK

Johnston, A. C. (1987). Suppression of earthquakes by large continental ice sheets: Nature, v. 330, no. 6147, p. 467-469.

Jop, P., Forterre, Y., Pouliquen, O. (2006) A constitutive law for dense granular flows. Nature 441 (7094): 727–730. DOI 10.1038/nature04801.

Judd, A., Hovland, M. (2007). Seabed fluid flow: the impact on geology, biology and the marine environment. Cambridge University Press. Online version 2009: https://doi.org/10.1017/CBO9780511535918.

Karakosta, C., Pappas, C., Marinakis, V., & Psarras, J. (2013). Renewable energy and nuclear power towards sustainable development: Characteristics and prospects. Renewable and Sustainable Energy Reviews, 22, 187-197.

Karstens, J., Haflidason, H., Becker, L. W., Berndt, C., Rüpke, L., Planke, S., Liebetrau, V., Schmidt, M., and Mienert, J., 2018, Glacigenic sedimentation pulses triggered post-glacial gas hydrate dissociation: Nature communications, v. 9, no. 1, p. 635.

Kaynia, A.M. (2019). Seismic considerations in design of offshore wind turbines. Soil Dynamics and Earthquake Engineering, 124, 399–407.

Kettlety, T., Martuganova, E., Kühn, D., Schweitzer, J., Weemstra, C., Baptie, B., Dahl-Jensen, T., Jerkins, A., Voss, P. H., Michael, J., & Skurtveit, E. (2024). A Unified Earthquake Catalogue for the North Sea to Derisk European CCS Operations. First Break, 42(5), 31–36. https://doi.org/10.3997/1365-2397.fb2024036

Kim, J., Løvholt, F., Issler, D., and Forsberg, C. F. (2019). Landslide material control on tsunami genesis—the Storegga Slide and tsunami (8,100 years BP). Journal of Geophysical Research: Oceans 124(6): 3607–3627, DOI 10.1029/2018JC014893.

King, E.L., Sejrup, H.P., Haflidason, H., Elverhøi, A., and Aarseth, I., 1996, Quaternary seismic stratigraphy of the North Sea Fan: glacially-fed gravity flow aprons, hemipelagic sediments and large submarine slides: Marine Geology, v. 130, p. 295-315, https://doi.org/10.1016/0025-3227(95)00168-9.

King, E.L., Haflidason, H., Sejrup, H.P., and Løvlie, R., 1998, Glacigenic debris flow on the North Sea Trough Mouth Fan during ice stream maxima: Marine Geology, v. 152, p. 217-246, https://doi.org/10.1016/S0025-3227(98)00072-3.

Kirby, J. T., Grilli, S. T., Horrillo, J., Liu, P. L.-F., Nicolsky, D., Abadie, S., Ataie-Ashtiani, B., Castro, M.J., Clous, L., Escalante, C., Fine, I., González-Vida, J.M., Løvholt, F., Lynett, P., Ma, G., Macías, J.,

Ortega, S., Shi, F., Yavari-Ramshe, S., and Zhang, C. (2022). Validation and inter-comparison of models for landslide tsunami generation. Ocean Modelling, 170, 101943.

Kirkham, J.D, Hogan, K.A., Larter, R.D, Arnold, N.S., Ely, J.C., Clark, C>D>, Games, K, Huuse, M, Stewart, M.A., Ottesen, D, Dowdeswell, J.A. (2024). Tunnel valley formation beneath deglaciating mid-latitude ice sheets: Observations and modelling. Quaternary Science Reviews, v. 323, 2974–2981.

Kishankov, A., Serov, P., Bünz, S., Patton, H., Hubbard, A., Mattingsdal, R., ... & Andreassen, K. (2022). Hydrocarbon leakage driven by Quaternary glaciations in the Barents Sea based on 2D basin and petroleum system modeling. Marine and Petroleum Geology, 138, 105557.

Kjær, Kurt H. "Mode of subglacial transport deduced from till properties, Mýrdalsjökull, Iceland." Sedimentary Geology 128.3-4 (1999): 271-292.

Kjørlaug RA, Kaynia AM (2015). Vertical earthquake response of megawatt-sized wind turbine with soil-structure interaction effects. Earthq Eng Struct Dyn, 44:2341–58.

Knies, J., Matthiessen, J., Vogt, C., Laberg, J. S., Hjelstuen, B. O., Smelror, M., ... & Vorren, T. O. (2009). The Plio-Pleistocene glaciation of the Barents Sea–Svalbard region: a new model based on revised chronostratigraphy. Quaternary Science Reviews, 28(9-10), 812-829.

Knutsen, S.-M., Richardsen, G., Vorren, T.O. (1993) Late Miocene–Pleistocene sequence stratigraphy and mass-movements on the western Barents Sea margin, Norwegian Petroleum Society Special Publications, Volume 2, 573-606, https://doi.org/10.1016/B978-0-444-88943-0.50038-1.

Knutz, P.C. and Cartwright, J.A. (2003) Seismic stratigraphy of the West Shetland Drift: Implications for late Neogene paleocirculation in the Faeroe-Shetland gateway. Paleoceanography. v. 18, No. 4, 1093.

Knutz, P.C. (2010) 3D seismic imaging of aggradational channels related to geostrophic currents through the Pliocene North Sea basin. Geo-Temas, 11, 89-90.

Kortekaas, S., Peuchen, J, 2008. Measured Swabbing Pressures and Implications for Shallow Gas Blowout. OTC.08: Proceedings 2007 Offshore Technology Conference, Houston, Texas, USA, OTC Paper 19280.

Kremer, K., Wirth, S. B., Reusch, A., Fäh, D., Bellwald, B., Anselmetti, F. S., ... & Strasser, M. (2017). Lake-sediment based paleoseismology: Limitations and perspectives from the Swiss Alps. Quaternary Science Reviews, 168, 1-18.

Krämer, K., Holler, P., Herbst, G., Bratek, A., Ahmerkamp, S., Neumann, A., ... & Winter, C. (2017). Abrupt emergence of a large pockmark field in the German Bight, southeastern North Sea. Scientific reports, 7(1), 5150.

Kristensen, T. B., Huuse, M., Piotrowski, J. A., & Clausen, O. R. (2007). A morphometric analysis of tunnel valleys in the eastern North Sea based on 3D seismic data. Journal of Quaternary Science: Published for the Quaternary Research Association, 22(8), 801-815.

Kuenen, P. H. (1937). Experiments in connection with Daly's hypothesis on the formation of submarine canyons. Leidse Geologische Mededelingen 8: 327–335.

Kuhlmann, G., Wong, T.E. 2008. Pliocene paleoenvironment evolution as interpreted from 3D-seismic data in the southern North Sea, Dutch offshore sector. Marine and Petroleum Geology, Volume 25, Issue 2, 173-189. https://doi.org/10.1016/j.marpetgeo.2007.05.009.

Kuhlmann, G., Langereis, C., Munsterman, D., van Leeuwen, R.J., Verreussel, R., Meulenkamp, J. and Wong, T., 2006. Chronostratigraphy of Late Neogene sediments in the southern North Sea Basin and paleoenvironmental interpretations. Palaeogeography, Palaeoclimatology, Palaeoecology, 239(3-4), pp.426-455.

Kurjanski, B., Rea, B. R., Spagnolo, M., Cornwell, D. G., Howell, J., & Archer, S. (2020). A conceptual model for glaciogenic reservoirs: From landsystems to reservoir architecture. Marine and Petroleum Geology, 115, 104205. https://doi.org/10.1016/j.marpetgeo.2019.104205.

Kurjański, B., Rea, B. R., Spagnolo, M., Cornwell, D. G., Howell, J., Comte, J., Quirós, A. G., Palmu, J., Oien, R. P., & Gibbard, P. L. (2021). Cool deltas: Sedimentological, geomorphological and geophysical characterization of ice-contact deltas and implications for their reservoir properties (Salpausselkä, Finland). Sedimentology, sed.12884. https://doi.org/10.1111/sed.12884

Kvalstad TJ, Andresen L, Forsberg CF, Berg K, Bryn P, Wangen M (2005a) The Storegga slide: evaluation of triggering sources and slide mechanics. Mar Pet Geol 22: 245-256.

Kvalstad TJ, Nadim F, Kaynia AM, Mokkelbost KH, and Bryn P (2005b) Soil conditions and slope stability in the Ormen Lange area. Marine and Petroleum Geology 22: 299–310. https://doi.org/10.1016/j.marpetgeo.2004.10.021.

Kvenvolden, K. A., 2000, Natural gas hydrate: Background and history of discovery, Natural Gas Hydrate: In Oceanic and Permafrost Environments, Springer, p. 9-16.

Laberg, J.S., Vorren, T.O., 1993. A Late Pleistocene submarine slide on the Bear Island Trough Mouth Fan. Geo-Mar. Lett. 13, 227-234.

Laberg, J.S., Vorren, T.O., 1996. The Middle and Late Pleistocene evolution of the Bear Island Trough Mouth Fan. Global Planet. Change 12, 309-330.

Laberg, J.S., and Vorren, T.O., 2000, Flow behaviour of the submarine glacigenic debris flows on the Bear Island Trough Mouth Fan, western Barents Sea: Sedimentology, v. 47, p. 1105-1117, https://doi.org/10.1046/j.1365-3091.2000.00343.x.

Laberg, J.S., Vorren, T.O., Dowdeswell, J.A., Kenyon, N.H., Taylor, J., 2000. The Andøya Slide and the Andøya Canyon, north-eastern Norwegian-Greenland Sea. Mar. Geol. 162, 259-275.

Laberg, J.S., Vorren, T.O., Mienert, J., Bryn, P., Lien, R., 2002. The Trænadjupet Slide: a large slope failure affecting the continental margin of Norway 4,000 years ago. Geo-Mar. Lett. 22, 19-24.

Laberg, J.S., Guidard, S., Mienert, J., Vorren, T.O., Haflidason, H., Nygård, A., 2007. Morphology and morphogenesis of a high-latitude canyon; the Andøya Canyon, Norwegian Sea, Marine Geology, 246, Pages 68-85, https://doi.org/10.1016/j.margeo.2007.01.009.

Laberg, J.S., Eilertsen, R.S. & Vorren, T.O. 2009: The paleo–ice stream in Vestfjorden, north Norway, over the last 35 ky: Glacial erosion and sediment yield. Geological Society of America Bulletin 121, 434–447. https://doi.org/10.1130/B26277.1

Laberg, J. S., Andreassen, K., Knies, J., Vorren, T. O., & Winsborrow, M. (2010). Late Pliocene–Pleistocene development of the Barents Sea ice sheet. Geology, 38(2), 107-110.

Laberg, J. S., Andreassen, K., & Vorren, T. O. (2012). Late Cenozoic erosion of the high-latitude southwestern Barents Sea shelf revisited. Bulletin, 124(1-2), 77-88.

Laberg, J.S., Baeten, N.J., Vanneste, M., Forsberg, C.F., Forwick, M., Haflidason, H. (2016). Sediment Failure Affecting Muddy Contourites on the Continental Slope Offshore Northern Norway: Lessons Learned and Some Outstanding Issues. In: Lamarche, G., et al. Submarine Mass Movements and their Consequences. Advances in Natural and Technological Hazards Research, vol 41. Springer, Cham. https://doi.org/10.1007/978-3-319-20979-1_28

Lacasse, S., L'Heureux, J.S., Liu, Z. 2022. Reducing landslide risk - Emerging challenges and novel technologies. Geohazards VIII.

Lamb, R.M., Huuse, M., Stewart, M.A. (2017). Early Quaternary sedimentary processes and palaeoenvironments in the central North Sea. Journal of Quaternary Science, 32(2), 127-144.

Lamb, R.M., Harding, R., Huuse, M., Stewart, M.A., Brocklehurst, S.H. (2018). The early quaternary North Sea basin. Journal of the Geological Society, 175(2), 275-290.

Lambeck, K., Rouby, H., Purcell, A., Sun, Y. and Sambridge, M. 2014. Sea-level and global ice volumes from the Last Glacial Maximum to the Holocene. PNAS, 111, 15296–15303, https://doi.org/10.1073/pnas.1411762111

Landva, A. O. (2006). "Characterisation of Escuminac peat and construction on peatland." Proc., Proc. of Characterisation and Engineering Properties of Natural Soils, 2135-2191.

Larsson, R. (1990). Behaviour of organic clay and gyttja. Report No. 38.

Lasabuda, A.P.E., Hanssen, A., Laberg, J.S. et al. Paleobathymetric reconstructions of the SW Barents Seaway and their implications for Atlantic–Arctic ocean circulation. Commun Earth Environ 4, 231 (2023). https://doi.org/10.1038/s43247-023-00899-y

Lasabuda, A., Geissler, W.H., Laberg, J.S., Knutsen, S.-M., Rydningen, T.A., and Berglar, K., 2018, Late Cenozoic erosion estimates for the Northern Barents Sea: Quantifying Glacial Sediment Input to the Arctic Ocean: Geochemistry, Geophysics, Geosystems, v. 19, p. 4876-4903, https://doi.org/10.1029/2018GC007882.

Lee, J. R., Busschers, F. S., & Sejrup, H. P. (2012). Pre-Weichselian Quaternary glaciations of the British Isles, The Netherlands, Norway and adjacent marine areas south of 68 N: implications for long-term ice sheet development in northern Europe. Quaternary Science Reviews, 44, 213-228.

Lee, J. R., & Phillips, E. (2013). Glacitectonics - a key approach to examining ice dynamics, substrate rheology and ice-bed coupling. Proceedings of the Geologists' Association, 124(5), 731–737. https://doi.org/10.1016/j.pgeola.2013.07.006

Leifer, I., & Judd, A. (2015). The UK22/4b blowout 20 years on: Investigations of continuing methane emissions from sub-seabed to the atmosphere in a North Sea context. Marine and Petroleum Geology, 68, 706–717. https://doi.org/10.1016/j.marpetgeo.2015.11.012

Lengkeek, H. J., & Brinkgreve, R. B. J. (2022). CPT-based classification of soft organic clays and peat. In Cone Penetration Testing 2022 (pp. 509–514). CRC Press. https://doi.org/10.1201/9781003308829-72.

Leynaud, D., Mienert, J., Vanneste, M., 2009. Submarine mass movements on glaciated and non-glaciated European continental margins: a review of triggering mechanisms and preconditions to failure. Mar. Petrol. Geol. 26, 618-632.

L'Heureux, J.-S., Glimsdal, S., Longva, O., Hansen, L., and Harbitz, C.B. (2011). The 1888 shoreline landslide and tsunami in Trondheimsfjorden, central Norway. Marine Geophysical Research, Vol. 32, Issue 1, 313-329. DOI 10.1007/s11001-010-9103-z.

L'Heureux, J. S., Vanneste, M., Rise, L., Brendryen, J., Forsberg, C. F., Nadim, F., ... & Haflidason, H. (2013a). Stability, mobility and failure mechanism for landslides at the upper continental slope off Vesterålen, Norway. Marine Geology, 346, 192-207.

5272 L'Heureux, J.S., Hansen, L., Longva, O. Eilertsen, R.S. (2013b). Landslides along Norwegian fjords:
5273 causes and hazard assessment. Landslide Science and Practice: Volume 5: Complex Environment,
5274 pp.81-87.

5275 L'Heureux, J. S., Ø. A. Høydal, A. P. Paniagua Lopez, and S. Lacasse. (2018). Impact of climate change
5276 and human activity on quick clay landslide occurrence in Norway. Paper to the Second JTC1 Workshop
5277 on Triggering and Propagation of Rapid Flow-lik e Landslides, Hong Kong, pp. 3-5. 2018.

5278 L'Heureux, J.-S., Long, M. (2017). Relationship between Shear-Wave Velocity and Geotechnical
5279 Parameters for Norwegian Clays. J. Geotech. Geoenvironmental Eng. 143, 4017013.
5280 https://doi.org/10.1061/(ASCE)GT.1943-5606.0001645

5281 L'Heureux, J.-S., Longva, O., Hansen, L., Vanneste, M. (2014). The 1930 Landslide in Orkdalsfjorden:
5282 Morphology and Failure Mechanism. In: Krastel, S., Behrmann, J.-H., Völker, D., Stipp, M., Berndt,
5283 C., Urgeles, R., Chaytor, J., Huhn, K., Strasser, M., and Harbitz, C.B. (Eds.), Submarine Mass
5284 Movements and Their Consequences: Proceedings of the 6th International Symposium, Kiel, September
5285 2013. Advances in Natural and Technological Hazards Research, vol. 37 (pp. 239-248). Cham: Springer
5286 International Publishing.

5287 L'Heureux, Jean-Sébastien, Steinar Nordal, and Synnøve W. Austefjord. (2017) "Revisiting the 1959
5288 quick clay landslide at Sokkelvik, Norway." Landslides in sensitive clays: From research to
5289 implementation: 395-405.

5290 Li, M. Z., Shaw, J., Todd, B. J., Kostylev, V. E., Wu, Y. (2014). Sediment transport and development
5291 of banner banks and sandwaves in an extreme tidal system: Upper Bay of Fundy, Canada. Continental
5292 Shelf Research, 83, 86–107. https://doi.org/10.1016/j.csr.2013.08.007

5293 Li, X.; Sovilla, B.; Ligneau, C.; Jiang, C. and Gaume, J. (2022). Different erosion and entrainment
5294 mechanisms in snow avalanches. Mechanics Research Communications 124: 103914, DOI
5295 10.1016/j.mechrescom.2022.103914.

5296 Lien, Ø. F., Hjelstuen, B. O., Zhang, X., Sejrup, H. P. (2022). Late Plio-Pleistocene evolution of the
5297 Eurasian Ice Sheets inferred from sediment input along the northeastern Atlantic continental margin.
5298 Quaternary Science Reviews, 282, 107433.

5299 Ligneau, C.; Sovilla, B. Gaume, J. (2024). Modelling erosion, entrainment and deposition in cohesive
5300 granular flows: Application to dense snow avalanches. Cold Regions Science and Technology 219:
5301 104103, DOI 10.1016/j.coldregions.2023.104103.

5302 Ligtenberg, J. (2005) Detection of fluid migration pathways in seismic data: implications for fault seal
5303 analysis: Basin Research, v. 17, no. 1, p. 141-153.

Lindberg, B., Laberg, J.S., Vorren, T.O. (2004). The Nyk Slide – morphology, progression, and age of a partly buried submarine slide offshore northern Norway. Mar. Geol. 213, 277-289.

Lindholm, C., Bungum, H., Ghione, F., Meslem, A., Huang, C., Oye, V. (2025). Earthquakes and seismic hazard for Norway and Svalbard. Journal of Seismology, https://doi.org/10.1007/s10950-024-10270-z.

Lisiecki, L. E., & Raymo, M. E. (2005). A Pliocene-Pleistocene stack of 57 globally distributed benthic δ18O records. Paleoceanography, 20(1).

Liu, Z., L'heureux, J. S., Glimsdal, S., and Lacasse, S. (2021). Modelling of mobility of Rissa landslide and following tsunami. Computers and Geotechnics, 140, 104388.

Llopart, J., Urgeles, R., Forsberg, C. F., Camerlenghi, A., Vanneste, M., Rebesco, M., ... & Lantzsch, H. (2019). Fluid flow and pore pressure development throughout the evolution of a trough mouth fan, western Barents Sea. Basin Research, 31(3), 487-513.

Lloyd, C., Huuse, M., Barrett, B.J., Stewart, M.A. Newton, A.M.W. (2021a) regional CO2 containment assessment of the northern Utsira Formation seal and overburden, northern North Sea. Basin Research, 33(3), pp.1985-2017.

Lockhart, E.A., Scourse, J.D., Praeg, D., Van Landeghem, K.J.J., Mellett, C., Saher, M., Callard, L., Chiverrell, R.C., Benetti, S., Ó Cofaigh, C., Clark, C.D. (2018) A stratigraphic investigation of the Celtic Sea megaridges based on seismic and core data from the Irish-UK sectors. Quat. Sci. Rev. 198, 156–170. https://doi.org/10.1016/j.quascirev.2018.08.029

Long, D., Stevenson, A. G., Wilson, C. K., Bulat, J. (2003) Slope failures in the Faroe–Shetland Channel. 281–289 in Submarine mass movements and their consequences. Locat, J, and Mienert, J (editors). Advances in Natural and Technological Hazards Research Series. (Dordrecht: Kluwer Academic Publishers.)

Long, D., Ziska, H., Musson, R. (2011) Geohazards. In: Ritchie, J.D., Ziska, H., Johnson, H. & Evans, D. (eds) Geology of the Faroe–Shetland Basin and Adjacent Areas. British Geological Survey Research Report, RR/11/01, Jarðfeingi Research Report, RR/11/01, HMSO for the British Geological Survey, London, pp 239-253.

Long, M. L., Tucker, G. T., Leth, C. T. L. (2024). Experience of in situ geotechnical tests and their interpretation in organic soils and peat. 7th International Conference on Geotechnical and Geophysical Site Characterization (ISC 24). https://doi.org/10.23967/ISC.2024.182

Louge, M. Y., Carroll, C. S., Turnbull, B. (2011). Role of pore pressure gradients in sustaining frontal particle entrainment in eruption currents: The case of powder snow avalanches. Journal of Geophysical Research 116: F04030, DOI 10.1029/2011JF002065.

Lund, B., Schmidt, P., Hieronymus, C. (2009). Stress evolution and fault stability during the Weichselian glacial cycle. Swedish Nuclear Fuel and Waste Management Co., Stockholm (Sweden) Technical Report SKB-TR-09-15. https://www.osti.gov/etdeweb/biblio/971759

Lundsten, E., Paull, C. K., Gwiazda, R., Dobbs, S., Caress, D. W., Kuhnz, L. A., ... & Addison, J. (2024). Pockmarks offshore Big Sur, California provide evidence for recurrent, regional, and unconfined sediment gravity flows. Journal of Geophysical Research: Earth Surface, 129(5), e2023JF007374.

Lunne, T., Andersen, K.H., Low, H.E., Randolph, M.F., Sjursen, M. (2011). Guidelines for offshore in situ testing and interpretation in deepwater soft clays. Can. Geotech. J. 48, 543–556. https://doi.org/10.1139/t10-088

Lunne, T., Long, M. (2006). Review of long seabed samplers and criteria for new sampler design. Mar. Geol. 226, 145–165. https://doi.org/10.1016/j.margeo.2005.07.014

Lunne, T., Robertson, P.K., Powell, J.J.M. (1997). Cone Penetration Testing in Geotechnical Practice. Blackie Academic & Professional, London.

Lunne, T., Strandvik, S., Kasin, K., L'Heureux, J.S., Haugen, E., Uruci, E., Veldhuijzen, A., Carlson, M., Kassner, M. (2018). Effect of cone penetrometer type on CPTU results at a soft clay test site in Norway, in: Cone Penetration Testing 2018. https://doi.org/10.1088/1755-1315/710/1/012010

Løseth, H. (2021) Comment on 'A Miocene age for the Molo Formation, Norwegian Sea shelf off Vestfjorden, based on marine palynology'. Norwegian Journal of Geology 101, 202102. https://doi.org/10.17850/njg101-1-2

Løseth, H. (2023). The Norwegian strandflat reviewed and constrained in an offshore perspective. Norwegian Journal of Geology, 103.

Løseth, H., Kyrkjebø, R., Hilde, E., Wild, R.J., Bunkholt, H. (2017) 500 m of rapid base level rise along an inner passive margin–Seismic observations from the Pliocene Molo Formation, mid Norway. Marine and Petroleum Geology 86, 268–287. https://doi.org/10.1016/j.marpetgeo.2017.05.039

Løseth, H., Dowdeswell, J.A., Batchelor, C.L., Ottesen, D. (2020). 3D sedimentary architecture showing the inception of an Ice Age. Nat. Commun. https://doi.org/ 10.1038/s41467-020-16776-7.

Løseth, H., Nygård, A., Batchelor, C. L., & Fayzullaev, T., 2022. A regionally consistent 3D seismic-stratigraphic framework and age model for the Quaternary sediments of the northern North Sea. Marine and Petroleum Geology, 142, 105766.

Løseth, H., Nygård, A., Batchelor, C.L., Fayzullaev, T. (2022). A regionally consistent 3D seismic-stratigraphic framework and age model for the Quaternary sediments of the northern North Sea. Marine and Petroleum Geology, 142, p.105766.

Løvholt, F., Harbitz, C.B., Haugen, K.B. (2005). A parametric study of tsunamis generated by submarine slides in the Ormen Lange/Storegga area off western Norway. Ormen Lange Special Issue, Marine and Petroleum Geology 22, 219-231; doi: 10.1016/j.marpetgeo.2004.10.0017.

Løvholt, F., Pedersen, G., Harbitz, C.B., Glimsdal, S., Kim, J. (2015) On the characteristics of landslide tsunamis. Philosophical Transactions of the Royal Society A: Mathematical, Physical and Engineering Sciences 373(2053): 20140376.

Løvholt, F., Pedersen, G., Harbitz, C.B. (2016) Tsunami-genesis due to retrogressive landslides on an inclined seabed. In: Submarine Mass Movements and Their Consequences, pp. 569–578. Cham: Springer.

Løvholt, F., Bondevik, S., Laberg, J.S., Kim, J., Boylan, N. (2017) Some giant submarine landslides do not produce large tsunamis. Geophysical Research Letters 44(16): 8463–8472. DOI 10.1002/2017gl074062.

Løvholt, F., Schulten, I., Mosher, D., Harbitz, C., Krastel, S. (2019). Modelling the 1929 Grand Banks slump and landslide tsunami. Geological Society, London, Special Publications 477(1): 315–331.

Løvholt, F., Glimsdal, S., and Harbitz, C. B. (2020). On the landslide tsunami uncertainty and hazard. Landslides, 17(10): 2301–2315.

Løvholt, F., Urgeles, R.E., Harbitz, C.B., Vanneste, M., Carlton, B. (2022). Submarine Landslides. In Treatise on Geomorphology (Second Edition), Vol. 8, 919-959. https://doi.org/10.1016/B978-0-12-818234-5.00139-5.

Macías, J., Escalante, C., Castro, M. J. (2021). Multilayer-HySEA model validation for landslide-generated tsunamis–Part 1: Rigid slides. Natural Hazards and Earth System Sciences, 21(2), 775-789.

Magnin, F., Etzelmüller, B., Westermann, S., Isaksen, K., Hilger, P., Hermanns, R. L. (2019). Permafrost distribution in steep rock slopes in Norway: measurements, statistical modelling and implications for geomorphological processes, Earth Surf. Dynam., 7, 1019–1040, https://doi.org/10.5194/esurf-7-1019-2019.

Majcher, J., Quinn, R., Smyth, T., Plets, R., McGonigle, C., Westley, K., Sacchetti, F., & Coughlan, M. (2022). Using difference modelling and computational fluid dynamics to investigate the evolution of complex, tidally influenced shipwreck sites. Ocean Engineering, 246, 110625. https://doi.org/10.1016/J.OCEANENG.2022.110625

Mangerud, J. A. N., Dokken, T., Hebbeln, D., Heggen, B., Ingólfsson, Ó., Landvik, J. Y., ... & Vorren, T. O. (1998). Fluctuations of the Svalbard–Barents Sea Ice Sheet during the last 150 000 years. Quaternary Science Reviews, 17(1-3), 11-42.

Maramai A., Graziani L., Brizuela B. (2014). Euro-Mediterranean Tsunami Catalogue (EMTC) (Version 1.0). Istituto Nazionale di Geofisica e Vulcanologia (INGV). https://doi.org/10.13127/tsunami/emtc.1.0

Marr JG, Elverhøi A, Harbitz CB, Imran J, Harff P (2002) Numerical simulation of mud-rich subaqueous debris flows on the glacially active margins of the Svalbard-Barents Sea. Marine Geology 188: 351–364.

Masson, D.G. (2001). Sedimentary processes shaping the eastern slope of the Faroe–Shetland Channel. Continental Shelf Research 21, 825-857. doi: 10.1016/S0278-4343(00)00115-1.

Masson, D.G., Wynn, R.B., Bett, B.J. (2004). Sedimentary environment of the Faroe–Shetland and Faroe Bank Channels, north-east Atlantic, and the use of bedforms as indicators of bottom current velocity in the deep ocean. Sedimentology 51, 1207-1241. doi: 10.1111/j.1365-3091.2004.00668.x.

Mazzini, A., Svensen, H. H., Planke, S., Forsberg, C. F., Tjelta, T. I. (2016). Pockmarks and methanogenic carbonates above the giant Troll gas field in the Norwegian North Sea. Marine Geology, 373, 26-38.

Mazzini, A., Svensen, H. H., Forsberg, C. F., Linge, H., Lauritzen, S. E., Haflidason, H., ... & Tjelta, T. I. (2017). A climatic trigger for the giant Troll pockmark field in the northern North Sea. Earth and Planetary Science Letters, 464, 24-34.

McCabe, A.M., Clark, P.U., Clark, J. (2005). AMS C dating of deglacial events in the Irish Sea Basin and other sectors of the British – Irish ice sheet. Quat. Sci. Rev. 1673–1690. https://doi.org/10.1016/j.quascirev.2004.06.019

McCabe, A.M., Clark, P.U., Clark, J., Dunlop, P. (2007). Radiocarbon constraints on readvances of the British – Irish Ice Sheet in the northern Irish Sea Basin during the last deglaciation. Quat. Sci. Rev. 26, 1204–1211. https://doi.org/10.1016/j.quascirev.2007.01.010

Meier, M., Schlindwein, V., Scholz, J. -R., Geils, J., Schmidt-Aursch, M.C., Krüger, F., Czuba, W., Janik, T. (2021). Segment-scale seismicity of the ultraslow spreading Knipovich Ridge. Geochem. Geophys. Geosystems 1–21. https://doi.org/10.1029/2020gc009375

Mellett, C. L., Long, D., Carter, G. D. O. (2015). Geology of the seabed and shallow subsurface: The Irish Sea. British Geological Survey Commissioned Report, CR/15/057. 52pp.

Mellett, C. L., Phillips, E., Lee, J. R., Cotterill, C. J., Tjelta, T. I., James, L., & Duffy, C. (2020). Elsterian ice-sheet retreat in the southern North Sea: antecedent controls on large-scale glaciotectonics and subglacial bed conditions. Boreas, 49(1), 129-151.

Mesri, G., Ajlouni, M. (2007). "Engineering properties of fibrous peats." Journal of Geotechnical and Geoenvironmental Engineering, ASCE, 133(7), 850-866.

Michel, G., Coughlan, M., Arosio, R., Emery, A.R., Wheeler, A.J. (2023). Stratigraphic and palaeo-geomorphological evidence for the glacial-deglacial history of the last British-Irish Ice Sheet in the north-western Irish Sea. Quat. Sci. Rev. 300, 107909. https://doi.org/https://doi.org/10.1016/j.quascirev.2022.107909

Mikalsen, H. (2015). Reservoir Structure and Geological Setting of the Shallow PEON Gas Reservoir (Master's Thesis. UiT The Arctic University of Norway.

Minasny, B., Berglund, Ö., Connolly, J., Hedley, C., de Vries, F., Gimona, A., ... & Widyatmanti, W. (2019). Digital mapping of peatlands–A critical review. Earth-Science Reviews, 196, 102870.

Minshull, T. A., Marín-Moreno, H., Betlem, P., Bialas, J., Bünz, S., Burwicz, E., Cameselle, A. L., Cifci, G., Giustiniani, M., Hillman, J. I. (2020) Hydrate occurrence in Europe: A review of available evidence: Marine and Petroleum Geology, v. 111, p. 735-764.

Mohrig, D., Marr, J. G. (2003). Constraining the efficiency of turbidity current generation from submarine debris flows and slides using laboratory experiments. Marine and Petroleum Geology 20: 883–899, DOI 10.1016/j.marpetgeo.2003.03.002.

Mohrig, D.; Elverhøi, A. Parker, G. (1999). Experiments on the relative mobility of muddy subaqueous and subaerial debris flows, and their capacity to remobilize antecedent deposits. Marine Geology 154: 117–129, DOI 10.1016/s0025-3227(98)00107-8.

Monrigal, O., de Jong, I., Duarte, H. (2017). An ultra-high-resolution 3D marine seismic system for detailed site investigation. Near Surface Geophysics 15, 335–345. https://doi.org/10.3997/1873-0604.2017025

Montelli, J.A. Dowdeswell, D. Ottesen, S.E. Johansen, (2017). Ice-sheet dynamics through the Quaternary on the mid-Norwegian continental margin inferred from 3D seismic data, Marine and Petroleum Geology, Volume 80, Pages 228-242, https://doi.org/10.1016/j.marpetgeo.2016.12.002.

Moreau, J., Huuse, M. (2014). Infill of tunnel valleys associated with landward-flowing ice sheets: The missing Middle Pleistocene record of the NW European rivers? Geochemistry, Geophysics, Geosystems 15, 1–9. https://doi.org/10.1002/2013gc005007.

Morency, C., Huismans, R.S., Beaumont, C. Fullsack, P. (2007). A numerical model for coupled fluid flow and matrix deformation with applications to disequilibrium compaction and delta stability. Journal of Geophysical Research: Solid Earth, 112(B10).

Morgan, E. C., Vanneste, M., Lecomte, I., Baise, L. G., Longva, O., McAdoo, B. (2012). Estimation of free gas saturation from seismic reflection surveys by the genetic algorithm inversion of a P-wave attenuation model. Geophysics, 77(4), R175-R187.

Mortimore, R. N. (2014). Logging the Chalk (pp. 48-117). Dunbeath, Scotland: Whittles Publishing.

Mosar, J., 2003, Scandinavia's North Atlantic passive margin: Journal of Geophysical Research: Solid Earth, v. 108, no. B8.

Mosca, I., Baptie, B., Haslam, R., Gafeira, J., Jenkins, G. (2024). Seismic Hazard Assessment for the UK Offshore Exclusive Economic Zone. British Geological Survey Open Report, OR/24/012.

Muir Wood, R. (1988). The Scandinavian Earthquakes of 22 December 1759 and 31 August 1819. Disasters 12, 223–236. https://doi.org/10.1111/j.1467-7717.1988.tb00672.x

Muir-Wood, R., King, G. C. (1993). Hydrological signatures of earthquake strain. Journal of Geophysical Research: Solid Earth, 98(B12), 22035-22068.Murray, A. B., & Thieler, E. R. (2004). A new hypothesis and exploratory model for the formation of large-scale inner-shelf sediment sorting and "rippled scour depressions." Continental Shelf Research, 24(3), 295–315. https://doi.org/10.1016/J.CSR.2003.11.001

Murray, A. B., Thieler, E. R. (2004). A new hypothesis and exploratory model for the formation of large-scale inner-shelf sediment sorting and "rippled scour depressions." Continental Shelf Research, 24(3), 295–315. https://doi.org/10.1016/J.CSR.2003.11.001

Murton, J. B., & Ballantyne, C. K. (2017). Periglacial and permafrost ground models for Great Britain. In J. S. Griffiths and C. J. Martin (Eds.), Engineering Geology and Geomorphology of Glaciated and Periglaciated Terrains (pp. 501-583). The Geological Society.

Mäntyniemi, P., Sørensen, M.B., Tatevossian, R.E. (2020). Testing the Environmental Seismic Intensity Scale on Data Derived from the Earthquakes of 1626, 1759, 1819, and 1904 in Fennoscandia, Northern Europe. Geosciences 11, 14. https://doi.org/10.3390/geosciences11010014.

Mörner, N. A. (2013). Patterns in seismology and palaeoseismology, and their application in long-term hazard assessments–the Swedish case in view of nuclear waste management. Pattern Recognition in Physics, 1(1), 75-89.

Nadim, F., T.J. Kvalstad, and T. Guttormsen (2005): Quantification of risks associated with seabed instability at Ormen Lange. Marine and Petroleum Geology, 22, 311-318.

Nazarov, A. N. (1991). Mathematical modelling of a snow-powder avalanche in the framework of the equations of two-layer shallow water. Fluid Dynamics 26: 70–75, DOI 10.1007/BF01050115.

Neilson, G., Musson, R.M.W., Burton, P.W. (1984). The “London” earthquake of 1580, April 6 Engineering Geology. 20 (1–2). 113-141.

Németh, A. A., Hulscher, S. J. M. H., De Vriend, H. J. (2002). Modelling sand wave migration in shallow shelf seas. Continental Shelf Research, 22(18–19), 2795–2806. https://doi.org/10.1016/S0278-4343(02)00127-9

Newton, A. M., & Huuse, M. (2017). Late Cenozoic environmental changes along the Norwegian margin. Marine Geology, 393, 216-244.

Newton, A. M., Montelli, A., Batchelor, C. L., Bellwald, B., Harding, R., Huuse, M., ... & Planke, S. (2024a). Glacial seismic geomorphology and Plio-Pleistocene ice sheet history offshore NW Europe.

Newton, A.M.W., et al., 2024b. Late Cenozoic Glaciers, Landscapes, Climates, and Ecosystems of the North Sea (GLACE-NS): 1236-1012-Full. Available at: https://www.iodp.org/docs/proposals/1236-1012-full-newton-cover/file.

NGU (2009). Rock avalanches — distribution and frequencies in the inner part of Storfjorden, Møre og Romsdal County, Norway. Geological Survey of Norway Report 2009.002.

NGU (2025). Marine limits and the possibility for quick clay – Marine limits and formerly submerged areas. Geological Survey of Norway. https://geo.ngu.no/kart/losmasse_mobil/?lang=nor&map=9

Noble-James, T., Bullimore, R., McBreen, F., O’Connor, J., Highfield, J., McCabe, C., Archer-Rand, S., Downie, A.L., Hawes, J. and Mitchell, P., 2023. Monitoring benthic habitats in English Marine Protected Areas: Lessons learned, challenges and future directions. Marine Policy, 157, p.105852.

Noble-James, T., Judd, A., Diesing, M., Clare, D., Eggett, A., Silburn, B., & Duncan, G. (2020). Monitoring shallow methane-derived authigenic carbonate: Insights from a UK Marine Protected Area. Aquatic Conservation: Marine and Freshwater Ecosystems, 30(5), 959-976.

NPD (2014). CO2 Storage Atlas Norwegian Continental Shelf. Norwegian Petroleum Directorate (NPD). Editors: Eva K. Halland, Jasminka Mujezinović, Fridtjof Riis. https://www.sodir.no/en/whats-new/publications/co2-atlases/co2-atlas-for-the-norwegian-continental-shelf/. Accessed 05. May 2025.

NVE (2021). Årsaksvurdering Kvikkleireskredet ved Kråkne i Alta 3. Juni 2020. External report Nr. 4/2021. Norges vassdrags- og energidirektorat. 200 pp. 978-82-410-2113-8.

Nygård, A., Sejrup, H.P., Haflidason, H., and King, E.L., 2002, Geometry and genesis of glacigenic debris flows on the North Sea Fan: TOBI imagery and deep-tow boomer evidence: Marine Geology, v. 188, p. 15-33, https://doi.org/10.1016/S0025-3227(02)00273-6.

Nygård, A., Sejrup, H.P., Haflidason, H., Cecchi, M., Ottesen, D., 2004. Deglaciation history of the southwestern Fennoscandian Ice Sheet between 15 and 13 14C ka BP. Boreas, 33: 1-17. https://doi.org/10.1111/j.1502-3885.2004.tb00992.x

Nygård, A., Sejrup, H.P., Haflidason, H., and Bryn, P., 2005, The glacial North Sea Fan, southern Norwegian Margin: architecture and evolution from the upper continental slope to the deep-sea basin: Marine and Petroleum Geology, v. 22, p. 71-84, https://doi.org/10.1016/j.marpetgeo.2004.12.001.

Obst, K., Nachtweide, C., Müller, U., 2017. Late Saalian and Weichselian glaciations in the German Baltic Sea documented by Pleistocene successions at the southeastern margin of the Arkona Basin. Boreas 46, 18–33. https://doi.org/10.1111/bor.12212

Ó Cofaigh, C., Hogan, K. A., Jennings, A. E., Callard, S. L., Dowdeswell, J. A., Noormets, R., Evans, J. (2018). The role of meltwater in high-latitude trough-mouth fan development: the Disko Trough-Mouth Fan, West Greenland. Marine Geology, 402, 17-32.

Oh, T.-M., Bang, E.-S., Cho, G.-C., Park, E.-S., 2017. Estimation of undrained shear strength for saturated clay using shear wave velocity. Mar. Georesources Geotechnol. 35, 236–244. https://doi.org/10.1080/1064119X.2016.1140855

Ojala, A. E., Mattila, J., Hämäläinen, J., & Sutinen, R. (2019). Lake sediment evidence of paleoseismicity: timing and spatial occurrence of late-and postglacial earthquakes in Finland. Tectonophysics, 771, 228227.

Okal EA and Synolakis CE (2004). Source discriminants for near-field tsunamis. Geophysical Journal International 158(3): 899–912.

Olesen, O., Blikra, L. H., Braathen, A., Dehls, J. F., Olsen, L., Rise, L., Roberts, D., Riis, F., Faleide, J. I., and Anda, E., 2004, Neotectonic deformation in Norway and its implications: a review: Norwegian Journal of Geology/Norsk Geologisk Forening, v. 84, no. 1.

Olesen, O., Bungum, H., Dehls, J., Lindholm, C., Pascal, C. & Roberts, D. (2013). Neotectonics, seismicity and contemporary stress field in Norway - mechanisms and implications. Geological Survey of Norway, Special Publication 13, 145–174.

Olesen, O., Olsen, L., Gibbons, S.J., Ruud, B.O., Høgaas, F., Johansen, T.A., Kværna, T., 2021. Postglacial Faulting in Norway, in: Steffen, H., Olesen, O., Sutinen, R. (Eds.), Glacially-Triggered Faulting. Cambridge University Press, pp. 198–217.

O'Reilly, S.S., Hryniewicz, K., Little, C.T.S., Monteys, X., Szpak, M.T., Murphy, B.T., Jordan, S.F., Allen, C.C.R., Kelleher, B.P., 2014. Shallow water methane-derived authigenic carbonate mounds at the Codling Fault Zone, western Irish Sea. Mar. Geol. 357, 139–150. https://doi.org/10.1016/j.margeo.2014.08.007

OSIG (Offshore Site Investigation and Geotechnics Committee), 2022. Guidance for the Planning and execution of geophysical and geotechnical ground investigations for offshore renewable energy developments. Society Underwater Technology (SUT) ISBN 0 906940 59 1.

Osmond, J.L., Mulrooney, M.J., Holden, N., Skurtveit, E., Faleide, J.I., Braathen, A., 2022. Structural traps and seals for expanding CO2 storage in the northern Horda platform, North Sea. AAPG Bull. 106, 1711–1752. https://doi.org/10.1306/03222221110

Ottemöller, L., Nielsen, H.H., Atakan, K., Braunmiller, J., Havskov, J. (2005) The 7 May 2001 induced seismic event in the Ekofisk oil field, North Sea. J. Geophys. Res. 110, B10301+. https://doi.org/10.1029/2004jb003374

Ottemöller, L., Michalek, J., Christensen, J., Baadshaug, U., Halpaap, F., Natvik, Ø., Kværna, T., Oye, V. (2021) UiB-NORSAR EIDA Node: Integration of Seismological Data in Norway. Seismol. Res. Lett. https://doi.org/10.1785/0220200369

Ottesen, D., Rise, L., Knies, J., Olsen, L. and Henriksen, S. (2005b) The Vestfjorden-Trænadjupet palaeo-ice stream drainage system, mid-Norwegian continental shelf. Marine Geology 218, 175–189. https://doi.org/10.1016/j.margeo.2005.03.001

Ottesen, D., Rise, L., Andersen, E.S., Bugge, T. & Eidvin, T. (2009) Geological evolution of the Norwegian continental shelf between 61ºN and 68ºN during the last 3 million years. Norwegian Journal of Geology Vol. 89, pp. 251-265. Trondheim 2009, ISSN 029-196x

Ottesen, D., Dowdeswell, J.A., Rise, L., Bugge, T. (2012) Large-scale development of the mid-Norwegian shelf over the last three million years and potential for hydrocarbon reservoirs in glacial sediments. Geol. Soc. Lond. Spec. Publ. 368 (1), 53–73.

Ottesen, D., Dowdeswell, J. A., Bugge, T. (2014). Morphology, sedimentary infill and depositional environments of the Early Quaternary North Sea Basin (56–62 N). Marine and Petroleum Geology, 56, 123-146.

Ottesen, D., Batchelor, C.L., Dowdeswell, J.A., Løseth, H. (2018) Morphology and pattern of Quaternary sedimentation in the North Sea Basin (52–62◦ N). Mar. Petrol. Geol. 98, 836–859.

Ottesen, D., Stewart, M., Brönner, M., Batchelor, C. L. (2020) Tunnel valleys of the central and northern North Sea (56 N to 62 N): Distribution and characteristics. Marine Geology, 425, 106199.

Ottesen, D., Batchelor, C., Bjarnadóttir, L.R., Wiberg, D.H., Dowdeswell, J.A., (2022) Glacial landforms reveal dynamic ice-sheet behaviour along the mid-Norwegian margin during the last glacial-deglacial cycle, Quaternary Science Reviews, Volume 285, 107462, https://doi.org/10.1016/j.quascirev.2022.107462.

Ottesen, D., Batchelor, C. L., Løseth, H., & Brunstad, H. (2024). 3D seismic evidence for a single Early Pleistocene glaciation of the central North Sea. Science Advances, 10(50), eadq6089.

Overeem, I., Weltje, G.J., Bishop-Kay, C., Kroonenberg, S.B. (2001) The Late Cenozoic Eridanos delta system in the Southern North Sea Basin: a climate signal in sediment supply? Basin Research, v. 13, 293-312. 10.1046/j.1365-2117.2001.00151.x

OWA (2020). Offshore Wind Accelerator. Guidance for Geophysical Surveying for UXO and Boulders Supporting Cable Installation. Report No. C862R04-3a. Carbon Trust.

Özmaral, A., A. Abegunrin, H. Keil, D. A. Hepp, T. Schwenk, H. Lantzsch, T. Mörz, and V. Spiess (2022), The Elbe Palaeovalley: Evolution from an ice-marginal valley to a sedimentary trap (SE North Sea), Quaternary Science Reviews 282, 107453, doi:https://doi.org/10.1016/j.quascirev.2022.107453.

Paolo, F., Kroodsma, D., Raynor, J., Hochberg, T., Davis, P., Cleary, J., ... & Halpin, P. (2024). Satellite mapping reveals extensive industrial activity at sea. Nature, 625(7993), 85-91.

Parker, G.; Fukushima, Y. and Pantin, H. M. (1986). Self-accelerating turbidity currents, Journal of Fluid Mechanics 171: 145–181, DOI 10.1017/S0022112086001404.

Parker, G.; Garcia, M.; Fukushima, Y. and Yu, W. (1987). Experiments on turbidity currents over an erodible bed. Journal of Hydraulic Research 25(1): 123–147, DOI 10.1080/00221688709499292.

Pantin, H.M. (1978). Quaternary sediments from the north-east Irish Sea: Isle of Man to Cumbria. Bull. Geol. Surv. G. B. 64.

Passchier, S., & Kleinhans, M. G. (2005). Observations of sand waves, megaripples, and hummocks in the Dutch coastal area and their relation to currents and combined flow conditions. Journal of Geophysical Research: Earth Surface, 110(F4), n/a-n/a. https://doi.org/10.1029/2004JF000215

Pastor, M.; Tayyebi, S. M.; Hernández, A.; Zheng, J.; Suárez, G. and Reyes, M. E. (2024). Modeling fast flows with variable water content: A depth-integrated SPH approach. Computers and Geotechnics 174: 106581, DOI 10.1016/j.compgeo.2024.106581.

Patton, H., Hubbard, A., Andreassen, K., Auriac, A., Whitehouse, P.L., Stroeven, A.P., Shackleton, C., Winsborrow, M., Heyman, J., Hall, A.M. (2017) Deglaciation of the Eurasian ice sheet complex: Quaternary Science Reviews, v. 169, p. 148-172, https://doi.org/10.1016/j.quascirev.2017.05.019.

Patton, H., Hubbard, A., Heyman, J. et al. The extreme yet transient nature of glacial erosion. Nat Commun 13, 7377 (2022). https://doi.org/10.1038/s41467-022-35072-0

Paul, M.A., Jobson, L.M. (1991). Geotechnical properties of soft clays from the Witch Ground Basin, central North Sea. Geol. Soc. Eng. Geol. Spec. Publ. 7, 151–156. https://doi.org/10.1144/GSL.ENG.1991.007.01.12

Paull, C., Ussler, W., Lorenson, T., Winters, W., Dougherty, J. (2005), Geochemical constraints on the distribution of gas hydrates in the Gulf of Mexico: Geo-Marine Letters, v. 25, p. 273-280.

Paull, C. K.; Talling, P. J.; Maier, K. L.; Parsons, D.; Xu, J.; Caress, D. W.; Gwiazda, R.; Lundsten, E. M.; Anderson, K.; Barry, J. P.; Chaffey, M.; O'Reilly, T.; Rosenberger, K. J.; Gales, J. A.; Kieft, B.; McGann, M.; Simmons, S. M.; McCann, M.; Sumner, E. J.; Clare, M. A. and Cartigny, M. J. (2018). Powerful turbidity currents driven by dense basal layers. Nature Communications 9: 4114, DOI 10.1038/s41467-018-06254-6.

Pedersen, S. (2014). Architecture of Glaciotectonic Complexes. Geosciences, 4(4), 269–296. https://doi.org/10.3390/geosciences4040269

Pedersen, S. A. S., & Boldreel, L. O. (2015). Thrust-fault architecture of glaciotectonic complexes in Denmark. GEUS Bulletin, 33(JUNE), 17–20. https://doi.org/10.34194/GEUSB.V33.4479

Peters, J.L., Benetti, S., Dunlop, P., Ó Cofaigh, C. (2015). Maximum extent and dynamic behaviour of the last British–Irish Ice Sheet west of Ireland. Quaternary Science Reviews, v. 128, 48-68. https://doi.org/10.1016/j.quascirev.2015.09.015

Peuchan, J., Terwindt, J. (2014). Introduction to CPT accuracy, in: 3rd International Symposium on Cone Penetration Testing CPT14: May 12-14, 2014. Las Vegas, Nevada, USA, p. 45 pp.

Pile Buck International, Inc.(2022). Pile Buck Magazine, www.pilebuck.com.

Piper, D. J., Shor, A. N., & Clarke, J. E. H. (1988). The 1929 "Grand Banks" earthquake, slump, and turbidity current.

Plaza-Faverola, A., Bünz, S., Mienert, J. (2012) The free gas zone beneath gas hydrate bearing sediments and its link to fluid flow: 3-D seismic imaging offshore mid-Norway: Marine Geology, v. 291, p. 211-226.

Plaza-Faverola, A., Vadakkepuliyambatta, S., Hong, W. L., Mienert, J., Bünz, S., Chand, S., & Greinert, J. (2017). Bottom-simulating reflector dynamics at Arctic thermogenic gas provinces: An example from Vestnesa Ridge, offshore west Svalbard. Journal of Geophysical Research: Solid Earth, 122(6), 4089-4105.

Plets, R., Dix, J., Bastos, A., & Best, A. (2007). Characterization of buried inundated peat on seismic (Chirp) data, inferred from core information. Archaeological Prospection, 14(4), 261–272. https://doi.org/10.1002/ARP.318

Porz, L., Zhang, W., Hanebuth, T.J.J., Schrum, C., 2021. Physical processes controlling mud depocenter development on continental shelves – Geological, oceanographic, and modeling concepts. Mar. Geol. 432, 106402. https://doi.org/https://doi.org/10.1016/j.margeo.2020.106402

Pouliquen, O., 1999. Scaling laws in granular flows down rough inclined planes. Physics of Fluids 11(3): 542–548. DOI 10.1063/1.869928.

Poulos, H.G., 2022. Use of shear wave velocity for foundation design. Geotech. Geol. Eng. 40, 1921–1938. https://doi.org/10.1007/s10706-021-02000-w.

Praeg, D., McCarron, S., Dove, D., Ó Cofaigh, C., Scott, G., Monteys, X., ... & Coxon, P. (2015). Ice sheet extension to the Celtic Sea shelf edge at the Last Glacial Maximum. Quaternary Science Reviews, 111, 107-112.

Prins, L. T., & Andresen, K. J. (2019). Buried late Quaternary channel systems in the Danish North Sea–Genesis and geological evolution. Quaternary Science Reviews, 223, 105943.

Prins, L. T., Andresen, K. J., Owen, M., and Knutz, P. C. (2025). A review of subsurface geosystems and de-risking offshore construction in the Danish North Sea. GEUS Bulletin 52. 8371. https://geusbulletin.org/index.php/geusb/article/view/8371/14568

Qiao, H., Liu, L., He, H., Liu, Xiaoyan, Liu, Xuening, Peng, P., 2023. The Practice and Development of T-Bar Penetrometer Tests in Offshore Engineering Investigation: A Comprehensive Review. J. Mar. Sci. Eng. 11. https://doi.org/10.3390/jmse11061160

Ramírez, L., Fraile, D., & Brindley, G. (2020). Offshore wind in Europe: Key trends and statistics 2019.

Rasmussen, E.S., Dybkjær, K., Toft, J.C., Nielsen, O.B., Sheldon, E., Mørk, F (in press): Lithostratigraphy of the Neogene succession of the Danish North Sea. GEUS Bulletin

Rauter, M. and Köhler, A. (2020). Constraints on entrainment and deposition models in avalanche simulations from high-resolution radar data. Geosciences 10(1): 9, DOI 10.3390/10010009.

Rauter M, Hoße L, Mulligan RP, Take WA, and Løvholt F (2021) Numerical simulation of impulse wave generation by idealized landslides with OpenFOAM. Coastal Engineering 165: 103815.

Rauter, M., Viroulet, S., Gylfadóttir, S. S., Fellin, W., and Løvholt, F. (2022). Granular porous landslide tsunami modelling – the 2014 Lake Askja flank collapse. Nature Communications, 13(1), 678.

Raymo, M. E., Lisiecki, L. E., & Nisancioglu, K. H. (2006). Plio-Pleistocene ice volume, Antarctic climate, and the global $\delta^{18}O$ record. Science, 313(5786), 492–495.

Rea, B. R., Newton, A. M., Lamb, R. M., Harding, R., Bigg, G. R., Rose, P., Spagnolo, M., Huuse, M., Cater, J. M. L., Archer, S., Buckley, F., Halliyeva, M., Huuse, J., Cornwell, D. G., Brocklehurst, S. H., Howell, J. A. (2018). Extensive marine-terminating ice sheets in Europe from 2.5 million years ago. Science Advances, 4(6), eaar8327.

Revelas, E.C., Sackmann, B.S., Maher, N.M., Jones, C.A. (2020). Mapping of benthic habitats at marine renewable energy sites using multibeam echosounder and sediment profile imaging technologies. Offshore Technology Conference. Houston, Texas. May. doi.org/10.4043/30733-MS

Riis, F., Berg, K., Cartwright, J., Eidvin, T., & Hansch, K. (2005). Formation of large, crater-like evacuation structures in ooze sediments in the Norwegian Sea. Possible implications for the development of the Storegga Slide. In Ormen Lange–an Integrated Study for Safe Field Development in the Storegga Submarine Area (pp. 257-273). Elsevier.

Rijsdijk, K.F., Passchier, S., Weerts, H.J.T., Laban, C., Van Leeuwen, R.J.W., Ebbing, J.H.J. (2005) Revised Upper Cenozoic stratigraphy of the Dutch sector of the North Sea Basin: towards and integrated lithostratigraphic, seismostratigraphic and allostratigraphic approach. Netherlands Journal of Geosciences — Geologie en Mijnbouw, Vol. 84, 129–146.

Rise, K., Ottesen, D., Berg, K., Lundin, E. (2005). Large-scale development of the mid-Norwegian margin during the last 3 million years. Marine and Petroleum Geology 22(1–2), 33–44, https://doi.org/10.1016/j.marpetgeo.2004.10.010.

Rise, L., Ottesen, D., Longva, O., Solheim, A., Andersen, E.S., Ayers, S. (2006). The Sklinnadjupet slide and its relation to the Elsterian glaciation on the mid-Norwegian margin: Marine and Petroleum Geology, v. 23, p. 569-583, https://doi.org/10.1016/j.marpetgeo.2006.05.005.

Rise, L., Chand, S., Hjelstuen, B.O., Haflidason, H., Bøe, R. (2010). Late Cenozoic geological development of the south Vøring margin, mid-Norway. Marine and Petroleum Geology 27, 1789-1803.

Rise, L., Bøe, R., Riis, F., Bellec, V. K., Laberg, J. S., Eidvin, T., ... & Thorsnes, T. (2013). The Lofoten-Vesterålen continental margin, North Norway: Canyons and mass-movement activity. Marine and Petroleum Geology, 45, 134-149.

Ritchie, J.D., Ziska, H., Johnson, H., Evans, D. (2011) Geology of the Faroe–Shetland Basin and Adjacent Areas. British Geological Survey Research Report, RR/11/01, Jarðfeingi Research Report, RR/11/01, HMSO for the British Geological Survey, London.

Roberts, A. M., Yielding, G. (1991). Deformation around basin-margin faults in the North Sea/mid-Norway rift. Geological Society, London, Special Publications, 56(1), 61-78.

Roberts, D. H., Dackombe, R. V., Thomas, G. S. (2007). Palaeo-ice streaming in the central sector of the British—Irish Ice Sheet during the Last Glacial Maximum: evidence from the northern Irish Sea Basin. Boreas, 36(2), 115-129.

Roberts, D.H., Grimoldi, E., Callard, S.L., Evans, D.J.A., Clark, C.D., Stewart, H.A., Dove, D., Saher, M., Ó Cofaigh, C., Chiverrell, R.C., Bateman, M.D., Moreton, S.G., Bradwell, T., Fabel, D., Medialdea, A. (2019) The mixed-bed glacial landform imprint of the North Sea Lobe in the western North Sea. Earth Surface Processes and Landforms, v. 44: 1233-1258.

Robertson, P.K. (1990). Soil classification using the cone penetration test. Can. Geotech. J. 27, 151–158.

Robertson, P.K., Campanella, R.G., Gillespie, D., Greig, J. (1986). Use of Piezometer Cone data, in: ASCE Speciality Conference In-Situ ’86: Use of In-Situ Testing in Geotechnical Engineering. American Society of Engineers (ASCE). ASCE, Reston, Blacksburg, pp. 1263–1280.

Rose P., Byerley, G., Vaughan, O., Cater, J., Rea, B. R., Spagnolo, M., Archer, S. (2018). Aviat: a Lower Pleistocene shallow gas hazard developed as a fuel gas supply for the Forties Field. From: Bowman, M. & Levell, B. (eds) 2018. Petroleum Geology of NW Europe: 50 Years of Learning – Proceedings of the 8th Petroleum Geology Conference, 485–505, https://doi.org/10.1144/PGC8.16

Rosentau, A., Bennike, O., Uścinowicz, S., & Miotk-Szpiganowicz, G. (2017). The baltic sea basin. Submerged landscapes of the European continental shelf: quaternary paleoenvironments, 103-133.

Rydningen, T.A., Laberg, J.S., Kolstad, V. (2015). Seabed morphology and sedimentary processes on high-gradient trough mouth fans offshore Troms, northern Norway, Geomorphology, 246, 205–219. https://doi.org/10.1016/j.geomorph.2015.06.007.

Rydningen, T.A., Laberg, J.S., Kolstad, V. (2016). Late Cenozoic evolution of high-gradient trough mouth fans and canyons on the glaciated continental margin offshore Troms, northern Norway—

Paleoclimatic implications and sediment yield. GSA Bulletin; 128 (3-4): 576–596. doi: https://doi.org/10.1130/B31302.1

Rydningen, T. A., Høgseth, G. V., Lasabuda, A. P. E., Laberg, J. S., Safronova, P. A., Forwick, M. (2020). An early Neogene—Early Quaternary contourite drift system on the SW Barents Sea continental margin, Norwegian Arctic. Geochemistry, Geophysics, Geosystems, 21(11), e2020GC009142.

Römer, M., Blumenberg, M., Heeschen, K., Schloemer, S., Müller, H., Müller, S., Hilgenfeldt, C., Barckhausen, U., Schwalenberg, K. (2021). Seafloor methane seepage related to salt diapirism in the northwestern part of the German North Sea. Frontiers in Earth Science 9, 319. https://doi.org/10.3389/feart.2021.556329

Römer-Stange, N., Wenau, S., Bihler, V., Keil, H., Ramos Córdova, C.A., Spiess, V. (2022). Boulder detection in the shallow sub-seafloor by diffraction imaging with beamforming on ultra-high resolution seismic data—a feasibility study. Earth and Space Science 9, e2021EA002156. https://doi.org/10.1029/2021EA002156

Rüther, D. C., Mattingsdal, R., Andreassen, K., Forwick, M., Husum, K. (2011). Seismic architecture and sedimentology of a major grounding zone system deposited by the Bjørnøyrenna Ice Stream during Late Weichselian deglaciation. Quaternary Science Reviews, 30(19-20), 2776-2792.

Safronova, P. A., Laberg, J. S., Andreassen, K., Shlykova, V., Vorren, T. O., Chernikov, S. (2015). Late Pliocene–early Pleistocene deep-sea basin sedimentation at high-latitudes: mega-scale submarine slides of the north-western Barents Sea margin prior to the shelf-edge glaciations. Basin Research, 29, 537-555, https://doi.org/10.1111/bre.12161

Salmanidou, D.M., Guillas, S., Georgiopoulou, A., Dias, F. (2017). Statistical emulation of landslide-induced tsunamis at the Rockall Bank, NE Atlantic. Proceedings of the Royal Society A: Mathematical, Physical and Engineering Sciences 473(2200): 20170026.

Sauvin, G., Vanneste, M., Vardy, M., Klinkvort, R., Forsberg, C.F. (2019) "Machine Learning and Quantitative Ground Models for Improving Offshore Wind Site Characterization." Paper presented at the Offshore Technology Conference, Houston, Texas, May 2019. doi: https://doi.org/10.4043/29351-MS

Scheidegger, A. E. (1973). On the prediction of the reach and velocity of catastrophic rockfalls. Rock Mechanics 5: 231–236.

Schiøler, P., Andsbjerg, J., Clausen, O.R., Dam, G., Dybkjær, K., Hamberg, L., Heilmann-Clausen, C., Johannessen, E.P., Kristensen, L.E., Prince, I., Rasmussen, J.A. (2007). Lithostratigraphy of the Palaeogene – Lower Neogene succession of the Danish North Sea. GEUS Bulletin, 12, 1–77. https://doi.org/10.34194/geusb.v12.5249

Schmitt, T., Mitchell, N. C., Ramsay, T. S. (2007). Use of swath bathymetry in the investigation of sand dune geometry and migration around a near shore “banner” tidal sandbank. Geological Society Special Publication, 274, 53–64. https://doi.org/10.1144/GSL.SP.2007.274.01.07

Schroot B. M., Schüttenhelm R.T.E. (2003). Expressions of shallow gas in the Netherlands North Sea. Netherlands Journal of Geosciences / Geologie en Mijnbouw 82 (1): 91-105.

Scourse, J. D., Chiverrell, R. C., Smedley, R. K., Small, D., Burke, M. J., Saher, M., ... & Clark, C. D. (2021). Maximum extent and readvance dynamics of the Irish sea ice stream and Irish Sea Glacier since the last glacial maximum. Journal of Quaternary Science, 36(5), 780-804.

Sejrup H. P., Aarseth I., Ellingsen K. L., Reither E., Jansen E. (1987) Quaternary stratigraphy of the Fladden area, central North Sea: a multidisciplinary study. Journal of Quaternary Science, v. 2, 35–58.

Sejrup, H. P., Aarseth, I., Haflidason, H., Løvlie, R., Bratten, Å., Tjøstheim, G., ... & Ellingsen, K. L. (1995). Quaternary of the Norwegian Channel: glaciation history and palaeoceanography. Norsk geologisk tidsskrift, 75(2-3), 65-87.

Sejrup, H. P., Clark, C. D., Hjelstuen, B. O. (2016). Rapid ice sheet retreat triggered by ice stream debuttressing: Evidence from the North Sea. Geology, v. 44, 355–358.

Sejrup, H. P., King, E. L., Aarseth, I., Haflidason, H., & Elverhøi, A. (1996). Quaternary erosion and depositional processes: western Norwegian fjords, Norwegian Channel and North Sea Fan. Geological Society, London, Special Publications, 117(1), 187-202.

Sejrup, H. P., Larsen, E., Landvik, J., King, E. L., Haflidason, H., & Nesje, A. (2000). Quaternary glaciations in southern Fennoscandia: evidence from southwestern Norway and the northern North Sea region. Quaternary Science Reviews, 19(7), 667-685.

Sejrup, H. P., Hjelstuen, B. O., Dahlgren, K. T., Haflidason, H., Kuijpers, A., Nygård, A., ... & Vorren, T. O. (2005). Pleistocene glacial history of the NW European continental margin. Marine and Petroleum Geology, 22(9-10), 1111-1129.

Sejrup, H. P., Hjelstuen, B. O., Patton, H., Esteves, M., Winsborrow, M., Rasmussen, T. L., ... & Hubbard, A. (2022). The role of ocean and atmospheric dynamics in the marine-based collapse of the last Eurasian Ice Sheet. Communications Earth & Environment, 3(1), 119.

Selby, N.D., Eshun, E., Patton, H.J., Douglas, A. (2005). Unusual long-period Rayleigh wave radiation from a vertical dip-slip source: The 7 May 2001 North Sea earthquake. J. Geophys. Res. Solid Earth 110, 2005JB003721. https://doi.org/10.1029/2005JB003721

Serié, C., Huuse, M., Schødt, N. H., Brooks, J. M., & Williams, A. (2017). Subsurface fluid flow in the deep-water Kwanza Basin, offshore Angola. Basin Research, 29(2), 149-179.

Serov, P., Mattingsdal, R., Winsborrow, M., Patton, H., and Andreassen, K., 2023, Widespread natural methane and oil leakage from sub-marine Arctic reservoirs: Nature Communications, v. 14, no. 1, p. 1782.

Shanmugam, G. (1996). High-density turbidity currents: Are they sandy debris flows? Journal of Sedimentary Research 66(1), 2–10. DOI: 10.1306/D426828E-2B26-11D7-8648000102C1865D.

Shennan, I., Bradley, S. L., & Edwards, R. (2018). Relative sea-level changes and crustal movements in Britain and Ireland since the Last Glacial Maximum. Quaternary Science Reviews, 188, 143-159.

Shennan, I., Milne, G. and Bradley, S. (2012), Late Holocene vertical land motion and relative sea-level changes: lessons from the British Isles. J. Quaternary Sci., 27: 64-70. https://doi.org/10.1002/jqs.1532

Shipp, 2017. Marine Geohazards. Workshop handout. Submarine Mass Movements and Their Consequences. 4th International Symposium. Vancouver Island, Canada. November 2017.

Si P, Shi H, and Yu X. (2018) A general numerical model for surface waves generated by granular material intruding into a water body. Coastal Engineering 142: 42–51.

Sibson, R. H., 1994, Crustal stress, faulting and fluid flow: Geological Society, London, Special Publications, v. 78, no. 1, p. 69-84.

Singhroha, S., Bünz, S., Plaza-Faverola, A., and Chand, S., 2020, Detection of gas hydrates in faults using azimuthal seismic velocity analysis, Vestnesa Ridge, W-Svalbard Margin: Journal of Geophysical Research: Solid Earth, v. 125, no. 2, p. e2019JB017949.

SINTEF Offshore Blowout Database, http://www.sintef.no/home/Technology-and-Society/Safety-Research/Projects/SINTEF-Offshore-Blowout-Database/ Trondheim, Norway, 2011

Sloan, E. D. (1998a). Gas hydrates: review of physical/chemical properties. Energy & fuels, 12(2), 191-196.

Sloan, E. D. (1998b). Physical/chemical properties of gas hydrates and application to world margin stability and climatic change. Geological society, London, special publications, 137(1), 31-50.

Sloan, E. D., and Koh, C. A., 2007, Clathrate hydrates of natural gases, CRC press.

Small, D., Smedley, R. K., Chiverrell, R. C., Scourse, J. D., Ó Cofaigh, C., Duller, G. A., ... & Clark, C. D. (2018). Trough geometry was a greater influence than climate-ocean forcing in regulating retreat of the marine-based Irish-Sea Ice Stream. GSA Bulletin, 130(11-12), 1981-1999.

Smedley, R. K., Scourse, J. D., Small, D., Hiemstra, J. F., Duller, G. A. T., Bateman, M. D., ... & Xu, S. (2017). New age constraints for the limit of the British–Irish Ice Sheet on the Isles of Scilly. Journal of Quaternary Science, 32(1), 48-62.

Smith, D. E., Cullingford, R. A., and Haggart, A., 1985. Major Coastal Flood During the Holocene in Eastern Scotland, E&G Quaternary Sci. J., 35, 109–118

Smith, D.E., Shi, S., Cullingford, R.A., Dawson, A.G., Dawson, S., Firth, C.R., Foster, I.D.L., Fretwell, P.T., Haggart, B.A., Holloway, L.K., Long, D., 2004. The Holocene Storegga Slide tsunami in the United Kingdom. Quaternary Science Reviews 23, 2291-2321.

Smith, S. A., Vanneste, M., Faleide, T. S. and Bertrand, A., 2024. Multi-sensor core logging of marine sediments for continuous thermal conductivity profiles. In Proceedings of the 7th International Conference on Geotechnical and Geophysical Site Characterization (Vol. 18, p. 21).

Solheim, A., Berg, K., Forsberg, C.F., Bryn, P., 2005a. The Storegga Slide complex: repetitive large scale sliding with similar cause and development. Marine and Petroleum Geology, 22, 97–107. https://doi.org/10.1016/j.marpetgeo.2004.10.013.

Solheim, A., Bryn, P., Berg, K., Sejrup, H.P. & Mienert, J. 2005b: Ormen Lange: An integrated study for the safe development of a deep-water gas field within the Storegga Slide Complex, NE Atlantic continental margin. Thematic Volume. Marine and Petroleum Geology 22, 1–9. https://doi.org/10.1016/j.marpetgeo.2004.10.001.

Soraghan, C., 2016. Management of Hydrogen Sulphide (H2S) Gas in Wind Turbine Sub-Structures: identifying and managing H2S. Case Study published by Catapult Offshore renewable Energy, TLI-CS-00006.

Sovilla, B., McElwaine, J. N. and Louge, M. Y, (2015). The structure of powder snow avalanches. Comptes Rendus Physique 16(1), 97–104. DOI: 10.1016/j.crhy.2014.11.005.

Standards Australia. (2001). AS/NZS 4801 Occupational health and safety management systems - Specification with guidance for use. Sydney: Standards Australia.

Stewart, S. A. (2007). Salt tectonics in the North Sea Basin: a structural style template for seismic interpreters.

Stewart, S.A., Davies, R.J. (2006). Structure and emplacement of mud volcano systems in the South Caspian Basin. AAPG bulletin, 90(5), pp.771-786.

Stewart, H.A., Bradwell, T., Carter, G.D.O., Dove, D., Gafeira, J. (2021) Chapter 6: Geomorphology of the Offshore Continental Shelf. 117-134 in World Geomorphological Landscapes: Landscapes and Landforms of Scotland (J. Gordon and C. Ballantyne Editors). (London Springer) DOI: 10.1007/978-3-030-71246-4_6

Stewart, H. A., Cooper, R. M., Lewis, W. D. (2022) Reprocessing of CHP datasets (HI1567 & HI1570) and Seafloor Substrate Interpretation for Selected Areas: Inner Sound off Skye on the West Coast of

Scotland. British Geological Survey Commissioned Report, 44 pp. (CR/21/080). https://nora.nerc.ac.uk/id/eprint/531840

Stewart, H.A., Hinxman, D., Dyer, N., Moore, J., Baker, A., Plenderleith, G., Terente, V., Holland, R., Rose, M. (2023) Ice sheet and retreat dynamics of the eastern sector of the British–Irish Ice Sheet: implications for sustainable offshore wind development, Berwick Bank Wind Farm. Quaternary Research Association Annual Discussion Meeting, 5-6 January 2023, Geological Society of London.

Stewart, H. A., Long, D. (2012) The timing and significance of gully incision on the eastern flank of the Faroe-Shetland channel and its impact on seafloor infrastructure. European Association of Geoscientists & Engineers. Near Surface Geophysics. V.10 n.4, 317-331.

Stewart, H.A., Long, D. (2016). Glacigenic debris flows observed in 3D seismic high-resolution seafloor imagery, Faroe–Shetland Channel, NE Atlantic. From: Dowdeswell, J A, Canals, M, Jakobsson, M, Todd, B J, Dowdeswell, E K and Hogan, K A (eds). Atlas of Submarine Glacial Landforms: Modern, Quaternary and Ancient. Geological Society, London, Memoirs, v. 46, 361–362.

Stewart, M. A., Lonergan, L. (2011) Seven glacial cycles in the middle-late Pleistocene of northwest Europe: geomorphic evidence from buried tunnel valleys. Geology, v. 39, 283–286.

Stoker, M. S., 1995. The influence of glacigenic sedimentation on slope-apron development on the continental margin off Northwest Britain. In Scrutton, R. A., Stoker, M. S., Shimmield, G. B. & Tudhope, A. W. (eds), 1995. The Tectonics, Sedimentation and Palaeoceanography of the North Atlantic Region, Geological Society Special Publication No. 90, 159-177.

Stoker M.S. (2002). Late Neogene development of the UK Atlantic mar-gin. In Doré A.G., Cartwright J.A., Stoker M.S., Turner J.P. and White N. (eds) Exhumation of the North Atlantic Margin: Timing, Mechanisms and Implications for Petroleum Exploration, Geological Society of London Special Publication, v. 196, 313-329.

Stoker, M.S. (2013) Cenozoic sedimentary rocks. In: Hitchen, K., Johnson, H. & Gatliff, R. W. (eds) Geology of the Rockall Basin and Adjacent Areas. British Geological Survey Research Report, RR/12/03, HMSO for the British Geological Survey, London, pp 96-136.

Stoker, M.S., Balson, P.S., Long, D., Tappin, D.R. (2011) An overview of the lithostratigraphical framework for the Quaternary deposits on the United Kingdom continental shelf. British Geological Survey Research Report, RR/11/03. 48pp. www.bgs.ac.uk/downloads/start.cfm?id=2084

Stoker, M.S., Bent, A.J.A. (1985) Middle Pleistocene glacial and glaciomarine sedimentation in the west Central North Sea. Boreas, v. 14, 325–332.

Stoker, M.S., Hitchen, K., Graham, C.C. (1993). United Kingdom offshore regional report: The geology of the Hebrides and West Shetland shelves, and adjacent deep-water areas. London: HMSO for the British Geological Survey.

Stoker, M.S., Praeg, D., Hjelstuen, B.O., Laberg, J.S., Nielsen, T., Shannon, P. M. (2005). Neogene stratigraphy and the sedimentary and oceanographic development of the NW European Atlantic margin. Marine and Petroleum Geology, v. 22, 977–1005.

Stoker, M.S., Varming, T. (2011) Cenozoic (sedimentary). In: Ritchie, J.D., Ziska, H., Johnson, H. & Evans, D. (eds) Geology of the Faroe–Shetland Basin and Adjacent Areas. British Geological Survey Research Report, RR/11/01, Jarðfeingi Research Report, RR/11/01, HMSO for the British Geological Survey, London, pp 151–208.

Stolt, M. H., & Lindbo, D. L. (2010). Soil Organic Matter. Interpretation of Micromorphological Features of Soils and Regoliths, 369–396. https://doi.org/10.1016/B978-0-444-53156-8.00017-9

Stow, J., 1601. The Chronicles of England, London.

Stow, D.A.V., Hernandez-Molina, F.J., Llave, E., Sayago-Gil, M., Diaz del Rio, V., Branson, A. (2009). "Bedform-velocity matrix: The estimation of bottom current velocity from bedform observations". Geology. 37 (4): 327–330

Sturt, F., Garrow, D., & Bradley, S. (2013). New models of North West European Holocene palaeogeography and inundation. Journal of Archaeological Science, 40(11), 3963-3976.

Sultan, N., Voisset, M., Marsset, T., Vernant, A.-M., Cauquil, E., Colliat, J., and Curinier, V., 2007, Detection of free gas and gas hydrate based on 3D seismic data and cone penetration testing: An example from the Nigerian Continental Slope: Marine Geology, 240 (1–4), 235–255.

Sultan, N., Plaza-Faverola, A., Vadakkepuliyambatta, S., Buenz, S., & Knies, J. (2020). Impact of tides and sea-level on deep-sea Arctic methane emissions. Nature communications, 11(1), 5087.

Sumer, B.M., Kirca, V.S.O., 2022. Scour and liquefaction issues for anchors and other subsea structures in floating offshore wind farms: A review. Water Sci. Eng. 15, 3–14. https://doi.org/10.1016/j.wse.2021.11.002

SUT (2022). Guidance Notes for the Planning and Execution of Geophysical and Geotechnical Ground Investigations for Offshore Renewable Energy Developments. Cook, M (Editor). (The Society for Underwater Technology: London) ISBN 0 906940 59 1. 71pp.

Svennevig, K., Hicks, S.P., Forbriger, T., Lecocq, T., Widmer-Schnidrig, R., Mangeney, A., Hibert, C., Korsgaard, N.J., Lucas, A., Satriano, C., Anthony, R.E., Mordret, A., Schippkus, S., Rysgaard, S., Boone, W., Gibbons, S.J., Cook, K.L., Glimsdal, S., Løvholt, F., Van Noten, K., Assink, J.D.,

Marboeuf, A., Lomax, A., Vanneste, K., Taira, T., Spagnolo, M., De Plaen, R.S.M., Koelemeijer, P., Ebeling, C., Cannata, A., Harcourt, W.D., Cornwell, D.G.., Caudron, C., Poli, P., Bernard, P., Larose, E., Stutzmann, E., Voss, P.H., Lund, B., Cannavo, F., Castro-Díaz, M.J., Chaves, E.J., Dahl-Jensen, T., Pinho Dias, N. De, Déprez, A., Develter, R., Dreger, D., Evers, L.G., Fernández-Nieto, E.D., Ferreira, A.M.G., Funning, G.J., Gabriel, A.-A., Hendrickx, M.E., Kafka, A.L., Keiding, M., Kerby, J., Khan, S.A., Dideriksen, A.K., Lamb, O.D., Larsen, T.B., Lipovsky, B., Magdalena, I., Malet, J.-P., Myrup, M., Rivera, L., Ruiz-Castillo, E., Wetter, S.; Wirtz, B. (2024). A rockslide-generated tsunami in a Greenland fjord rang Earth for 9 days. Science 385 (6714), 1196–1205.

Svendsen, J. I., Alexanderson, H., Astakhov, V. I., Demidov, I., Dowdeswell, J. A., Funder, S., ... & Stein, R. (2004). Late Quaternary ice sheet history of northern Eurasia. Quaternary Science Reviews, 23(11-13), 1229-1271.

Sørensen, M.B., Haga, T., Nesje, A. (2023). Earthquake-induced landslides in Norway. Nat. Hazards Earth Syst. Sci., 23, 1577–1592.

Tam, C. 2023. Leveraging the use of repurposed Oil and Gas 2D seismic data to de-risk offshore wind farm development projects. A case study from the Central North Sea. EGC1 Conference poster, Aberdeen

Tappin, D. R., Chadwick, R. A., Jackson, A. A., Wingfield, R. T. R. and Smith, N. J. P., 1995. The geology of Cardigan Bay and the Bristol Channel, United Kingdom Offshore Regional Report. British Geological Survey. London: HMSO

Tappin, D.R., Pearce, B., Fitch, S., Dove, D., Gearey, B., Hill, J.M., Chambers, C., Bates, R., Pinnion, J., Diaz Doce, D. and Green, M. (2011). The Humber regional environmental characterisation. Marine Aggregate Levy Sustainability Fund.

Tasianas, A., Bünz, S., Bellwald, B., Hammer, Ø., Planke, S., Lebedeva-Ivanova, N., & Krassakis, P. (2018). High-resolution 3D seismic study of pockmarks and shallow fluid flow systems at the Snøhvit hydrocarbon field in the SW Barents Sea. Marine Geology, 403, 247-261.

Taylor, M., Ralon, P., Anuta, H., & Al-Zoghoul, S. (2020). IRENA renewable power generation costs in 2019. International Renewable Energy Agency: Abu Dhabi, UAE.

Thakur, V., L'Heureux, J. S., & Locat, A. (2017). Landslides in sensitive clays. Advances in Natural and Technological Hazards Research, 46, 593.

Thöle, H., Gaedicke, C., Kuhlmann, G., Reinhardt, L., 2014. Late Cenozoic sedimentary evolution of the German North Sea – A seismic stratigraphic approach. Newsletters on Stratigraphy 299–329. https://doi.org/10.1127/0078-0421/2014/0049

Tommasi, P., Avalle, A., Budillon, F., Romeo, R., Caburlotto, A., Conforti, A., Di Martino, G., Pagliaroli, A., Magagnoli, M., Urgeles, R., Llopart, J., Camerlenghi, A., 2019. Evaluation of disturbance induced on soft offshore sediments by two types of gravity piston coring techniques. Mar. Geol. 417, 106005. https://doi.org/10.1016/j.margeo.2019.106005

Toorman, E. A. (1997). Modelling the thixotropic behavior of dense cohesive sediment suspensions. Rheologica Acta 36: 56–65, DOI 10.1007/bf00366724.

Tóth, Z., Spiess, V., Mogollón, J.M., Jensen, J.B., 2014a. Estimating the free gas content in Baltic Sea sediments using compressional wave velocity from marine seismic data. Journal of Geophysical Research: Solid Earth 119, 8577–8593. https://doi.org/10.1002/2014JB010989

Tóth, Z., Spieß, V., Jensen, J., 2014b. Seismo-acoustic signatures of shallow free gas in the Bornholm Basin, Baltic Sea. Cont. Shelf Res. 88, 228–239. https://doi.org/https://doi.org/10.1016/j.csr.2014.08.007

Tóth, Z., McCarron, S., Wheeler, A. J., Wenau, S., Davis, S., Lim, A., & Spiess, V. (2020). Geomorphological and seismostratigraphic evidence for multidirectional polyphase glaciation of the northern Celtic Sea. Journal of Quaternary Science, 35(3), 465-478.

Trafford, A., & Long, M. (2020). Relationship between Shear-Wave Velocity and Undrained Shear Strength of Peat. Journal of Geotechnical and Geoenvironmental Engineering, 146(7), 04020057. https://doi.org/10.1061/(ASCE)GT.1943-5606.0002298/ASSET/F2C1F035-9C2D-4E63-A96E-E6C0F55BB547/ASSETS/IMAGES/LARGE/FIGURE9.JPG

Trafford, A., Ellwood, R., Wacquier, L., Godfrey, A., Minto, C., Coughlan, M., Donohue, S., 2022. Distributed acoustic sensing for active offshore shear wave profiling. Sci. Rep. 12, 9691. https://doi.org/10.1038/s41598-022-13962-z

Tran, Q. A.; Grimstad, G. and Ghoreishian Amiri, S. A. (2024). MPMICE: A hybrid MPM-CFD model for simulating coupled problems in porous media. Application to earthquake-induced submarine landslides. Intl. J. Num. Meth. Eng. 125(5) : e7383, DOI 10.1002/nme.7383. 10.1002/nme.7383.

Tregaskis, C. (2020). Granular Avalanches Past Obstacles and Erosion and Deposition Processes in Shallow Granular Flows. PhD thesis, Dept. of Mathematics, University of Manchester, Manchester, UK. https://pure.manchester.ac.uk/ws/portalfiles/portal/213186161/FULL_TEXT.PDF.

Trivedi, A., Sarkar, S., Ker, S., and Minshull, T. A., 2023, An improved Weichselian seismic stratigraphic framework of the Kongsfjorden-Isfjorden Interfan region off western Svalbard from high-frequency deep-towed seismic data and its implication on fluid migration and methane venting: Copernicus Meetings.

Trujillo-Vela, M. G.; Ramos-Canón, A. M.; Escobar-Vargas, J. A. and Galindo-Torres, S. A. (2022). An overview of debris-flow mathematical modelling. Earth-Science Reviews 232: 104135, DOI 10.1016/j.earscirev.2022.104135.

Tuuling, I., & Flodén, T. (2016). The Baltic Klint beneath the central Baltic Sea and its comparison with the North Estonian Klint. Geomorphology, 263, 1-18.

Tylmann, K., & Uścinowicz, S. (2022). Timing of the last deglaciation phases in the southern Baltic area inferred from Bayesian age modeling. Quaternary Science Reviews, 287, 107563.

Uehara, K., Scourse, J. D., Horsburgh, K. J., Lambeck, K., & Purcell, A. P. (2006). Tidal evolution of the northwest European shelf seas from the Last Glacial Maximum to the present. Journal of Geophysical Research: Oceans, 111(C9).

Unnithan, V., Shannon, P. M., McGrane, K., Readman, P. W., Jacob, A. W. B., Keary, R., & Kenyon, N. H. (2001). Slope instability and sediment redistribution in the Rockall Trough: constraints from GLORIA.

Upstreamonline (2025). Equinor sharpens its exploration tools to bring gas to Europe. https://www.upstreamonline.com/exclusive/equinor-sharpens-its-exploration-tools-to-bring-gas-to-europe/2-1-1749879. Accessed on 05 May 2025.

Urlaub, M., Talling, P.J., Masson, D.G., 2013. Timing and frequency of large submarine landslides: implications for understanding triggers and future geohazard, Quaternary Science Reviews 72, 63-82, https://doi.org/10.1016/j.quascirev.2013.04.020.

Uścinowicz, S. (2006). A relative sea-level curve for the Polish Southern Baltic Sea. Quaternary International, 145, 86-105.

Uścinowicz, S. (2014). The baltic sea continental shelf.

Vachon, R., Schmidt, P., Lund, B., Plaza-Faverola, A., Patton, H., and Hubbard, A., 2022, Glacially Induced Stress Across the Arctic From the Eemian Interglacial to the Present—Implications for Faulting and Methane Seepage: Journal of Geophysical Research: Solid Earth, v. 127, no. 7, p. e2022JB024272.

Vadakkepuliyambatta, S., Chand, S., & Bünz, S. (2017). The history and future trends of ocean warming-induced gas hydrate dissociation in the SW Barents Sea. Geophysical Research Letters, 44(2), 835-844.

van Dijk, T. A. G. P., Best, J., & Baas, A. C. W. (2021). Subaqueous and Subaerial Depositional Bedforms. In Encyclopedia of Geology (pp. 771–786). Elsevier. https://doi.org/10.1016/B978-0-08-102908-4.00187-9

Van Landeghem, K. J., Uehara, K., Wheeler, A. J., Mitchell, N. C., & Scourse, J. D. (2009a). Post-glacial sediment dynamics in the Irish Sea and sediment wave morphology: Data–model comparisons. Continental Shelf Research, 29(14), 1723-1736.

Van Landeghem, K. J., Wheeler, A. J., Mitchell, N. C., & Sutton, G. (2009b). Variations in sediment wave dimensions across the tidally dominated Irish Sea, NW Europe. Marine Geology, 263(1-4), 108-119.

Van Landeghem, K. J., Niemann, H., Steinle, L. I., O'Reilly, S. S., Huws, D. G., & Croker, P. F. (2015). Geological settings and seafloor morphodynamic evolution linked to methane seepage. Geo-Marine Letters, 35, 289-304.

Van Landeghem, K. J., & Chiverrell, R. C. (2020). Bed erosion during fast ice streaming regulated the retreat dynamics of the Irish Sea Ice Stream. Quaternary Science Reviews, 245, 106526.

Van Rensbergen, P., Hillis, R. R., Maltman, A. J. & Morely, C. K. (editors) 2003. Subsurface Sediment Remobilization. Geological Society, London, Special Publications 216; https://doi.org/10.1144/GSL.SP.2003.216.01.34

Vanneste, M., Mienert, J., and Bünz, S., 2006, The Hinlopen Slide: A giant, submarine slope failure on the northern Svalbard margin, Arctic Ocean: Earth and Planetary Science Letters, v. 245, p. 373-388, https://doi.org/10.1016/j.epsl.2006.02.045.

Vanneste, M., Sultan, N., Garziglia, S., Forsberg, C. F., & l'Heureux, J. S. (2014). Seafloor instabilities and sediment deformation processes: The need for integrated, multi-disciplinary investigations. Marine Geology, 352, 183-214.

Vanneste M, Løvholt F, Issler D, Liu Z, Boylan N, and Kim J (2019) A novel quasi-3D landslide dynamics model: From theory to applications and risk assessment. In: Proceedings of the Offshore Technology Conference 2019, OTC-29363-MS. ISBN: 978-1-61399-641-6.

van Vliet-Lanoë, B., Magyari, A., and Meilliez, F., 2004, Distinguishing between tectonic and periglacial deformations of quaternary continental deposits in Europe: Global and Planetary Change, v. 43, no. 1-2, p. 103-127.

Vardy, M.E., Vanneste, M., Henstock, T.J., Clare, M.A., Forsberg, C.F., and G. Provenzano, 2017. State-of-the-art remote characterization of shallow marine sediments: the road to a fully integrated solution. Near Surface Geophysics, 15, 387-402.

Vasskog, K., Waldmann, N., Bondevik, S., Nesje, A., Chapron, E., & Ariztegui, D. (2013). Evidence for Storegga tsunami run-up at the head of Nordfjord, western Norway. Journal of Quaternary Science, 28(4), 391-402.

6052 Vattenfall, 2019: Horns Rev III Wind Farm Zone, Location E03 Seabed and soils. Report, 102 pages

6053 Vaughan-Hirsch, D. P., & Phillips, E. R. (2017). Mid-Pleistocene thin-skinned glaciotectonic thrusting
6054 of the Aberdeen Ground Formation, Central Graben region, central North Sea. Journal of Quaternary
6055 Science, 32(2), 196–212. https://doi.org/10.1002/JQS.2836

6056 Vejbæk, O.V., 2008. Disequilibrium compaction as the cause for Cretaceous–Paleogene overpressures
6057 in the Danish North Sea. AAPG bulletin, 92(2), pp.165-180.

6058 Velenturf, A. P. M., Emery, A. R., Hodgson, D. M., Barlow, N. L. M., Mohtaj Khorasani, A. M., Van
6059 Alstine, J., ... & Thorp, M. (2021). Geoscience solutions for sustainable offshore wind development.
6060 Earth Science, Systems and Society, 1(1), 10042.

6061 Vimpere, L., Spangenberg, J. E., Roige, M., Adatte, T., De Kaenel, E., Fildani, A., ... & Castelltort, S.
6062 (2023). Carbon isotope and biostratigraphic evidence for an expanded Paleocene–Eocene Thermal
6063 Maximum sedimentary record in the deep Gulf of Mexico. Geology, 51(4), 334-339.

6064 Viner, D. (1991). Accident analysis and risk control. Derek Viner Pty Ltd, Melbourne.

6065 Vinnem, JE., Røed, W. (2020). Lessons from Major Accidents. In: Offshore Risk Assessment Vol. 1.
6066 Springer Series in Reliability Engineering. Springer, London. https://doi.org/10.1007/978-1-4471-
6067 7444-8_4

6068 Virtanen, E. A., Lappalainen, J., Nurmi, M., Viitasalo, M., Tikanmäki, M., Heinonen, J., ... & Moilanen,
6069 A. (2022). Balancing profitability of energy production, societal impacts and biodiversity in offshore
6070 wind farm design. Renewable and Sustainable Energy Reviews, 158, 112087.

6071 Voellmy, A. (1955). Über die Zerstörungskraft von Lawinen [On the destructive power of avalanches]
6072 (in German). Schweiz. Bauztg 73(12, 15, 17, 19) : 159–165, 212–217, 246–249, 280–285.

6073 Vorren, T.O., and Laberg, J.S., 1997, Trough mouth fans – palaeoclimate and ice-sheet monitors:
6074 Quaternary Science Reviews, v. 16, p. 865-881, https://doi.org/10.1016/S0277-3791(97)00003-6.

6075 Vorren, T. O., Laberg, J. S., Blaume, F., Dowdeswell, J. A., Kenyon, N. H., Mienert, J., ... & Werner,
6076 F. (1998). The Norwegian–Greenland Sea continental margins: morphology and late Quaternary
6077 sedimentary processes and environment. Quaternary Science Reviews, 17(1-3), 273-302.

6078 Vorren, T.O., Mangerud, J., Blikra, L.H., Nesje, A., and Sveian, H. (2008). The emergence of modern
6079 Norway. In: Ramberg, I.B., Bryhni, I., Nøttvedt, A., Rangnes, K. (Eds.) The Making of a Land —
6080 Geology of Norway. Norsk Geologisk Forening, Trondheim, 534–559.

6081 Voss, P., Dahl-Jensen, T. & Larsen, T. B. (2015) Earthquake hazard in Denmark, GEUS. Danmarks

6082 og Grønlands Geologiske Undersøgelse Rapport Vol. 2015 No. 24 https://doi.org/10.22008/gpub/30674

Wagner, B., Bennike, O., Klug, M., Cremer, H., 2007. First indication of Storegga tsunami deposits from East Greenland. Journal of Quaternary Science 22, 321-325.

Waldmann N, Vasskog K, Simpson G, Chapron E, Støren EWN, Hansen L, Loizeau J-L, Nesje A and Ariztegui D (2021) Anatomy of a Catastrophe: Reconstructing the 1936 Rock Fall and Tsunami Event in Lake Lovatnet, Western Norway. Front. Earth Sci. 9:671378. doi: 10.3389/feart.2021.671378

Waller, M., & Kirby, J. (2021). Coastal peat-beds and peatlands of the southern North Sea: their past, present and future. Biological Reviews, 96(2), 408–432. https://doi.org/10.1111/brv.12662

Wallmann, K., Riedel, M., Hong, W. L., Patton, H., Hubbard, A., Pape, T., ... & Bohrmann, G. (2018). Gas hydrate dissociation off Svalbard induced by isostatic rebound rather than global warming. Nature communications, 9(1), 83.

Walker, J., Gaffney, V., Fitch, S., Muru, M., Fraser, A., Bates, M., & Bates, R. (2020). A great wave: the Storegga tsunami and the end of Doggerland?. Antiquity, 94(378), 1409-1425.

Walker, J.D. and Geissman, J.W., compilers. (2022). Geologic Time Scale v. 6.0. Geological Society of America. https://doi.org/10.1130/2022.CTS006C.

Walker, J., Gaffney, V., Harding, R., Fraser, A.I., Fitch, S., Boothby, V. (2024). Winds of Change: Urgent Challenges and Emerging Opportunities in Submerged Prehistory, a Perspective from the North Sea. Heritage 2024, 7, 1947–1968. https://doi.org/10.3390/heritage7040093

Waller, M. and Kirby, J. (2021). Coastal peat-beds and peatlands of the southern North Sea: their past, present and future. Biol. Rev. (2021), 96, pp. 408–432. 408 doi: 10.1111/brv.12662

Ward, S.L., Neill, S.P., Van Landeghem, K.J.J., Scourse, J.D., 2015. Classifying seabed sediment type using simulated tidal-induced bed shear stress. Mar. Geol. 367, 94–104. https://doi.org/10.1016/j.margeo.2015.05.010

Watts, P., Grilli, S. T., Tappin, D. R., and Fryer, G. J. (2005). Tsunami generation by submarine mass failure. II: Predictive equations and case studies. Journal of waterway, port, coastal, and ocean engineering, 131(6), 298-310.

Watts, R., Lee, A., and Snieckus, D. (2021). Saipem woe as 'soil and foundations' issues hit work on North Sea wind farm installation. UpStream. https://www.upstreamonline.com/energy-transition/saipem-woe-as-soil-and-foundations-issues-hit-work-on-north-sea-wind-farm-installation/2-1-971065 (accessed April 2025).

Weaver, P. P., Wynn, R. B., Kenyon, N. H., & Evans, J. (2000). Continental margin sedimentation, with special reference to the north-east Atlantic margin. Sedimentology, 47, 239-256.

Webb, K. E., Barnes, D. K., & Plankea, S. (2009). Pockmarks: Refuges for marine benthic biodiversity. Limnology and Oceanography, 54(5), 1776-1788.

Wentworth, C.K., 1922. A scale of grade and class terms for clastic sediments. The Journal of Geology, 30, pp. 377-392

Westerhold, T., Marwan, N., Drury, A. J., Liebrand, D., Agnini, C., Anagnostou, E., ... & Zachos, J. C. (2020). An astronomically dated record of Earth's climate and its predictability over the last 66 million years. science, 369(6509), 1383-1387.

Wheeler, A. J., Walshe, J., & Sutton, G. D. (2001). Seabed mapping and seafloor processes in the Kish, Burford, Bray and Fraser Banks area, South-Western Irish Sea. Irish Geography, 34(2), 194-211.

Whitehouse, R.J.S., Harris, J.M., Sutherland, J., Rees, J., 2011. The nature of scour development and scour protection at offshore windfarm foundations. Mar. Pollut. Bull. 62, 73–88. https://doi.org/10.1016/j.marpolbul.2010.09.007

Whittington, R.J. (1977). A late-glacial drainage pattern in the Kish Bank area and post-glacial sediments in the Central Irish Sea. In Kidson, C., Toolet, M.J. (Eds.), The Quaternary History of the Irish Sea. Seel House, Liverpool, pp. 55–68.

WindEurope (2024). Wind energy in Europe. Statistics 2024 and the outlook for 2025-2030. 64 pp.

Winkelmann, D., Geissler, W., Schneider, J., Stein, R., 2008. Dynamics and timing of the Hinlopen/Yermak Megaslide north of Spitsbergen, Arctic Ocean. Marine Geology, Volume 250, 34-50, https://doi.org/10.1016/j.margeo.2007.11.013.

Winsborrow, M. C., Andreassen, K., Corner, G. D., & Laberg, J. S. (2010). Deglaciation of a marine-based ice sheet: Late Weichselian palaeo-ice dynamics and retreat in the southern Barents Sea reconstructed from onshore and offshore glacial geomorphology. Quaternary Science Reviews, 29(3-4), 424-442.

Winsborrow, M., Andreassen, K., Hubbard, A., Plaza-Faverola, A., Gudlaugsson, E., & Patton, H. (2016). Regulation of ice stream flow through subglacial formation of gas hydrates. Nature Geoscience, 9(5), 370-374.Woods, M.A., Wilkinson, I.P., Leng, M.J., Riding, J.B., Vane, C.H., Lopes dos Santos, R.A., Kender, S., De Schepper, S., Hennissen, J.A.I., Ward, S.L., Gowing, C.J.B., Wilby, P.R., Nichols, M.D., Rochelle, C.A., 2019. Tracking Holocene palaeostratification and productivity changes in the Western Irish Sea: A multi-proxy record. Palaeogeogr. Palaeoclimatol. Palaeoecol. 532, 109231. https://doi.org/https://doi.org/10.1016/j.palaeo.2019.06.004

Winsemann, J., Koopmann, H., Tanner, D. C., Lutz, R., Lang, J., Brandes, C., & Gaedicke, C. (2020). Seismic interpretation and structural restoration of the Heligoland glaciotectonic thrust-fault complex:

Implications for multiple deformation during (pre-)Elsterian to Warthian ice advances into the southern North Sea Basin. Quaternary Science Reviews, 227, 106068. https://doi.org/10.1016/J.QUASCIREV.2019.106068

Wrona, T., Magee, C., Jackson, C. A., Huuse, M., & Taylor, K. G. (2017). Kinematics of polygonal fault systems: Observations from the northern North Sea. Frontiers in Earth Science, 5, 101.

Yavari-Ramshe S and Ataie-Ashtiani B (2016) Numerical modeling of subaerial and submarine landslide-generated tsunami waves—Recent advances and future challenges. Landslides 13(6): 1325–1368.

Yuan, F., Bennell, J.D., Davis, A.M., 1992. Acoustic and physical characteristics of gassy sediments in the western Irish Sea. Cont. Shelf Res. 12, 1121–1134.

Zakeri, A.; Høeg, K. and Nadim, F. (2009). Submarine debris flow impact on pipelines – Part II: Numerical analysis. Coastal Engineering 56: 1–10, DOI 10.1016/j.coastaleng.2008.06.005.

Zarifi, Z., Köhler, A., Ringrose, P., Ottemöller, L., Furre, A.-K., Hansteen, F., Jerkins, A., Oye, V., Dehghan Niri, R., Bakke, R., 2022. Background Seismicity Monitoring to Prepare for Large-Scale CO2 Storage Offshore Norway. Seismol. Res. Lett. https://doi.org/10.1785/0220220178

Zengaffinen T, Løvholt F, Pedersen GK, and Harbitz CB (2020) Effects of rotational submarine slump dynamics on tsunami genesis: New insight from idealized models and the 1929 grand banks event. Geological Society, London, Special Publications 500(1): 41–61. Zhang C, Kirby JT, Shi F, Ma G, and Grilli ST (2021).

Zhang C, Kirby JT, Shi F, Ma G, and Grilli ST (2021) A two-layer non-hydrostatic landslide model for tsunami generation on irregular bathymetry. 1. Theoretical basis. Ocean Modelling 159: 101749.

Zhao, Y., & Si, B. (2019). Thermal properties of sandy and peat soils under unfrozen and frozen conditions. Soil and Tillage Research, 189, 64–72. https://doi.org/10.1016/j.still.2018.12.026

Zhao, Y., Si, B., Zhang, Z., Li, M., He, H., & Hill, R. L. (2019). A new thermal conductivity model for sandy and peat soils. Agricultural and Forest Meteorology, 274, 95–105. https://doi.org/10.1016/j.agrformet.2019.04.004

Zoback, M. D., & Gorelick, S. M. (2012). Earthquake triggering and large-scale geologic storage of carbon dioxide. Proceedings of the National Academy of Sciences, 109(26), 10164-10168.

Zoback, M. D., and Lund Snee, J.-E., 2018, Predicted and observed shear on pre-existing faults during hydraulic fracture stimulation, SEG Technical Program Expanded Abstracts 2018, Society of Exploration Geophysicists, p. 3588-3592.